18. SITE 686[1]

Shipboard Scientific Party[2]

HOLE 686A

Date occupied: 1730 L, 1 December 1986

Date departed: 1130 L, 2 December 1986

Time on hole: 18 hr

Position: 13°28.81′S, 76°53.49′W

Water depth (sea level; corrected m, echo-sounding): 446.8

Water depth (rig floor; corrected m, echo-sounding): 457.3

Bottom felt (m, drill pipe): 458.7

Penetration (m): 205.7

Number of cores: 23

Total length of cored section (m): 205.7

Total core recovered (m): 181.71

Core recovery (%): 88.3

Oldest sediment cored
Depth (mbsf): 205.7
Nature: diatomaceous mud
Age: Quaternary

HOLE 686B

Date occupied: 1130 L, 2 December 1986

Date departed: 0030 L, 3 December 1986

Time on hole: 13 hr

Position: 13°28.81′S, 76°53.49′W

Water depth (sea level; corrected m, echo-sounding): 446.8

Water depth (rig floor; corrected m, echo-sounding): 457.3

Bottom felt (m, drill pipe): 458.3

Penetration (m): 303.0

Number of cores: 32

Total length of cored section (m): 303.0

Total core recovered (m): 225.53

Core recovery (%): 74.4

Oldest sediment cored
Depth (mbsf): 303.0
Nature: diatomaceous mud
Age: Quaternary; possibly Pliocene

Principal results: Site 686, the southernmost point of the paleoceanographic north-south transect along the outer Peru shelf, is located in the West Pisco Basin. This site was selected (1) to obtain a high-resolution record of upwelling and climatic histories from Quaternary and possibly Neogene sediments, (2) to calculate mass accumulation rates of biogenic constituents from an upwelling regime, and (3) to document in detail early diagenetic reactions and products specific to the coastal upwelling environment.

Two holes were drilled at Site 686. Hole 686A was cored to a total depth of 205.7 mbsf using the hydraulic piston (APC) tool to 64.7 mbsf, followed by coring using the extended-core barrel (XCB) tool. Using these same drilling operations, Hole 686B was cored to 303.0 mbsf. In both holes, overall core recovery was good (80%); recovery was only moderate, however, in several sand layers. Cores from both holes were readily correlated using lithostratigraphic and biostratigraphic markers as well as physical index properties.

The sediments at Site 686 are made up of diatomaceous mud. Three major laminated intervals (Units I, III, and V) alternate with three bioturbated intervals (Units II, IV, and VI). All sediments recovered are of Quaternary age, based on the occurrence of an ash layer at 153.6 mbsf (which was also recognized at Site 687), where its age assignment was well constrained and estimated as between 0.7 and 0.9 m.y. At Site 686, the bioturbated intervals commonly contain silty, sandy, and shelly beds, whereas the laminated intervals, having friable phosphate layers, are more phosphoritic. Dolomites are common in all units except Unit I between 0–16 mbsf, which is a laminated diatomaceous mud with peloidal phosphorites. The major cyclic sequences contain numerous smaller cycles alternating between bioturbated and laminated diatomaceous muds. These cycles may record fluctuations in sea level and the position and intensity of the oxygen-minimum zone. Diatoms can be grouped into floras indicative of strong-, intermediate-, and low-intensity coastal upwelling, with oceanic admixtures. At least three prolonged phases of intense coastal upwelling appear to coincide with lithologic Units I, II, and III. Superimposed on these major and minor cycles is a clear

---

[1] Suess, E., von Huene, R., et al., 1988. *Proc. ODP, Init. Repts.*, 112: College Station, TX (Ocean Drilling Program).

[2] Erwin Suess (Co-Chief Scientist), Oregon State University, College of Oceanography, Corvallis, OR 97331; Roland von Huene (Co-Chief Scientist), U.S. Geological Survey, Branch of Pacific Marine Geology, 345 Middlefield Rd. M/S 999, Menlo Park, CA 94025; Kay-Christian Emeis (ODP Staff Scientist), Ocean Drilling Program, Texas A&M University, College Station, TX 77843; Jacques Bourgois, Département de Géotectonique, Université Pierre et Marie Curie, 4 Place Jussieu, 75230 Paris Cedex 05, France; José del C. Cruzado Castañeda, Petroleos del Peru S. A., Paseo de la Republica 3361, San Isidro, Lima, Peru; Patrick De Wever, CNRS, Laboratoire de Stratigraphie, Université Pierre et Marie Curie, 4 Place Jussieu, 75230 Paris Cedex 05, France; Geoffrey Eglinton, University of Bristol, School of Chemistry, Cantock's Close, Bristol BS8 1TS, England; Robert Garrison, University of California, Earth Sciences, Applied Sciences Building, Santa Cruz, CA 95064; Matt Greenberg, Lamont-Doherty Geological Observatory, Columbia University, Palisades, NY 10964; Elard Herrera Paz, Petroleos del Peru, S. A., Paseo de la Republica 3361, San Isidro, Lima, Peru; Phillip Hill, Atlantic Geoscience Centre, Bedford Institute of Oceanography, Box 1006, Dartmouth, Nova Scotia B2Y 4A2, Canada; Masako Ibaraki, Geoscience Institute, Faculty of Science, Shizuoka University, Shizuoka 422, Japan; Miriam Kastner, Scripps Institution of Oceanography, SVH, A-102, La Jolla, CA 92093; Alan E. S. Kemp, Department of Oceanography, The University, Southampton SO9 5NH, England; Keith Kvenvolden, U.S. Geological Survey, Branch of Pacific Marine Geology, 345 Middlefield Rd., M/S 999, Menlo Park, CA 94025; Robert Langridge, Department of Geological Sciences, Queen's University at Kingston, Ontario K7L 3A2, Canada; Nancy Lindsley-Griffin, University of Nebraska, Department of Geology, 214 Bessey Hall, Lincoln, NE 68588-0340; Janice Marsters, Department of Oceanography, Dalhousie University, Halifax, Nova Scotia B3H 4J1, Canada; Erlend Martini, Geologisch-Paläontologisches Institut der Universität Frankfurt, Senckenberg-Anlage 32-34, D-6000, Frankfurt/Main, Federal Republic of Germany; Robert McCabe, Department of Geophysics, Texas A&M University, College Station, TX 77843; Leonidas Ocola, Laboratorio Central, Instituto Geofisico del Peru, Lima, Peru; Johanna Resig, Department of Geology and Geophysics, University of Hawaii, Honolulu, HI 96822; Agapito Wilfredo Sanchez Fernandez, Instituto Geologico Minero y Metalurgico, Pablo Bermudez 211, Lima, Peru; Hans-Joachim Schrader, College of Oceanography, Oregon State University, Corvallis, OR 97331 (currently at Department of Geology, University of Bergen, N-5000 Bergen, Norway); Todd Thornburg, College of Oceanography, Oregon State University, Corvallis, OR 97331; Gerold Wefer, Universität Bremen, Fachbereich Geowissenschaften, Postfach 330 440, D-2800 Bremen 33, Federal Republic of Germany; Makoto Yamano, Earthquake Research Institute, University of Tokyo, Bunkyo-ku, Tokyo 113, Japan.

tectonic trend of subsidence in the depositional environment of the West Pisco Basin from 1.5 Ma to the present. Benthic foraminifer assemblages record four successively deeper habitats from the shelf (50–100 m) at 300 mbsf to upper middle-bathyal depths (500–1500 m) at 14.5 mbsf. Calcite formation followed by dolomitization is the ubiquitous diagenetic sequence along the Peru margin. We recognized this sequence at Site 686 by its reflection in maxima and minima of dissolved calcium and magnesium profiles. A subsurface brine, clearly seen as a chloride anomaly, continually replenishes calcium and magnesium used up in the formation of carbonate minerals. At Site 686, the brine contains large quantities of dissolved ammonia and phosphate and is depleted in sulfate, quite unlike the brines found along the transect at 11°S. We believe that this reflects the brine's passage through organic-rich sediments that undergo mineralization by sulfate reduction and the injection of dissolved metabolites.

BACKGROUND AND SCIENTIFIC OBJECTIVES

Sites 686 and 687 are important stations on the main paleoceanographic transects across upper-slope water masses and along the latitudinal range of sedimentary basins underlying the Peru coastal upwelling regime. These transects were designed to study the history of the upwelling environment in a three-dimensional framework. The sites that constitute the water depth transect are Site 681 at 146 m deep, Site 680 at 252 m, Site 687 at 307 m, and 686 at 443 m. The sites of the latitudinal transect are Sites 684 at 9°S, Site 679 at 11°S, and Site 686 at 13°S (see Site 679 chapter, Fig. 1); these latter sites are all within the same water depth of 450 ± 20 m. Some general considerations apply equally to Sites 686 and 687, whereas others apply specifically to each site. Therefore, the first part of the respective "Background and Scientific Objectives" sections of the Site 686 and 687 chapters are identical, but the second parts contain separate discussions for each site.

General Objectives

Site 686 in the West Pisco Basin (Fig. 1) and Site 687 at the southernmost end of the Lima Basin were selected to provide a continuous high-resolution record of upwelling and climatic histories, mass accumulation rates of biogenic constituents from an upwelling regime, and detailed documentation of early diagenetic reaction pathways and products of Quaternary and possibly Neogene sediments. Upwelling objectives address the development of (1) the oxygen-minimum zone and its role in organic-matter sedimentation and preservation through time, (2) latitudinal shifts of upwelling centers during climate cycles, and (3) records of water column parameters, especially temperature.

History of Oxygen Minima and Upwelling

The oxygen-minimum zone in the Peruvian upwelling regime today is strongly developed and intensifies from north to south because of cumulative oxygen consumption within the poleward-flowing undercurrent (Packard et al., 1983; Codispoti, 1983). Consequently, this zone shoals along the path of the undercurrent by about 300 m through the depth interval bracketed by Sites 684 and 686. Sea-level fluctuations and tectonism superimpose additional long-term trends on the depth distribution of those sediments that were deposited within the oxygen-minimum zone. We expected that sampling the latitudinal and water-depth transects would allow us to evaluate these trends separately.

Upwelling plumes generated along today's eastern-boundary current system off Peru show a distinct zonation along their paths (Fig. 2). The temperature increases from the center near the shore toward the margin offshore. The nutrient pattern changes from silica-dominated to nitrogen-dominated compositions, and the resulting biological succession likewise displays a zonal nearshore-offshore pattern, changing roughly from phytoplankton to zooplankton dominance (Jones et al., 1983; Dugdale, 1983). Site 686 is located at the northern fringe of a prominent upwelling center around Capo Nazca (14.5°S), and Site 687 is located at its extreme edge. Comparing both sites to each other and to Site 681, which is in the middle of the upwelling center at 11°S, may document the zonal structure and probable spatial shifts during climatic cycles. Bulk-sediment accumulation rates and accumulation rates of individual components (i.e., organic matter, calcium carbonate, phosphate, nitrogen, and silica) will be calculated later from the samples drilled at these sites.

Early Diagenesis

Rapid sedimentation rates of organic-rich sediments promote extreme sulfate reduction, methanogenesis, and associated early diagenetic carbonate reactions. Calcite and dolomite are the most widespread authigenic minerals formed during these carbon-fueled biogeochemical processes. Sites 686 and 687, with their continuous and rapid sedimentation of biogenic silica, phosphorus, and carbon, should provide exhaustive data about dissolved and gaseous compounds of pore waters, about isotope characteristics, and, hence, about *in-situ* temperatures of dolomite formation. With these data, we will be able to model the reactions of diagenesis by a detail and extent in time rarely possible before.

Effects of Hypersaline Fluids

A new objective emerged after Leg 112 drilling began that affected early diagenetic dolomitization processes, because we consistently found indications of saline brines at sites on the shelf and upper slope. These fluids were discovered in the subsurface at Sites 680, 681, and 684. The extent of their area over the Peru margin appears enormous, but their origin remains uncertain. This is of great significance because hypersaline pore fluids exert a strong influence on reaction pathways. Preliminary interstitial-water and gas analyses suggest that the brine continuously replenishes dissolved sulfate, the oxygen donor used by sulfate-reducing bacteria. Consequently, the competing effective pathway of microbial methanogenesis is suppressed. Such a process could strongly alter the carbon-isotope signal of the metabolic carbon dioxide that is incorporated in dolomites or any other authigenic carbonate mineral. The brine also is an inexhaustible source of calcium and magnesium for dolomitization. Therefore, sampling of interstitial water was intensified at Sites 686 and 687. Special attention was directed toward detecting elevated salinity; sulfate, magnesium, and calcium contents; and any change in the intensity of methanogenesis. The data acquired from Sites 686 and 687 about the distribution and chemistry of this brine will help us understand the full implications of this phenomenon.

Specific Objectives

The drilling area is located between two structural ridges that separated the shelf and upper-slope region. This part of the West Pisco Basin is heavily sedimented and underwent long and continuous subsidence and, hence, preserved a largely undisturbed record (Thornburg and Kulm, 1981). The East Pisco Basin contains an even thicker sediment cover, probably with a large terrigenous component. Both basins are adjacent to exposures on land of the famous Miocene Pisco Formation, a classic association of diatomites, cherts, and dolomites believed to have formed under coastal upwelling conditions (Muizon and Bellon, 1980).

The site lies landward of the depositional center of the West Pisco Basin (Fig. 1). The distance from shore is 66 km. We expected sedimentation rates to be high but thought that terrigenous input might be reduced because of the more proximal East Pisco Basin acting as a trap. Seismic data across the site indicate a shallow mud lens, about 40 m thick, that progrades seaward over older strata that conformably follow the basin morphol-

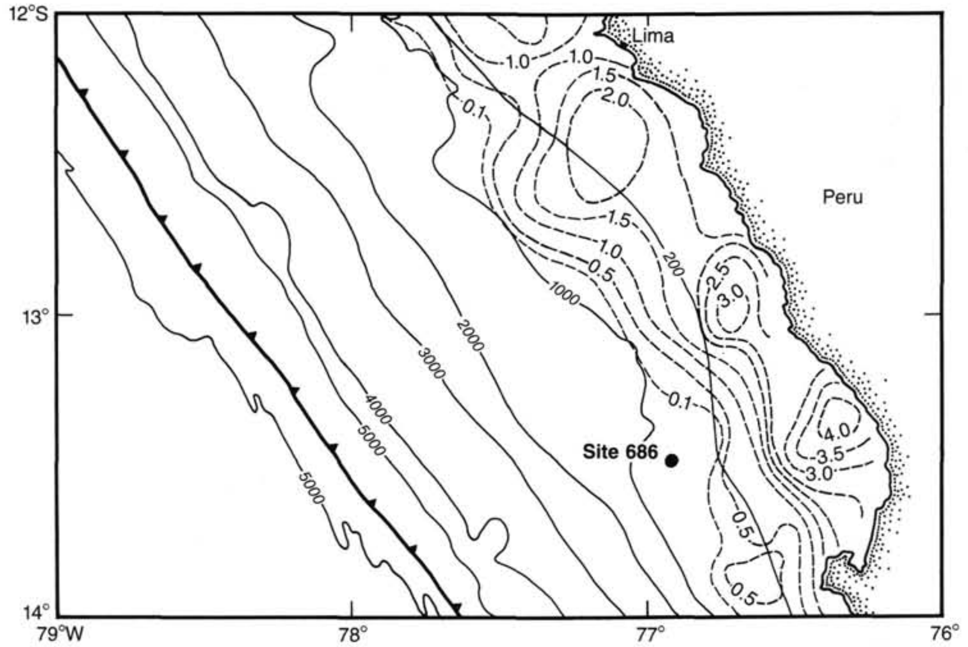

Figure 1. Bathymetry and sediment isopachs along the Peru Continental Margin at Site 686; depths are in intervals of 1000 m, beginning at a water depth of 200 m; sediment isopachs are in increments of 0.5 km, beginning at 0.1 km; for an overview of all sites, see Figure 1, Site Chapter 679 (this volume).

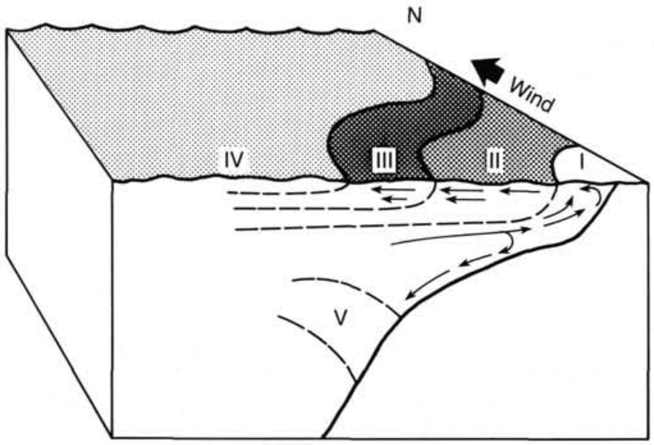

Figure 2. Idealized structure of an upwelling center in the southern hemisphere (Jones et al., 1983). The coastline is depicted on the right. The arrows indicate hypothetical stream lines of the cross-shelf flow. Zone I is the zone of intense upwelling; temperature is lowest, nutrients are highest, and biomass is generally low. As the water progresses outward (Zones II and III), it begins to warm, and the phytoplankton begin to adapt to both high nutrients and near-surface light intensities, which increases their rates of growth. Zone IV represents the oceanic conditions of the Peru Current regime. Zone V is the poleward-flowing countercurrent.

ogy. The mud lens shows strong multiple internal reflectors and thins out toward both ends, i.e., seaward and landward of Site 686. During its youngest history, the West Pisco Basin apparently subsided at a much faster rate than the adjacent Lima Basin, which would account for the thicker basin deposits (present water depth is 447 m). We believe that during deposition and high rates of subsidence this site traversed from shelf depths to its present depth and recorded the change in the oxygen-minimum zone and in oscillations of sea level during climatic cycles on an expanded scale of continuous high rates of sedimentation. Two holes were planned at Site 686 using the APC and XCB coring tools so as to reach 300 meters below seafloor (mbsf). This target depth was intended to provide sufficient sample coverage for high-resolution studies of the uppermost sediment sequence in the area of strongest coastal upwelling.

OPERATIONS

The ship approached Site 686 after a transit of 30 hr from the northern area at 2100 UTC (1600 L) on 1 December, 1986. (All times are UTC, Universal Time Coordinated, formerly GMT, Greenwich Mean Time, unless otherwise indicated.) The course followed SCS line YALOC 12-03-74 (Fig. 3) to locate the new site, which was situated on the broad, heavily sedimented and gently dipping flank of the West Pisco Basin at a water depth of 447 m. We deployed our geophysical gear, reduced speed to 6 kt, and began seismic surveying at 2120 hr. The survey was designed to ascertain that no acoustic turbulent features, "wipe-out" zones, or "pull-down" structures were present in the subsurface that might signal the presence of free methane gas. We did not observe such features. During this run, both the water-gun and 3.5-kHz records quickly showed a morphology and subbottom topography that allowed us to correlate clearly with existing YALOC seismic records, as well as to recognize its features. Thus, we had no trouble recognizing the new site, and dropped a wide-angle positioning beacon at 2200 hr. After retrieving the geophysical gear, the *JOIDES Resolution* came to a position on the new site. About 2 hr later, after running drill string to the bottom and shortly before spudding, our dynamic positioning alarm sounded because the beacon signal was weak and erratic. A backup beacon was lowered on taut wire, and we regained dynamic positioning mode at 0100 hr, 2 December. During this adjustment, we moved the ship about 200 m south. Checking the 3.5-kHz record showed us that the gently dipping sub-bottom reflectors and the thickness of near-surface strata remained unchanged.

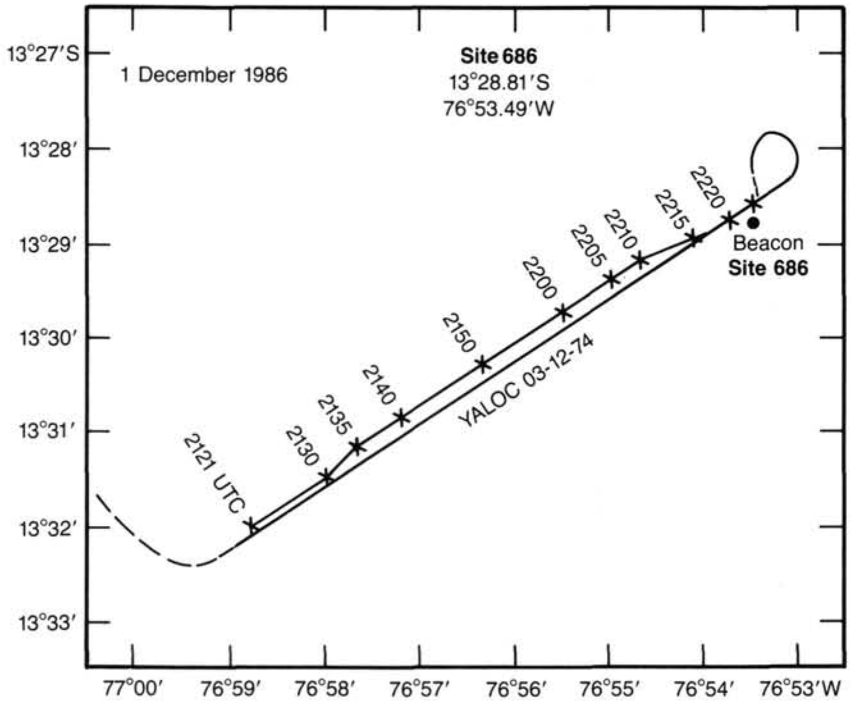

Figure 3. Tracking chart of approach to locating Site 686.

The first APC core came on deck at 0300 UTC, 2 December (2200 L, 1 December). We continued drilling Hole 686A to a total depth of 205.7 mbsf, using our APC tool to 64.7 mbsf and then the XCB mode for the rest of the hole (Table 1). Recovery of all APC and XCB cores was excellent (average of 89%). Modified jets on the drill bit and the soft formation encountered provided favorable conditions for improved core recovery. We measured temperatures in the hole at 33.6 and 52.6 mbsf using the heat-flow shoe and at 110.7 and 186.7 mbsf using the *in-situ* probe.

Hole 686B was cored at the same water depth, after moving the ship about 10 m south (Table 1). The APC-XCB combination again yielded good recovery rates (76%), with 100% recovery in the olive gray diatomaceous muds but <50% in frequent sand beds and silty layers. Phosphatic and dolomitic layers did not seem to affect recovery adversely. During these coring operations at shallow water depths, we accelerated retrieval of the core barrel from the hole significantly by running the wire line down the drill string before the core was completely cut. During this modified operation, 27 cores were brought on deck in 9 hr.

At about 1700 hr, 2 December, it was obvious that unfavorable global positioning system (GPS) conditions would delay the start of drilling the following day at Site 687. We decided to lengthen Hole 686B by 100 m. Our need to acquire a longer sediment section was prompted by the unexpectedly high sedimentation rates in the cored Quaternary sequence, which prevented our reaching the desired Neogene strata during 200 m of drilling. At 2250 hr, the last core was brought on deck. This core penetrated the first sediments of Pliocene age at 303.0 mbsf. The mud line was cleared at 2400 hr, and the ship was under way to the next site by 0200 L (0700 UTC), 3 December.

LITHOSTRATIGRAPHY

Lithologic Units

Sediments cored at Site 686 were divided into six lithologic units (Fig. 4 and Table 2), based on sediment composition and the dominance of either laminated or burrowed sequences.

Unit I

Cores 112-686A-1H through 112-686A-4H-3, 80 cm; depth: 0–27.9 mbsf.

Cores 112-686B-1H through 112-686B-3H-5, 30 cm; depth: 0–24.3 mbsf.

Unit I consists mainly of sandy diatomaceous muds that are predominantly, but not exclusively, laminated. These muds have 20% to 55% diatom frustules, 10% to 55% clay minerals, and 0% to 30% sand-sized terrigenous grains. Minor lithologies include phosphate nodules (both D and F types), a few layers of unlithified dolomitic muds, one layer of lithified dolomite, and thin beds of quartzo-feldspathic sand, silty sand, and silt, some of which are foraminifer-rich. D-phosphate nodules occur in a series of prominent gravel beds, some of which appear to be phosphatic hardgrounds and may mark hiatuses (Figs. 5 through 9; see following extended discussion).

Laminated muds are of two basic types. Type 1 laminations are typically thicker than 0.5 cm (Figs. 10 through 14). Some have sharp basal contacts and faint size grading and thus appear to have been deposited by currents. Others are diatom oozes (greater than 50% diatoms) with a distinctive olive color; these appear to be pelagic oozes recording either intervals of high diatom productivity or sorting by bottom currents. Still other type 1 laminations show subtle small bioturbation structures and originated through burrowing and disruption of type 2 laminations. Type 2 laminations are thinner (less than 0.5 cm) and more evenly spaced (Figs. 11 through 14). These likewise appear to have diverse origins; some are olive diatom oozes that probably record high productivity intervals, others show microripples and small scoured surfaces, indicating current activity. Laminated muds of both types have a variety of small-scale structures, including slump folds, microfaults, and dewatering veins.

Bioturbation occurs on several scales in Unit I. As noted before, very thin burrowed intervals produce some type 1 laminations (Fig. 13) and indicate shallow burrowing. Larger burrows disrupt bedding and contain sediments of a composition and texture different from the enclosing laminated muds (Figs. 14 through 16). Intense burrowing destroys all vestiges of bedding

Table 1. Coring summary for Site 686.

Core-section interval (cm)	Date (Dec. 1986)	Time (L)	Depth (mbsf)	Length cored (m)	Length recovered (m)	Recovery (%)
112-686A-1H	1	2155	0–5.1	5.1	5.12	100.0
2H	1	2210	5.1–14.6	9.5	9.88	104.0
3H	1	2230	14.6–24.1	9.5	9.85	103.0
4H	1	2300	24.1–33.6	9.5	9.88	104.0
5H	1	2320	33.6–43.1	9.5	9.92	104.0
6H	1	2350	43.1–52.6	9.5	7.15	75.2
7H	2	0030	52.6–62.1	9.5	3.13	32.9
8H	2	0100	62.1–64.7	2.6	2.68	103.0
9X	2	0143	64.7–72.7	8.0	7.01	87.6
10X	2	0214	72.7–82.2	9.5	4.73	49.8
11X	2	0240	82.2–91.7	9.5	9.69	102.0
12X	2	0308	91.7–101.2	9.5	6.70	70.5
13X	2	0334	101.2–110.7	9.5	10.05	105.8
14X	2	0515	110.7–120.2	9.5	2.56	26.9
15X	2	0559	120.2–129.7	9.5	13.37	140.7
16X	2	0620	129.7–139.2	9.5	11.08	116.6
17X	2	0645	139.2–148.7	9.5	9.65	101.0
18X	2	0704	148.7–158.2	9.5	11.43	120.3
19X	2	0728	158.2–167.7	9.5	9.53	100.0
20X	2	0750	167.7–177.2	9.5	9.58	101.0
21X	2	0807	177.2–186.7	9.5	9.66	101.0
22X	2	0941	186.7–196.2	9.5	0.56	5.9
23X	2	1005	196.2–205.7	9.5	8.50	89.5
112-686B-1H	2	1210	0–8.5	8.5	8.56	101.0
2H	2	1220	8.5–18.0	9.5	9.86	104.0
3H	2	1235	18.0–27.5	9.5	9.76	103.0
4H	2	1250	27.5–37.0	9.5	7.07	74.4
5H	2	1305	37.0–46.5	9.5	9.86	104.0
6X	2	1345	46.5–56.0	9.5	5.19	54.6
7X	2	1400	56.0–65.5	9.5	1.90	20.0
8X	2	1420	65.5–75.0	9.5	6.10	64.2
9X	2	1435	75.0–84.5	9.5	9.39	98.8
10X	2	1455	84.5–94.0	9.5	6.49	68.3
11X	2	1510	94.0–103.5	9.5	10.55	111.0
12X	2	1530	103.5–113.0	9.5	7.22	76.0
13X	2	1550	113.0–122.5	9.5	0.98	10.3
14X	2	1605	122.5–132.0	9.5	9.89	104.0
15X	2	1625	132.0–141.5	9.5	8.72	91.8
16X	2	1640	141.5–151.0	9.5	9.91	104.0
17X	2	1700	151.0–160.5	9.5	9.44	99.3
18X	2	1725	160.5–170.0	9.5	10.51	110.6
19X	2	1745	170.0–179.5	9.5	1.04	10.9
20X	2	1805	179.5–189.0	9.5	9.97	105.0
21X	2	1820	189.0–198.5	9.5	3.46	36.4
22X	2	1835	198.5–208.0	9.5	9.68	102.0
23X	2	1850	208.0–217.5	9.5	5.85	61.6
24X	2	1910	217.5–227.0	9.5	4.93	51.9
25X	2	1925	227.0–236.5	9.5	9.46	99.6
26X	2	1945	236.5–246.0	9.5	9.79	103.0
27X	2	2005	246.0–255.5	9.5	1.50	15.8
28X	2	2025	255.5–265.0	9.5	9.62	101.0
29X	2	2050	265.0–274.5	9.5	4.18	44.0
30X	2	2115	274.5–284.0	9.5	10.05	105.8
31X	2	2130	284.0–293.5	9.5	0.85	9.0
32X	2	2150	293.5–303.0	9.5	3.75	39.5

H = hydraulic piston; X = extended-core barrel; L = local time.

and produces massive, more or less homogeneous sediment. Such homogeneous intervals are relatively rare in Unit I, and those present are usually less than 1 m thick (Section 112-686A-2H-2).

Unit I also contains relatively small amounts of thin quartzofeldspathic sands and silts in layers of 1 to 10 cm thick (Section 112-686A-3H-6; Figs. 10 and 16 through 18). Some of these beds show sharp basal contacts, subtle graded bedding and, in a few cases, laminations (Fig. 18), characteristics that suggest deposition from a waning current. Several of these beds have concentrations of foraminifer tests and mollusk shell fragments (Fig. 18). Dispersed shell fragments are also present in some of the burrowed diatomaceous muds.

Unit II

Cores 112-686A-4H-3, 80 cm, through 112-686A-11X; depth, 27.9–91.7 mbsf.

Cores 112-686B-3H-5, 30 cm, through 112-686B-11X-3, 40 cm; depth, 24.3–97.4 mbsf.

Burrowed sandy diatomaceous muds, silts, and sands constitute most of Unit II. Completely bioturbated intervals of these lithologies occur in packets up to 7 m thick. These are separated from other bioturbated packets by thinner intervals (1–2 m) of laminated or slightly bioturbated, laminated diatomaceous mud. These alternations of bioturbated packets with laminated packets form about five or six cycles whose details are discussed later.

Superimposed on these cycles are graded beds 10 to 20 cm thick having sharp, scoured basal contacts and composed of quartzo-feldspathic sand and sandy silt. Two gravels containing reworked D-phosphate nodules occur in Unit II; one of these lies just above two dolomite beds and forms an excellent correlation between Holes 686A and 686B (Samples 112-686A-6H-4, 103–105 cm, and 112-686B-6X-2, 106–113 cm). F-phosphate nodules do occur at several levels in Unit II but are comparatively rare. A few thin dolomite beds up to 10 cm thick likewise are scattered throughout the unit in both the laminated and massive packets (Fig. 19).

Unit II differs from Unit I in (1) the dominance of burrowed intervals in Unit II vs. laminated intervals in Unit I, (2) the greater abundance of sand and silt layers in Unit II, and (3) a somewhat greater abundance of sand-sized terrigenous grains in the diatomaceous muds of Unit II. These attributes suggest a higher-energy, more-oxygenated, and perhaps shallower-water, environment for Unit II compared with Unit I. Laminated intervals in Unit II contain both type 1 and type 2 laminations as well as a variety of small structures, such as microfaults, dewatering veins, and slump folds (Figs. 20 and 21).

Unit III

Cores 112-686A-12X through 112-686A-17X-4; depth, 91.7–145.2 mbsf.

Cores 112-686B-11X-3, 40 cm, through 112-686B-16X-2; depth, 97.4–144.5 mbsf.

Laminated diatomaceous muds dominate Unit III and appear to be less sandy than comparable muds in lithologic Units I and II. As in Unit I, the laminated or slightly bioturbated laminated muds occur in packets up to 7.5 m thick, separated from other laminated packets by bioturbated intervals a few meters thick. The range of structures in the laminated muds resembles that of Units I and II. Thin graded beds of quartzofeldspathic- and lithic-rich sands and silts occur throughout the unit. Phosphate nodules are rare, but thin beds of dolomite are more common than in Unit II, particularly in the bottom one-half of Unit III. In addition, there are a few thin beds of micritic limestone. Two thin, ash-bearing beds occur in Section 112-686A-12X-3 but were not recognized in Hole 686B.

Unit IV

Cores 112-686A-17X-5 through 112-686A-23X; depth, 145.5–205.7 mbsf.

Cores 112-686B-16X-3 through 112-686B-24X-2, 25 cm; depth, 144.5–220.8 mbsf.

Burrowed, massive diatomaceous muds and distinctive shelly beds characterize Unit IV, which also contains a few interbedded packets of laminated or slightly burrowed laminated mud up to about 3 m thick. Also present are muddy sand layers having abundant reworked foraminifer tests. Concentrations of small mollusk shells and shell fragments occur in thin sand beds, in burrow fills, and also as dispersed grains in massive, bioturbated muds. Thin, lithified dolomite beds or nodular layers (Fig. 22) are common, and several such layers occur in nearly every core from lithologic Unit IV. A few F-phosphate nodules occur in both laminated and burrowed diatomaceous muds, and Section 112-686A-22X-1 contains D-phosphate nodules. A distinctive pair of volcanic ash layers occurs in both holes (Samples

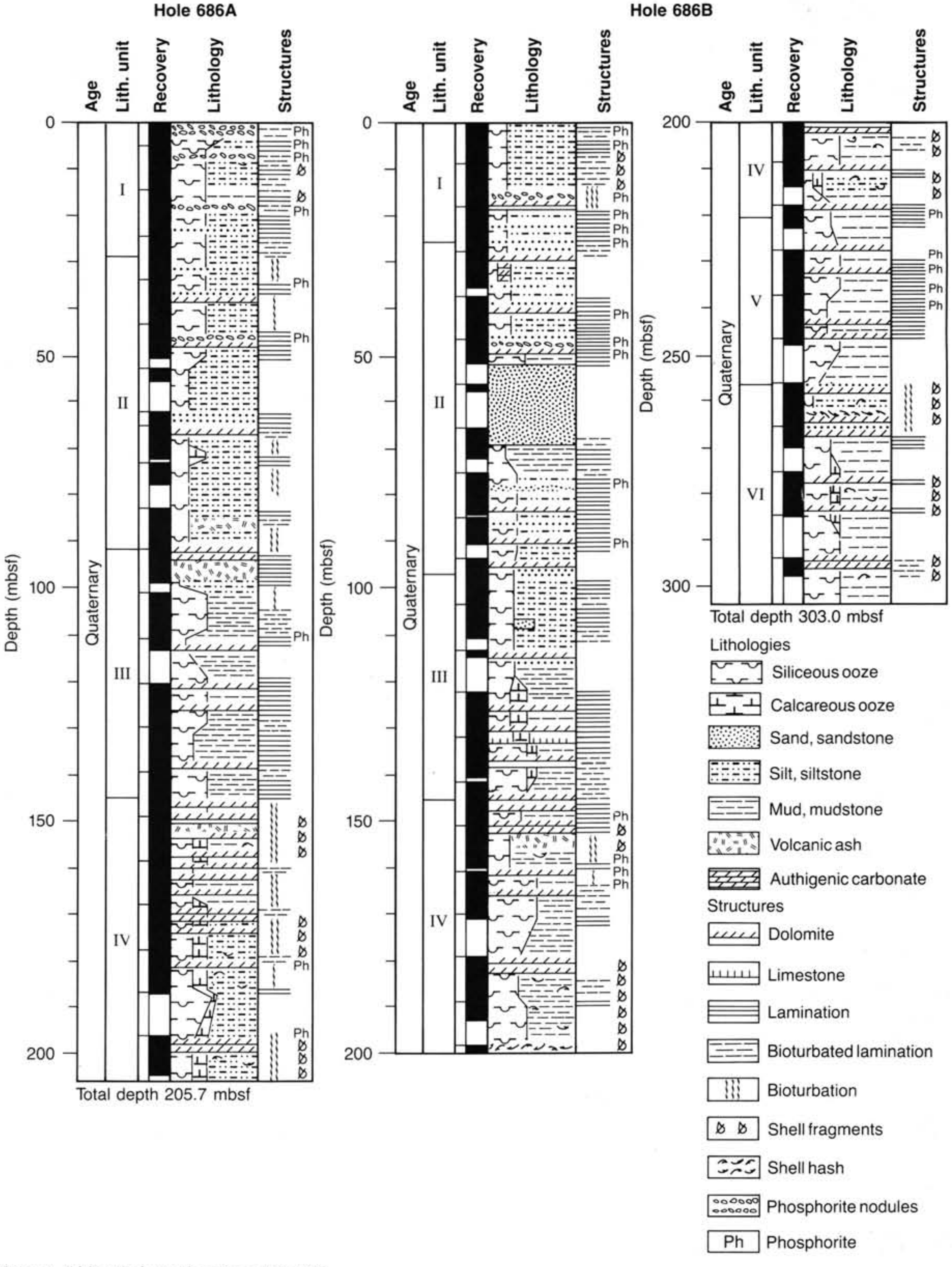

Figure 4. Lithostratigraphic units at Site 686.

112-686A-18X-5, 85–95 cm, and 112-686B-17X-3, 45–56 cm) and allows correlation between these layers, as well as between Sites 686 and 687, as subsequently discussed.

Unit V

Cores 112-686B-24X-2, 25 cm, through 112-686A-27X; depth, 220.8–255.5 mbsf.

The laminated diatomaceous muds that dominate Unit V also include a few thin burrowed intervals, some of which contain mollusk shells and shell fragments. Thin layers of lithified dolomite (Fig. 23) and micritic limestone occur throughout the unit, as do unlithified micritic (calcitic) and dolomitic diatomaceous mud layers. Thin sand and silt layers, present in most of the other units, are rare in Unit V.

Table 2. Lithologic units at Site 686.

Unit	Lithology	Core range	Approx. depth (mbsf)
I	Laminated diatomaceous mud with thin sand and silt layers	112-686A-1H through -4H-3, 80 cm	0-27.9
		112-686B-1H through -3H-5, 30 cm	0-24.3
II	Burrowed diatomaceous mud with beds of sand and silt	112-686A-4H-3, 80 cm through -11X	27.9-91.7
		112-686B-3H-5, 30 cm through -11X-3, 40 cm	24.3-92.4
III	Laminated diatomaceous mud	112-686A-12X through -17X-4	91.7-145.2
		112-686B-11X-3, 40 cm through -16X-2	97.4-144.5
IV	Burrowed diatomaceous mud with layers of shelly beds	112-686A-17X-5 through -23X	145.5-205.7
		112-686B-16X-3 through -24X-2, 25 cm	144.5-220.8
V	Laminated diatomaceous mud	112-686B-24X-2, 25 cm through -27X	220.8-255.5
VI	Burrowed diatomaceous mud with layers of shelly beds	112-686B-28X through -32X	255.5-303.0

Unit VI

Cores 112-686B-28X through 112-686B-32X; depth, 255.5-303.0 mbsf.

Unit VI closely resembles Unit IV in that the unit is largely bioturbated and contains distinctive shelly mollusk beds (Fig. 24) as well as dispersed mollusk fragments in burrowed diatomaceous muds and silts, the dominant lithologies of the unit. Interspersed with these burrowed muds and silts are the shelly beds noted above and a few thin (10-15 cm) beds of gray sand. The shelly beds contain concentrations of bivalves and gastropods (including distinctive "slipper" gastropods) as well as remains of crustaceans and fish.

In contrast to all other units, completely unbioturbated, laminated diatomaceous muds are very rare and thin in Unit VI (Fig. 25). A 1-cm-thick, white volcanic ash layer occurs in Sample 112-686B-29X-2, 65-66 cm. Both authigenic calcite and dolomite are present throughout Unit VI in thin lithified beds and as unlithified layers of calcite- and/or dolomite-rich diatomaceous mud. No D- or F-phosphate nodules were noted in Unit VI.

Carbonate Measurements

Downhole concentrations of carbonate in samples from Hole 686A are surprisingly low and rarely exceed 10% (Fig. 26 and Table 3). Considering the intense diagenetic overprinting of primary input signals observed in previous sites on the Peruvian shelf, we can comment on the formation of diagenetic carbonates, even though sample distribution along the lithologic section is widely spaced. From Table 3 and Figure 26 we can distinguish at least three intervals that differ in carbonate concentrations.

The first interval extends from the seafloor to about 12 mbsf and is characterized by fluctuations of carbonate content between 0% and about 5%. This most likely is mainly calcite of biogenic origin as little dolomite was observed in smear slides of this interval.

In the second interval (12 to about 35 mbsf), carbonate varies between 0.5% and a high of 41% calculated as $CaCO_3$, even though considerable contributions of authigenic dolomite may be present. This second interval is the zone of most intense carbonate diagenesis. From interstitial-water data (see "Inorganic Geochemistry" section, this chapter), we can see that in this interval, calcite is the dominant precipitate as a result of high alkalinity and Ca^{2+} concentrations. Lithified dolomite was first observed at a depth of 18 mbsf.

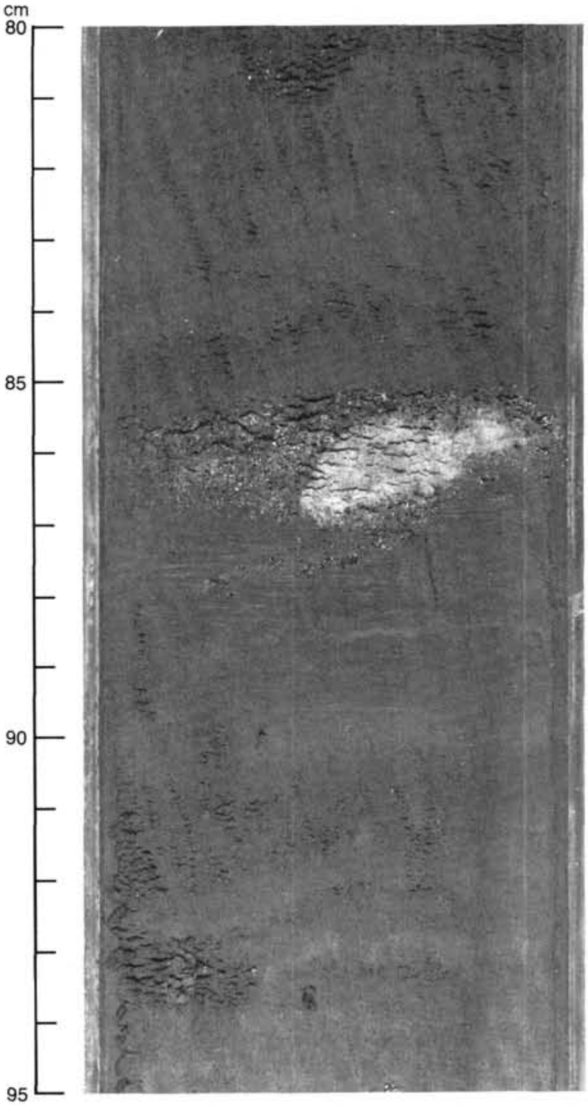

Figure 5. F-phosphate nodule in slightly burrowed laminated mud, lithologic Unit I (Sample 112-686B-1H-2, 80-95 cm).

The third interval (35 to 200 mbsf) indicates a slight increase in overall carbonate content from values near 1% to about 10%. This increase probably is caused by ongoing dolomitization of the lower sedimentary section, because the gain by diffusion of magnesium from the subsurface brine appears to be on the same order as the loss from precipitation of dolomite (see "Inorganic Geochemistry" section, this chapter). Closer sampling and analysis during shore-based programs may show whether the apparent cyclicity in the sedimentary facies (bioturbated vs. nonbioturbated) exerts any influence on diagenetic carbonate formation.

Diagenesis

Phosphates

Both F- and D-phosphates are present at Site 686, but they are common only in Unit I, perhaps because the remainder of the cored section was deposited at relatively rapid rates (see

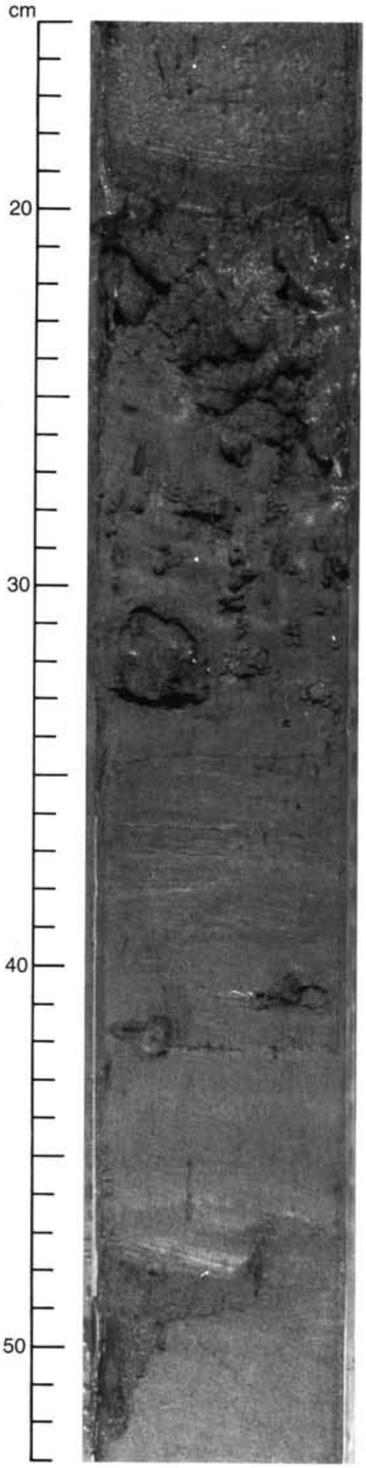

Figure 6. Layer of D-phosphate nodules, Unit I. Scattered nodules also occur in the laminated mud, possibly as burrow fill (Sample 112-686A-1H-2, 15–54 cm).

discussion below). F-phosphates (Fig. 5) are present in small amounts in all lithologic units. Unlike most other sites where they tend to occur only in laminated muds, here the F-phosphates are found in both laminated and burrowed muds. Unit III (Sample 112-686B-9X-2, 40–47 cm) contains a small slump fold in which a rotated F-phosphate nodule occurs in a deformed limb, which indicates that it formed before folding and during very early diagenesis.

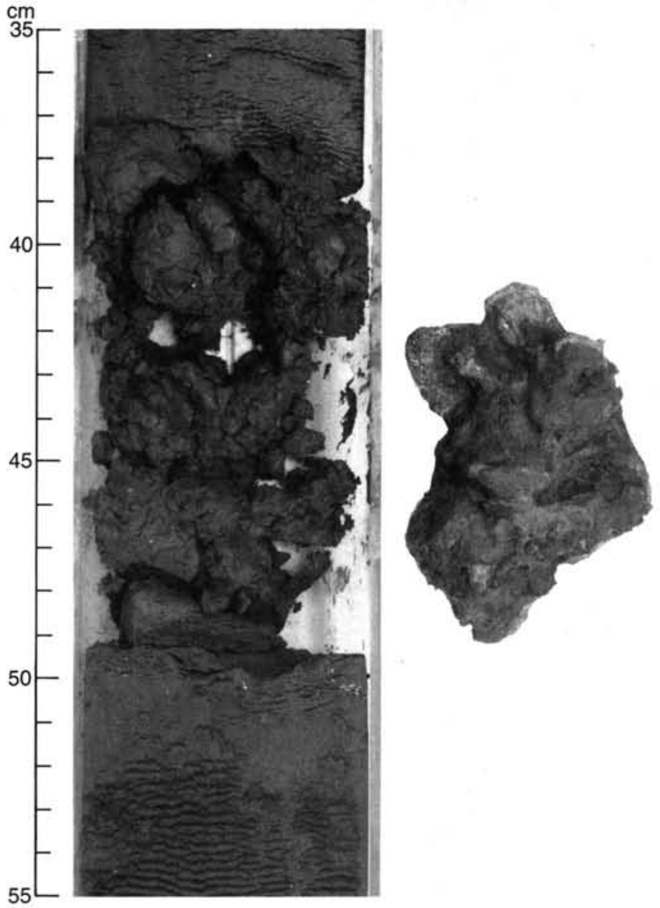

Figure 7. D-phosphate hardground, Unit I. The hardground was taken out of the core and turned upside down so that we are viewing its bulbous lower surface (Sample 112-686A-3H-1, 35–55 cm).

Thin gravel layers containing D-phosphate nodules occur in lithologic Unit I and in minor amounts in Units II (Sections 112-686A-6H-4, 112-686B-6X-2, and 112-686B-10X-4) and IV (Section 112-686A-21X-6 and 112-686A-23X-1), but were not observed in Units III, V, and VI. The most complete record of phosphates occurs in Unit I (Hole 686A), where Cores 112-686A-1H, 112-686A-2H, and 112-686A-3H contain four prominent beds of D-phosphate, along with five or six occurrences of F-phosphates (suggesting that perhaps Unit I is a condensed sequence containing several hiatuses). Some D-phosphate beds in Unit I are reworked gravels (Fig. 4), while in others the nodules have been cemented by later generations of phosphate to form phosphatic hardgrounds (Figs. 7 through 9). These hardgrounds have flat upper surfaces (perhaps from bioerosion) marked by organic borings (Fig. 9). In contrast, the lower surfaces protrude downward (Figs. 7 and 8) as if they had continued to grow irregularly down into the sediment at the same time the upper surfaces were being planed off.

Authigenic Carbonates

The degree of carbonate diagenesis increases with depth at Site 686 (Table 4). Unlike several other Leg 112 sites, however, there is no well-developed, near-surface zone where extensive precipitation of authigenic carbonates occurred. The unlithified diatomaceous muds of Unit I contain 1%–15% authigenic calcite and/or dolomite, but distribution of these phases is erratic, and most muds examined in smear slides contain 5% or less of authigenic carbonate minerals.

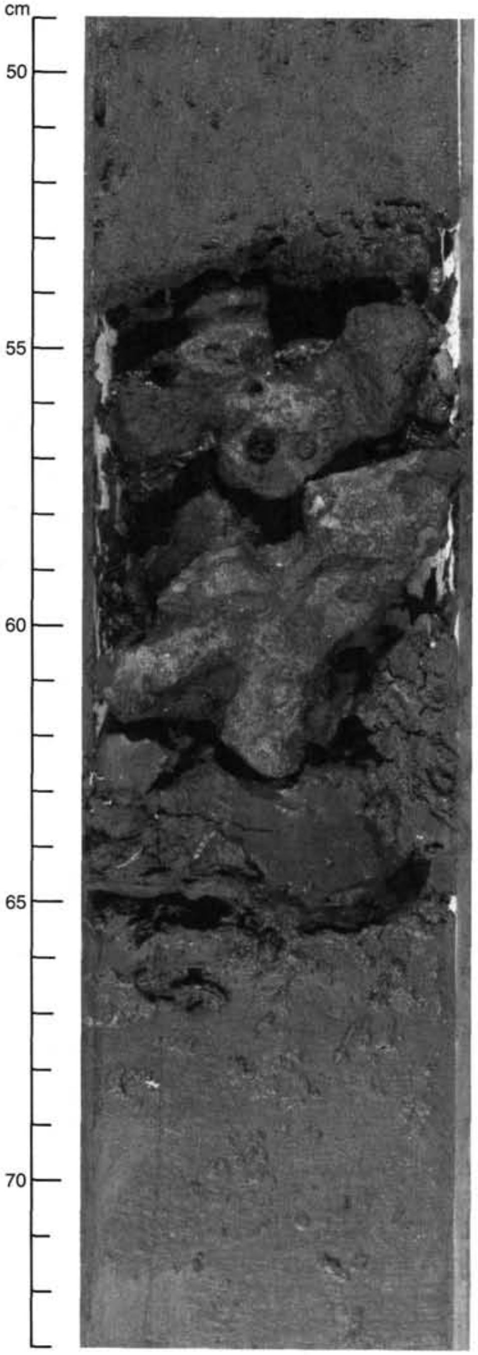

Figure 8. D-phosphate hardground, Unit I. The mottled appearance of the phosphate results from different generations of phosphatization, each of which produces slightly different colors and textures. See Figure 9 for a more detailed view of this hardground surface (Sample 112-686A-2H-2, 49–73 cm).

Figure 9. Closeup view of slabs from D-phosphate hardground seen in Figure 8. The slab at bottom has light-colored phosphatic clasts cemented by a later generation of dark-colored phosphate. The slab at bottom has a small hole made by a boring organism (Unit I, Sample 112-686A-2H-2, 48–59 cm).

The shallowest lithified carbonate is a dolomite layer at about 18 mbsf (Sample 112-686B-2H-7, 34–70 cm); this dolomite bed is directly overlain by a D-phosphate gravel, a juxtaposition noted at several other sites (e.g., Sites 680 and 681). Dolomite beds become progressively more common with depth and are most abundant in Units III through VI, where in some places nearly every core has two or more lithified or unlithified dolomite layers along with micritic limestone beds.

Below about 100 mbsf, small amounts of dispersed authigenic calcite and dolomite are common in diatomaceous muds, with calcite apparently more abundant than dolomite. However, in the lithified beds the situation is reversed, dolomite is much more abundant than calcite, although some of the hard beds fizz vigorously in weak acid and appear to be mixtures of dolomite and calcite (e.g., a hard bed in Sample 112-686B-17X-1, 117 cm, contains an estimated 45% calcite and 35% dolomite). Authigenic limestone beds were noted in Cores 112-686B-15X and 112-686B-25X.

At least four varieties of lithified dolomite layers are present at Site 686. The most common are thin beds or nodular layers of hard, well-lithified dolomite having distinct upper and lower contacts (Fig. 22). These occur in both laminated and burrowed muds, and many of them show a pronounced moldic porosity brought about by dissolution of foraminifer tests. A second variety appears to replace or partly replace laminated diatomaceous muds to form slightly friable, relatively thick layers (up to 30 cm thick) having somewhat diffuse upper and lower contacts (Figs. 19 and 23). The third variety is dolomite-cemented sandstones and siltstones, which are most common in Units IV and VI. The fourth variety occurs in Unit IV, where some shelly beds appear to have localized the sites of dolomitization. An example was found in Sample 112-686B-28X-2, 72–75 cm, where mud-filled internal casts of mollusks were preferentially dolomitized.

Depositional Environments

The lithological characteristics summarized above suggest a cyclic alternation between low-energy, low-oxygen environments (Units I, III, and V) and higher-energy, more-oxygenated environments having substantial terrestrial influx and enhanced sed-

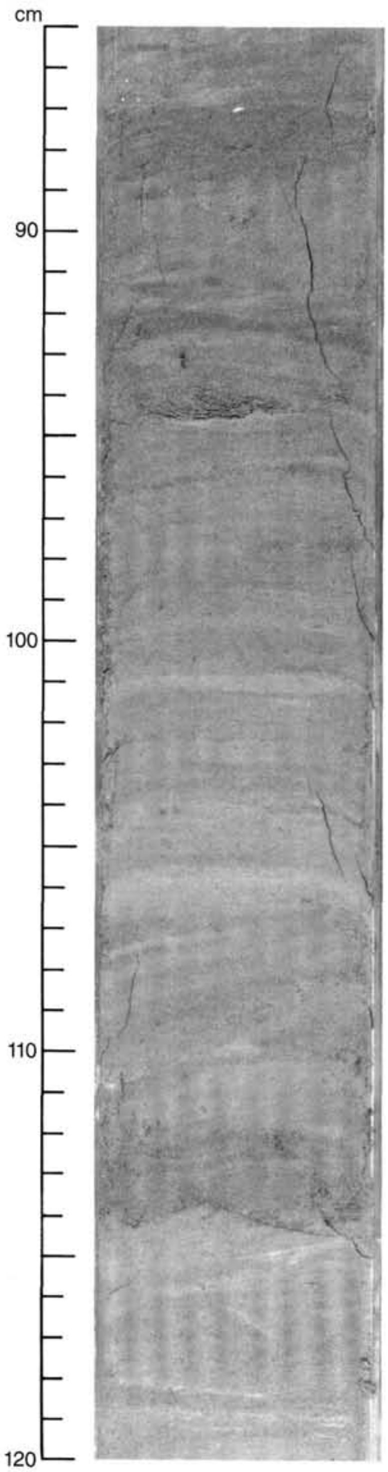

Figure 10. Laminated diatomaceous mud from Unit I showing type 1 laminations (Sample 112-686B-3H-4, 85-120 cm).

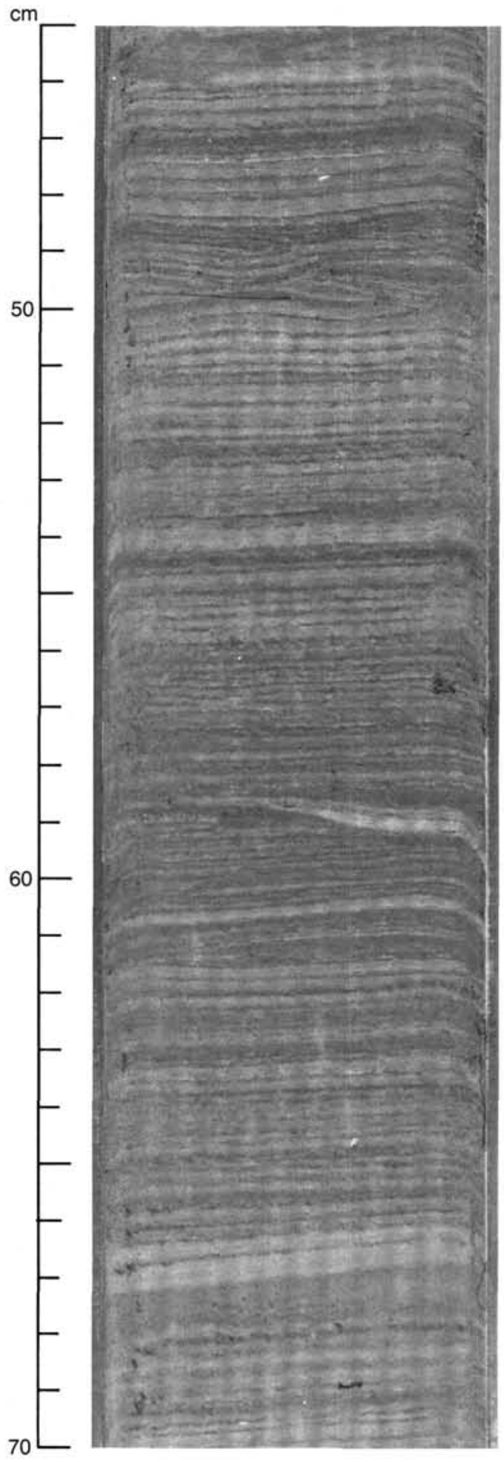

Figure 11. Laminated diatomaceous mud from Unit I showing type 2 laminations. Note small-scale scour structures in the middle and near the top of this core segment and several small slump folds between 48 cm and 50 cm (Sample 112-686B-3H-2, 45-70 cm).

iment reworking (Units II, IV, and VI). Our preliminary interpretation is that these cycles may record fluctuations in sea level and in the position and intensity of the oxygen-minimum zone. In this interpretation, the dominantly laminated units represent periods of high sea-level stands and an expanded oxygen-minimum zone, while the burrowed, coarser units represent low sea-level stands and the imposition of higher-energy, more-oxygenated environments. These fluctuations were superimposed on an overall deepening trend at Site 686, as indicated by paleontological evidence (see "Biostratigraphy" section, this chapter). Benthic foraminifer assemblages suggest that Units VI through IV

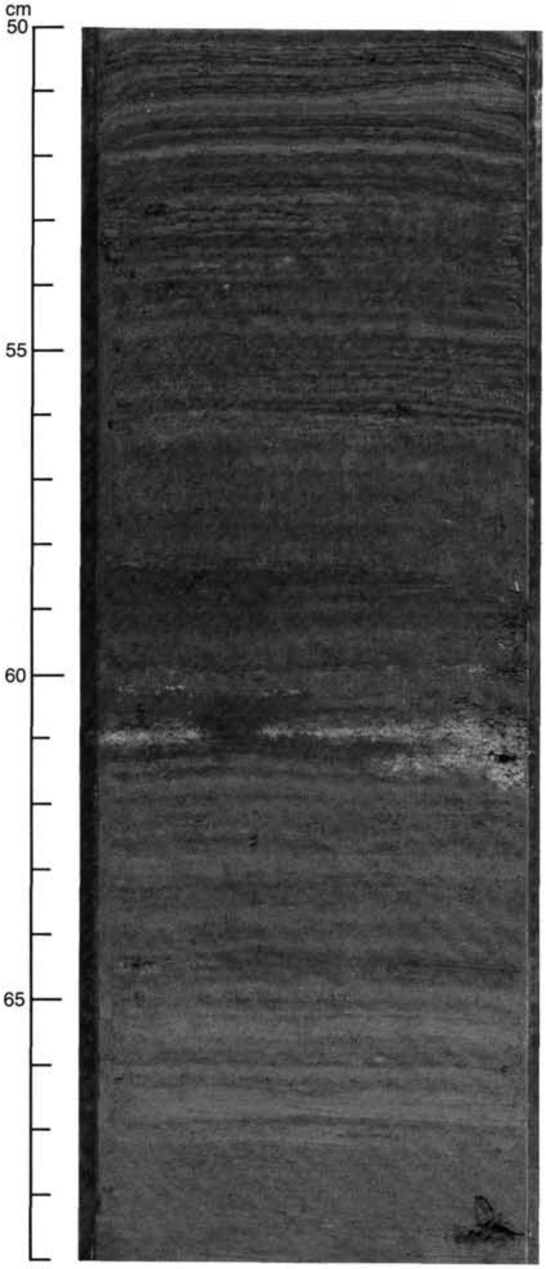

Figure 12. Interlayered type 1 and type 2 laminations in diatomaceous muds of Unit I. The light-colored lamina at 61 cm is dolomitic diatom ooze (Sample 112-686A-3H-4, 50-69 cm).

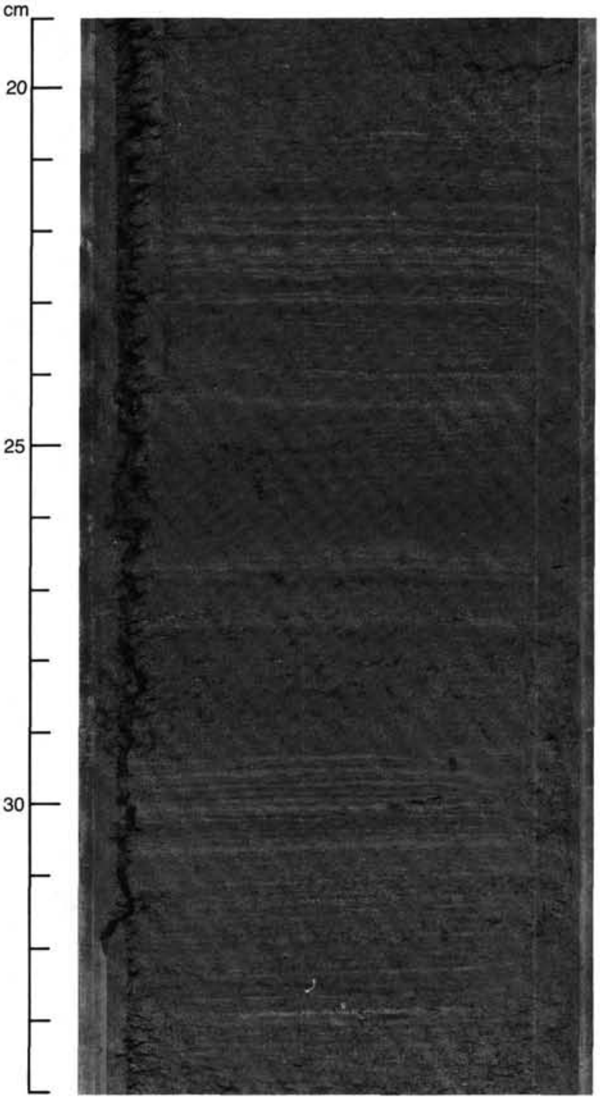

Figure 13. Alternations of type 1 and type 2 laminations in diatomaceous muds of Unit I (Sample 112-686A-1H-4, 19-34 cm).

were deposited in an outer-shelf environment and Units III through I in middle- to upper-bathyal environments, perhaps at slope depths comparable to the present depth of Site 686.

Age of Section at Site 686 and Correlation with Site 687

The paleontological data summarized in the "Biostratigraphy" section (this chapter) suggest that the section cored at Site 686 is probably of Quaternary age, but no finer resolution was possible through fossil dating. The Brunhes/Matuyama boundary (0.73 Ma) lies between about 39 and 44 mbsf (see "Paleomagnetism" section, this chapter). Thus, the average sedimentation rate for the upper 40 m of sediment was about 55 to 60 m/m.y. However, sparse nannofossil assemblages constrain the average sedimentation rate for the rest of the section at this site to a value between a minimum of 160 and a maximum of 300 m/m.y.

A cross correlation with Site 687, where better age information was available, allowed a somewhat more precise estimate of the average sedimentation rate for the lower two-thirds of the section at Site 686. A distinctive volcanic-ash layer near the top of Unit IV at Site 686 can be recognized at about 50 mbsf at Site 687, where its radiometric age is 1.36 ± 0.05 Ma (see Site 687 chapter). At Site 686, this ash layer occurs at a depth of about 154 mbsf. Assuming the ash is about 1.36 m.y. old, the average sedimentation rate for the interval between 40 and 154 mbsf was approximately 180 m/m.y. Projecting this rate to the base of the section at Site 686 yielded an age of about 2 Ma (late Pliocene) for the oldest sediment recovered.

Cycles at Site 686

The six lithologic units at Site 686 represent long-term oscillations of oxygen levels and perhaps also of sea levels. Assuming sedimentation rates of 60 m/m.y. for Unit I and 180 m/m.y. for the other units, Table 3 shows the estimated durations for the six units. In Table 3 we have applied our interpretation of

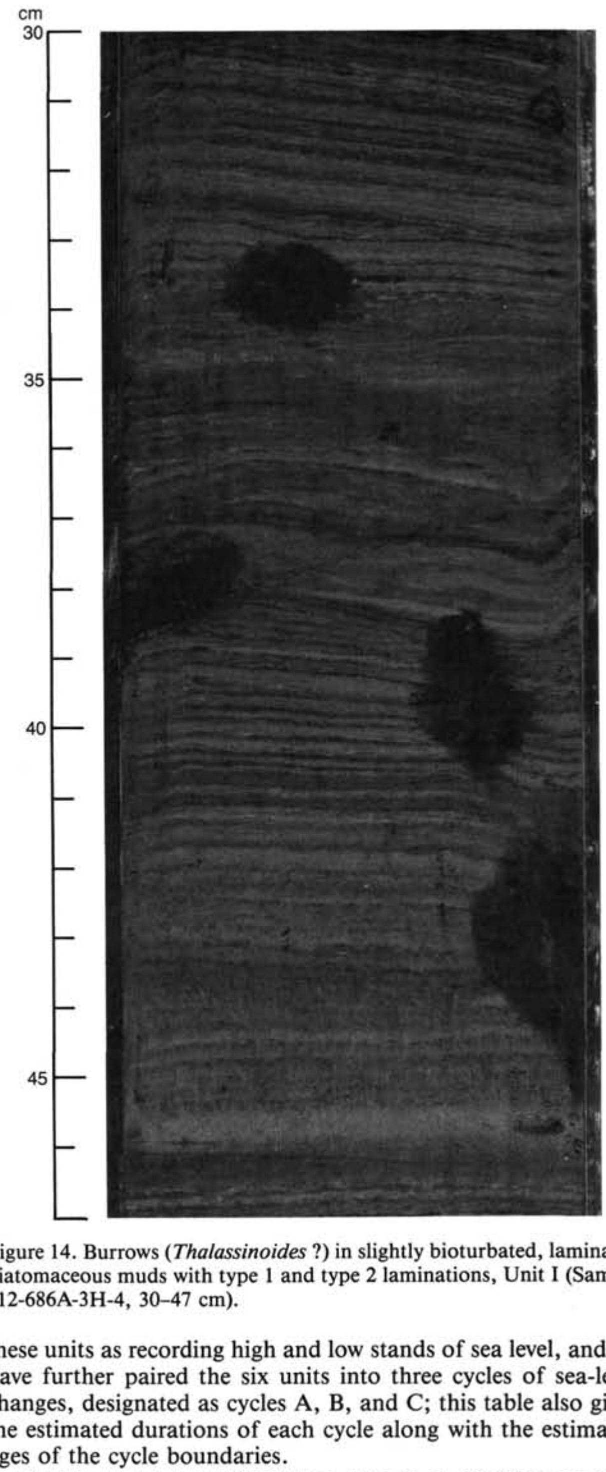

Figure 14. Burrows (*Thalassinoides* ?) in slightly bioturbated, laminated diatomaceous muds with type 1 and type 2 laminations, Unit I (Sample 112-686A-3H-4, 30–47 cm).

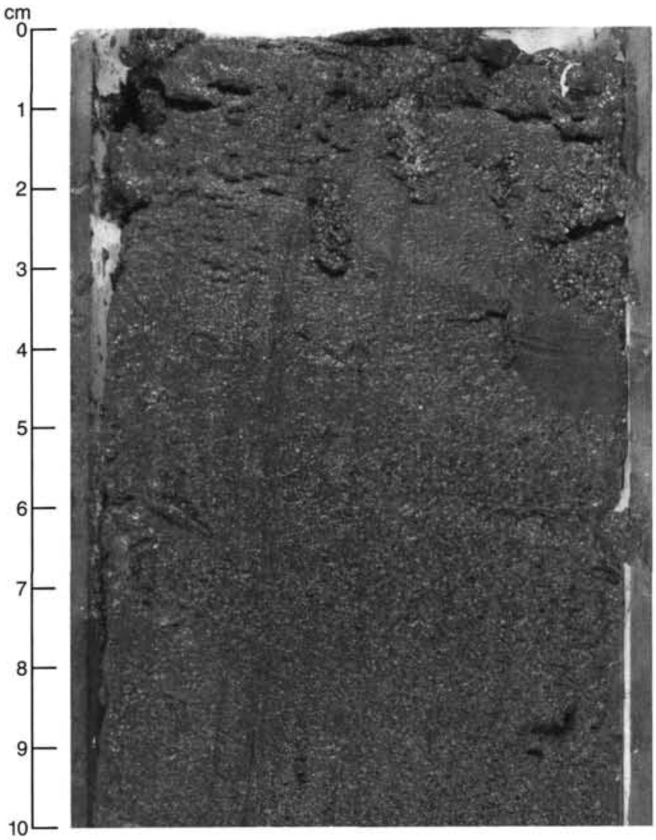

Figure 15. Burrows filled with foraminifer-rich mud, from, at, or near the sediment-water interface in Unit I (Sample 112-686A-1H-1, 0–10 cm).

these units as recording high and low stands of sea level, and we have further paired the six units into three cycles of sea-level changes, designated as cycles A, B, and C; this table also gives the estimated durations of each cycle along with the estimated ages of the cycle boundaries.

For the time interval 0–2.4 Ma, Haq et al. (1987) recognized four third-order cycles of sea-level change whose durations and boundary ages are listed in Table 3, along with the ages of the downlap surface for each cycle (the age of the downlap surface corresponds to the age of maximum flooding during a rise in sea level). Cycle A at Site 686 should encompass the youngest two cycles of Haq et al. (1987), but we were unable to resolve them. As noted previously, Unit I, with its numerous phosphatic layers, may be a condensed sequence in which a complex history of sea-level changes became greatly compressed at Site 686. We should emphasize that several Quaternary specialists question the validity of the major Quaternary cycles proposed by Haq et al. (1987). They prefer numerous shorter-term glacial/interglacial cycles (N. Shackleton, pers. comm., 1987). These shorter cycles are doubtless present within the larger cycles.

Superimposed on the long-term cycles represented by the six lithologic units are alternations of laminated and burrowed intervals at smaller scales. These range in thickness from decimeters to several meters to a few tens of meters (Fig. 25) and indicate short-term fluctuations in oxygen levels. The most prominent of these shorter cycles is recorded by the physical properties of the sediments (Fig. 27). As explained in the "Physical Properties" section (this chapter), these cycles, which have an average thickness of about 20 m, can be correlated plausibly by alternating low-density, water-rich, laminated diatomaceous muds with burrowed sands and silty muds having higher density and lower water content. Assuming an average cycle thickness of about 20 m and a more or less constant sedimentation rate of 180 m/m.y., the average cycle duration was 111,000 yr. This value is near the long-term variation in the earth's orbital eccentricity. The value also corresponds approximately to a cycle length that has been widely recognized in deep-sea pelagic sediments and attributed variously to climatically induced variations in productivity and/or preservation.

Structure

Structures observed in the cores of Site 686 include slump folds and convolute bedding, both normal and reversed microfaults, and rare dewatering veins. Although these features are present to some extent in all units, they are best observed in the laminated muds, especially in Unit I and the laminated parts of Unit II, because preservation is poor in the more massively bioturbated intervals.

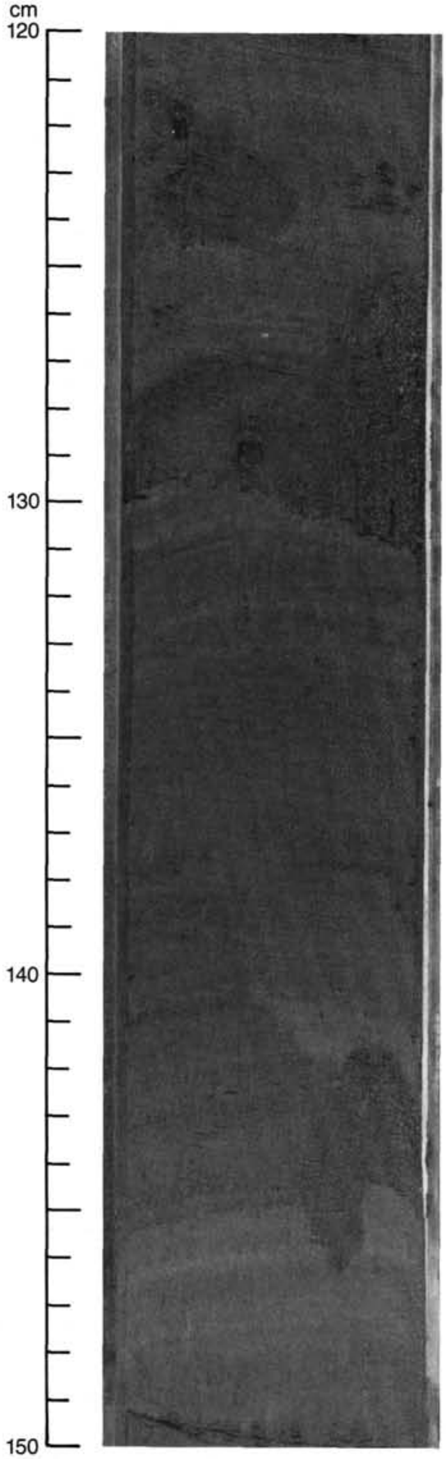

Figure 16. Large burrows (*Thalassinoides* ?) in moderately bioturbated diatomaceous mud having some residual type 1 laminations, Unit I (Sample 112-686A-1H-2, 120–150 cm).

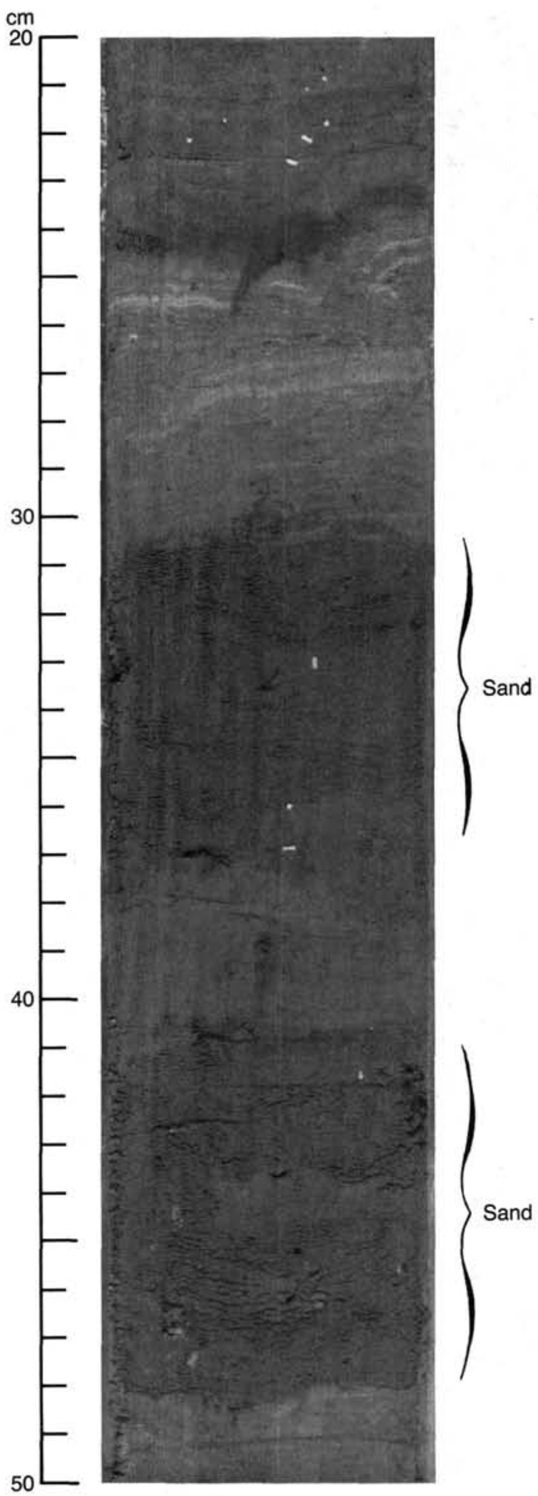

Figure 17. Thin sand layers interbedded with type 1 laminated diatomaceous muds, Unit I. Note small-scale deformation structures in the upper one-third of the core segment (Sample 112-686A-3H-6, 20–50 cm).

Slump Folds and Related Structures

Both Holes 686A and 686B exhibit well-developed slump folds in several cores (notably Samples 112-686A-1H-3, 11–25 cm, and 88–125 cm; 112-686B-1H-4, 60–117 cm; 112-686B-3H-1, 75 cm, through 112-686B-3H-3, 140 cm; 112-686B-5H, all sections; and 112-686B-10X-1, 20 cm, to 112-686B-10X-3, 50 cm). Slump folds appear in these cores both as fold noses (Fig. 20) and as zones of discordant bedding or convolute bedding, inclined at moderate to high angles relative to the surrounding bedding (Fig. 24). Typically, the lower contacts of the slump folds are defined by smeared-out beds that become thinner near the contact and wedge out into a zone of decollement, along which the folded beds were transported during slumping (Fig. 20). The up-

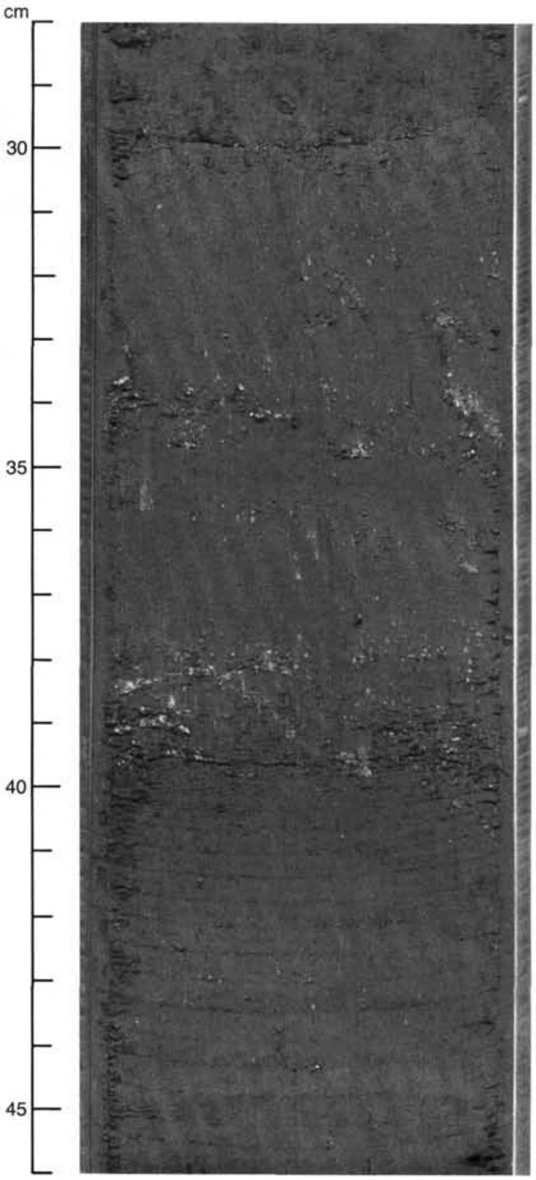

Figure 18. Foraminifer-rich sandy bed having some small mollusk(?) shell fragments lying above laminated sand layer, Unit I (Sample 112-686A-2H-7, 28–46 cm).

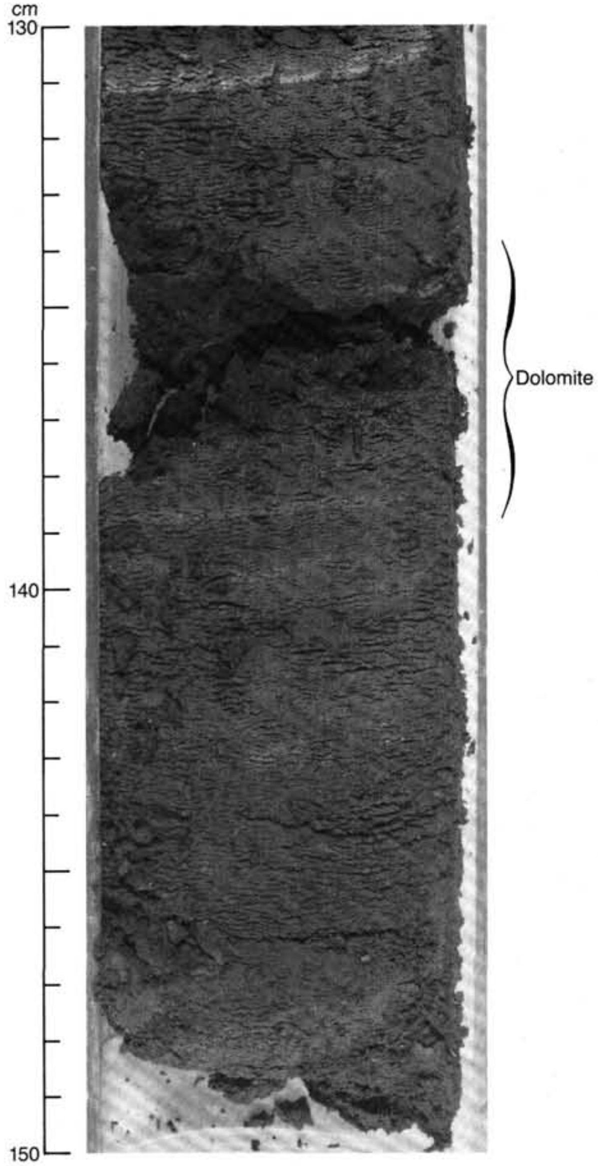

Figure 19. Friable, thin, dolomitic mud between 134 and 139 cm in type 1 laminated diatomaceous muds, Unit II. Light laminae are diatom oozes (Sample 112-686A-6H-3, 130–150 cm).

per contacts of these folds are sharply truncated, presumably due to scouring by bottom currents, and the folds are overlain by horizontal beds (Figs. 20 and 21).

Microfaults

Most of the microfaults observed in these cores are extensional (e.g., Samples 112-686A-2H-1, 105 cm; 112-686A-5H-1, 43 cm, and 66 cm; 112-686B-3H-4, 52–67 cm; and Sections 112-686B-5H-1 and 112-686B-5H-5), but compressional microfaults occur in four cores (Samples 112-686A-1H-2, 115–125 cm, and 112-686A-1H-4, 21 cm; 112-686A-3H-5, 80–85 cm; 112-686B-5H-3, 14–18 cm, 112-686B-5H-4, 65–67 cm; and 112-686B-10X-1, 30 cm, 48 cm, and 83 cm). Offsets on both types of faults are small, typically less than 1 cm, with a maximum throw of 2 cm. In Figure 21, the extensional microfaults visible just below the slump fold die out at the decollement that marks the base of the slump fold, which indicates that extensional microfaulting occurred before formation of the slump fold.

Dewatering Veins

Dewatering veins similar to those reported at other sites were observed in only two cores (Samples 112-686A-1H-3, 38–64 cm; 112-686B-5H-6, 67–68 cm, and 130–136 cm; and 112-686B-5H-7, 20–38 cm). These structures consist of mud-filled veins 1 to 3 mm wide that taper to points in both directions and commonly originate in coarse-grained laminae.

BIOSTRATIGRAPHY

Two holes were drilled at Site 686 in a water depth of 447 m to recover upwelling sediments of late Neogene and Quaternary age. Hole 686A penetrated 205.7 m and Hole 686B penetrated 303 m of Quaternary sediments. The base of the Quaternary was not reached.

As usual in upwelling areas, diatoms form the major part of microfossil assemblages, along with silicoflagellates and sponge

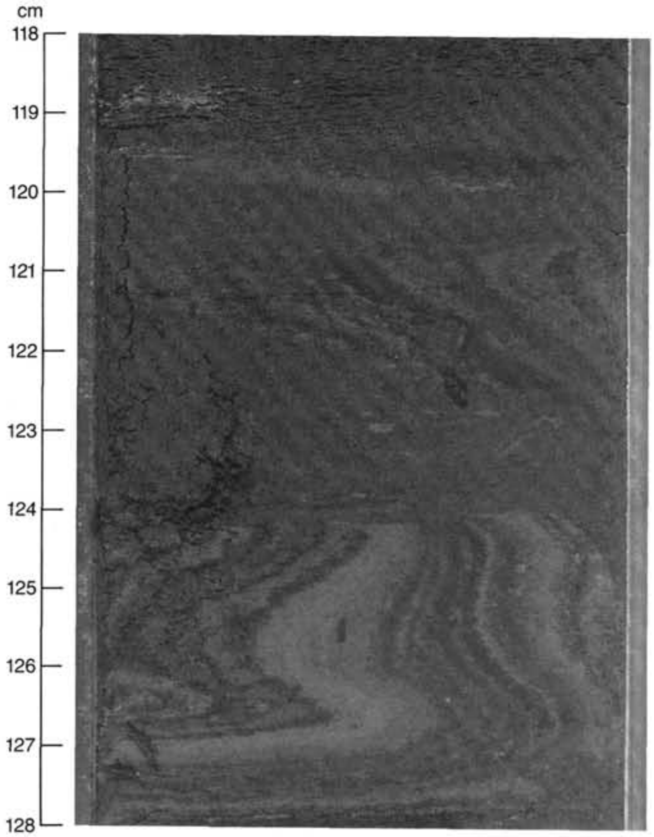

Figure 20. Nose of a complex slump fold exhibiting the characteristic change of shape from bed to bed and overlying a zone of decollement in which the beds on the lower fold limb are smeared out. Upper limb of the fold is truncated sharply, overlain by horizontal beds, and then by steeply inclined beds of a second slump fold (Unit II, Sample 112-686B-5H-4, 118–128 cm).

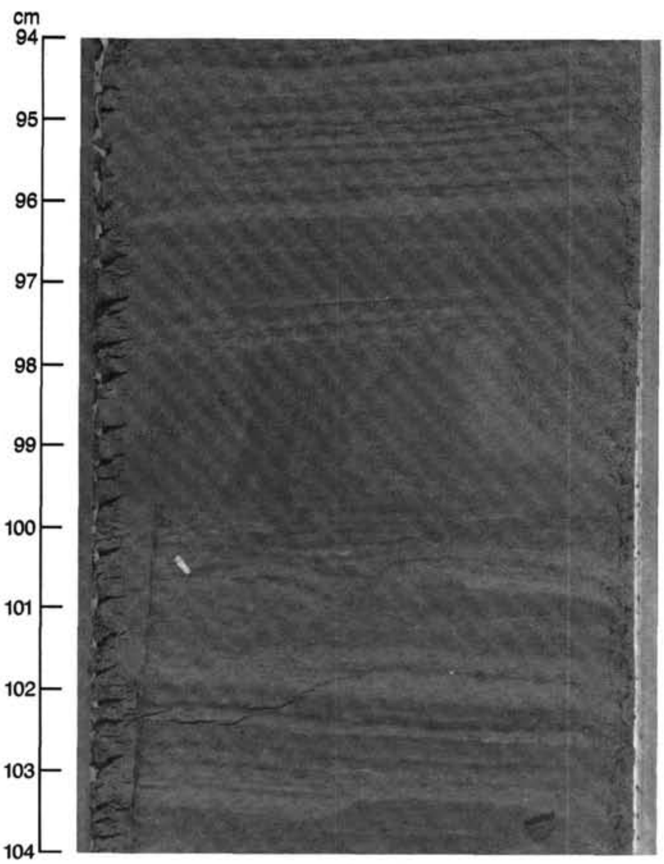

Figure 21. Steeply inclined beds of a slump fold nose. The extensional microfaults below this fault die out at the basal decollement of the fold, indicating that the faulting occurred before the slumping (Unit II, Sample 112-686B-5H-5, 94–104 cm).

spicules, and indicate frequent blooms as well as indications of cold- and warm-water masses at various times. Calcareous nannoplankton and planktonic foraminifers were found occasionally. Radiolarians are present in small numbers throughout, but all these groups are sparsely distributed throughout the Quaternary sequence at this site. Benthic foraminifers are present in two principal assemblages that indicate deposition in upper-bathyal environments for the upper part of the sequence. We noted a shallowing trend to an outer-shelf environment for the lower part of the sequence below 140 mbsf. Several sandy shell layers were encountered in the lower part of the sequence; these layers include mollusks and gastropods as well as remains of crustaceans and fish. Displaced lower to middle Miocene and middle to upper Eocene nannofossils, diatoms, and silicoflagellates were noted in much of the sequence, with concentrations in the shell-bed levels. According to nannoplankton data, sedimentation rates are at least 160 m/m.y.

Diatoms and Other Microfossils

All core-catcher samples from Hole 686A and the lower part of Hole 686B (Sections 112-686B-16X, CC through 112-686B-32X, CC) were examined for diatoms. These are abundant to common and frequently well preserved. The lowest sample, Section 112-686B-32X, CC contains *Pseudoeuntotia doliolus*, which places this sample in the *Pseudoeunotia doliolus* Zone; thus, the whole section cored at Site 686 is of Quaternary age.

Diatoms were categorized into three distinct floras: (1) strong coastal upwelling, (2) intermediate coastal upwelling, and (3) some coastal upwelling with oceanic admixtures. Since the core-catcher record was too spotty, we were unable to list samples according to the above scheme.

Floods of *Coscinodiscus asteromphalus*, girdle bands, *Actinocyclus ehrenbergii*, *Delphineis* sp. (new form, closely related to the northern *D.* "*ossiformis*") allowed us to correlate these species from hole to hole.

Terrestrial organic matter (in the form of cuticles and pieces of tracheoid wood) was found to occur sporadically in the coarse fraction, as did pollen. Fish scales and fish teeth formed another component in association with benthic and planktonic foraminifers as well as radiolarians.

Silicoflagellates

All core-catcher samples in Hole 686A were studied for silicoflagellates. In Hole 686B, only core-catcher samples from Core 112-686B-21X downward were examined. Both sequences are entirely Quaternary. The silicoflagellate assemblages are dominated by members of the *Dictyocha messanensis* group. *Mesocena quadrangula* was found in several levels from Section 112-686A-7H, CC (55.6 mbsf) throughout the sequence down to Section 112-686B-32X, CC at the terminal depth of 303 mbsf; the species indicated a long overlapping with *Distephanus bioctonarius bioctonarius*. The latter species was found between Section 112-686A-1H, CC (4.9 mbsf) and 112-686B-32X, CC (303 mbsf).

Calcareous Nannoplankton

All core-catcher samples from both holes, together with additional samples from sections within Hole 686A, were studied for calcareous nannoplankton.

Figure 22. Layers of nodular dolomite in moderately burrowed diatomaceous mud, Unit IV (Sample 112-686B-16X-4, 90–150 cm).

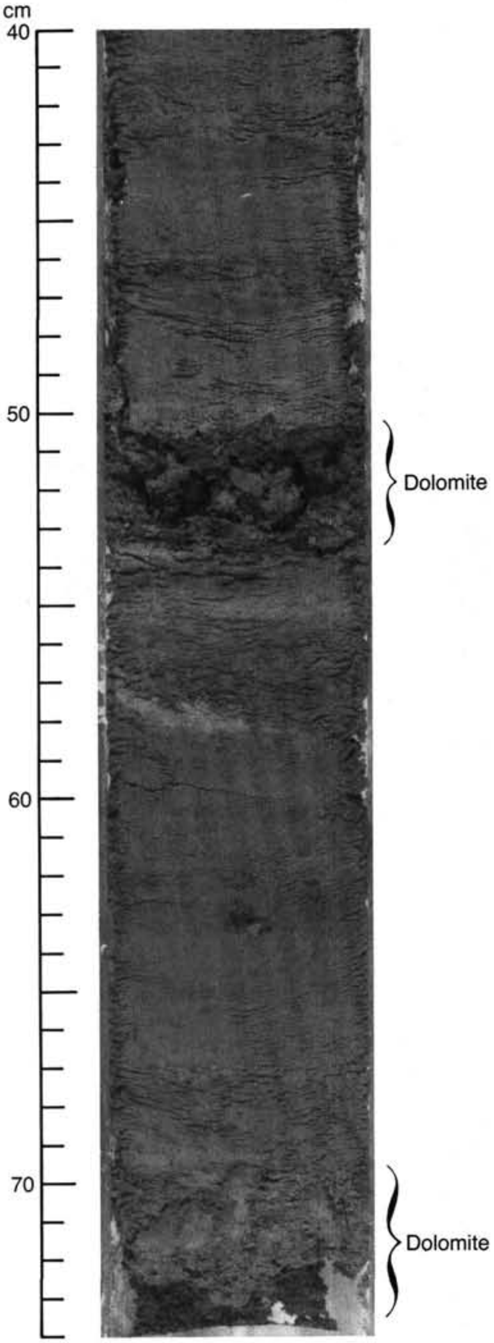

Figure 23. Two thin dolomite layers in moderately burrowed diatomaceous mud, Unit V (Sample 112-686B-25X-4, 40–74 cm).

Most samples are barren of calcareous nannoplankton. From approximately 60 mbsf down to approximately 284 mbsf, calcareous nannoplankton were occasionally encountered in impoverished and poorly preserved assemblages, usually *Gephyrocapsa* species and rare *Helicosphaera carteri*. Rare *Pseudoemiliania lacunosa* were found in Samples 112-686A-10X-2, 68–69 cm (74.9 mbsf) and 112-686A-21X, CC (186.6 mbsf), indicating the presence of nannoplankton Zone NN19 (*Pseudoemiliania lacunosa* Zone) in the lower part of the sequence. *Cyclococcolithus macintyrei* is present in Sections 112-686A-19X, CC (167.5 mbsf) and 112-686A-22X, CC (187.1 mbsf), which can be used to identify the lower part of the *Pseudoemiliania lacunosa* Zone (Zone NN19a, last occurrence [LO] of *Discoaster brouweri* to LO of *Cyclococcolithus macintyrei*) and the lowest part of the Quaternary.

In most cases, the meager Quaternary nannoplankton assemblages were associated with displaced lower to middle Miocene and middle to late Eocene nannoplankton species. The displaced species are especially frequent in the shell-bed interval around 190 mbsf. Here, in Section 112-686A-22X, CC (187.1

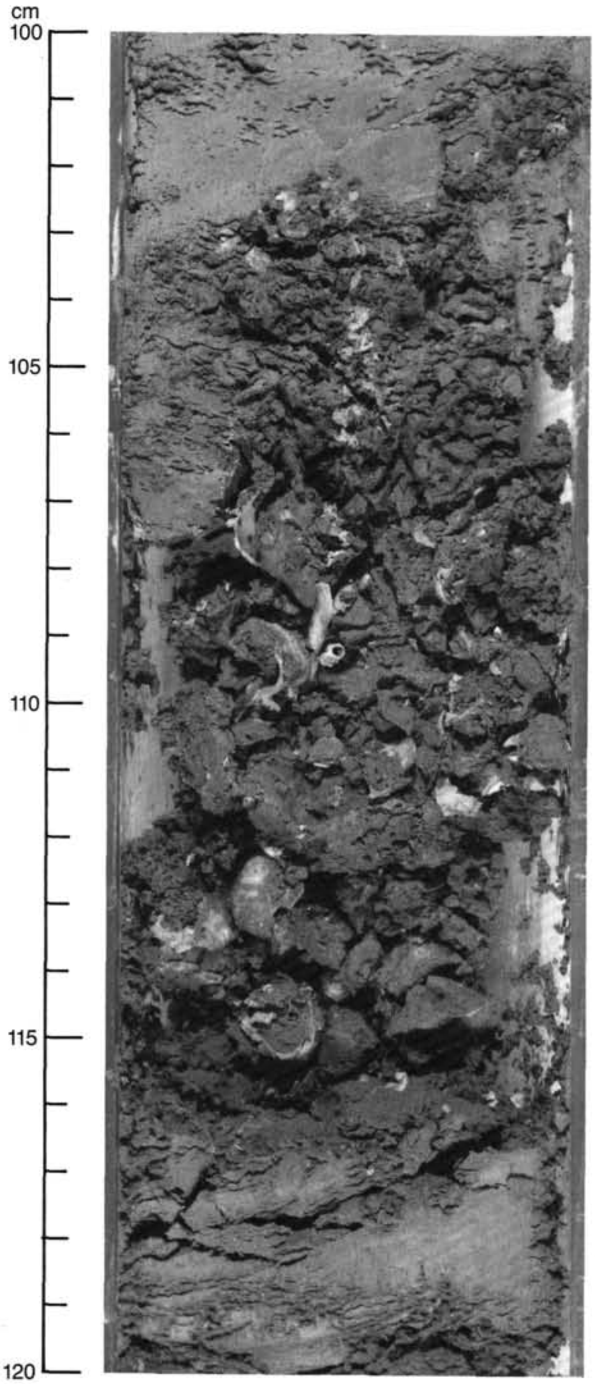

Figure 24. Sandy, shelly bed having mollusk fragments, Unit VI (Sample 112-686B-28X-5, 100–120 cm).

mbsf) *Discoaster deflandrei*, *Cyclococcolithus floridanus*, *Reticulofenestra pseudoumbilica*, *Dictyococcites dictyodus*, and *Reticulofenestra umbilica* were identified.

Sedimentation rates are at least 160 m/m.y., if one considers that the whole sequence represents the Quaternary calcareous nannoplankton Zones NN19 (*Pseudoemiliania lacunosa* Zone) to NN21 (*Emiliania huxleyi* Zone).

Radiolarians

All core-catcher samples from Hole 686A were studied for radiolarians. These are generally rare in all samples but are well to moderately well preserved.

A radiolarian assemblage that included *Lamprocyrtis nigriniae* was found in Sections 112-686A-2H, CC (14.7 mbsf), 112-686A-5H, CC (43.3 mbsf), 112-686A-9X, CC (71.6 mbsf), 112-686A-12X, CC (98.3 mbsf), and 112-686A-13X, CC (111.0 mbsf), indicating a Quaternary age. As no collosphaerids were found, we could not subdivide the Quaternary.

Planktonic Foraminifers

All core-catcher samples in Holes 686A and 686B were examined for planktonic foraminifers. In most cases, these were rare and well preserved.

Hole 686A

Above Section 112-686A-15X, CC (133.3 mbsf), samples are barren, except for Sections 112-686A-8H, CC (64.7 mbsf), 112-686A-9X, CC (71.6 mbsf), and 112-686A-14X, CC (113.1 mbsf). Below Section 112-686A-16X, CC (145.4 mbsf), rare planktonic foraminifers occur in Sections 112-686A-16X, CC (140.4 mbsf) through 112-686A-22X, CC (187.1 mbsf). Section 112-686A-23X, CC also is barren. *Globigerina bulloides*, *G. quinqueloba*, *Globigerinita glutinata*, *G. uvula*, and *Neogloboquadrina pachyderma* were found in most samples, indicating cool water. *Globigerinoides ruber* occurs only in Section 112-686A-21X, CC (186.6 mbsf), indicating warm water.

Hastigerinopsis riedeli occurs in Sections 112-686A-17X, CC (148.7 mbsf), 112-686A-19X, CC (167.5 mbsf), and 112-686A-20X, CC (177.1 mbsf) and ranges from Zone N22 to the Holocene (Poore, 1979). Based on planktonic foraminifers, the sequence recovered in this hole can be placed in the Quaternary.

Hole 686B

Planktonic foraminifers were found in Sections 112-686B-7X, CC (57.7 mbsf), 112-686B-13X, CC (113.8 mbsf), 112-686B-15X, CC (140.5 mbsf), 112-686B-20X, CC (189.3 mbsf) through 112-686B-23X, CC (213.6 mbsf), 112-686B-28X, CC (192.3 mbsf), and 112-686B-29X, CC (269.1 mbsf). *Globigerina bulloides*, *G. quinqueloba*, *Globigerinita glutinata*, *G. uvula*, and *Neogloboquadrina pachyderma* were found in most samples, which indicates cool water.

Hastigerinopsis riedeli occurs in Section 112-686B-21X, CC (207.9 mbsf), which has a range from Zone N22 to the Holocene (Poore, 1979). *Neogloboquadrina humerosa* was found in Section 112-686B-28X, CC. This species ranges from Zones N18 to N22, late Miocene to Pleistocene (Kennett, 1973). Foraminifers in Hole 686B indicate a Quaternary age.

Benthic Foraminifers

Hole 686A

Benthic foraminifers were concentrated in discrete layers in the upper part of the cored section, but were not retained in most of the core-catcher samples. A surface sample, 112-686A-1H-1, 0–1 cm, and a layer at Sample 112-686A-2H-7, 36–39 cm (14.5 mbsf), contain abundant, well- to moderately well-preserved benthic foraminifers, as do Sections 112-686A-8H, CC (64.7 mbsf) and 112-686A-9X, CC (71.6 mbsf). From Section 112-686A-13X, CC through 112-686A-23X, CC (11.1–204.6 mbsf), benthic foraminifers are generally abundant and well preserved. Sections 112-686A-1H, CC through 112-686A-7H, CC (5.0–55.6 mbsf) and 112-686A-10X, CC through 112-686A-12X, CC (77.2–98.3 mbsf) are barren of benthic foraminifers.

Two assemblages, described at previous sites, occur in this hole and are described as follows.

Cancris inflatus—Trifarina carinata Assemblage. This assemblage occurs in Sample 112-686A-1H-1, 0–1 cm (1 mbsf), and some species are present in Sample 112-686A-2H-7, 36–39 cm (14.5 mbsf). This species was noted previously in Sections 112-679B-1H, CC (96.3 mbsf), 112-679D-1H, CC (7.7 mbsf), 112-

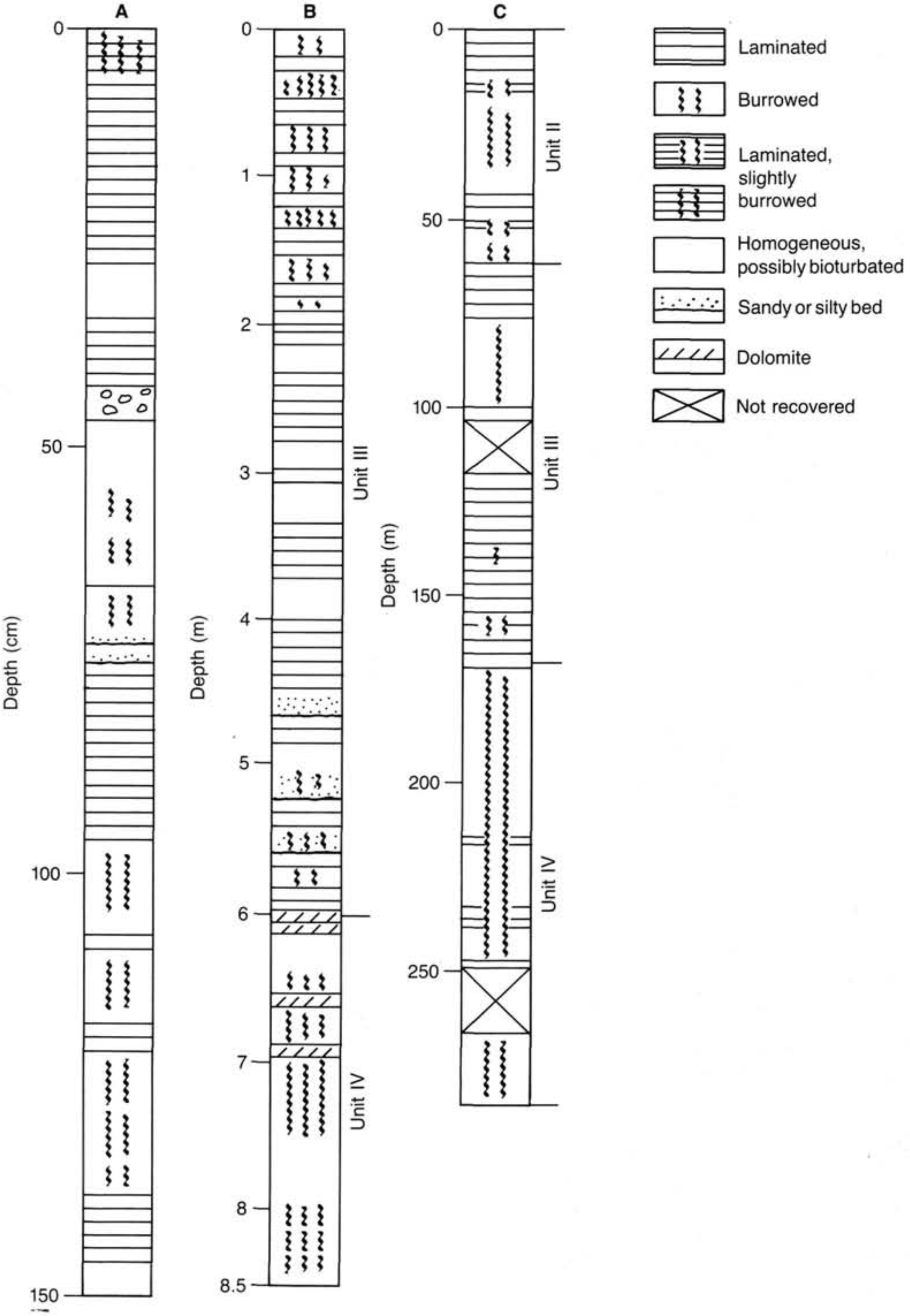

Figure 25. Alternating laminated and burrowed diatomaceous muds shown at different scales (note scales on the left side of the columns). A) a core section from Unit I (Section 112-686A-1H-1). B) a core that cuts across the contact between Units III and IV (Sections 112-686A-17X-1 to 112-686A-17X-5). C) a series of cores extending from the lower part of Unit II through Unit III into the upper part of Unit IV (Cores 112-686A-8X through 112-686A-23X).

680A-5H, CC (43.2 mbsf), 112-680B-3H, CC, and 112-680B-4H, CC (24.7–34.1 mbsf). The assemblage indicates an upper-bathyal environment.

Bolivina seminuda humilis Assemblage. *Bolivina rankini* occurs with or replaces *B. seminuda humilis* in some samples. This assemblage occurs in Sections 112-686A-8H, CC (64.7 mbsf), 112-686A-9X, CC (71.6 mbsf), and 112-686A-13X, CC through 112-686A-15X, CC (111.1–133.3 mbsf), where it indicates an upper-bathyal, low-oxygen environment. A large *Buliminella* occurs in abundance in Section 112-686A-16X, CC. From Sections 112-686A-16X, CC through 112-686A-23X, CC (140.4–204.6 mbsf), the assemblage is altered by the co-occurrence with

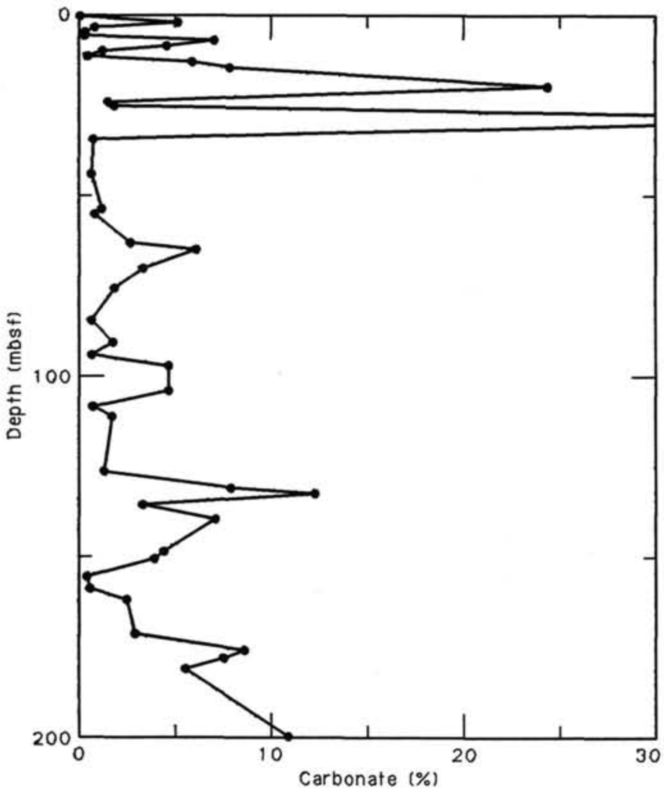

Figure 26. Carbonate contents in Hole 686A.

Bolivina of common to abundant *Nonionella* sp., which indicates a shallower seafloor in an outer-shelf environment. A similar assemblage with abundant *Nonionella* occurs in the upper part of Hole 681A, which was drilled in a water depth of 146 m. Using a sedimentation rate of 160 m/m.y., this implies a subsidence rate of at least 150 m/m.y. for the section above 140 mbsf, presuming the outer-shelf facies was deposited during a lower sea-level stand.

Hole 686B

Two samples from this hole (which repeats and extends the section cored in Hole 686A) were examined for benthic foraminifers to confirm the trend of shoaling noted in Hole 686A. Section 112-686B-30X, CC (284 mbsf) contains abundant, well-preserved benthic foraminifers and abundant mollusk shells. *Hanzawaia* sp., *Nonionella* spp., *Discorbis* sp., *Buliminella elegantissima*, *Bolivina costata*, and *Epistominella subperuviana* are the dominant species; *Buccella* sp. is rare. Section 112-686A-31X, CC (284.8 mbsf) contains abundant dolomitized foraminifers. The assemblage resembles that of the previous sample, but without *Hanzawaia* and with a few specimens of *Virgulinella*. These foraminifers indicate an outer-shelf (50 to 150 m) environment (Ingle, 1980).

Biogenic Groups (Coarse-Fraction Analysis)

The biogenic groups analyzed in Hole 686A show the following relative percentage distribution (Fig. 28). Diatoms and radiolarians are the dominant groups in Sections 112-686A-1H, CC (5.0 mbsf) to 112-686A-16X, CC (140.4 mbsf). Benthic foraminifers predominate from Section 112-686A-14X, CC (113.1 mbsf) to the bottom and reach up to 80% of the total biogenic remains in Section 112-686A-20X, CC (177.1 mbsf). Planktonic foraminifers are rare but conspicuously present from Section 112-686A-17X, CC (148.7 mbsf) downward. However, a few specimens also were found in Sections 112-686A-8X, CC (64.7 mbsf) and 112-686A-14X, CC (113.2 mbsf). Planktonic species identified include *Globigerina bulloides*, *G. parkerae*, *G. calida*, *Neogloboquadrina pachyderma*, *N. dutertrei*, *Globorotalia (Hirsutella) scitula*, and *Globigerinoides trilobus*. These species are small in size, become robust below Section 112-686A-19X, CC (167.6 mbsf), and are probably related to changes in oceanic conditions. Most species listed indicate temperate to warm, subtropical waters and range from the Miocene to Holocene.

ORGANIC GEOCHEMISTRY

Two holes were drilled at Site 686 to sample Quaternary upwelling sediments in the central part of West Pisco Basin (in a water depth of about 447 m). Organic-geochemical analyses were conducted on samples from Hole 686A down to 202.6 mbsf, whereas Hole 686B was sampled to 295.5 mbsf. The overlapping sediment interval in the upper parts of both holes gave us an opportunity to compare results. Hydrocarbon gases, organic carbon, and organic matter characteristics were routinely monitored. Details of methods and procedures are discussed in the "Organic Geochemistry" sections, Site 679 and 682 chapters (this volume). Instruments used are described in the "Explanatory Notes" (this volume).

Table 3. Profile of duration and age of sedimentary cycles at Site 686.

				Quaternary cycles at Site 686			Neogene cycles of sea-level changes (Haq et al., 1987)		
Lithologic unit[a]	Thickness (m)	Duration (m.y.)	Sea level	Cycle	Duration of cycle (m.y.)	Age of cycle boundaries (Ma)	Duration (m.y.)	Age of cycle boundaries (Ma)	Downlap surface age (Ma)
I	28	0.46	High stand			0		0	0.006
				A (Units I and II)	0.86		0.8		
II	73	0.40	Low stand						
						0.86		0.8	
III	53	0.29	High stand						
				B (Units III and IV)	0.71		0.8		1.3
IV	76	0.42	Low stand						
						1.57		1.6	
V	35	0.19	High stand						
				C (Units V and VI; base not exposed)	0.46+		0.8		2.0
VI	48+	0.27	Low stand						
						2.03+		2.4	

[a] Lithologic Units I, III, and V are predominantly laminated; Units II, IV, and VI are predominantly burrowed.

Table 4. Carbonate contents for Hole 686A.

Core-section interval (cm)	Depth (mbsf)	Carbonate (%)
112-686A-1H-1, 14–15	0.14	0.08
1H-2, 14–15	1.64	5.10
1H-3, 14–15	3.14	0.83
1H-4, 14–15	4.64	0.33
2H-1, 14–15	5.24	0.33
2H-2, 14-15	6.74	7.00
2H-3, 14–15	8.24	4.58
2H-4, 14–15	9.74	1.25
2H-5, 14–15	11.24	0.50
2H-6, 14–15	12.74	5.91
2H-7, 14–15	14.24	7.83
3H-4, 45–46	19.55	24.41
3H-7, 31–33	23.91	1.50
4H-1, 79–80	24.89	1.83
4H-3,106–107	28.16	41.23
5H-1, 68–69	34.28	0.75
6H-2, 26–27	43.70	0.67
7H-1, 85–86	53.45	1.17
7H-2, 85–86	54.95	0.83
8H-1, 77–78	62.87	2.67
8H-2, 86–87	64.46	6.08
9X-4, 66–67	69.86	3.33
10X-2,127–128	75.47	1.83
11X-2, 77–78	84.47	0.67
11X-6, 77–78	90.47	1.75
12X-2, 90–91	94.10	0.67
12X-4, 90–91	97.10	4.66
13X-2,120–121	103.90	4.66
13X-5,120–121	108.40	0.75
4X-1, 45–46	111.15	1.75
15X-8, 39–40	130.85	7.91
15X-5, 39–40	126.35	1.33
16X-3, 79–80	132.44	12.25
16X-5, 83–84	135.48	3.33
17X-1, 20–21	139.40	7.08
17X-7, 20–21	148.40	4.41
8X-2, 32–33	150.52	3.92
18X-5, 84–85	155.54	0.42
19X-1, 61–62	158.81	0.58
19X-3, 62–63	161.82	2.50
20X-3, 59–60	171.29	2.92
20X-6, 59–60	175.79	8.58
21X-1, 69–70	177.89	7.50
21X-3, 69–70	180.89	5.50
23X-3, 43–44	199.63	10.83

Hydrocarbon Gases

Vacutainer Gases

Enough gas was present for gas pockets to form in most of the core liners, starting with Core 112-686A-8H of Hole 686A (65.7 mbsf) and Core 112-686B-5H of Hole 686B (39.7 mbsf) to the bottom of the respective holes. The results of gas analyses are listed in Table 5. C_1 ranges from 54.5% to 90.0%; we assumed the balance gas was air, although significant amounts of CO_2 may be present. The concentrations of C_2 and C_3 are remarkably uniform, with C_2 ranging from 130 to 290 ppm, and C_3, when detected, ranging from 2.2 to 8.6 ppm. The uniformity of C_2 concentrations results in C_1/C_2 ratios that lie within a narrow range (between 2500 and 5700). The profiles of this ratio with depth (Fig. 29) are similar in both holes and decrease slightly with depth. However, this decrease is less pronounced than what we expected for oceanic sediments in general (Claypool and Kvenvolden, 1983) and probably results from the youth of the sediments drilled (Quaternary). The magnitude of the ratio was less than what we expected for hydrocarbon gases in young sediments. C_2 concentrations are anomalously large, which suggests the possibility that microbial generation of C_2 is intense at this location.

Extracted Gases

Table 6 lists the concentrations of hydrocarbon gases, based on results from the headspace procedure for both holes and on results from the can procedure at Hole 686B only. We detected only the hydrocarbon gases, C_1 and C_2. This contrasts with results from other sites, where C_3 and often $C_{2:1}$ were normally seen, although in small concentrations. The amount of extracted C_1 increases rapidly with depth and reaches its largest concentrations between 22.5 and 41.5 mbsf. Below these depths, the amount of C_1 remains about the same (Fig. 30). Results from both holes and from the two procedures are roughly comparable, although the C_1 concentrations in Hole 686A are usually slightly lower. The occurrence of the highest amounts of C_1 at a minimum depth of 22.5 mbsf corresponds to the depth at which sulfate concentrations decrease to zero (see "Inorganic Geochemistry" section, this chapter). This inverse correlation between C_1 and sulfate values reflects the competitive relationship between microbial sulfate reduction and methanogenesis (Claypool and Kaplan, 1974).

As measured by the headspace procedure, C_2 concentrations range from 10 to 52 μL/L of wet sediment. These amounts are anomalously large, as are the amounts of C_2 in the free gas obtained by vacutainers. C_1/C_2 ratios of the extracted gases follow a profile with depth (Fig. 31) that mimics the profile of C_1 concentrations (Fig. 30), and results from Holes 686A and 686B using the two procedures are roughly comparable. However, the trends shown by the C_1/C_2 ratios for gases collected by vacutainers (Fig. 29) and for extracted gases (Fig. 31) are very different. Values for the C_1/C_2 ratios of extracted gases remain about the same below about 75 mbsf. In general, C_1/C_2 ratios tend to be lower in extracted gas than in free gas (obtained by vacutainers); the trends with depth are usually the same (Kvenvolden and McDonald, 1986). The reason that the C_1/C_2 ratios of extracted gas and free gas do not show the same trends with depth at this site may have to do with the geologically young age of the sediments here and the range over which the C_1/C_2 ratios vary. The range is small and perhaps insufficient to reveal any trend with depth in the extracted gas data.

Carbon

Part of the 14 "squeeze cakes" left after the procedures used to obtain pore-water samples for inorganic geochemistry studies (see "Inorganic Geochemistry" section, this chapter) were examined for total carbon, carbonate carbon, and organic carbon (OC). In addition, total organic carbon (TOC) and organic matter characteristics, as measured by Rock-Eval pyrolysis, were determined. Data concerning the carbon content of these samples are given in Table 7, and OC and TOC are compared with depth in Figure 32. The OC content of these samples varies, ranging from 0.52% to 4.97% for OC and from 0.48% to 4.64% for TOC. As at the previous site (see "Organic Geochemistry" section, Site 685 chapter), OC and TOC values are comparable, but the TOC values are consistently lower (Fig. 32). The largest amounts of OC occur in the near-surface sediments (upper 25 m); below this depth, a trend of decreasing OC continues to the bottom of the hole. We could not correlate the profile of OC with depth with any major lithologic boundaries; however, higher organic values are usually associated with laminated sediments; but lower values were measured on burrowed sediments.

Rock-Eval pyrolysis parameters are listed in Table 8 and depicted graphically in Figure 33. The organic matter in these samples is immature (T_{max} values of 402°C or less). The trends with depth of TOC and the hydrogen index (HI) are similar and are partially mirrored by the oxygen index (OI) values. Thus, samples with higher amounts of OC have a higher HI. We be-

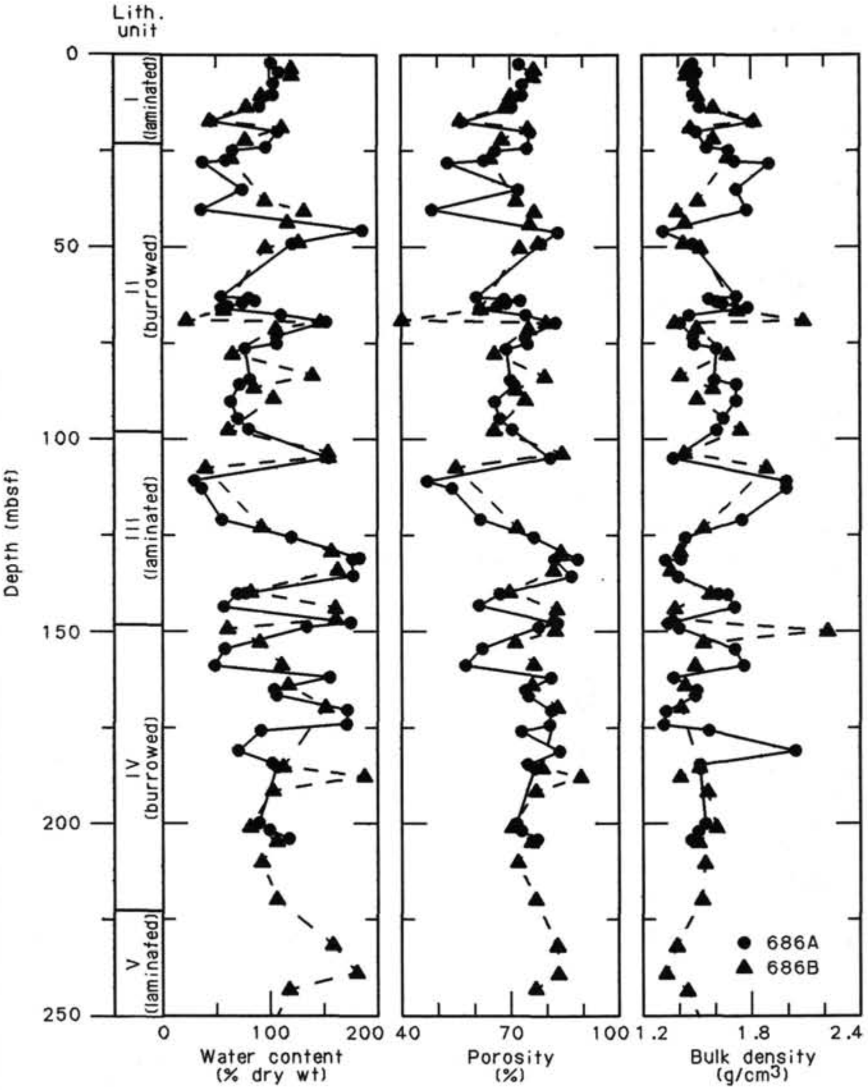

Figure 27. Physical properties for Unit I through the upper part of Unit V. Note cyclic variation in properties, interpreted as a reflection of oceanographic cycles (see discussion in "Lithostratigraphy" and "Physical Properties" sections, this chapter).

lieve these samples contain organic matter of mainly marine origin. On the other hand, samples containing lower amounts of OC have lower HIs and higher OIs. One interpretation is that these samples may contain a significant component of terrigenous organic matter, the expected result for sediments deposited on the upper continental slope and near the coast. On the other hand, the high OIs may reflect the immaturity of marine organic matter, which contains many oxygenated compounds. Figure 34 shows that the organic matter at Site 686 falls between a type II and type III classification (Tissot and Welte, 1984). Many of the OIs are higher than those encountered at previous shallow-water sites (e.g., see "Organic Geochemistry" section, Site 684 chapter, this volume).

INORGANIC GEOCHEMISTRY

Introduction and Operation

Two holes were cored in Quaternary sediments at Site 686 at a water depth of 446.8 m. Two *in-situ* water samples were obtained from Hole 686A, at 110.7 and 186.7 mbsf. All the interstitial-water samples from Hole 686B were squeezed from 5-cm-thick, whole-round sediment samples in Cores 112-686B-1H to 112-686B-12X and from 10-cm-thick samples in Cores 112-686B-18X to 112-686B-32X. The results from both holes are summarized in Table 9 and Figures 35 through 45.

Unlike the deeper-water Sites 682, 683, and 685, the *in-situ* water sampler, which was deployed in softer sediments, obtained pristine interstitial waters, with no admixed drill-hole water at this site (shown in Table 9).

The correlation coefficients of the alkalinity titration measurements were not as high as at all previous sites, and ranged from 0.91 to 0.98 instead of 0.99 to 1.00 at Site 686. This was caused by long time drifts of the combination electrode as a response of continuous exposure to unusually harsh geochemical conditions encountered in the two preceding sites (e.g., Site 685, with extreme alkalinity values of 156.4 mmol/L, and Site 684, the most saline site encountered during Leg 112). To alleviate the drift, the combination electrode was conditioned in standard seawater between each of the two extreme measurements and correlation coefficients of the alkalinity measurements again were 0.99 to 1.00.

At Site 686, systematic downhole increases in salinity, chloride, and calcium were observed (Figs. 35 and 42; Table 9). However, these gradients were significantly more moderate than at

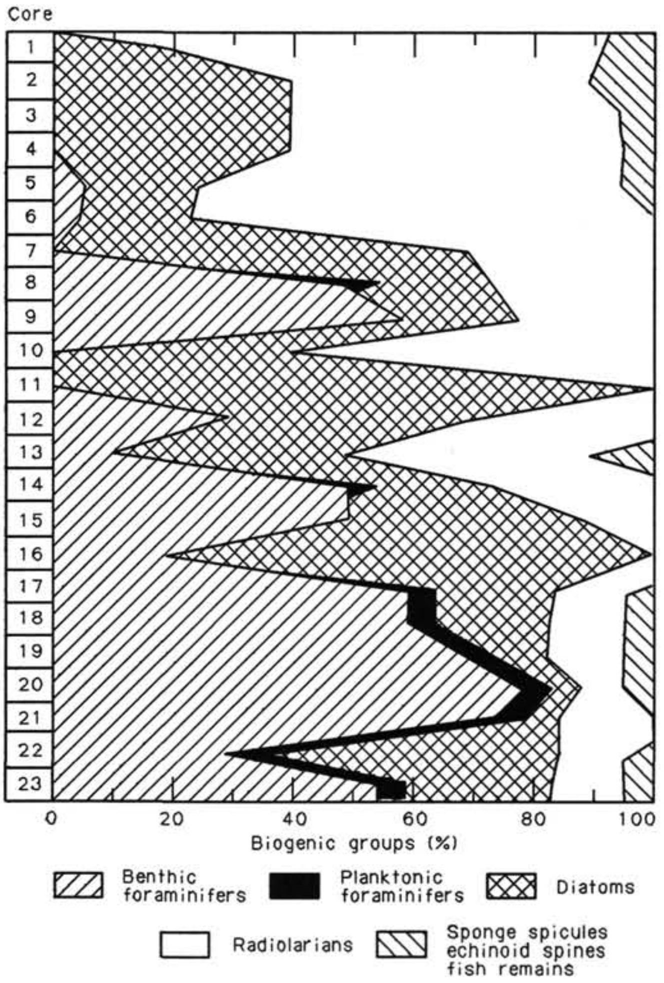

Figure 28. Biogenic groups in the coarse fraction of core-catcher samples from Hole 686A.

Table 5. Vacutainer gases at Site 686.

Core-section interval (cm)	Depth (mbsf)	C_1 (%)	C_2 (ppm)	C_3 (ppm)	C_1/C_2
112-686A-8H-2, 90	64.5	65.7	140	3.3	4600
9X-4, 80	70.0	84.6	170		4900
10X-2, 95	75.2	67.4	160		4300
11X-6, 15	89.9	85.1	180		4700
12X-3, 90	95.6	78.5	180	4.3	4300
13X-6, 45	109.2	82.1	190	3.4	4400
14X-2, 53	112.7	66.4	130		5300
15X-6, 25	128.0	82.8	190	5.0	4300
16X-7, 11	138.8	67.1	180	4.5	3700
17X-5, 50	145.7	90.0	190	3.9	4400
18X-5, 115	155.9	81.4	180		4500
19X-5, 80	165.4	82.6	190	5.4	4300
20X-5, 135	175.1	75.7	190	5.0	3900
21X-6, 15	184.9	83.7	200	5.7	4200
23X-5, 37	202.6	75.2	210	7.3	3600
112-686B-5H-2, 115	39.7	85.6	170	4.6	4900
6X-3, 91	50.4	79.5	140	3.2	5700
7X-1, 119	57.2	74.8	140	4.1	5500
8X-3, 124	69.7	72.0	170	2.2	4300
9X-4, 140	80.9	74.2	150		4900
10X-4, 69	89.7	54.5	130		4200
11X-7, 10	103.1	87.5	180	5.3	4800
12X-4, 55	108.6	72.2	140		5200
14X-6, 40	130.4	86.1	190	6.0	4600
15X-4, 135	137.9	78.0	190		4100
16X-6, 96	150.0	75.7	160	4.8	4900
17X-5, 124	158.2	77.1	180	5.2	4300
18X-4, 47	165.5	85.6	200	5.4	4300
20X-7, 56	188.5	66.2	200	8.6	3300
22X-5, 58	205.1	79.7	200	4.2	4100
23X-4, 15	212.7	70.0	160	4.6	4500
24X-3, 83	221.3	64.1	180	5.3	3500
25X-6, 101	235.5	63.0	220		2800
26X-5, 102	243.5	78.7	200	4.4	3900
28X-4, 115	261.2	76.8	190	5.0	4100
29X-3, 15	268.2	64.8	200		3300
30X-6, 100	283.0	68.4	200		3400
32X-2, 50	295.5	70.3	290	6.0	2500

Units of (%) and (ppm) are in volume of gas component per volume of gas mixture. All measurements were performed on the Hach-Carle Gas Chromatograph.

previous saline sites (680, 681, and 684), as well as at the nearby shallower Site 687. The chloride gradients at the five saline sites cored during Leg 112 are shown in Figure 36. However, sulfate and magnesium concentrations do not increase with depth at this site (Figs. 37 and 43). At these high sedimentation rates of approximately 160 m/m.y. (see "Biostratigraphy" section, this chapter), the deepest sample analyzed at 296.4 mbsf was still within the sulfate-depleted (0 mmol/L) and methanogenesis zones. Nearly constant magnesium concentrations from ~106 mbsf to the bottom of the hole implies that the dolomitization rate equals the Mg^{2+} diffusion rate from the subsurface brine. Indeed, in lithological Units III through VI between 104 and 303 mbsf, dolomite is a common phase.

The profiles of chloride and calcium concentrations as well as the salinity profile are primarily diffusion profiles between a subsurface brine and bottom seawater for Cl^-, and between the same brine and a diagenetic reactive zone at 20–40 mbsf for Ca^{2+} and salinity.

Chloride and Salinity

The chloride gradient at Site 686 is ~6 mmol/L/10 m, compared with 40 mmol/L/10 m at Site 684 (Figs. 35 and 36 and Table 9). At 296 mbsf, Cl^- concentration is only 129% of seawater Cl^-. Similarly, the salinity gradient is moderate at this site.

The observed distinct salinity minimum of 33.8 g/kg in Samples 112-686B-2H-3, 145–150 cm, and 112-686B-3H-3, 145–150 cm, between about 10 and 25 mbsf (Fig. 35) may result from either extensive diagenesis within this depth interval, as suggested by the Ca^{2+} and SO_4^{2-} minima, phosphate, and Mg^{2+}/Ca^{2+} maxima (Figs. 37 and 42, and 39 and 42, respectively), or (less likely) to dilution during the last interglacial, represented by the top of the lithostratigraphic Unit I. Diffusion calculations will be conducted later for the latter possibility.

Sulfate and Alkalinity

Not surprisingly in this high-sedimentation environment, sulfate reduction is already complete at about 15 mbsf and remains at zero concentrations throughout the hole. At the depth of minimum sulfate concentration, methane production increases rapidly (Figs. 30 and 36). At Sites 681 and 684, two other saline sites at ~11°S and ~9°S, respectively, where sedimentation rates are slower, the SO_4^{2-} reduction zone is almost 40 m thick. Because of carbonate diagenesis, the alkalinity maximum is reached deeper in the section than the sulfate minimum. Note that within the depth range of the burial zone cored at Site 686, sulfate does not seem to be replenished, as was the case at saline Sites 680 and 681.

Ammonia and Phosphate

Ammonia concentrations increase systematically and sharply from ~1.5 mmol/L at 4.5 mbsf to >45 mmol/L at 296 mbsf. These NH_4^+ values are 140% higher than the maximum value of 32.3 observed at Site 685, where the record high alkalinity value of 156.4 mmol/L was observed. We believe it reasonable to sug-

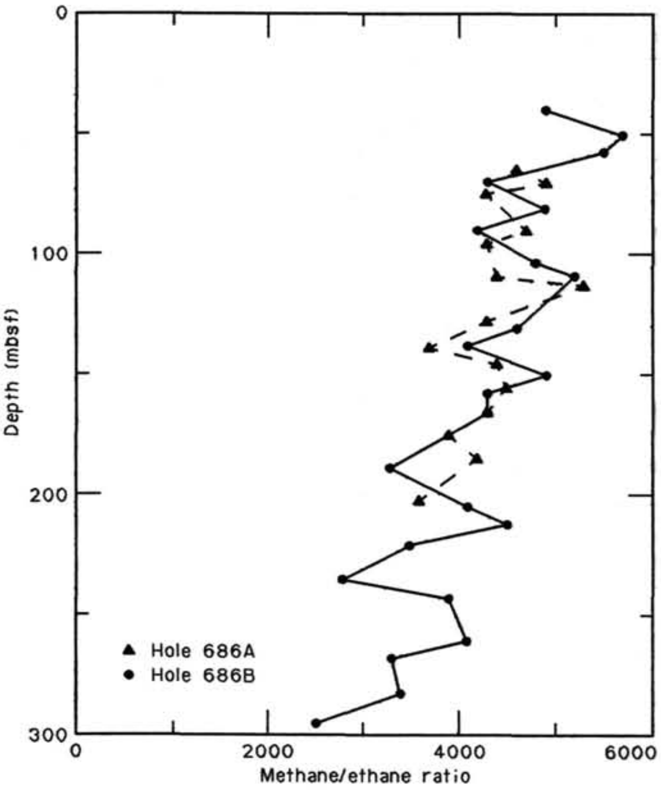

Figure 29. Methane/ethane ratios in gas collected by means of vacutainers from Holes 686A and 686B.

Table 6. Extracted gases at Site 686.

Core-section interval (cm)	Depth (mbsf)	C_1 (μL/L)	C_2 (μL/L)	C_1/C_2
Headspace Gases				
112-686A-2H-4, 149–150	11.1	770	17	45
4H-4, 0–1	28.6	200,000	52	3900
6X-5, 0–1	49.1	7,300	10	700
8H-2, 0–1	63.6	17,000	18	960
10X-3, 0–1	75.7	8,900	14	1400
12X-4, 0–1	96.2	15,000	14	1100
14X-2, 0–1	112.2	16,000	12	1300
16X-6, 0–1	137.2	16,000	27	600
18X-6, 0–1	156.2	23,000	14	1600
20X-5, 0–1	173.7	20,000	33	620
23X-5, 0–1	202.2	11,000	15	720
112-686B-1H-4, 0–1	4.5	110		
3H-4, 0–1	22.5	100,000	32	3300
5H-4, 0–1	41.5	140,000	37	3700
7X-1, 149–150	57.5	27,000	14	2000
9X-7, 0–1	84.0	33,000	32	1000
11X-7, 0–1	103.0	36,000	39	930
14X-3, 0–1	125.5	29,000	42	690
15X-5, 0–1	138.0	26,000	37	700
17X-5, 0–1	157.0	28,000	22	1300
20X-7, 0–1	188.5	26,000	22	1200
21X-2, 134–135	191.9	14,000	14	960
23X-3, 149–150	212.5	23,000	12	1900
25X-5, 149–150	234.5	29,000	32	910
28X-6, 0–1	263.0	26,000	15	1700
29X-3, 0–1	268.0	19,000	23	830
32X-2, 134–135	296.4	30,000	27	1100
Canned Gases				
112-686B-1H-3, 145–150	4.5	62	3.0	21
3H-3, 140–145	22.5	54,000	23	2300
6X-2, 140–145	49.5	38,000	14	2700
9X-6, 140–145	84.0	28,000	24	1200
15X-5, 135–140	139.4	16,000	13	1300
21X-2, 135–140	191.9	15,000	13	1200
28X-4, 145–150	261.5	9,200	6.9	1300
32X-2, 135–140	296.4	18,000	18	1000

Units are in microliters (μL) of gas component per liter (L) of wet sediment. All measurements were performed on the Hach-Carle Gas Chromatograph.

gest diffusion from depth, that is, from an ammonia source related to the subsurface brine.

This suggestion was supported by a most unusual phosphate profile (shown in Fig. 39). Although the anticipated pronounced phosphate maximum at shallow burial depth can be seen, deeper phosphate concentrations never decrease below 60 μmol/L; and between 106 to 296 mbsf, phosphate concentrations increase with depth. This zone corresponds to the depth interval of constant Mg^{2+} concentrations (Fig. 43). Unusually high NH_4^+ concentrations also were observed at the most saline site (Site 684) and discussed in the Site 684 chapter (this volume).

Silica

Silica concentrations ranged between 900 and 1165 μmol/L. A general trend of increasing concentration with depth was observed (Fig. 40 and Table 9).

pH

pH values are constant (7.8 to 8.0) to about 280 mbsf, where the pH increases steeply to a value of 8.4 at 296 mbsf (Fig. 41 and Table 9). We believe that the high NH_4^+ concentrations are responsible for the pH increase, as well as for some of the observed depth increases in SiO_2.

Calcium and Magnesium

As at the other three saline sites, concentrations of Ca^{2+} and Mg^{2+} decrease below those of seawater at 4.5 mbsf (Figs. 42 and 43 and Table 9). Ca^{2+} concentrations decrease dramatically to <50% seawater concentration in the first 22.5 m of Site 686. Below 22.5 mbsf, these concentrations increase with depth because of Ca^{2+} provided by diffusion from the subsurface brine and from dolomitization.

At this site, Mg^{2+} concentrations also decrease with depth in the uppermost 90 m; in the first 20 m, these Ca^{2+} decreases are steeper than the Mg^{2+} decreases, which raises the Mg^{2+}/Ca^{2+} ratio to 7.15 at ~13 mbsf. These observations indicate that calcite precipitates first, after which dolomite forms rapidly. The first dolomite was observed at 18 mbsf ("Lithostratigraphy" section, this chapter), just below the Mg^{2+}/Ca^{2+} maximum and at the depth where SO_4^{2-} reached a concentration of zero. The Mg^{2+} profile below 100 mbsf was discussed in the "Introduction" (this volume).

The Chemistry of the Subsurface Brine

On the basis of chemical analyses of four saline sites, we believe that the observed brine is a concentrated solution of Cl^- (and alkalies), SO_4^{2-}, Mg^{2+}, and, to some degree, Ca^{2+}. This brine apparently acquires ammonia and phosphate from the organic-rich sediments as it "ages" when passing from its source to the present site (Figs. 44 and 45). During that passage, dissolved SO_4^{2-} is lost from the brine concurrently with the injection of metabolites. The implications for diagenesis are considerable.

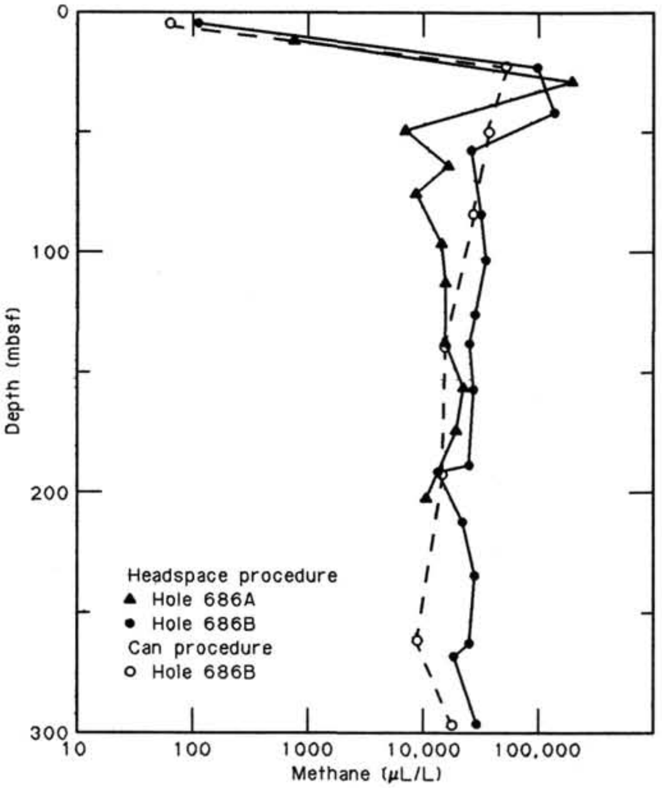

Figure 30. Comparison of extracted methane concentrations with depth at Holes 686A and 686B. Results from the headspace procedure are indicated by triangles (Hole 686A) and closed circles (Hole 686B). The open circles are the results from the can procedure applied to samples from Hole 686B.

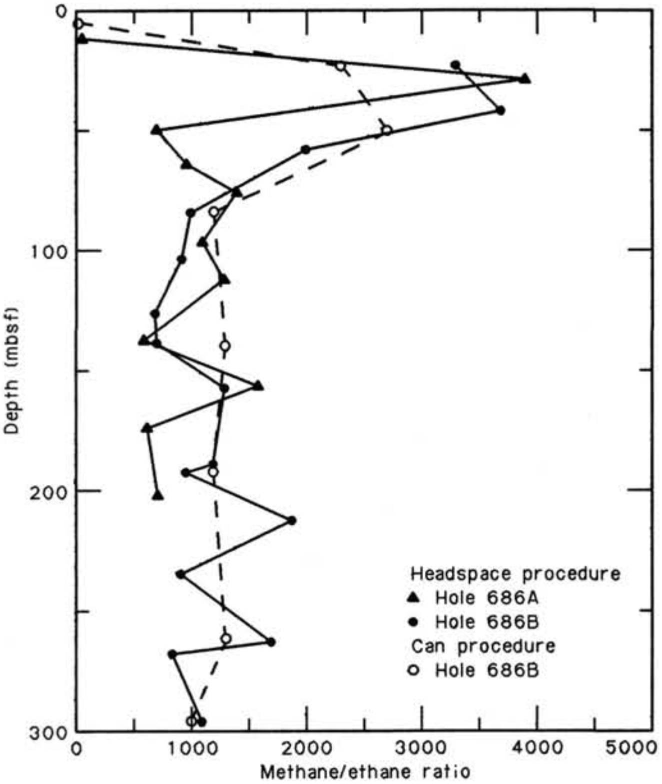

Figure 31. Methane/ethane ratios in gas extracted from sediments by the headspace procedure from Holes 686A and 686B. The open circles are the results from the can procedure applied to samples from Hole 686B.

Table 7. Organic carbon and carbonate carbon for Hole 686B.

Core-section interval (cm)	Depth (mbsf)	Total carbon (%)	Inorganic carbon (%)	Organic carbon (%)	TOC (%)
112-686B-1H-3, 145-150	4.5	5.02	0.05	4.97	4.64
2H-3, 145-150	13.0	4.16	0.18	3.98	3.58
3H-3, 145-150	22.5	1.10	0.12	0.98	0.73
5H-3, 145-150	41.5	3.46	0.03	3.43	2.93
6X-2, 145-150	49.5	2.64	0.37	2.27	1.91
9X-6, 145-150	82.7	2.96	0.22	2.74	2.41
12X-2, 145-150	106.5	1.39	0.29	1.10	0.85
15X-5, 140-150	139.4	2.48	0.80	1.68	1.49
18X-4, 140-150	165.7	3.31	0.49	2.82	2.51
21X-2, 140-150	191.9	2.34	0.92	1.42	1.38
24X-2, 140-150	220.4	2.55	0.39	2.16	1.80
28X-5, 140-150	262.9	1.33	0.81	0.52	0.48
30X-4, 140-150	280.4	2.89	0.36	2.53	2.03
32X-2, 140-150	296.4	1.58	0.57	1.01	0.87

TOC = total organic carbon from Rock-Eval pyrolysis.

PALEOMAGNETICS

Introduction

At Site 686, the upper six cores (0-49.2 mbsf) contained a strong and stable magnetization that was easy to measure with the shipboard spinner magnetometer. Vector plots from these six cores show that the magnetization exhibited a straight-line decay in the magnetic vector upon demagnetization. Below Core 112-686A-6H, the magnetization became complex, and samples gave evidence of remagnetization by a high coercivity phase, which we were unable to unblock by alternating-field demagnetization. Because of this high coercivity remagnetization, alternating-field demagnetization was not effective in isolating primary from secondary magnetizations below Core 112-686A-6H. Although preliminary study was conducted on samples from below Core 112-686A-6H (results are shown in Fig. 46), we believe our results are unreliable. Until we can demagnetize these samples later using the thermal method, our results should not be used for magnetostratigraphic correlations.

Results

Figure 46 shows the declination, inclination, and intensity values vs. depth for the samples measured. The value reported in the plots is the 150-Oe demagnetization value, which was selected on the basis of the vector plots and low circular standard deviations. The magnetization of the first six cores indicated that all were of normal polarity acquired during the Brunhes Chron. Although Core 112-686A-11X appears to show a reversed magnetization, the magnetic carrier of this signal appears to be a high coercivity phase that cannot be demagnetized by the alternating-field method. Figure 47 depicts a vector plot of a sample collected from Section 112-686A-11X-5. This plot shows that after removing the low coercivity magnetization, we found a high coercivity phase that does not indicate any decay with magnetic fields of up to 400 Oe.

PHYSICAL PROPERTIES

A detailed suite of measurements was performed at Site 686 in an attempt to better define the cyclic nature of physical-property parameters, as indicated by data from other sites. Samples were taken from split cores, generally at an interval of one every two sections (3 m) in the first hole. Gaps in data were filled in

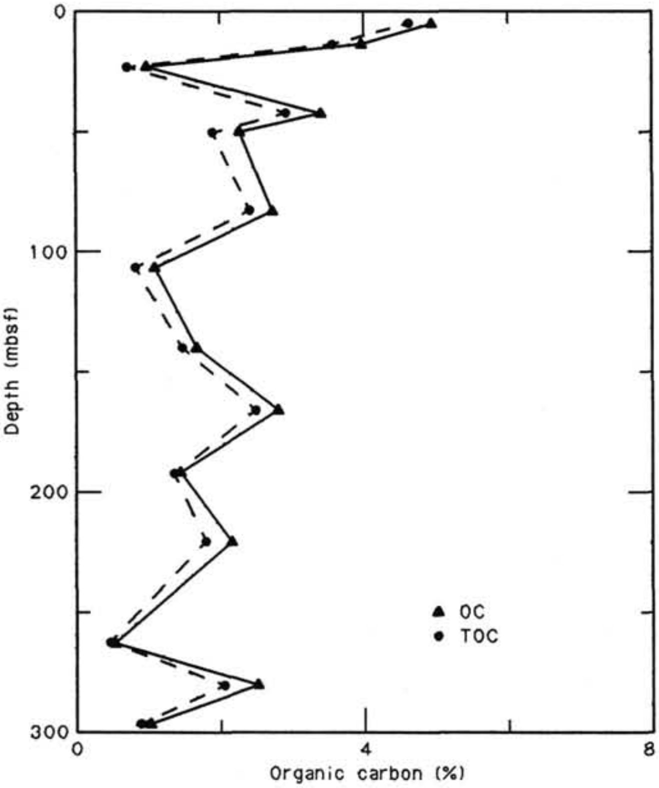

Figure 32. Comparison of organic carbon with total organic carbon from Rock-Eval pyrolysis at Site 686.

by more extensive sampling in Hole 686B. We were careful to retrieve samples in the major lithologic cycles, which were separated by turbidite sand layers.

Good recovery in the cores allowed a high sampling density. Data from both holes correlate well with each other (within the limits of the slightly different lithologies) and clearly exhibit cyclic behavior.

Index Properties

The index properties measured at Site 686 include water content (presented as a percentage of dry sample weight), porosity, bulk density, and grain density (Table 10). The methods specified in the "Explanatory Notes" (this volume) were used to measure these index properties at Site 686. The measured salinity of the pore water (see "Inorganic Geochemistry" section, this chapter) at each sample depth was used to calculate index properties. Figure 48 illustrates the downhole trends in water content and porosity with depth and the lithology for this site.

Core sections from both holes were run through the GRAPE, depending on time allowed by our hectic coring schedule. Figure 49 gives the bulk-density data obtained from samples of split cores superimposed on GRAPE profiles. In general, correlation is excellent between the GRAPE data and the bulk-density values obtained from index-property samples.

The index properties at this site do not show a uniform downhole trend but instead are dominated by a cyclic profile. The profiles appear to show less cyclicity in lithologic Units V and VI, but this may relate to fewer data collected in these units.

As established at several previous sites, diatomaceous sediments are characterized by very high water contents and porosities and correspondingly low bulk densities. Water-content values higher than 180% were measured at Site 686 and correspond to intervals of highly diatomaceous mud (e.g., 186% in Sample 112-686A-6H-4, 61 cm, or at 46 mbsf). These muds are also commonly laminated and were probably deposited in a low-oxygen environment ("Lithostratigraphy" section, this chapter). However, at Site 686 highly diatomaceous sediments may also be bioturbated and/or interbedded with more terrigenous intervals. Where the diatom content remains high and the degree of bioturbation is only moderate, water contents also remain high (e.g., 176% in Sample 112-686A-17X-6, 107 cm, i.e., at 148 mbsf). In contrast, sediments that contain a high proportion of terrigenous silt and low diatom content have low water contents (e.g., 39% in Sample 112-686A-5H-5, 52 cm, i.e., at 40 mbsf). Apparently, a range of mixed lithologies gives intermediate water-content values.

Porosity profiles indicate behavior similar to that of the water-content profiles. Porosities of almost 90% were measured and correspond to intervals of highly diatomaceous sediment (e.g., 89% in Sample 112-686A-15X-8, 62 cm, or at 131 mbsf). Sediments that contain a high proportion of terrigenous silt and low diatom content have much lower porosities (as low as 40%).

Similar cyclic variation can be seen in bulk density profiles (Fig. 49). Detailed analysis of GRAPE data indicate that cyclicity can be detected on a smaller scale within each core. Figure 50 shows the GRAPE bulk density for Core 112-686A-4H. Four distinct intervals are present in the undisturbed part of this core. Lithologic Unit II consists of very silty mud and shows prominent bioturbation. This unit also has a relatively high average bulk density (slightly less than 1.8 g/cm^3). Several graded silt/sand beds within this sequence give even higher values. By contrast, Unit III consists of highly diatomaceous, laminated mud with low bulk densities that average less than 1.6 g/cm^3. Unit I consists of silty diatomaceous mud that is partly bioturbated and is characterized by an intermediate bulk density on the order of 1.75 g/cm^3.

Compressional-Wave Velocities

The *P*-Wave Logger, which is run in conjunction with the GRAPE, was used to measure velocities through the sediments in the APC cores before they were split. However, few data were obtained. The cores were very gassy, which led to poor data. Reliable velocity profiles were obtained only for the first few cores. We tried to obtain samples for measuring with the Hamilton Frame. However, the sediments were too soft to provide samples that would give reasonable velocity values.

Figure 51 shows velocity profiles for Sections 112-686A-2H-3 and 112-686A-3H-5. These profiles reflect the variations in index properties of these sediments. The mean velocity was 1530 m/s, with a low of 1525 m/s and high spikes of up to 1590 m/s. These values are generally low because of the high porosities and water contents of the sediments.

Vane Shear Strength

Undrained vane shear strengths for Site 686 were measured using the Wykham Farrance vane apparatus in split cores of Holes 686A and 686B. Values obtained for peak undrained vane shear strength are presented in Table 11 and are shown vs. depth below seafloor in Figure 52. In general, the highly variable shear strengths reflect the cyclicity of the index properties. These shear-strength values are scattered in the zones of highly diatomaceous muds, and coarser sediments may be the result of some degree of draining during the test.

Total overburden stresses were calculated for Site 686 using bulk-density measurements and assuming hydrostatic pore-pressure conditions. The profiles for total stress and the assumed hydrostatic conditions for the combined data from both holes are shown vs. depth below seafloor in Figure 53. The cyclicity of the bulk densities is reflected in the cyclicity about the polynomial approximation curve of total stresses. The ratio of peak undrained shear strength to effective overburden pressure (C_u/

Table 8. Summary of Rock-Eval pyrolysis data for Site 686.

Core-section interval (cm)	Depth (mbsf)	Weight (mg)	T_{max}	S_1	S_2	S_3	PI	S_2/S_3	PC	TOC	HI	OI
112-686B-1H-3, 145–150	4.45	96.7	401	2.55	18.74	3.24	0.12	5.78	1.77	4.64	403	69
2H-3, 145–150	12.95	93.5	394	2.34	14.66	2.90	0.14	5.05	1.41	3.58	409	81
3H-3, 145–150	22.45	101.0	395	0.38	1.86	0.96	0.17	1.93	0.18	0.73	254	131
5H, 145–150	41.45	97.9	397	1.88	12.24	2.12	0.13	5.77	1.17	2.93	417	72
6X, 145–150	49.45	100.7	389	1.41	6.79	1.83	0.17	3.71	0.68	1.91	355	95
9X, 145–150	82.73	97.9	400	1.45	8.51	2.20	0.15	3.86	0.83	2.41	353	91
12X, 145–150	106.45	102.1	396	0.47	1.86	1.45	0.20	1.28	0.19	0.85	218	170
15X, 140–150	139.40	101.5	402	0.66	3.91	1.84	0.14	2.12	0.38	1.49	262	123
18X, 140–150	165.71	100.8	401	1.35	8.74	2.22	0.13	3.93	0.84	2.51	348	88
21X, 140–150	191.90	100.4	396	0.66	3.23	1.92	0.17	1.68	0.32	1.38	234	139
24X, 140–150	220.40	96.5	396	1.12	6.32	1.92	0.15	3.29	0.62	1.80	351	106
28X, 140–150	262.90	99.1	392	0.17	0.71	0.89	0.19	0.79	0.07	0.48	147	185
30X, 140–150	280.40	88.4	395	1.54	7.70	2.17	0.17	3.54	0.77	2.03	379	106
32X-2, 140–150	296.40	100.0	393	0.38	1.77	1.22	0.18	1.45	0.17	0.87	203	140

Note: Rock-Eval parameters are defined in "Organic Geochemistry" section, Site 679 chapter.

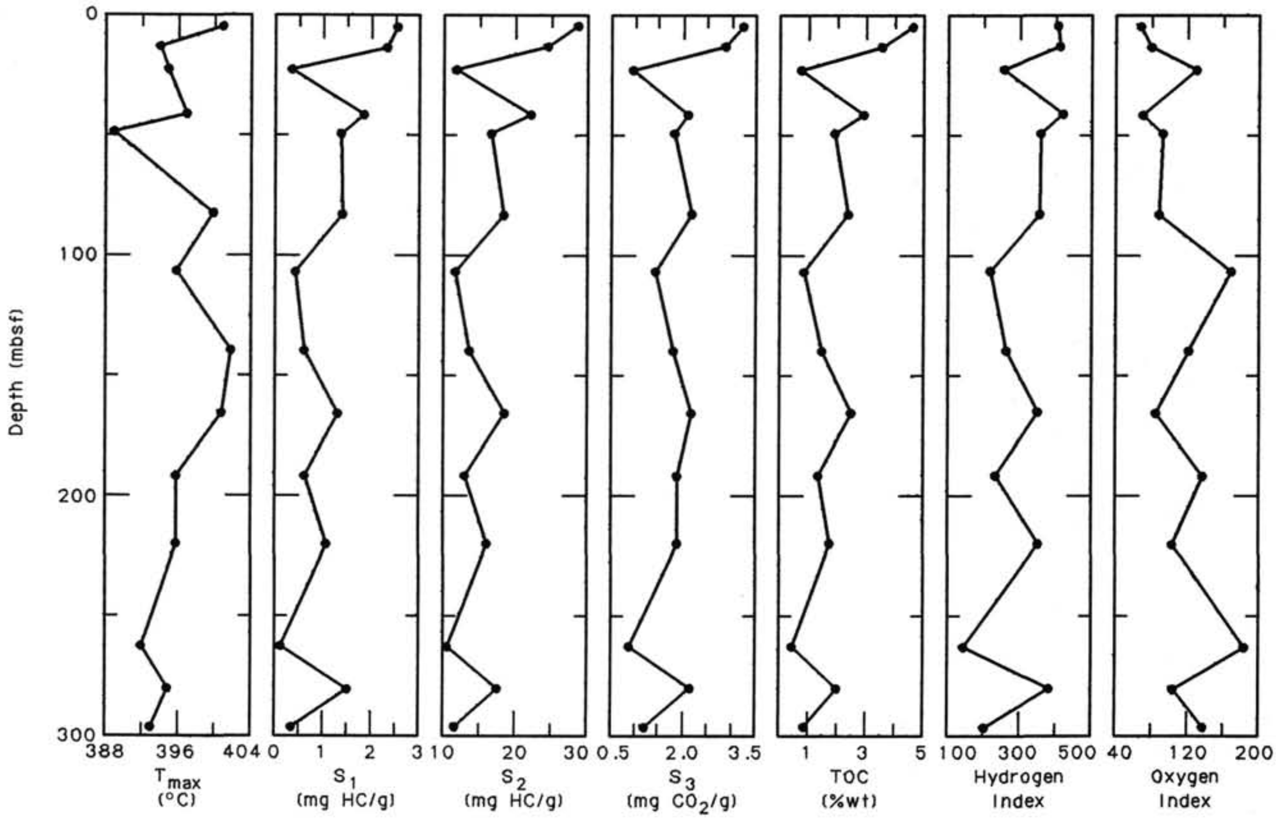

Figure 33. Comparison of Rock-Eval parameters T_{max}, S_1, S_2, S_3, TOC, HI, and OI in sediments from Hole 686B.

P') is plotted vs. depth below seafloor for Holes 686A and 686B (Fig. 54). The C_u/P' profile deviates from the theoretical curve, again because of variations in bulk density. However, the spikes in the profile indicate that, in some cases, a high shear strength corresponds to a low bulk density (and higher water content), the opposite of the usual situation.

Thermal Conductivity

Thermal conductivity was measured in Hole 686B samples by the needle-probe method. Conductivities were measured before splitting the cores. Although the samples were examined carefully through the core liners to avoid gas cracks and disturbed zones, some data were discarded as the measurements were apparently disturbed. Results are shown in Table 12 and Figure 55.

Several extremely high thermal-conductivity values can be seen. These obviously correlate with the presence of sandy beds. All values higher than 1.1 W/m·K were obtained in sand or very sandy layers; the average thermal conductivity of these layers is 1.22 W/m·K. Thermal conductivity (including the high values) correlates well with the index properties (Figs. 48 and 49) and shows cyclicity between the seafloor and 70 mbsf. Below 70 mbsf, the relation between thermal conductivity and water contents is less clear. Possibly, some of the low values resulted from the poor thermal contact among grains owing to gas expansion or drilling disturbance.

Summary and Discussion

Pronounced variations among index properties can be clearly seen at Site 686. These variations can be correlated between

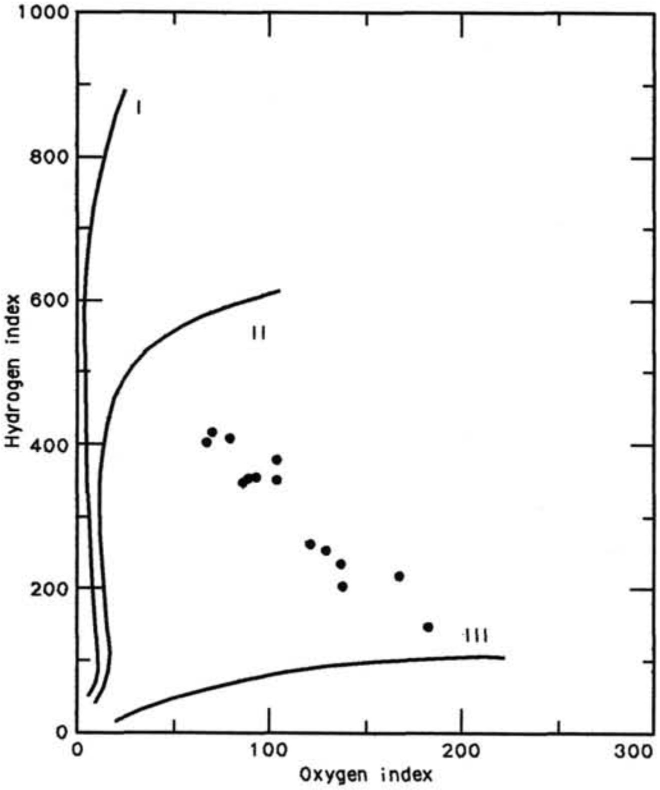

Figure 34. Hydrogen and oxygen indices (HI and OI) obtained from Rock-Eval pyrolysis of sediments from Hole 686B and plotted on a van Krevelen-type diagram (Tissot and Welte, 1984).

Holes 686A and 686B. A similar cyclicity was observed at Site 681; we believe this cyclicity was closely related to glacial/interglacial cycles. Further inspection of the cycles at Site 686 indicated that the index properties are controlled by lithologic variations and that a large contrast in properties occurs between different facies. Further study will be required to quantify the different parameters, such as grain size, diatom content, bioturbation, and diagenesis, and their effects on the physical properties of these upwelling-related sediment sequences.

GEOPHYSICS

Structure and Seismic Records

In the area of the southern transect sites, between 12.5°S and 13.5°S, a block-faulted, well-developed basement high along the outer shelf forms the landward flank of two important slope basins—the Lima Basin and the West Pisco Basin (Thornburg and Kulm, 1981). This outer shelf high, known as the Lima Platform, apparently has a structural limb extending southward, which divides the northern end of the West Pisco Basin from the southern end of the Lima Basin. This margin-transverse structure is best defined near 13.2°S by sharp bathymetry and free-air gravity gradients (Thornburg and Kulm, 1981; Couch and Whitsett, 1981).

Farther north, the Lima Basin flank is located at the much greater depth of nearly 1000 m. The thickness of the Neogene–Quaternary sections is approximately 2 to 3 km, as projected by seismic and gravity modeling in both the Lima and West Pisco basins. Landward of the outer-shelf structural high, the East Pisco Basin shoals to the north against acoustic basement at the latitude of Site 686. Farther south, the emerging outer-shelf structural high forms the Coastal Cordillera, and the East Pisco Basin is exposed on land. These onshore exposures are of the famous Miocene–Pliocene Pisco Formation—a classic association of diatomites, cherts, phosphorites, and dolomites believed to have formed under coastal upwelling conditions.

Offshore, the West Pisco Basin is reduced to thin, discontinuous sediment accumulations along the shelf and upper slope. Thornburg and Kulm (1981) speculated that the convergence of the Nazca Ridge with the Peru Continental Margin may have caused the uplift and emergence of the Coast Range and East Pisco Basin and the sparse and patchy sediment distribution offshore. The passage of the Nazca Ridge as it migrates southward along the margin may have resulted in the accelerated subsidence of the Lima Basin during late Neogene and Quaternary time. The vertical motion may be reflected in the sediment record cored at Sites 686 and 687.

Site 686 was located on the heavily sedimented, landward flank of the West Pisco Basin. Site selection was based initially on the SCS Line YALOC 12-03-74, which was obtained during the Nazca Plate Project (Kulm et al., 1981). An interpreted section of this line is shown in Figure 56, and a part of the original single-channel record appears in Figure 57. This information was supplemented during approach to the site by a seismic record shot with our 80-in.^{3} water gun and by concurrent 3.5-kHz profiling from *JOIDES Resolution* (Fig. 58). The combined information shows a thick sediment package with strong multiple reflectors conformably following the landward flank of the West Pisco Basin. Two sequences can be distinguished: a lower one that thickens seaward and an upper one that thickens landward to form a downlapping interface between the two. At Site 686, this contact is located at approximately 150 mbsf and coincides with a marked lithologic change from laminated diatomaceous mud (Unit III) above to a burrowed diatomaceous mud with abundant bivalve shells and shelly layers below (Unit IV). Unit I

Table 9. Interstitial-water geochemical data from Site 686, Leg 112.

Sample	Depth (mbsf)	pH	Salinity (g/kg)	Cl^- (mmol/L)	Alkalinity (mmol/L)	SO_4^{2-} (mmol/L)	PO_4^{3-} (μmol/L)	NH_4^+ (mmol/L)	SiO_2 (μmol/L)	Ca^{2+} (mmol/L)	Mg^{2+} (mmol/L)	Mg^{2+}/Ca^{2+}
112-686B-1H, 145-150	4.45	7.9	35.1	542.78	10.60	19.11	66.01	1.39	904	9.09	48.61	5.35
2H-3, 145-150	12.95	8.0	33.8	548.53	25.84	1.79	76.71	6.67	985	5.67	40.52	7.15
3H-3, 145-150	22.45	8.0	33.8	554.23	27.12	0.0	81.57	7.36	1029	5.11	36.10	7.07
5H-3, 145-150	41.45	8.0	34.2	557.09	33.96	0.0	74.76	13.07	1040	5.50	33.28	6.05
6X-3, 145-150	49.45	7.9	34.6	569.49	38.06	0.0	83.52	15.84	1123	5.42	32.72	6.04
9X-3, 145-150	83.95	7.8	36.4	578.08	54.28	0.0	66.01	26.65	1046	5.85	30.69	5.25
12X-3, 145-150	106.45	8.0	37.5	588.57	56.71	0.0	63.09	31.60	1089	5.90	26.61	4.51
112-686A *In-situ* #1	110.70	—	37.8	604.79	59.09	0.0	88.38	32.13	1085	5.94	26.57	4.47
112-686B-15X-5, 140-150	139.45	7.8	38.7	600.97	61.30	0.0	64.06	37.67	1081	6.21	27.99	3.74
18X-4, 140-150	166.40	7.8	39.9	626.73	63.58	0.0	66.01	40.00	1081	7.49	27.68	3.61
112-686A *In-situ* #2	186.70	7.8	40.2	645.81	66.48	0.0	86.43	42.15	1091	8.68	24.87	2.87
112-686B-24X-2, 140-150	220.40	7.9	41.8	638.18	59.57	0.0	76.71	44.66	1240	8.07	26.93	3.34
28X-5, 140-150	262.90	7.9	42.3	686.83	54.89	0.0	73.79	43.90	1166	8.68	24.40	2.81
30X-4, 140-150	280.40	8.1	43.7	707.81	53.15	0.0	75.73	43.38	1112	9.63	27.22	2.83
32X-2, 140-150	296.40	8.4	43.9	718.31	49.66	0.0	73.79	45.13	1164	9.80	26.98	2.75

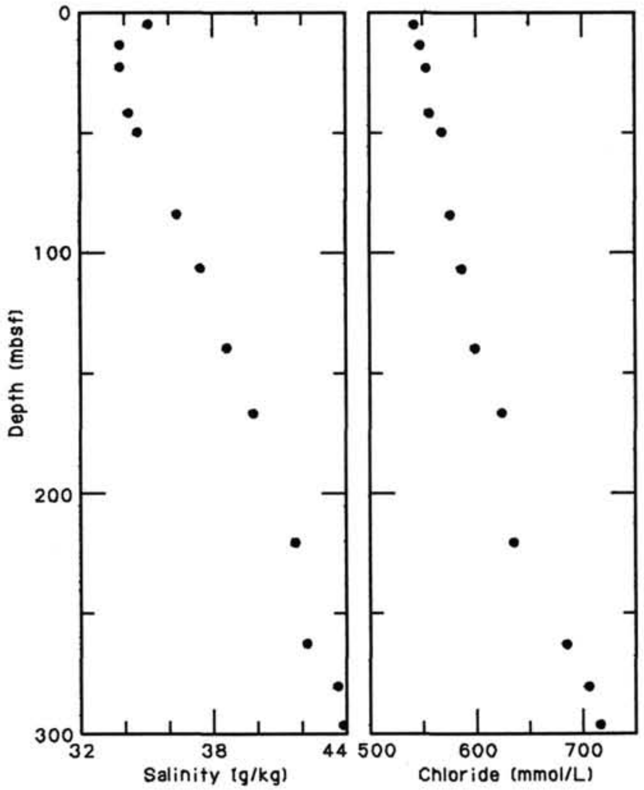

Figure 35. Profiles of salinity and chloride at Site 686.

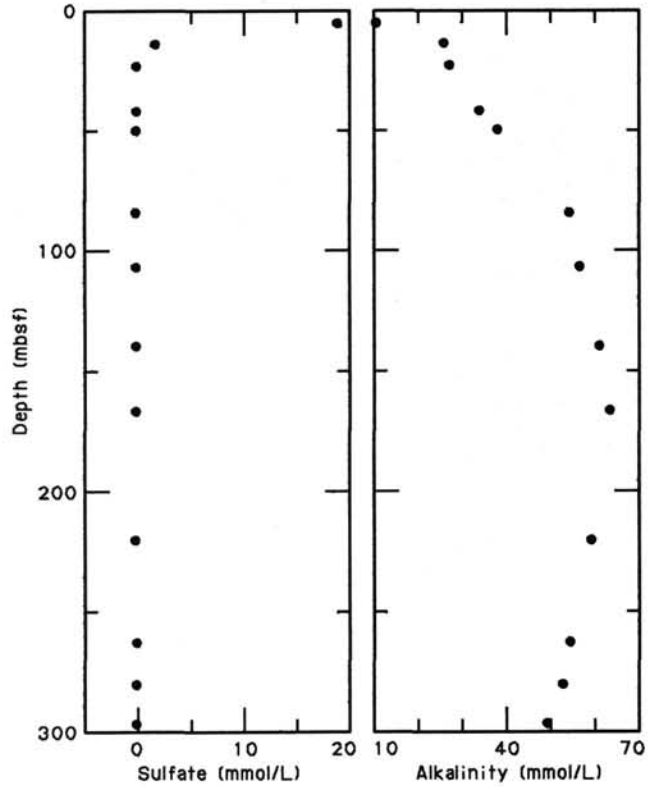

Figure 37. Profiles of sulfate and alkalinity at Site 686.

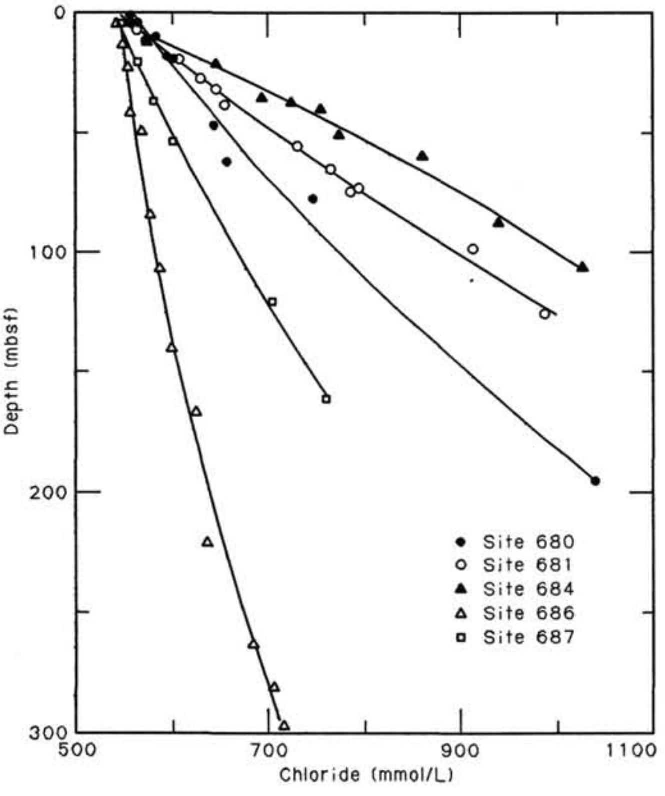

Figure 36. The chloride gradients for Sites 680, 681, 684, 686, and 687.

is a transgressive sequence with strong "upwelling" character that was deposited during a progressive increase in water depth, while Unit IV is interpreted as a reworked and diagenetically imprinted sequence laid down in shallower water. Seaward of Site 686, a subsurface fault, which also was observed during approach to the site, causes the overlying sequence to thicken and show downwarping above the fault zone. The same geometry was evident in the shallow subsurface topography at Site 686 (Fig. 58), which depicts a mud lens about 47 m thick that progrades seaward over older strata and terminates against the fault-induced flexure. The underlying strata dip at a lower angle than the slope, thus forming outcrops downslope. Several subbottom reflectors of the mud lens could be correlated to lithologic changes within the recovered section. Most were in Unit II, a burrowed diatomaceous mud with laminated interlayers and common interbeds of silt and sand.

Heat Flow

Temperature Measurements

Temperatures were measured in Hole 686A using the APC tool and the T-probe. The APC tool was deployed twice while retrieving Cores 112-686A-4H and 112-686A-6H. The first measurement gave an equilibrium temperature of 9.1°C ±0.3°C at 33.6 mbsf. On the second run (Fig. 59), the increased temperature resulting from frictional heating caused by penetration was very high, probably because the sediment was sandy and hard to penetrate. In addition, the temperature record shows two spikes and unexplained oscillatory variations having an 80-s period. The exact periodicity of the temperature variation suggests that the trouble is with the instrument. Similar temperature varia-

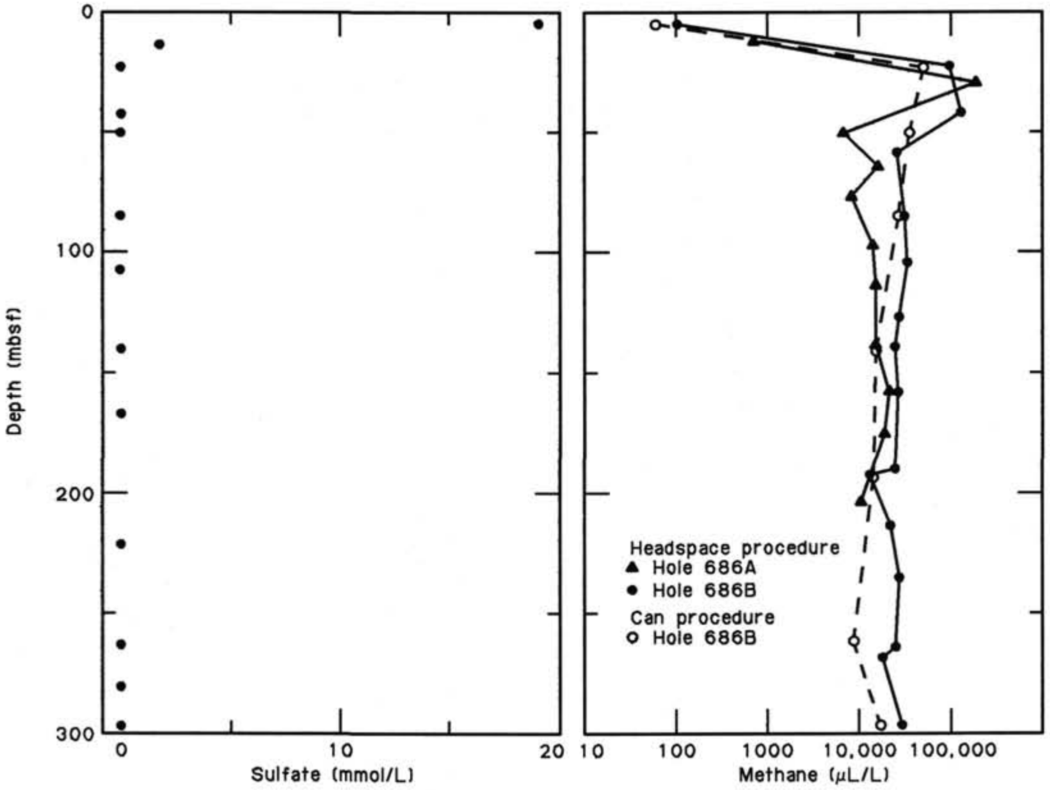

Figure 38. Profiles of sulfate and extracted methane at Site 686. (the extracted methane profile shows results from the headspace procedure for Holes 686A and 686B and from the can procedure at Hole 686B.

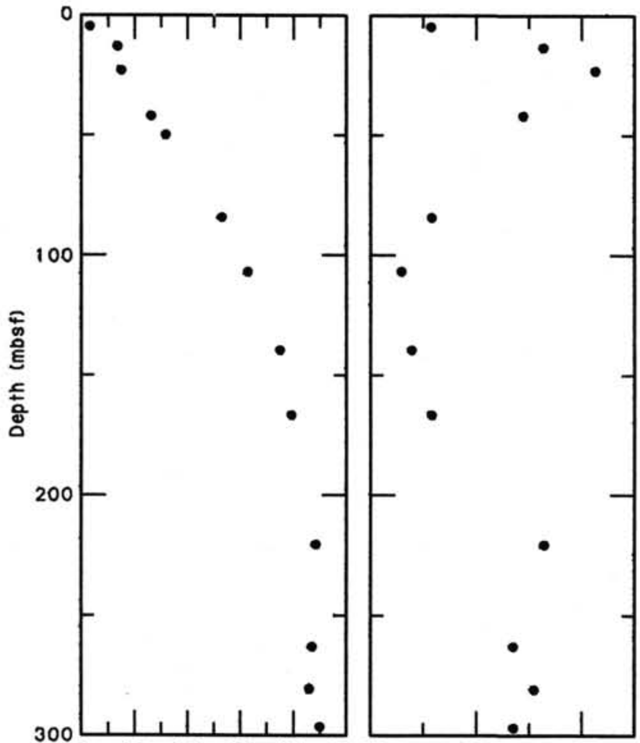

Figure 39. Interstitial ammonia and phosphate at Site 686.

tions also were observed in these measurements while retrieving Core 112-680C-3H; "Geophysics" section, Site 680 chapter). Fortunately, the instrument was in the sediment longer than usual, which allowed us to extrapolate the temperature record. We estimated that the equilibrium temperature was 11.0°C ±0.3°C at 52.6 mbsf.

The T-probe was in operation during pore-water sampling after Cores 112-686A-13X and 112-686A-21X (Fig. 60). In both cases, the APC tool and T-probe were run together for intertool calibration; the two instruments were kept in the water at the mud line for about 10 min after measuring the sediment temperature. The T-probe did not collect temperature data during the first measurement. On the second run, we obtained relatively good temperature data, although some anomalous values were recorded before penetration and after the temperature was measured at the mud line. Extrapolation of the temperature record in the sediment results in a final temperature of 17.2°C ± 0.1°C at 186.7 mbsf. However, after Site 687 we found that the connection between the temperature recorder and the sensor was unstable. This makes the reliability of the temperature data somewhat lower, and the error in the formation temperature may reach 0.5°C in the worst-case scenario.

Estimating Heat Flow

Three equilibrium temperature values are plotted vs. depth in Figure 60. We calculated the average geothermal gradient as 50 $\times 10^{-3}$ K/m, using the least-squares method (indicated by a solid line in Fig. 60). This gradient indicates that the average bottom-water temperature is 7.8°C. At Site 686, a bottom-water temperature of 8.04°C was measured with a current meter. The triangle shown in Figure 60 is the bottom-water temperature

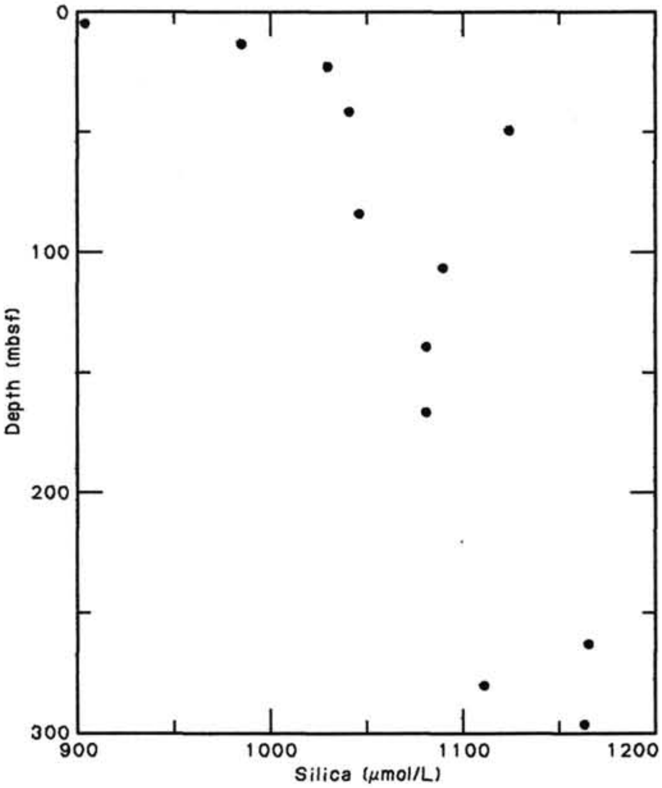

Figure 40. Interstitial silica at Site 686.

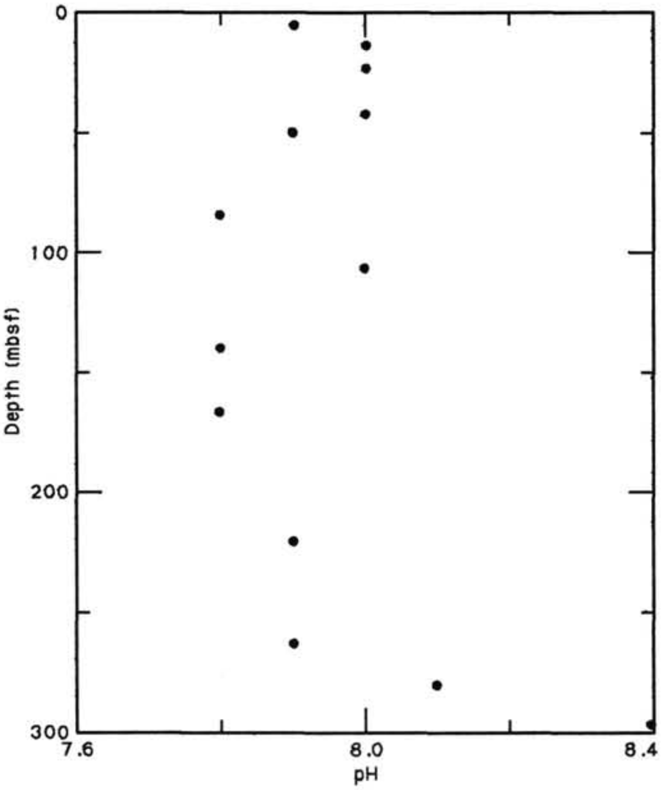

Figure 41. Interstitial pH at Site 686.

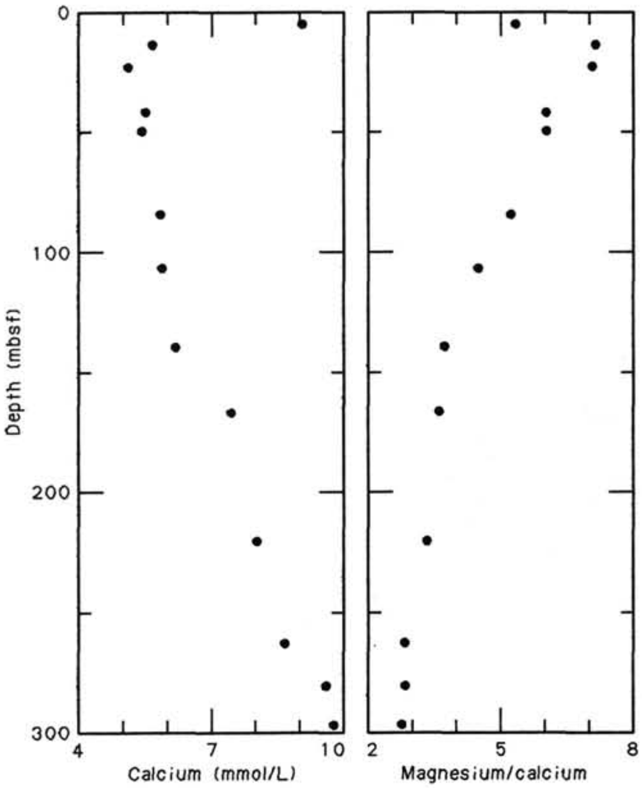

Figure 42. Interstitial calcium and Mg^{2+}/Ca^{2+} ratios at Site 686.

(8.24°C) measured with the current meter after correcting for the characteristic of the APC tool (see "Explanatory Notes," this volume). The water depth of 447 m at Site 686 is relatively shallow, thus the measured bottom-water temperature does not necessarily equal the average bottom-water temperature. The small difference in the two values, however, might suggest that the calculated temperature gradient is reliable.

Thermal-conductivity data obtained from Hole 686B samples were converted to thermal resistance after correcting to the *in-situ* temperature and pressure conditions. The temperature data are plotted vs. thermal resistance in Figure 61. The heat flow calculated by the least-squares fit was 40 mW/m^2 (represented by the solid line in Fig. 61). Below 70 mbsf, however, some of the thermal-conductivity values may be affected by gas expansion or drilling disturbance (see "Physical Properties" section, this chapter). If we assume that the higher values among the thermal-conductivity data measured below 70 mbsf (about 0.9 $W/m \cdot K$) are representative for this depth range, then heat flow becomes slightly higher, about 45 mW/m^2. Therefore, the heat flow at Site 686 was estimated as 45 ± 5 mW/m^2.

SUMMARY AND CONCLUSIONS

Site 686, at the southern end of the north-south paleoceanographic transect along the Peru outer shelf, was located in the West Pisco Basin at a water depth of 446.8 m. This site was selected (1) to obtain a high-resolution record of upwelling and climatic history from Quaternary and possibly Neogene sediments, (2) to calculate mass accumulation rates of biogenic constituents from an upwelling regime, and (3) to document in detail early diagenetic reactions and products specific to the coastal upwelling environment.

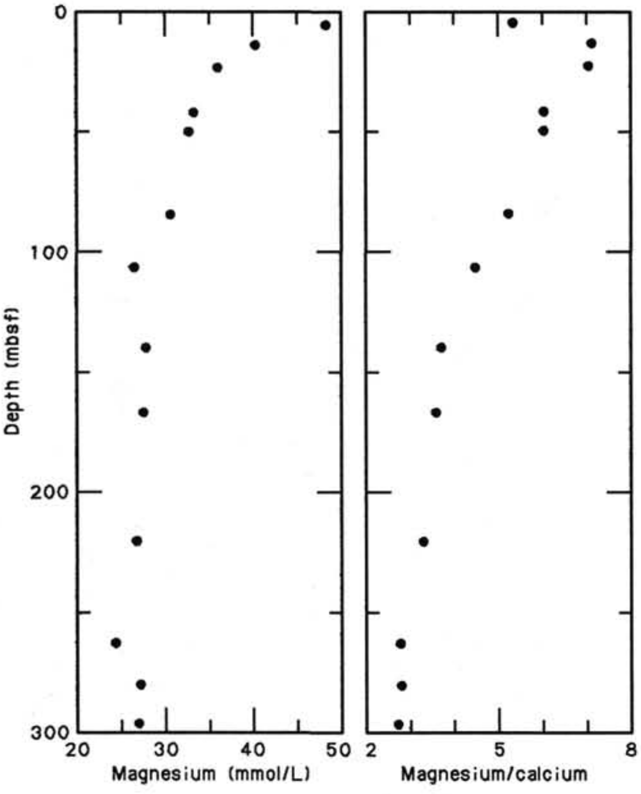

Figure 43. Interstitial magnesium and Mg^{2+}/Ca^{2+} ratios at Site 686.

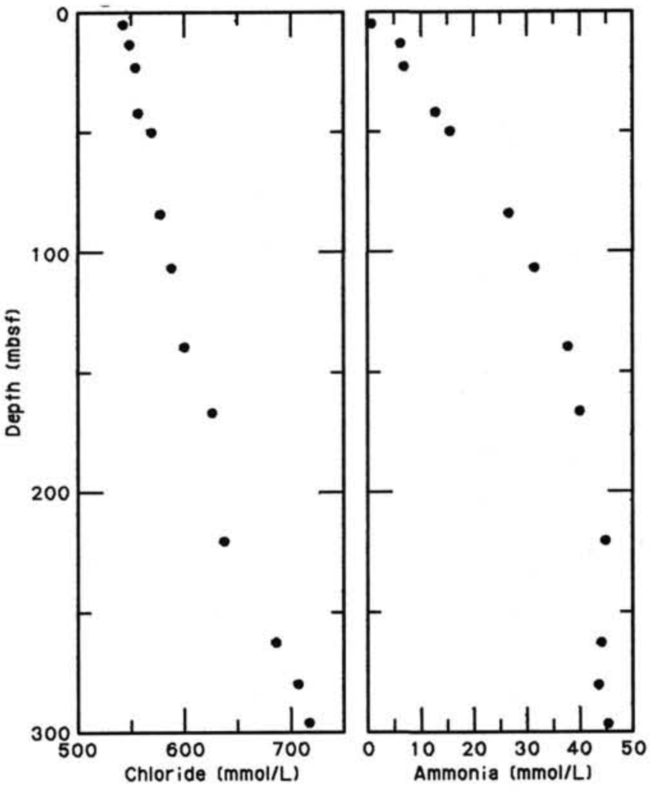

Figure 45. Interstitial chloride and ammonia at Site 686.

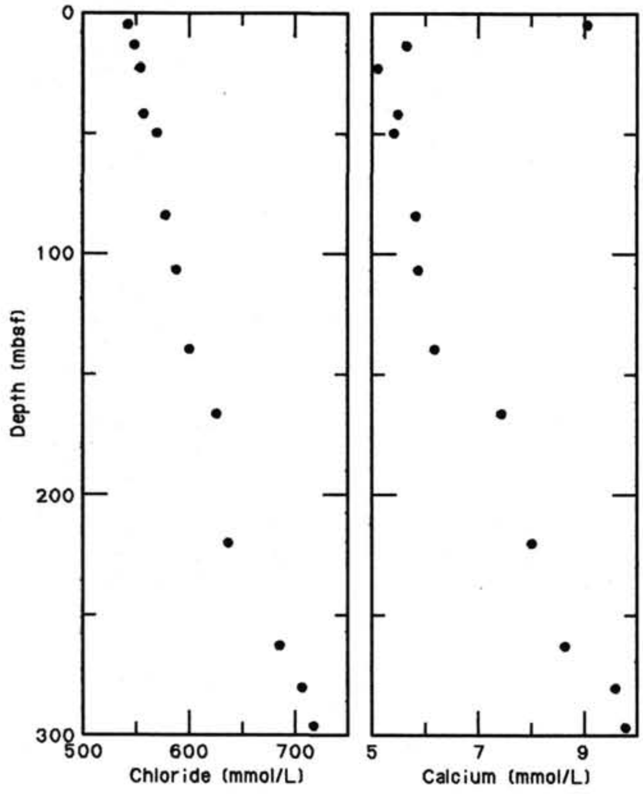

Figure 44. Interstitial chloride and calcium at Site 686.

Two holes were drilled at Site 686. Hole 686A was cored to a total depth of 205.7 mbsf using the APC mode to 64.7 mbsf, then followed by the XCB mode. Hole 686B was cored to 303.0 mbsf using the same combination of drilling modes. Core recovery overall was good (80%) in both holes; however, recovery in several sand layers was only moderate. Cores from both holes were readily correlated, based on lithostratigraphic and biostratigraphic markers as well as on physical properties. One marker was a distinct ash bed located at 154.6 m that consisted of a 2-cm-thick white part below a 10-cm-thick gray part. This marker was also found at Site 687 below the Brunhes/Matuyama boundary and above a fine sand unit believed to be about 0.9 m.y. old. This correlation enabled us to assign age easily (0.7–0.9 Ma) for Site 686, which otherwise contains few fossils.

The sediments at Site 686 consist of diatomaceous mud in three major cyclic alternations. Each cycle consists of laminated (Units I, III, and V) and bioturbated (Units II, IV, and VI) intervals. The bioturbated intervals commonly contain silty, sandy, and shelly beds. The laminated intervals are more phosphoritic and contain layers of friable phosphate. Dolomites are common in all units except for a zone in Unit I from 0 to 16 mbsf, which is a laminated diatomaceous mud with peloidal phosphorites. In turn, the major cyclic sequences contain numerous smaller cyclic alternations between bioturbated and laminated diatomaceous muds. These cycles can best be recognized in the physical index properties, i.e., water content, porosity, and bulk density. Obviously, this signal is caused by textural changes. The cyclicity may record fluctuations in sea level and the concurrent changes in the influx of fine sand and silt. The laminated units probably represent periods of high sea-level stands and an expanded oxygen-minimum zone. In these phases preservation of

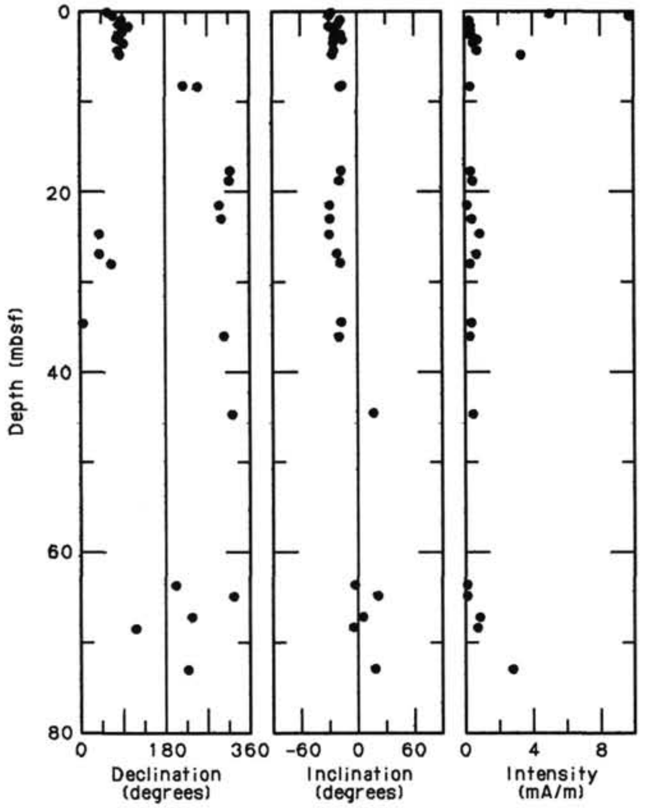

Figure 46. Declination, inclination, and magnetic intensity plots vs. depth below seafloor at Site 686. Although the diagram suggests that a reversal occurred at about 45 mbsf, we were unable to interpret this change as a magnetic reversal because of a complex magnetic overprinting with a high coercivity phase. Shipboard paleontological and stratigraphic studies (see "Lithostratigraphy" section, this chapter) suggest the deposition rate of Site 686 was 189 m/m.y. This independent evidence suggests that the Brunhes-Matuyama transition should occur much deeper in the section (120–140 mbsf). The intensity-vs.-depth plot does not appear to show the cyclicity noted in Sites 680 and 683.

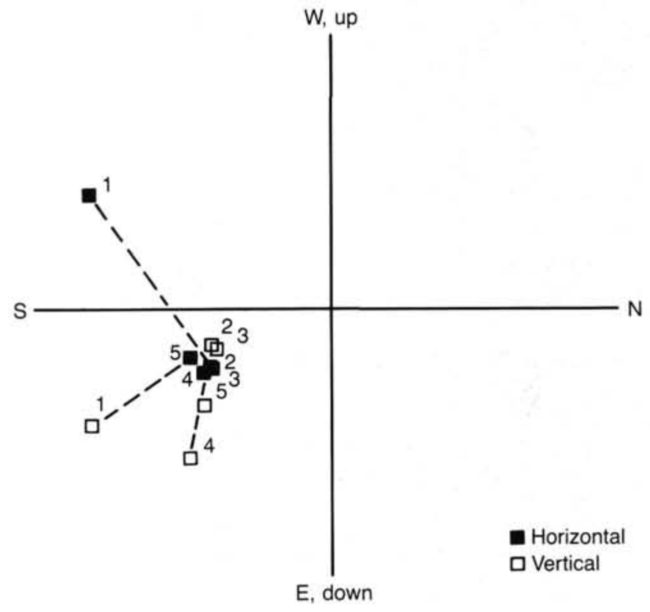

Figure 47. Vector plot of a sample collected from Core 112-686A-11H. This plot shows that the sample contains a high coercivity magnetic phase that cannot be removed by alternating-field demagnetization. On the basis of this type of demagnetization behavior, data from the lower cores of this site should be looked at cautiously until results from thermal demagnetization can be obtained.

organic matter derived from upwelling is enhanced by lack of bioturbation. The smaller cycles appear similar in duration, amplitude, and age to Pleistocene oxygen-isotope stages.

Diatoms were grouped into floras indicative of strong-, intermediate-, and low-intensity coastal upwelling having oceanic character. At least three prolonged phases of intense coastal upwelling appear to coincide with lithologic Units I, II, and III. Superimposed on these major and minor cycles is a clear trend of subsidence in the West Pisco Basin during the past 1.5 m.y. Benthic foraminifer assemblages record four successively deeper habitats from a shelf-edge (50–100 m) environment in early Pleistocene time to upper-middle bathyal depths (500–1500 m) at the present time.

Diagenetic products are common throughout the cores of Site 686. Single phosphate nodules are most abundant within the laminated units, but these can also occur as gravel layers within the bioturbated units. Lithified dolomite first appears at 18 mbsf, becomes progressively more abundant downhole, and is distributed with the same frequency in both laminated and bioturbated units. Authigenic calcite forms just below the sulfate-depletion zone where methanogenesis begins. In this zone, biogenic methane is accompanied by persistent and anomalously high ethane contents, the source of which remains unclear. Intense microbial production, perhaps favored by specific organic substrates at Site 686, is one mechanism; another is influx from a subsurface brine, the salinity effect of which becomes significant at the same depth as ethane increases.

Diagenetic reactions over the entire shelf and upper slope off Peru are influenced by this saline brine, which extends throughout the subsurface over an enormous area. The diagenetic sequence of calcite formation followed by dolomitization, ubiquitous along the Peru margin, can be seen again at Site 686 and is reflected in maxima and minima of dissolved Ca^{2+} and Mg^{2+} profiles. The subsurface brine, clearly seen in a chloride anomaly (132% of normal seawater) continually replenishes the interstitial water with Ca^{2+} and Mg^{2+} ions, which are depleted by carbonate mineral formation. At Site 686, the brine contains large quantities of dissolved ammonia (>45 mmol/L) and phosphate (>0.08 mmol/L), alkalinity (>63 mmol/L) is anomalously high, and sulfate (<0.1 mmol/L) is depleted. These are characteristics unlike those observed at previous brine-rich sites along the transect at 11°S. These concentrations reflect the history of the brine and its subsurface passage through organic-rich sediments that undergo mineralization by sulfate reduction and loading of the brine with dissolved metabolites.

The sediments from Site 686 contain all the components of a well-developed and variable coastal upwelling facies of Quaternary age. The sediment record is expanded in time, continuous, and reveals low-temperature diagenetic reactions typical of organic-rich environments, particularly precipitation of dolomite and phosphate. These diagenetic reactions are strongly influenced by dissolved ion fluxes from a saline subsurface brine.

REFERENCES

Claypool, G. E., and Kaplan, I. R., 1974. The origin and distribution of methane in marine sediments. *In* Kaplan, I. R. (Ed.), *Natural Gases in Marine Sediments*: New York (Plenum), 94–129.

Claypool, G. E., and Kvenvolden, K. A., 1983. Methane and other hydrocarbon gases in marine sediment. *Annu. Rev. Earth Planet. Sci. 1983*, 11:299–327.

Codispoti, L. A., 1983. On nutrient variability and sediments in upwelling regions. *In* Suess, E., and Thiede, J. (Eds), *Coastal Upwelling: Its Sediment Record*: New York (Plenum Press), 125–145.

Couch, R., and Whitsett, R. M., 1981. Structures of the Nazca Ridge and continental shelf and slope of southern Peru. *In* Kulm., L. D., Dymond, J., Dasch, E. J., and Hussong, D. M. (Eds.), *Nazca Plate: Crustal Formation and Andean Convergence.* Geol. Soc. Am. Mem., 154:569–586.

Dugdale, R. C., 1983. Effects of source nutrient concentrations and nutrient regeneration on production of organic matter in coastal upwelling centers. *In* Suess, E., and Thiede, J. (Eds), *Coastal Upwelling: Its Sediment Record*: New York (Plenum Press), 175–182.

Haq, B. U., Hardenbol, J., and Vail, P. R., 1987. Chronology of fluctuating sea levels since the Triassic (250 million years ago to present). *Science*, 235:1150–1167.

Ingle, J., 1980. Cenozoic paleobathymetry and depositional history of selected sequences within the Southern California continental borderland. *Cushman Foundation Spec. Publ.*, 19:163–195.

Jones, B. H., Brink, K. H., Dugdale, R. C., Stuart, D. W., van Leer, J. C., Blasco, D., and Kelly, J. C., 1983. Observations of a persistent upwelling center off Point Conception, California. *In* Suess, E., and Thiede, J. (Eds), *Coastal Upwelling: Its Sediment Record*: New York (Plenum Press), 37–60.

Kennett, J. P., 1973: Middle and late Cenozoic planktonic foraminiferal biostratigraphy in the southwest Pacific—DSDP Leg 21. *In* Burns, R. E., Andrews, J. E., et al., *Init. Repts. DSDP*, 21: Washington (U.S. Govt. Printing Office), 575–640.

Kulm, L. D., Dymond, J., Dasch, E. J., and Hussong, D. M. (Eds.), 1981. *Nazca Plate: Crustal Formation and Andean Convergence.* Geol. Soc. Am. Mem., 154.

Kvenvolden, K. A., and McDonald, T. J., 1986. Organic geochemistry aboard *JOIDES Resolution*-an assay. ODP Technical Note, 6:5.

Muizon, C. de, and Bellon, H., 1980. L'age Mio-Pliocène de la formation Pisco, Peru. *C. R. Acad. Sci.*, 290(D):1063–1066.

Packard, T. T., Garfield, P. C., and Codispoti, L. A., 1983. Oxygen consumption and denitrification below the Peruvian upwelling. *In* Suess, E., and Thiede, J. (Eds), *Coastal Upwelling: Its Sediment Record*: New York (Plenum Press), 147–173.

Poore, R. Z., 1979. Oligocene through Quaternary planktonic foraminiferal biostratigraphy of the North Atlantic: DSDP Leg 49. *In* Luyendyk, B. P., Cann, J. R., et al., *Init. Repts. DSDP*, 49: Washington (U.S. Govt. Printing Office), 447–517.

Thornburg, T. M., and Kulm, L. D., 1981. Sedimentary basins of the Peru continental margin: structure, stratigraphy and Cenozoic tectonics from 6°S to 16°S latitude. *In* Kulm, L. D., Dymond, J., Dasch, J. E., and Hussong, D. M. (Eds.), *Nazca Plate: Crustal Formation and Andean Convergence*. Geol. Soc. Am. Mem., 154:393–422.

Tissot, B. P., and Welte, D. H., 1984. *Petroleum Formation and Occurrence* (2nd Ed.): Berlin-Heidelberg (Springer-Verlag).

Ms 112A-117

Table 10. Summary of index-properties data from Site 686.

Core-section interval (cm)	Depth (mbsf)	Water content (% dry wt)	Porosity (%)	Bulk density (g/cm³)	Grain density (g/cm³)
112-686A-1H-2, 77	2.27	102.94	73.39	1.48	2.53
1H-4, 16	4.66	110.98	76.79	1.50	2.58
2H-2, 84	7.44	105.01	74.19	1.48	2.47
2H-4, 68	10.28	104.67	74.12	1.48	2.46
2H-6, 84	13.44	92.16	71.15	1.52	2.51
3H-2, 108	17.18	47.59	56.81	1.81	2.60
3H-4, 77	19.87	109.65	76.36	1.50	2.53
3H-7, 29	23.89	98.07	75.47	1.56	2.49
4H-1, 65	24.75	68.31	66.61	1.68	2.70
4H-3, 23	27.33	61.23	63.39	1.71	2.59
4H-3, 78	27.88	39.85	52.91	1.90	2.69
5H-1, 124	34.84	76.35	72.86	1.72	2.73
5H-5, 52	40.12	38.59	48.36	1.78	2.66
6H-4, 61	45.88	186.81	84.10	1.32	2.26
6H-6, 82	49.09	122.95	79.55	1.48	2.66
8H-1, 70	62.80	57.12	61.20	1.72	2.62
8H-1, 120	63.30	82.00	69.08	1.57	2.41
8H-2, 30	63.90	87.90	73.31	1.61	2.58
8H-2, 83	64.43	76.43	69.35	1.64	2.56
9X-1, 64	65.34	63.00	67.04	1.78	2.68
9X-1, 114	65.84	57.73	62.18	1.74	2.69
9X-2, 125	67.45	112.26	75.25	1.46	2.51
9X-4, 27	69.47	153.26	83.53	1.41	2.69
10X-1, 44	73.14	108.04	74.83	1.48	2.49
10X-2, 81	75.01	108.73	75.61	1.49	2.45
10X-3, 60	76.30	79.25	69.55	1.61	2.71
11X-2, 65	84.35	83.81	71.26	1.60	2.61
11X-3, 33	85.53	74.52	71.74	1.72	2.79
11X-6, 20	89.90	65.56	66.55	1.72	2.68
12X-2, 117	94.37	72.80	67.85	1.65	2.61
12X-4, 108	97.28	82.37	71.13	1.61	2.59
13X-3, 56	104.76	155.92	81.70	1.37	2.42
13X-7, 35	110.55	31.57	46.90	2.00	2.64
14X-2, 25	112.45	38.12	53.88	2.00	2.85
15X-1, 43	120.63	57.30	62.10	1.75	2.68
15X-4, 99	125.45	122.17	77.26	1.44	2.35
15X-8, 62	131.08	183.96	89.10	1.41	2.68
16X-2, 98	131.13	177.68	82.87	1.33	2.33
16X-5, 90	135.55	178.25	87.46	1.40	2.40
16X-9, 46	139.15	71.48	67.98	1.67	2.73
17X-1, 84	140.04	79.01	69.60	1.62	2.59
17X-3, 128	143.48	59.14	62.01	1.71	2.66
17X-6, 107	147.77	175.70	83.60	1.34	2.48
18X-1, 20	148.90	136.11	78.64	1.40	2.30
18X-4, 128	154.48	60.43	62.81	1.71	2.57
18X-7, 86	158.56	50.96	57.92	1.76	2.58
19X-3, 69	161.89	156.62	81.73	1.37	2.37
19X-5, 84	165.04	105.11	74.97	1.50	2.48
19X-6, 85	166.55	107.63	75.61	1.49	2.47
20X-2, 130	170.50	172.31	82.01	1.33	2.13
20X-5, 38	174.08	171.98	81.35	1.32	2.02
20X-6, 37	175.57	93.26	73.82	1.57	2.49
21X-3, 71	180.91	72.58	84.14	2.05	2.51
21X-5, 112	184.32	102.92	75.36	1.52	2.56
21X-6, 60	185.30	108.42	77.30	1.52	2.40
23X-3, 83	200.03	91.35	72.31	1.55	2.41
23X-4, 119	201.89	100.57	73.69	1.51	2.49
23X-6, 48	204.18	119.76	77.96	1.47	2.47
112-686B-1H-3, 60	3.60	122.18	77.68	1.45	2.44
1H-4, 81	5.31	122.27	77.08	1.44	2.46
2H-2, 55	10.55	94.63	71.16	1.50	2.44
2H-4, 57	13.57	80.51	69.26	1.59	2.49
2H-6, 89	16.89	46.42	56.40	1.82	2.60
3H-1, 89	18.89	112.70	75.83	1.47	2.39
3H-3, 86	21.86	79.31	68.54	1.59	2.59
3H-6, 119	26.69	66.72	65.37	1.67	2.63
5H-1, 84	37.84	97.43	72.56	1.51	2.52
5H-3, 70	40.70	133.94	77.83	1.39	2.24
5H-5, 83	43.83	119.22	76.50	1.44	2.30
6X-2, 89	48.89	129.84	79.04	1.43	2.45
6X-3, 59	50.09	97.73	73.49	1.52	2.49
8X-1, 62	66.12	59.07	62.35	1.72	2.58
8X-3, 37	68.87	24.13	39.66	2.09	2.63
8X-3, 99	69.49	148.50	80.77	1.38	2.39
8X-4, 97	70.97	107.53	75.84	1.50	2.40

Table 10 (continued).

Core-section interval (cm)	Depth (mbsf)	Water content (% dry wt)	Porosity (%)	Bulk density (g/cm³)	Grain density (g/cm³)
112-686B-9X-3, 91	77.69	68.04	66.20	1.67	2.64
9X-7, 43	83.21	141.56	80.48	1.41	2.39
10X-2, 39	86.39	86.94	72.13	1.59	2.60
10X-4, 41	89.41	105.27	74.91	1.50	2.38
11X-3, 109	97.42	63.51	66.15	1.74	2.76
11X-7, 108	103.41	155.34	84.98	1.43	2.60
12X-1, 123	104.73	156.09	82.33	1.38	2.43
12X-3, 58	107.08	42.59	54.98	1.89	2.70
14X-1, 26	122.76	93.53	72.57	1.54	2.51
14X-5, 62	129.12	158.82	84.61	1.41	2.46
15X-2, 48	133.98	164.85	82.82	1.36	2.34
15X-6, 36	139.86	84.25	70.43	1.58	2.53
16X-2, 88	143.88	162.32	83.33	1.38	2.17
16X-4, 65	146.65	163.09	82.69	1.37	2.30
16X-6, 41	149.41	61.90	83.09	2.23	6.63
17X-2, 36	152.86	91.70	71.92	1.54	2.37
17X-6, 20	158.70	112.87	77.26	1.49	2.43
18X-3, 107	163.88	119.19	76.64	1.44	2.34
18X-7, 81	169.62	152.61	83.41	1.41	2.42
20X-5, 77	185.19	114.00	79.27	1.52	2.55
20X-7, 33	187.75	188.10	90.01	1.41	2.52
21X-2, 101	191.51	104.17	77.80	1.56	2.49
22X-2, 97	200.97	82.95	71.08	1.61	2.44
22X-5, 25	204.75	107.39	76.47	1.51	2.49
23X-2, 60	210.10	92.93	72.65	1.55	2.28
24X-2, 68	219.68	107.98	77.64	1.53	2.35
25X-4, 28	231.78	159.26	83.51	1.39	2.20
26X-2, 98	238.98	181.37	83.77	1.33	2.17
26X-5, 78	243.28	119.26	77.21	1.45	2.21
28X-3, 132	259.82	89.27	74.17	1.61	2.45
28X-6, 90	263.90	55.97	61.55	1.76	2.48

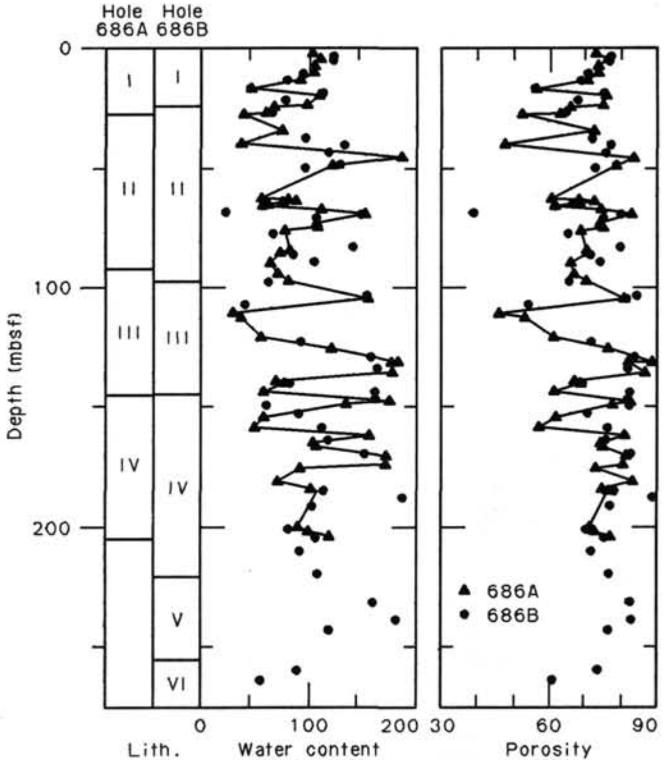

Figure 48. Water content and porosity profiles for Holes 686A and 686B at Site 686. Schematic of lithologic units also is shown.

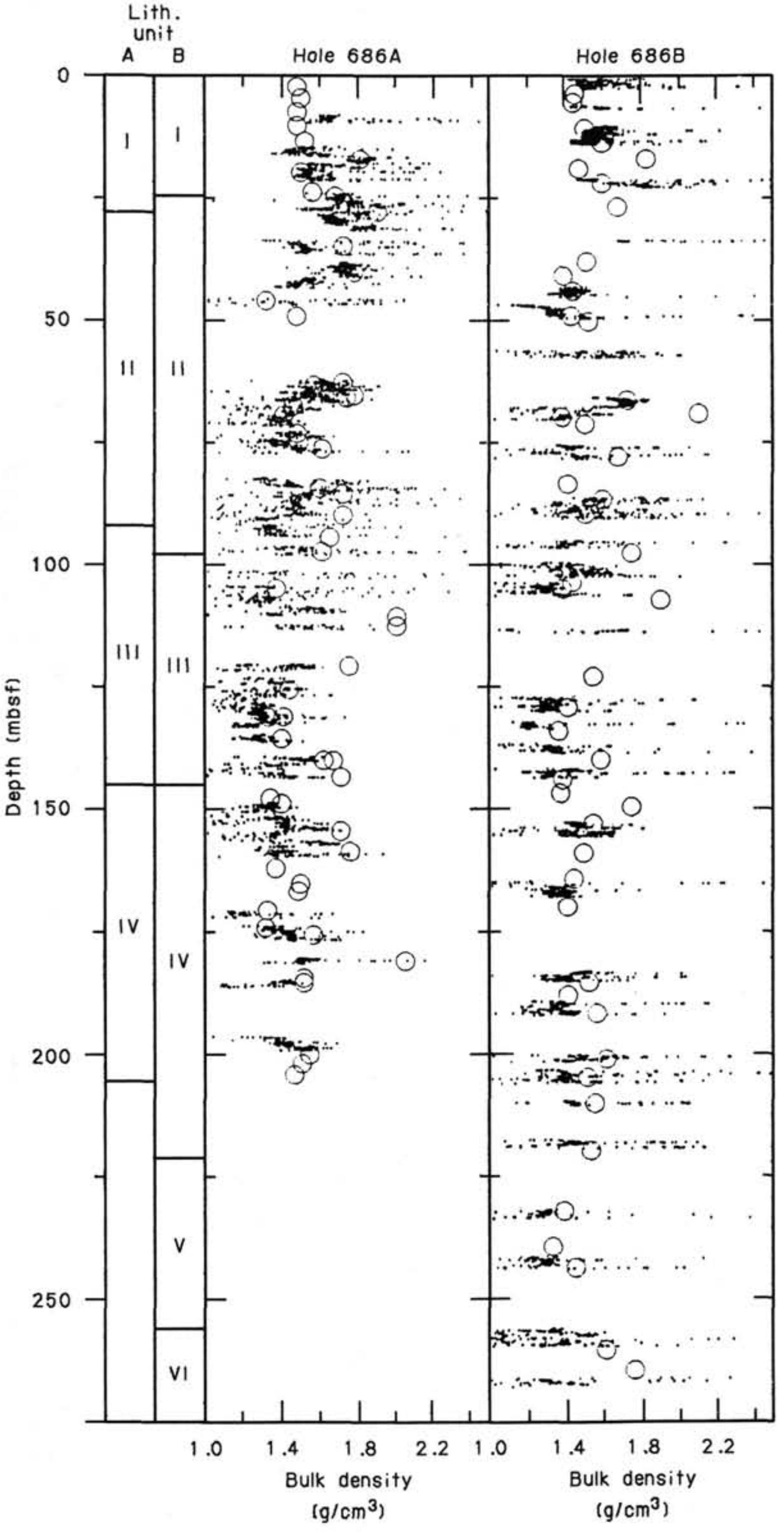

Figure 49. Sample bulk density superimposed on GRAPE bulk-density profiles for Holes 686A and 686B.

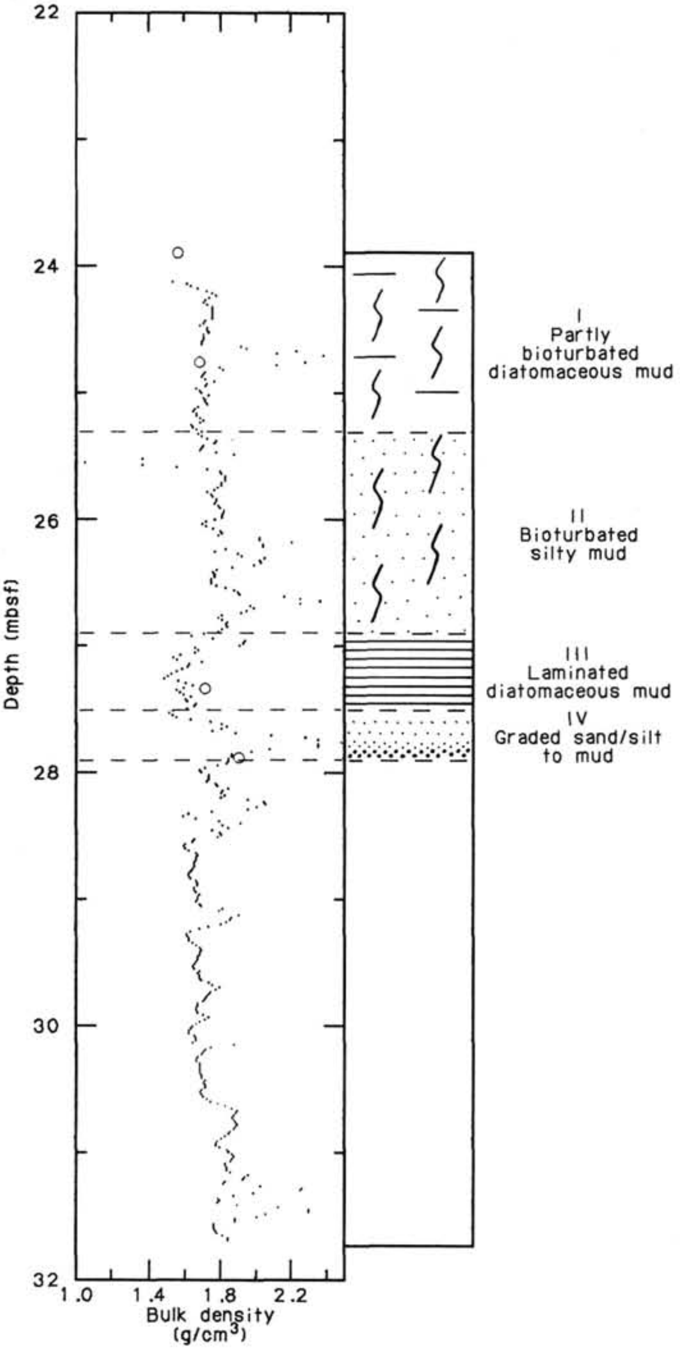

Figure 50. GRAPE bulk-density profile from Core 112-686A-4H, showing in detail the changes in profile that occur within one core from the varied lithology. Circles denote sample bulk densities, dots mark GRAPE measurements.

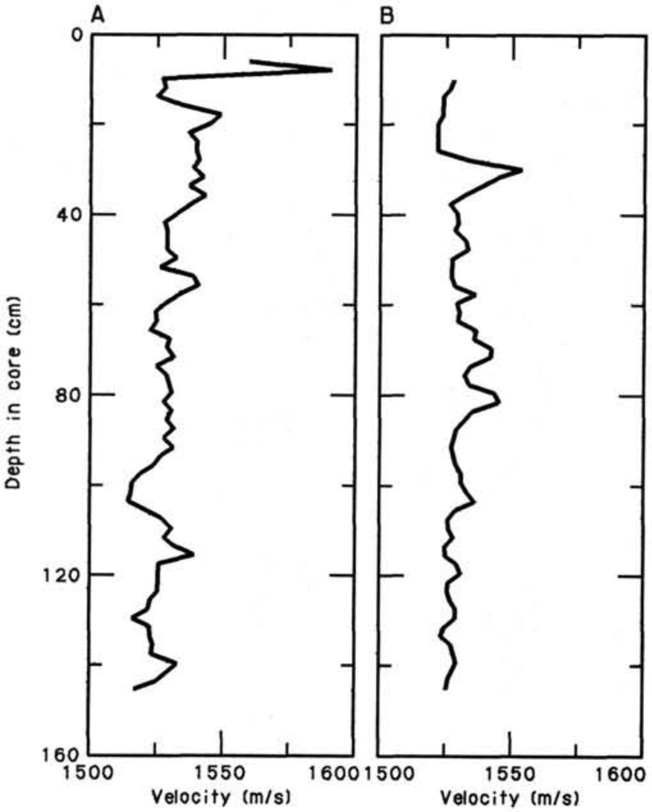

Figure 51. *P*-wave-velocity profiles for Sections 112-686A-2H-3 and 112-686A-3H-5.

Table 11. Summary of vane shear-strength data for Site 686.

Core-section interval (cm)	Depth (mbsf)	Peak (kPa)
112-686A-1H-2, 76	2.26	35.52
1H-4, 15	4.65	57.67
2H-2, 86	7.46	51.67
2H-4, 68	10.28	64.13
2H-6, 84	13.44	76.59
3H-2, 108	17.18	70.59
3H-4, 77	19.87	115.80
3H-7, 29	23.89	17.17
4H-1, 65	24.75	58.98
4H-3, 23	27.33	63.46
5H-1, 128	34.88	73.91
8H-1, 70	62.80	62.71
8H-1, 120	63.30	55.25
8H-2, 30	63.90	84.36
8H-2, 83	64.43	71.67
9X-2, 125	67.45	55.25
10X-1, 44	73.14	44.79
10X-3, 60	76.30	56.74
11X-2, 65	84.35	69.43
11X-3, 33	85.53	62.71
11X-6, 20	89.90	58.98
12X-4, 108	97.28	59.72
13X-3, 56	104.76	65.70
15X-4, 99	125.45	66.44
16X-2, 98	131.13	54.50
16X-6, 46	136.61	72.42
17X-1, 85	140.05	56.74
17X-3, 129	143.49	52.26
18X-4, 129	154.49	50.77
18X-7, 87	158.57	59.35
19X-5, 85	165.05	61.96
19X-6, 86	166.56	44.79
20X-5, 39	174.09	80.63
20X-6, 38	175.58	62.71
21X-3, 72	180.92	55.99
21X-5, 113	184.33	50.77
23X-4, 120	201.90	79.88
23X-6, 49	204.19	78.39
112-686B-1H-3, 61	3.61	45.21
1H-4, 82	5.32	52.13
2H-2, 56	10.56	59.05
2H-4, 57	13.57	77.51
2H-6, 90	16.90	60.90
3H-1, 89	18.89	94.07
3H-3, 87	21.87	89.59
3H-6, 119	26.69	62.71
5H-1, 85	37.85	61.96
5H-3, 71	40.71	114.22
5H-5, 84	43.84	132.89
6X-2, 89	48.89	64.95
6X-3, 60	50.10	77.64
8X-1, 63	66.13	65.70
8X-3, 99	69.49	67.94
8X-4, 98	70.98	47.03
9X-3, 92	77.70	49.27
9X-7, 44	83.22	59.72
10X-2, 40	86.40	58.23
10X-4, 42	89.42	61.96
11X-7, 109	103.42	80.63
14X-1, 26	122.76	66.44
14X-5, 62	129.12	67.19
16X-2, 88	143.88	88.84
16X-4, 65	146.65	94.07
17X-2, 37	152.87	73.16
17X-6, 21	158.71	76.90
18X-7, 81	169.62	86.60
20X-5, 77	185.19	80.63
22X-5, 25	204.75	78.39
26X-2, 98	238.98	103.79

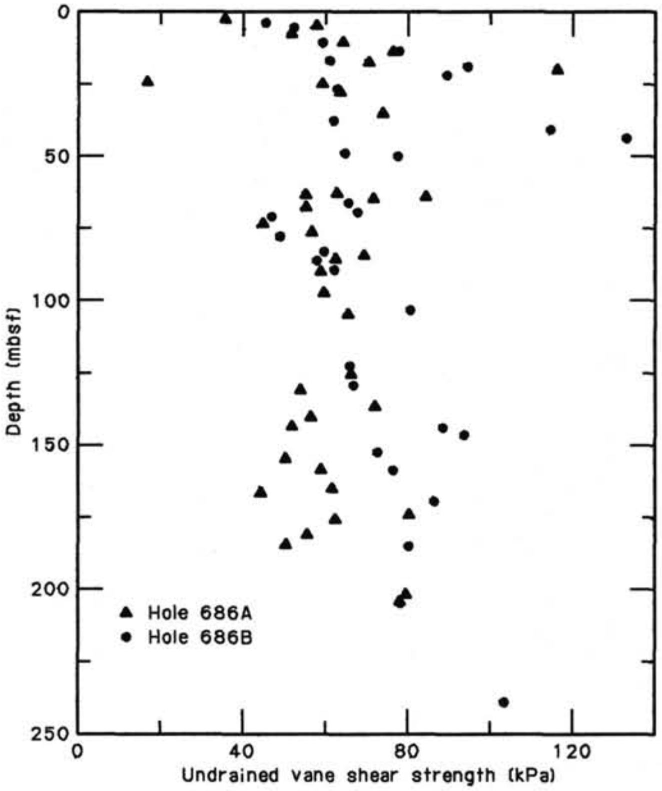

Figure 52. Profiles of peak undrained vane shear strength for Holes 686A and 686B.

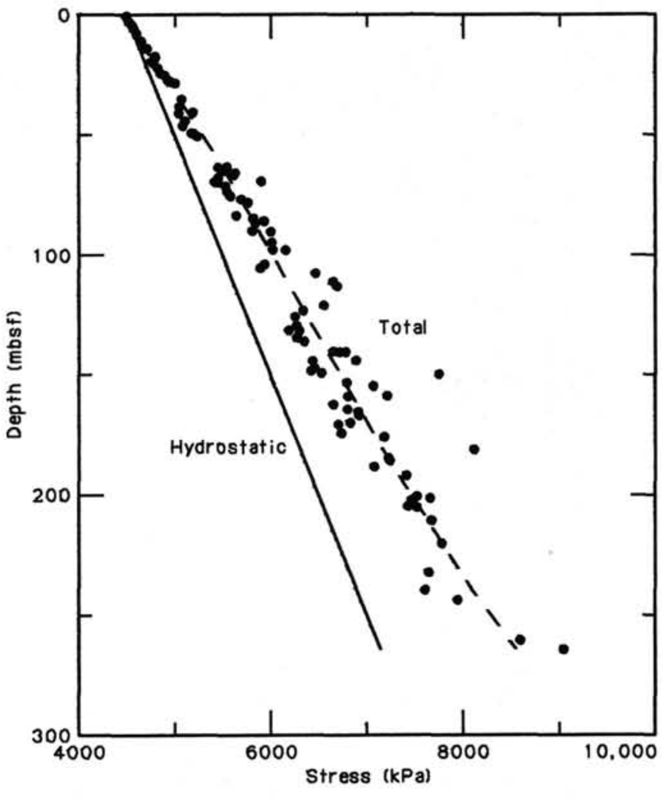

Figure 53. Profiles of assumed hydrostatic stress and calculated total stress for combined data from both holes of Site 686.

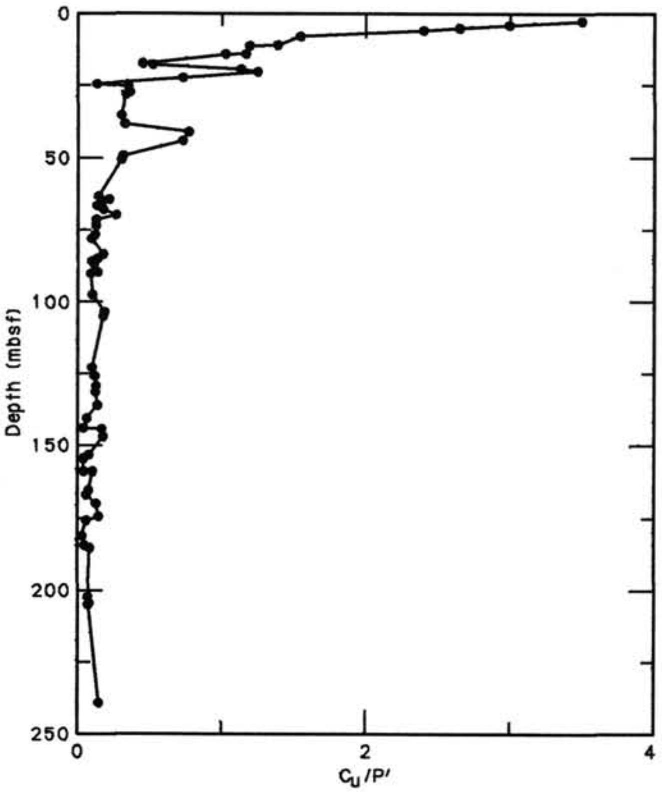

Figure 54. Ratio of peak undrained vane shear strength to effective overburden pressure vs. depth below seafloor for combined data from both holes of Site 686.

Table 12. Summary of thermal-conductivity data for Hole 686B.

Core-section interval (cm)	Depth (mbsf)	Thermal conductivity (W/m·K)
112-686B-1H-1, 90	0.90	0.948
1H-2, 68	2.18	0.932
1H-3, 70	3.70	0.820
1H-4, 70	5.20	0.792
1H-5, 70	6.70	1.031
1H-6, 50	8.00	1.073
2H-1, 70	9.20	0.946
2H-2, 65	10.65	0.893
2H-3, 70	12.20	0.985
2H-4, 70	13.70	1.045
2H-5, 70	15.20	0.835
2H-6, 70	16.70	1.334
3H-1, 80	18.80	0.975
3H-2, 70	20.20	0.945
3H-3, 70	21.70	0.902
3H-4, 76	23.26	1.086
3H-5, 69	24.69	1.099
3H-6, 87	26.37	1.334
5H-1, 37	37.32	0.897
5H-2, 130	39.75	1.226
5H-3, 67	40.62	0.835
5H-4, 92	42.37	0.758
5H-5, 80	43.75	0.898
5H-6, 70	45.15	0.885
6X-1, 82	47.32	0.788
6X-2, 67	48.67	0.796
6X-3, 64	50.14	0.818
6X-4, 37	51.37	0.911
8X-1, 99	66.49	1.163
8X-2, 22	67.22	1.083
8X-3, 143	69.93	0.796
8X-4, 100	71.00	0.886
9X-4, 90	80.40	0.792
9X-5, 61	81.61	0.885
9X-6, 90	83.40	0.752
10X-1, 46	84.96	0.913
10X-2, 78	86.78	0.953
10X-3, 109	88.59	0.767
10X-4, 57	89.57	0.893
11X-3, 72	96.84	0.931
11X-3, 118	97.30	0.940
11X-5, 139	99.55	0.801
11X-6, 94	100.60	0.944
12X-1, 21	103.71	0.718
12X-1, 125	104.75	0.720
14X-1, 102	123.52	0.685
14X-2, 64	124.64	0.773
14X-3, 12	125.62	0.796
14X-4, 91	127.37	0.762
14X-5, 60	128.56	0.744
14X-6, 96	130.42	0.734
15X-1, 83	132.83	0.670
15X-4, 101	137.51	0.764
15X-5, 66	138.66	0.793
16X-1, 60	142.10	0.907
16X-2, 98	143.98	0.723
16X-4, 8	146.08	0.742
16X-5, 126	148.76	0.730
17X-2, 47	152.97	0.875
17X-3, 140	155.40	1.963
17X-5, 10	157.10	0.737
17X-6, 83	159.33	0.885
18X-4, 68	164.28	0.741
18X-5, 105	166.07	0.781
18X-6, 29	166.81	0.802
18X-7, 110	169.05	0.782
20X-3, 80	182.67	0.827
20X-4, 62	183.99	0.867
20X-5, 116	185.84	0.801
20X-6, 54	186.72	0.728
21X-1, 53	189.53	0.864
21X-2, 76	191.26	0.864

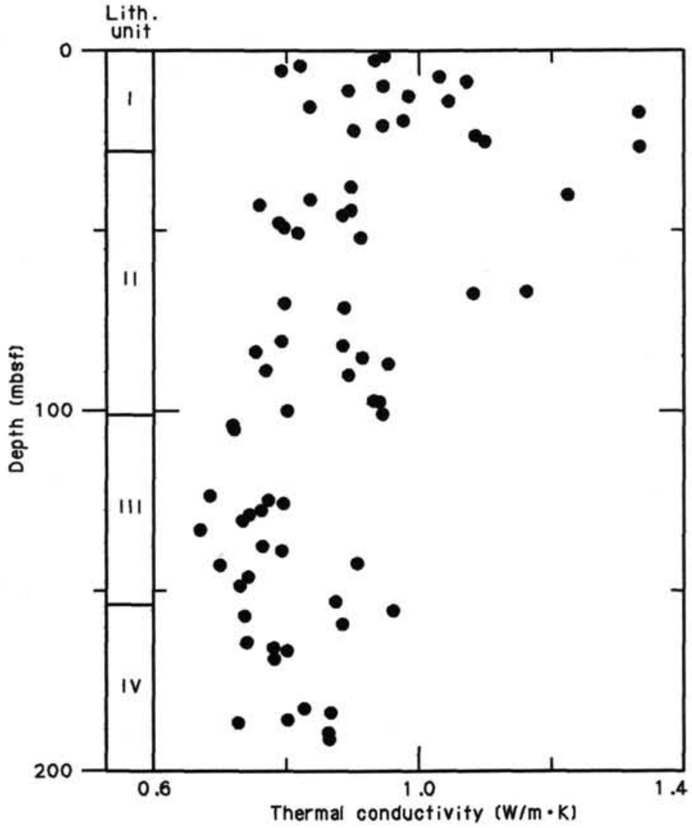

Figure 55. Thermal-conductivity profile for Hole 686B.

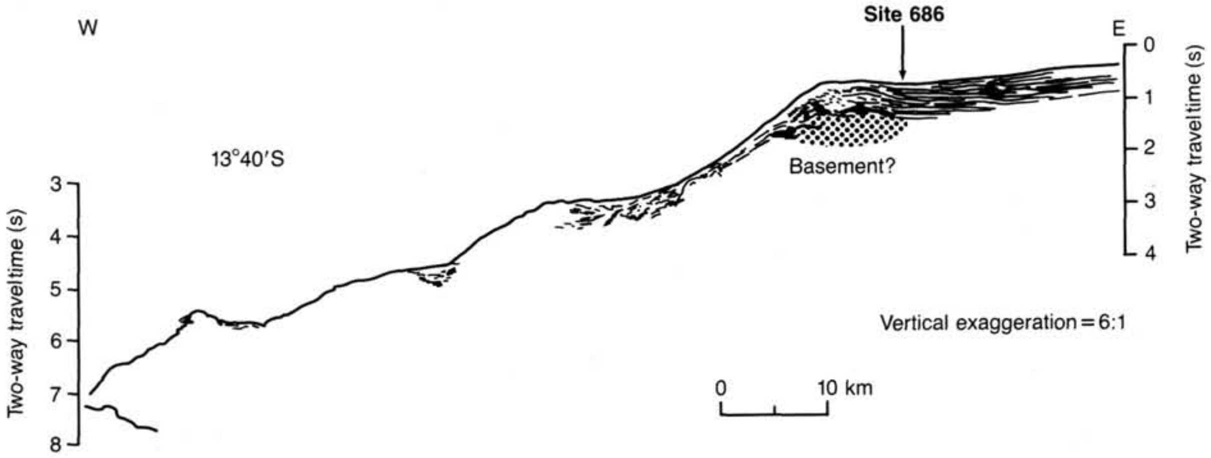

Figure 56. West Pisco Basin seismic stratigraphy and location of Site 686 from Thornburg and Kulm (1981).

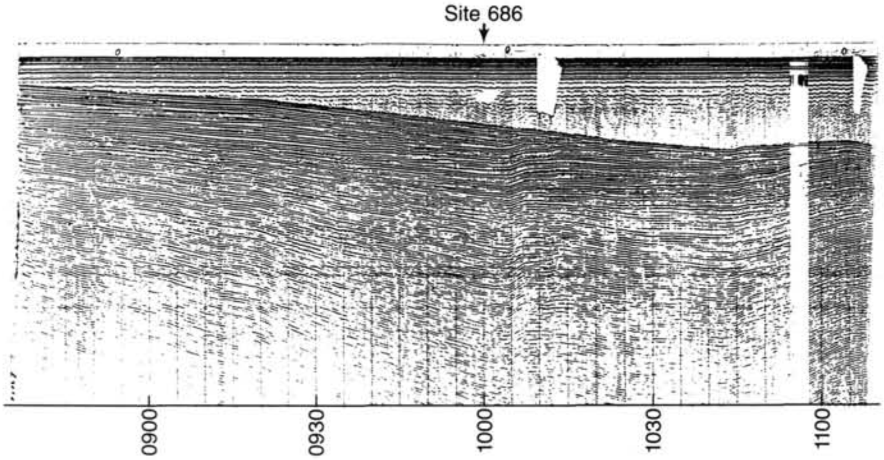

Figure 57. Part of single-channel seismic line YALOC 12-03-74, showing strata that lie nearly flat on the landward flank of the West Pisco Basin; note the location of Site 686.

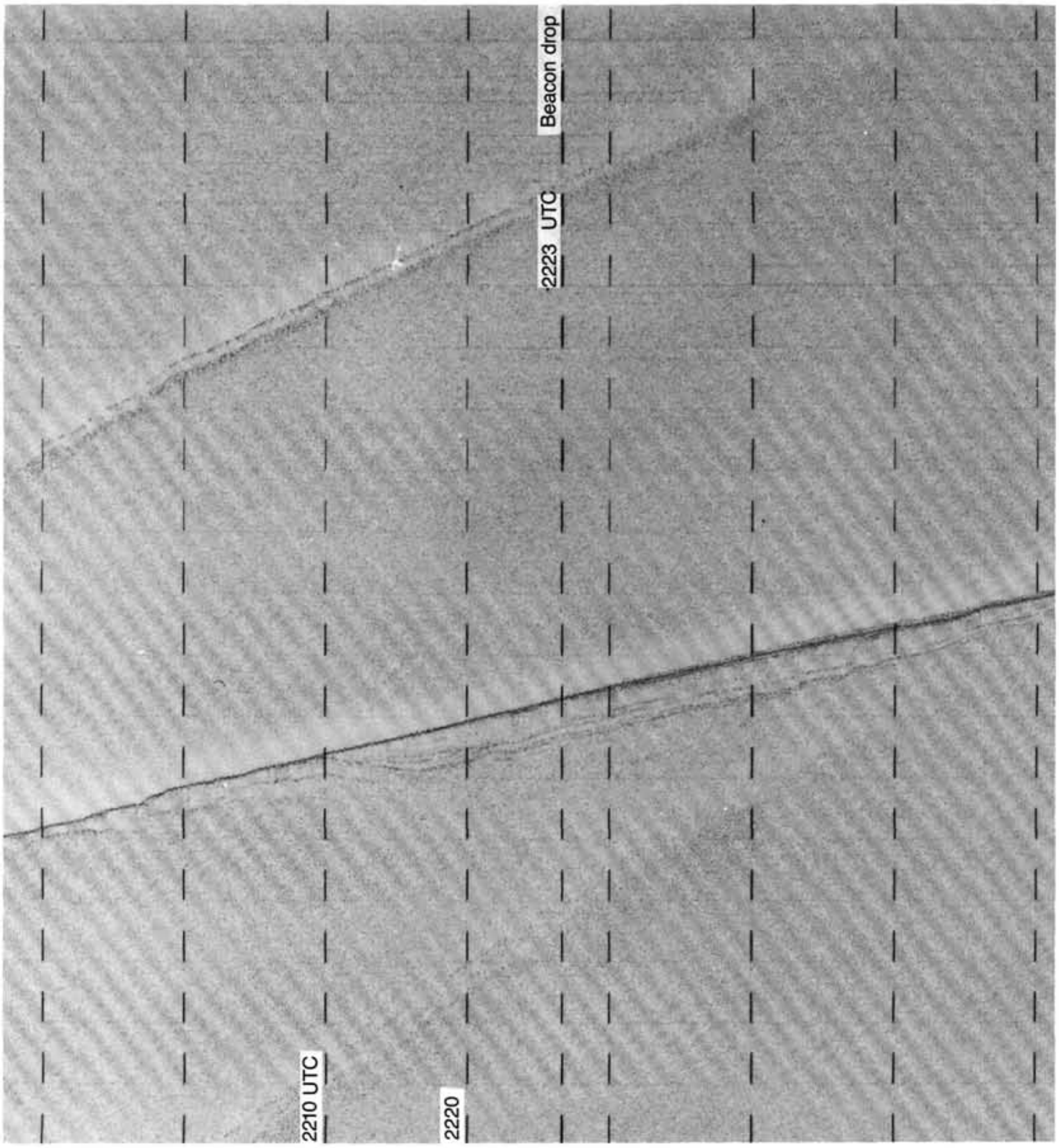

Figure 58. 3.5-kHz record at Site 686, obtained by *JOIDES Resolution* during approach to the site.

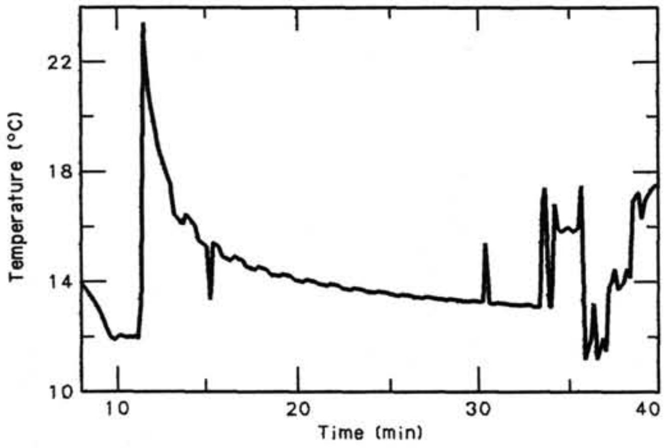

Figure 59. Temperature vs. time records obtained with the APC tool while retrieving Core 112-686A-6H (depth 52.6 m).

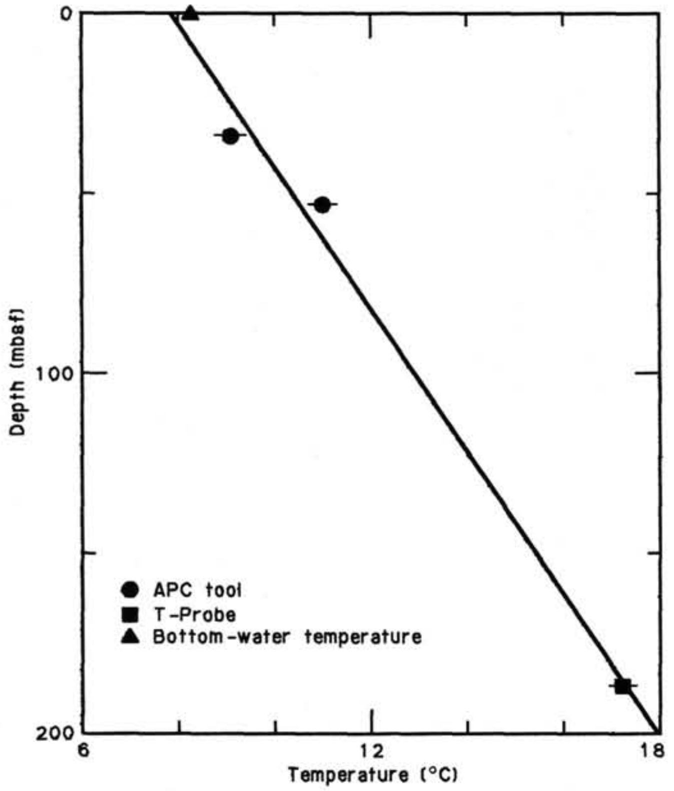

Figure 60. Temperature data in Hole 686A showing error bars plotted vs. depth. The solid line indicates the best-fitting geothermal gradient determined from the APC tool and T-probe temperature data.

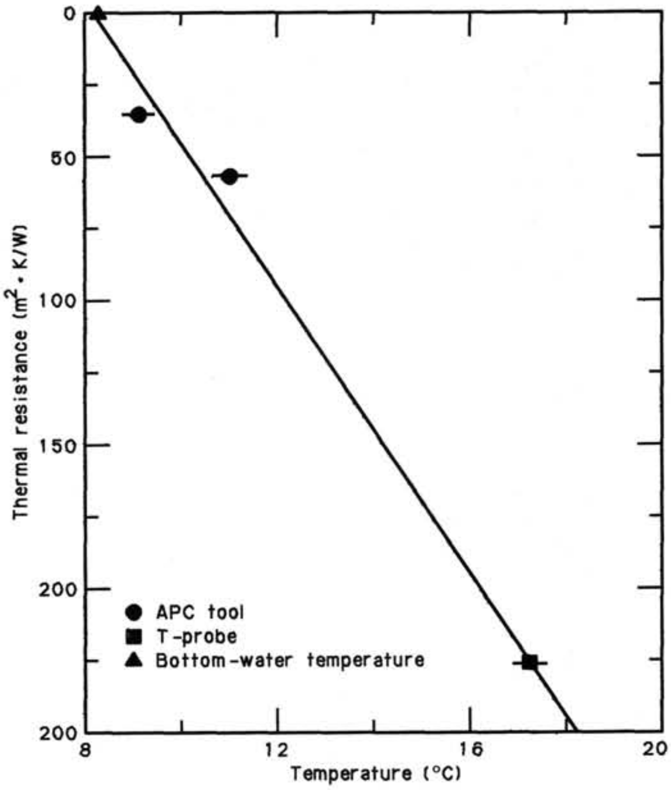

Figure 61. Temperature data in Hole 686A showing error bars plotted vs. thermal resistance. The solid line indicates the best-fitting geothermal gradient determined from the APC tool and T-probe temperature data.

SITE 686 HOLE A CORE 1H CORED INTERVAL 446.8-451.9 mbsl; 0.0-5.1 mbsf

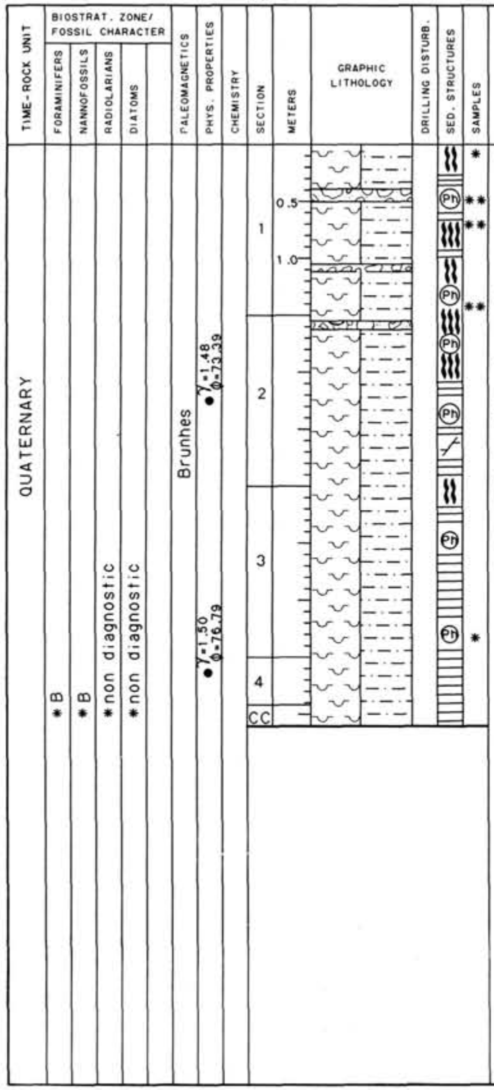

LITHOLOGIC DESCRIPTION

DIATOMACEOUS MUD

Major lithology: diatomaceous mud, olive gray (5Y 4/2 and 5Y 5/2), olive (5Y 5/4), and dark olive gray (5Y 3/2). Laminated with some intervals of soft sediment deformation and some burrowing.

Minor lithologies:
1. phosphate nodules and nodular gravels.
2. quartzo-feldspathic sand.

SMEAR SLIDE SUMMARY (%):

	1, 9 D	1, 43 M	1, 50 M	1, 73 M	1, 74 M	1, 143 M
TEXTURE:						
Sand	20	70	5	25	60	85
Silt	40	10	20	40	30	15
Clay	40	20	75	35	10	—
COMPOSITION:						
Quartz	5	15	2	5	30	15
Feldspar	5	15	3	12	20	20
Rock fragments	5	15	3	8	25	15
Mica	—	—	—	—	Tr	—
Clay	23	—	25	20	5	—
Volcanic glass	Tr	—	Tr	—	Tr	15
Calcite/dolomite	2	5	2	5	—	10
Accessory minerals	—	5	Tr	—	—	5
Pyrite	5	—	3	10	10	5
Amphibole	Tr	—	—	—	5	—
Phosphate	—	35	—	—	—	—
Glauconite	—	5	—	—	—	—
Diatoms	55	Tr	62	40	5	15
Sponge spicules	Tr	—	—	—	Tr	Tr
Fish remains	—	5	—	—	—	—

	1, 143 M	3, 128 M
TEXTURE:		
Sand	10	—
Silt	20	5
Clay	70	95
COMPOSITION:		
Quartz	3	Tr
Feldspar	2	Tr
Rock fragments	3	Tr
Clay	5	—
Volcanic glass	Tr	—
Calcite/dolomite	2	—
Accessory minerals		
Pyrite	10	—
Phosphate	—	100
Diatoms	75	—
Sponge spicules	Tr	—

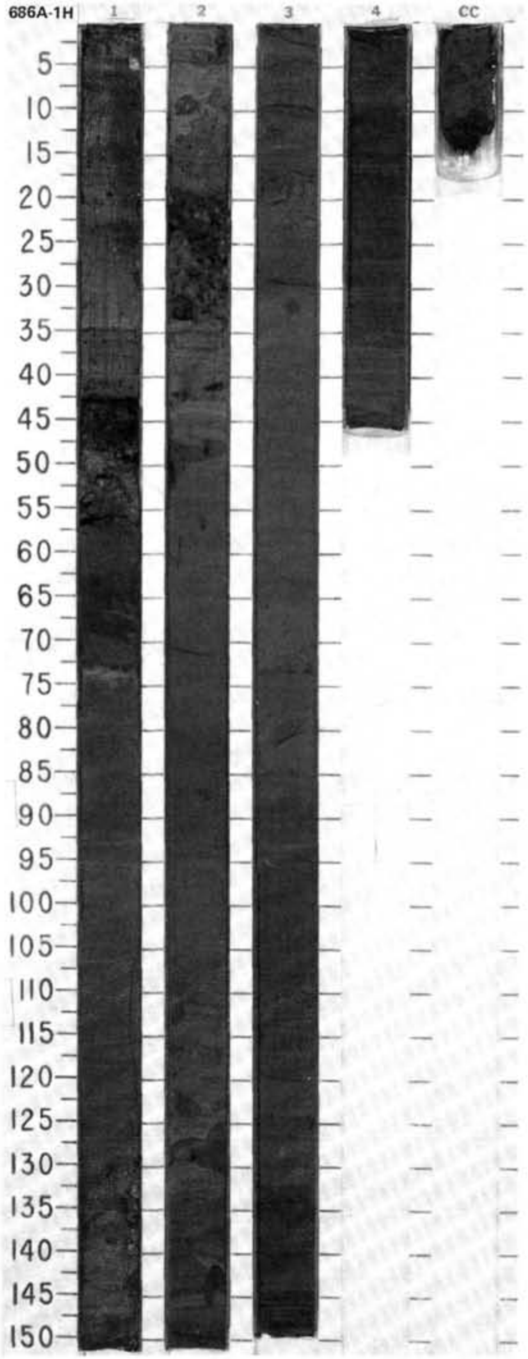

SITE 686 HOLE A CORE 2H CORED INTERVAL 451.9-461.4 mbsl; 5.1-14.6 mbsf

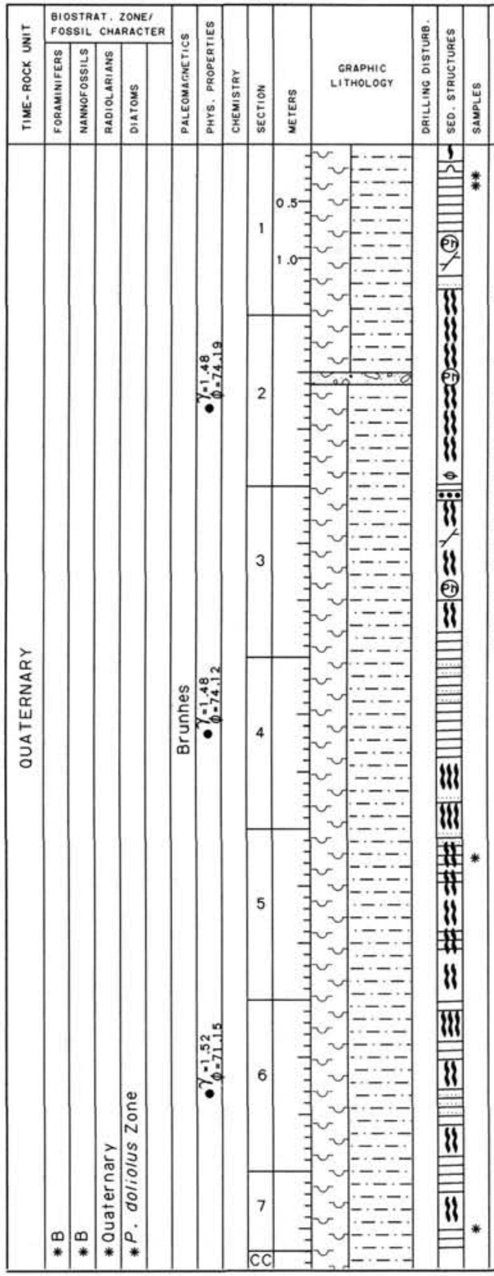

LITHOLOGIC DESCRIPTION

DIATOMACEOUS MUD and OOZE

Major lithology: diatomaceous mud and ooze, olive gray (5Y 3/2 and 5Y 4/2), laminated to burrowed, with scattered foraminiferal shells.

Minor lithologies:
1. phosphate nodules (N 4/).
2. scattered small bivalve shell fragments.
3. thin graded sand layer.

SMEAR SLIDE SUMMARY (%):

	1, 23 M	1, 25 D	5, 21 M	7, 46 D
TEXTURE:				
Sand	25	20	30	30
Silt	45	35	45	45
Clay	30	45	25	25
COMPOSITION:				
Quartz	5	15	10	15
Feldspar	5	10	15	5
Rock fragments	—	10	15	10
Clay	20	20	20	25
Volcanic glass	8	Tr	—	5
Calcite/dolomite	—	Tr	—	2
Accessory minerals	—	—	5	—
Pyrite	2	5	5	2
Amphibole	—	—	—	1
Diatoms	60	40	25	35
Sponge spicules	—	Tr	5	Tr
Silicoflagellates	Tr	—	—	—
Fish remains	—	—	—	Tr

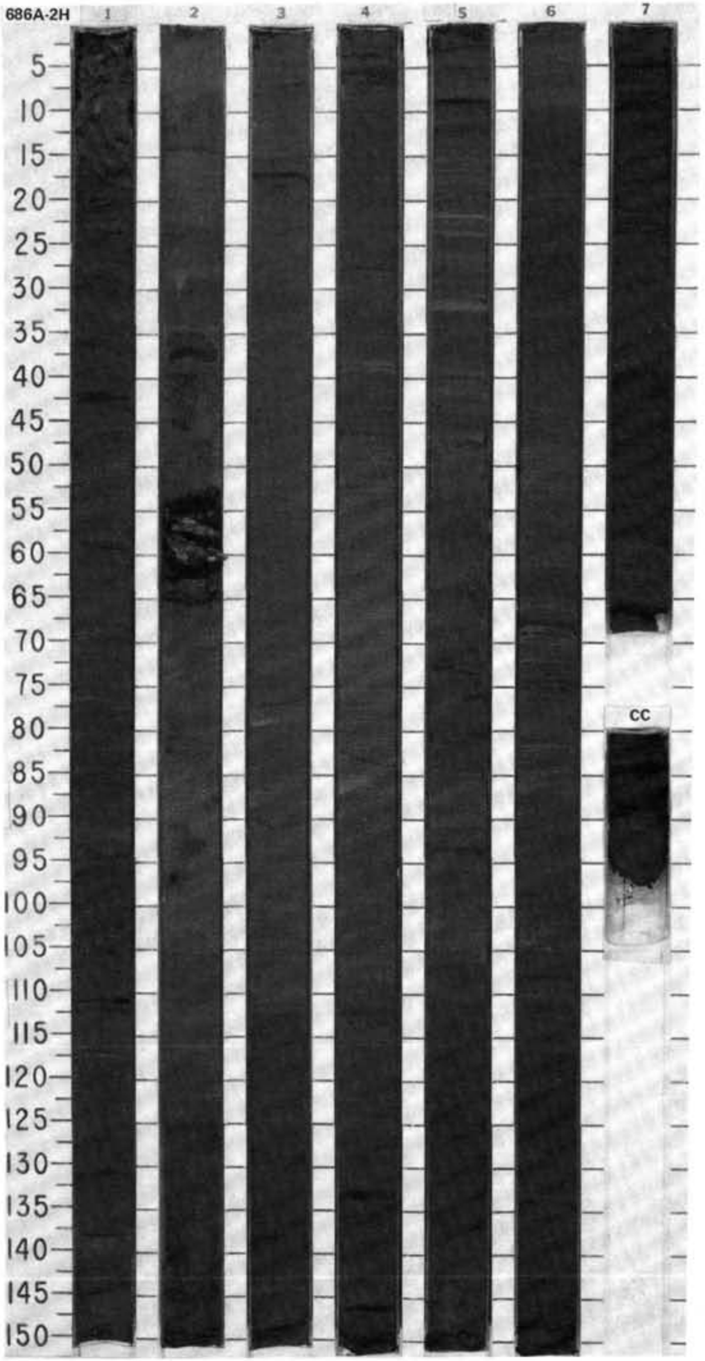

SITE 686 HOLE A CORE 3H CORED INTERVAL 461.4-470.9 mbsl; 14.6-24.1 mbsf

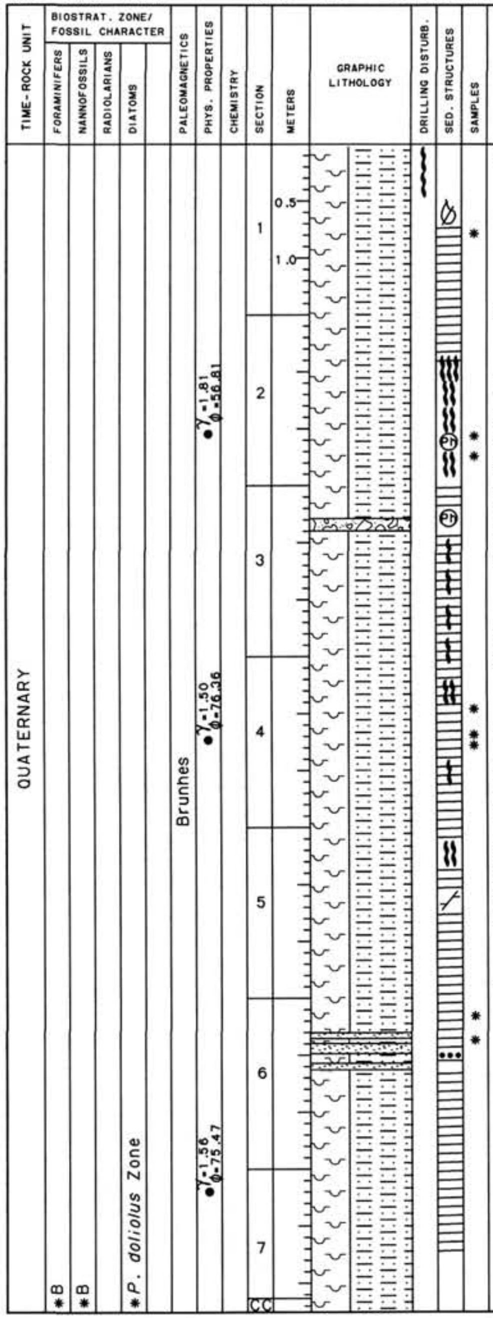

LITHOLOGIC DESCRIPTION

DIATOMACEOUS MUD and SILT

Major lithology: diatomaceous mud and silt, dark olive (5Y 2/5 and 5Y 3/3), olive (5Y 4/4) green gray (5GY 3/2) and olive gray (5Y 4/2). Laminated to burrowed and massive, in places dolomitic.

Minor lithologies:
1. phosphate nodules and lenses.
2. dolomitic diatomaceous ooze.
3. fine-grained, quartzo-feldspathic sand in laminae and thin layers.

SMEAR SLIDE SUMMARY (%):

	1, 75 D	2, 105 D	2, 123 M	4, 46 M	4, 61 M	4, 69 D
TEXTURE:						
Sand	—	15	—	—	—	—
Silt	50	55	65	50	100	83
Clay	50	30	35	50	—	20
COMPOSITION:						
Quartz	2	22	3	2	Tr	2
Feldspar	—	—	3	—	—	3
Clay	40	10	—	—	—	17
Volcanic glass	—	1	—	—	—	—
Calcite/dolomite	—	—	Tr	—	15	35
Accessory minerals						
Pyrite	3	7	—	2	Tr	1
Phosphate	—	—	94	—	—	1
Glauconite	—	—	—	—	—	1
Micrite	10	20	—	50	—	—
Diatoms	45	40	—	46	85	40
Radiolarians	—	—	—	—	—	Tr
Silicoflagellates	—	—	—	—	—	Tr

	6, 9 M	6, 32 D
TEXTURE:		
Sand	80	10
Silt	18	80
Clay	2	10
COMPOSITION:		
Quartz	40	70
Feldspar	30	10
Rock fragments	12	4
Mica	2	Tr
Calcite/dolomite	Tr	3
Accessory minerals	3	—
Pyrite	2	8
Glauconite	—	3
Micrite	—	2
Hornblende	3	—
Diatoms	8	—

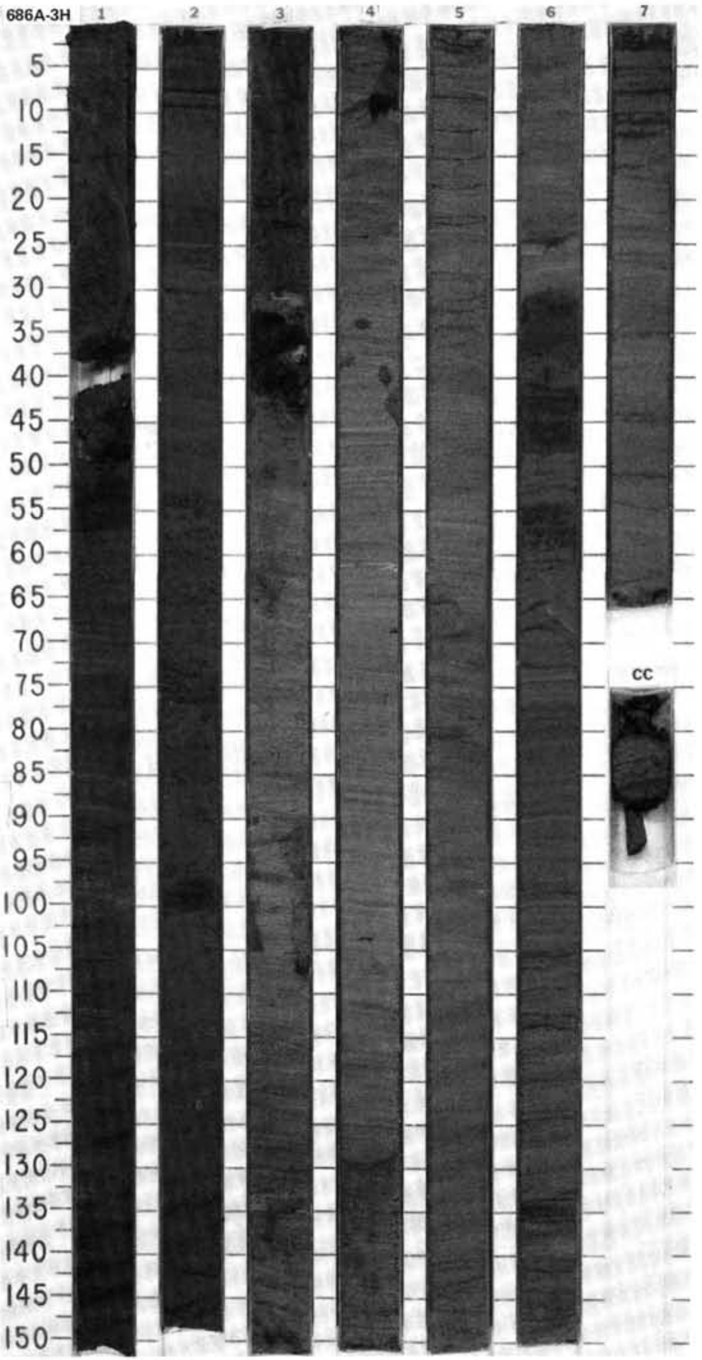

SITE 686 HOLE A CORE 4H CORED INTERVAL 470.9-480.4 mbsl; 24.1-33.6 mbsf

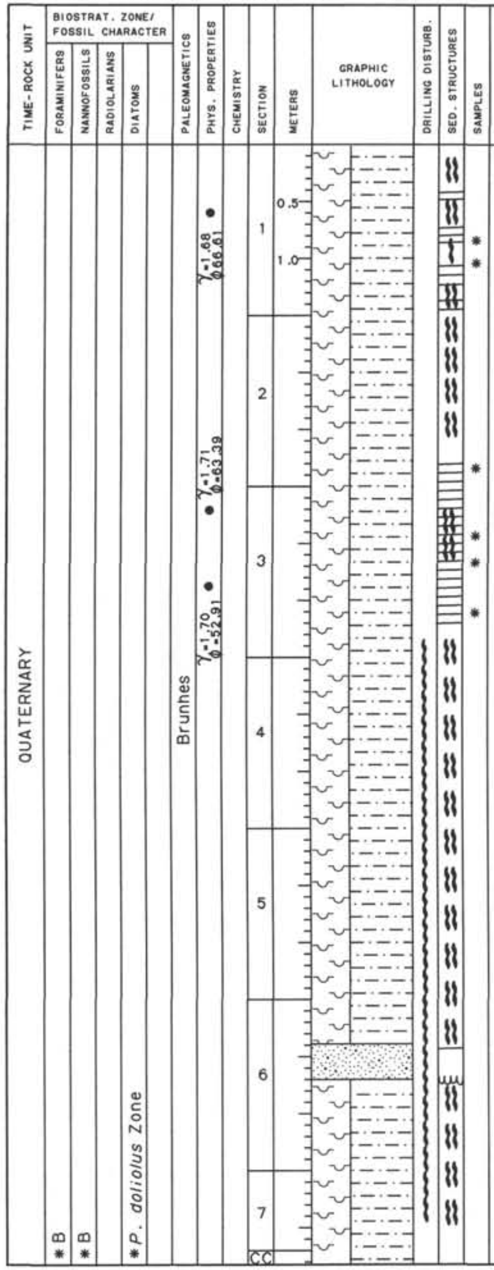

LITHOLOGIC DESCRIPTION

DIATOMACEOUS MUD and SILT

Major lithology: diatomaceous mud and silt, greenish gray (5GY 4/2) and olive (5Y 4/3), dark olive (5Y 3/5), gray (5GY 3/1), olive gray (5Y 4/2), and dark olive gray (5Y 3/2). Laminated to burrowed.

Minor lithologies:
1. quartzo-feldspathic silty sand.
2. phosphatic sandy silt, in graded layers.
3. vertebrate bone fragments.

SMEAR SLIDE SUMMARY (%):

	1, 85 D	1, 101 M	2, 127 M	3, 41 D	3, 71 D	3, 109 M
TEXTURE:						
Sand	10	75	40	—	90	25
Silt	60	17	60	70	10	70
Clay	30	8	—	30	—	5
COMPOSITION:						
Quartz	25	37	18	15	60	13
Feldspar	3	28	—	5	3	15
Rock fragments	2	8	5	Tr	2	5
Mica	—	1	—	—	Tr	1
Clay	10	7	—	22	—	5
Volcanic glass	1	—	—	1	4	—
Calcite/dolomite	—	3	4	—	—	43
Accessory minerals	—	4	3	—	—	—
Pyrite	5	—	12	5	20	5
Glauconite	3	—	2	Tr	—	—
Hornblende	—	7	5	—	—	2
Micrite	20	—	—	7	—	—
Phosphate	—	—	40	—	10	4
Foraminifers	1	—	—	—	—	—
Diatoms	30	—	6	45	1	7
Sponge spicules	—	—	—	Tr	—	—
Bioclasts	—	5	5	—	—	—

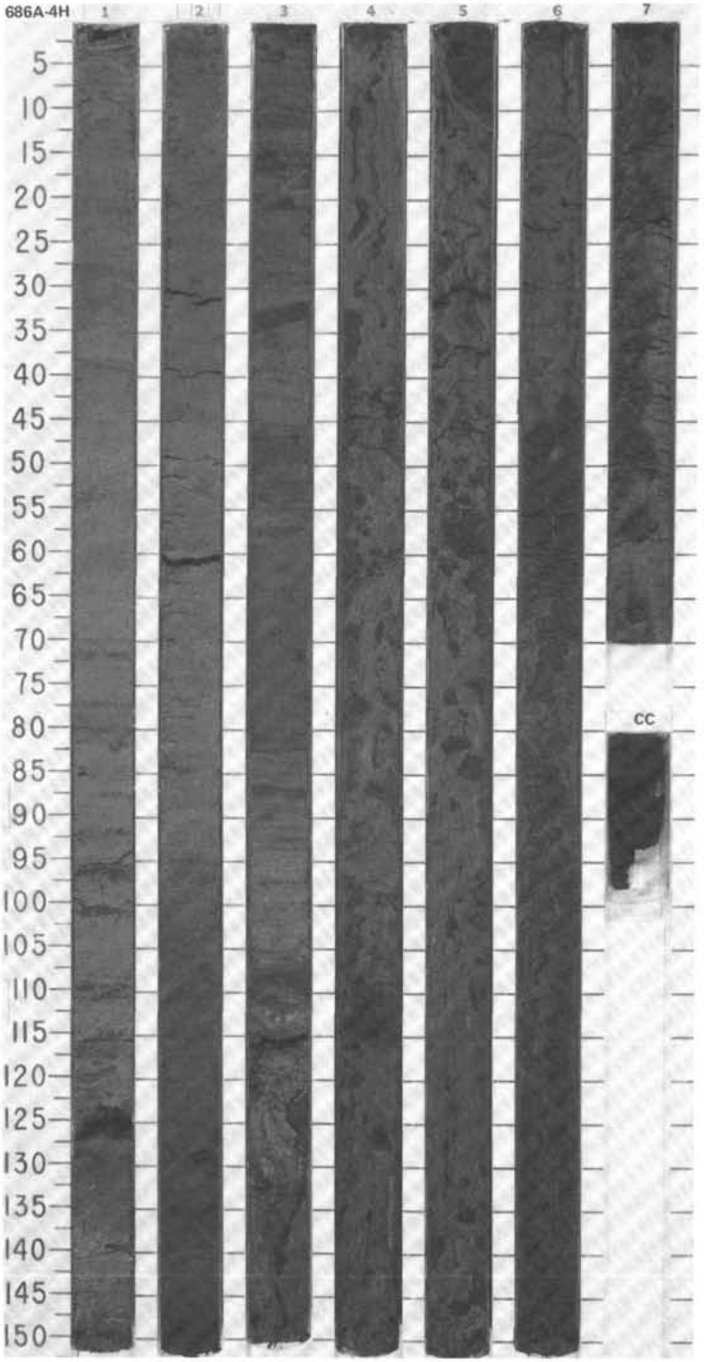

SITE 686 HOLE A CORE 5H CORED INTERVAL 480.4-489.9 mbsl; 33.6-43.1 mbsf

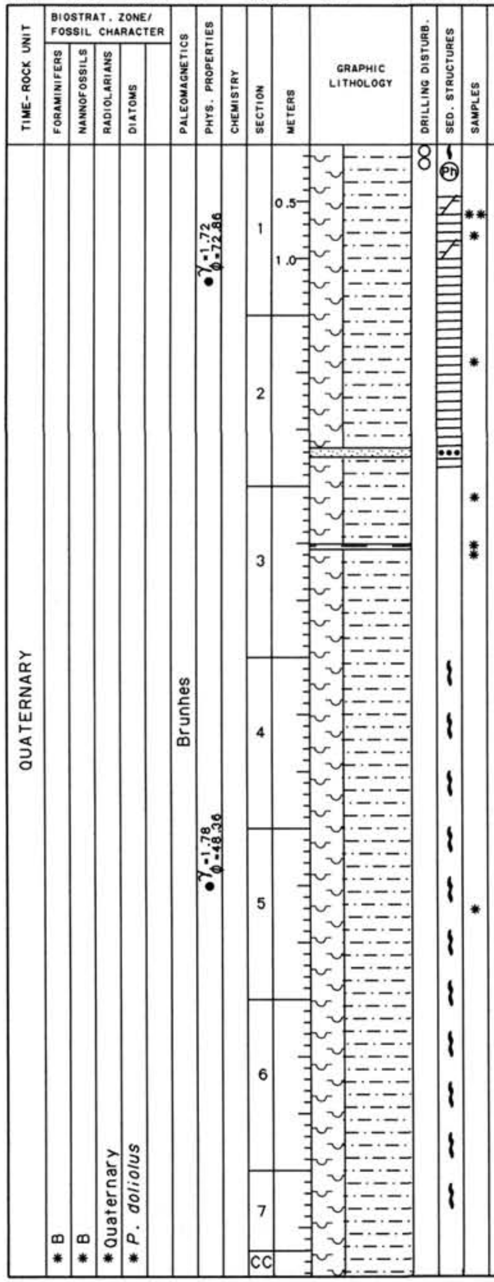

LITHOLOGIC DESCRIPTION

DIATOMACEOUS MUD AND OOZE

Major lithology: diatomaceous mud and ooze, dark olive gray (5Y 3/2 and 5Y 4/2), olive gray (5Y 4/2), green gray (5GY 5/1), olive (5Y 5/6), gray (5Y 5/1), dark green gray (5GY 4/1), very dark gray brown (2.5Y 3/2). Laminated to burrowed and massive.

Minor lithologies:
1. fine-grained sand, dark gray (5Y 4/1), in graded beds with sharp, erosional basal contacts.
2. quartz-rich sandy mud.

SMEAR SLIDE SUMMARY (%):

	1, 69 D	1, 69 M	1, 78 M	2, 42 M	3, 10 D	3,56 M
TEXTURE:						
Sand	5	—	5	5	40	10
Silt	20	30	70	55	30	60
Clay	75	70	25	40	30	30
COMPOSITION:						
Quartz	10	15	5	15	25	15
Feldspar	3	5	5	5	20	Tr
Rock fragments	—	—	Tr	5	—	—
Clay	35	—	20	25	15	—
Volcanic glass	Tr	—	—	5	—	—
Calcite/dolomite	—	—	Tr	5	5	80
Accessory minerals						
Pyrite	2	5	—	5	15	—
Glauconite	—	—	—	Tr	15	—
Hornblende	—	—	—	—	—	Tr
Opaques	—	—	—	—	—	5
Foraminifers	—	—	5	—	Tr	Tr
Diatoms	20	50	65	10	5	—
Sponge spicules	—	—	—	—	Tr	Tr
Pellets	30	25	—	25	—	—

	3, 63 D	5, 70 D
TEXTURE:		
Sand	10	30
Silt	40	30
Clay	50	40
COMPOSITION:		
Quartz	14	35
Feldspar	4	5
Rock fragments	Tr	—
Clay	35	30
Calcite/dolomite	—	Tr
Accessory minerals		
Pyrite	8	10
Glauconite	—	Tr
Apatite	1	—
Micrite	3	6
Diatoms	35	14

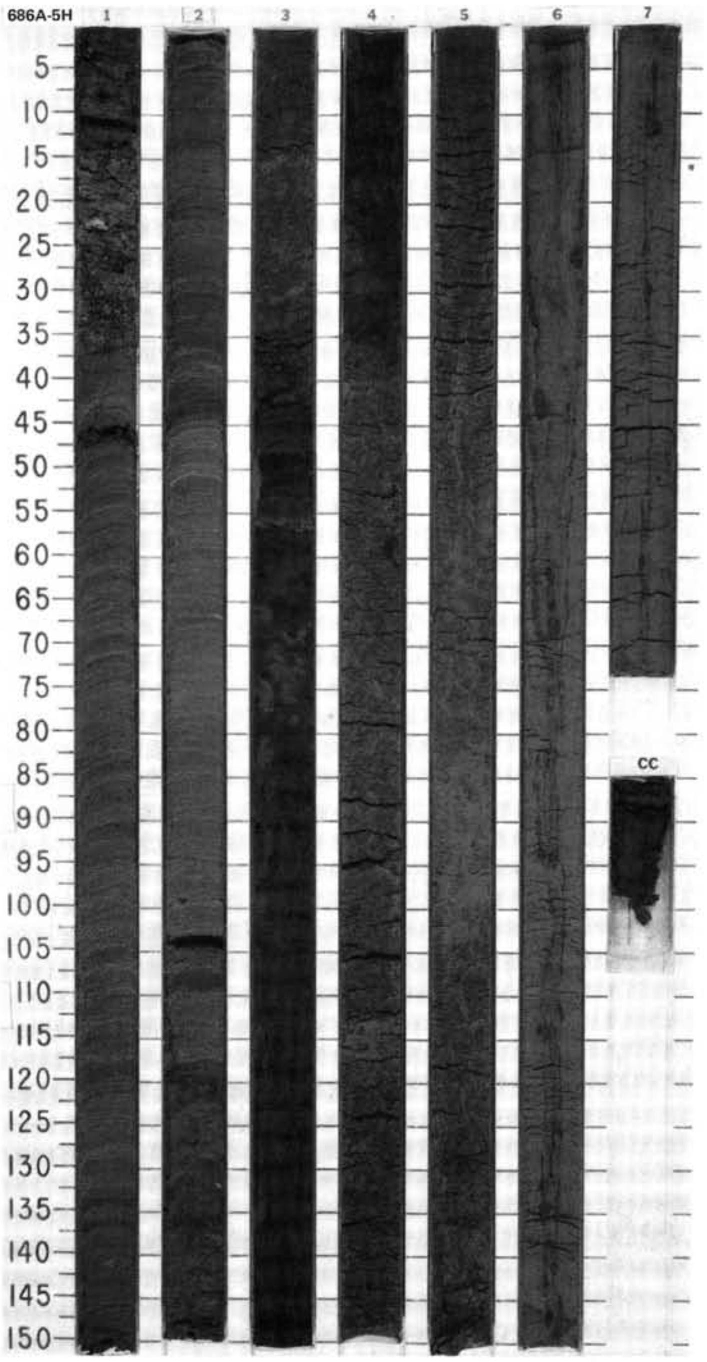

SITE 686 HOLE A CORE 6H CORED INTERVAL 489.9-499.4 mbsl; 43.1-52.6 mbsf

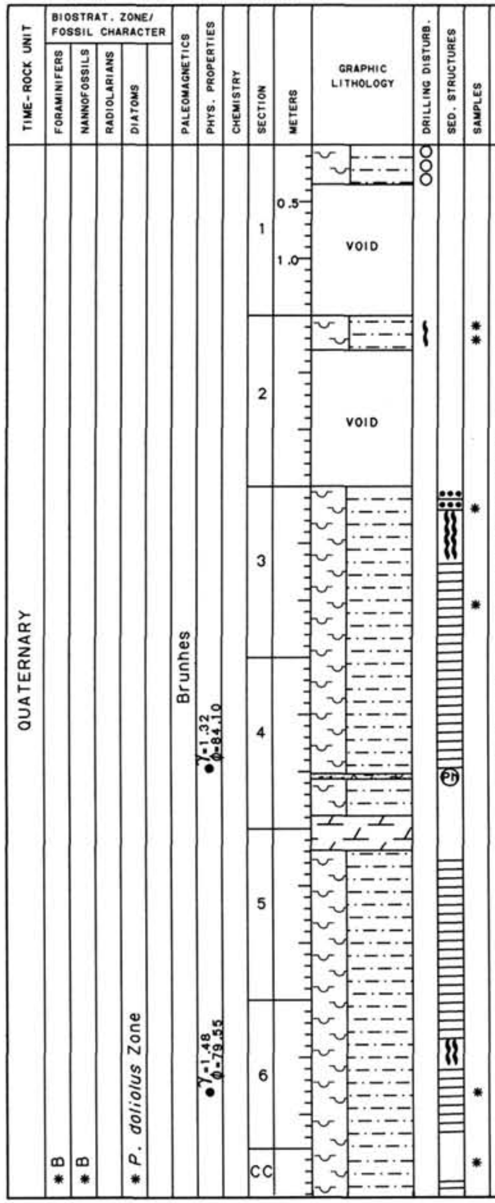

LITHOLOGIC DESCRIPTION

DIATOMACEOUS MUD and FINE-GRAINED SAND

Major lithology: diatomaceous mud, dark olive (5Y 3/2), olive gray (5Y 4/2), dark green gray (5GY 4/1), very dark gray brown (2.5Y 3/2), olive yellow (5Y 6/6), and light olive gray (5Y 5/4). Laminated to burrowed, *massive*. Fine-grained sand, dark gray (N 4/), dark greenish gray (5GY 3/1), massive (burrowed?) and graded.

Minor lithologies:
1. phosphatic gravel.
2. dolomitic diatomaceous mud.
3. diorite pebble.
4. dolomite nodules.

SMEAR SLIDE SUMMARY (%):

	2, 10 M	2, 13 D	3, 20 M	3, 104 D	6, 80 D	CC, 12 D
TEXTURE:						
Sand	60	15	20	5	15	25
Silt	10	40	55	65	45	35
Clay	30	45	25	30	40	40
COMPOSITION:						
Quartz	35	20	5	10	20	30
Feldspar	12	5	5	5	5	5
Rock fragments	10	—	5	5	5	2
Clay	30	38	22	20	40	37
Volcanic glass	—	1	—	—	5	Tr
Calcite/dolomite	Tr	—	Tr	Tr	10	—
Accessory minerals						
Pyrite	8	7	3	—	5	8
Glauconite	1	Tr	—	Tr	—	—
Hornblende	—	—	—	—	Tr	—
Micrite	Tr	4	—	—	—	3
Foraminifers	—	—	5	—	—	—
Nannofossils	—	—	Tr	—	—	—
Diatoms	4	25	55	40	10	15
Radiolarians	—	—	—	Tr	—	—
Sponge spicules	—	Tr	—	—	Tr	—
Silicoflagellates	—	—	—	Tr	—	—
Fish remains	—	—	—	Tr	Tr	—
Pellets	—	—	—	20	—	—

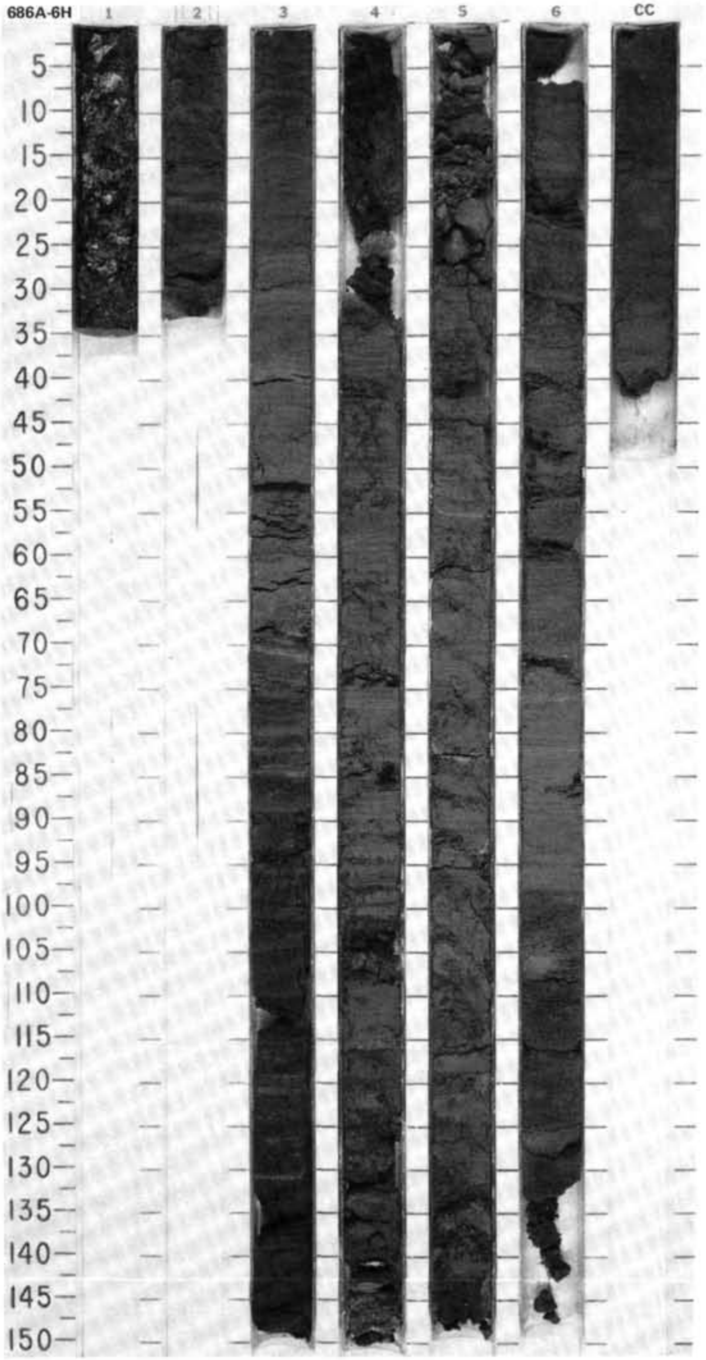

SITE 686 HOLE A CORE 7H CORED INTERVAL 499.4-508.9 mbsl; 52.6-62.1 mbsf

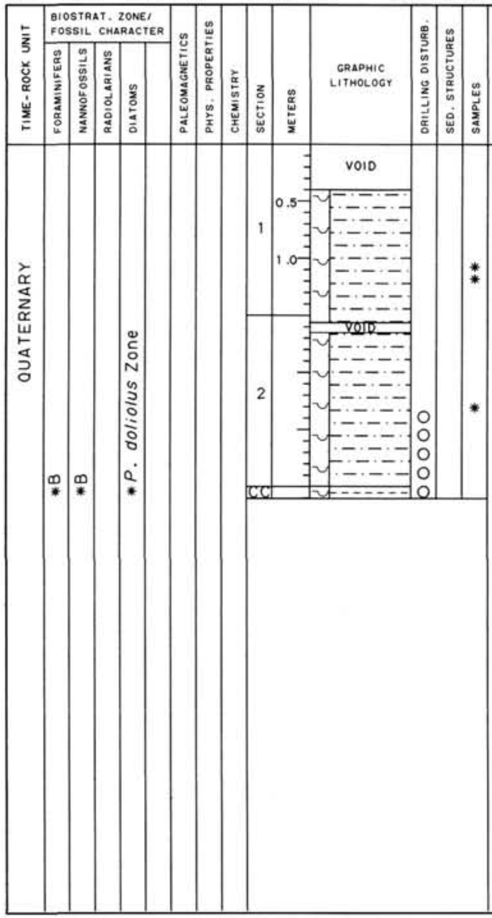

LITHOLOGIC DESCRIPTION

DIATOMACEOUS MUD, SANDY SILT and SAND

Major lithology: diatomaceous mud and sandy silt, dark greenish gray (5GY 9/1) and olive (5Y 4/3), massive, and sand, dark greenish gray (5G 4/1), massive with severe drilling disturbance.

SMEAR SLIDE SUMMARY (%):

	1, 112 M	1, 117 D	2, 79 M
TEXTURE:			
Sand	65	80	25
Silt	20	5	50
Clay	15	15	25
COMPOSITION:			
Quartz	15	50	20
Feldspar	20	12	15
Rock fragments	10	12	10
Mica	2	—	1
Clay	13	15	25
Calcite/dolomite	3	—	3
Accessory minerals			
Glauconite	1	—	—
Pyrite	3	6	2
Hornblende	2	Tr	2
Phosphate	Tr	—	2
Diatoms	20	5	20
Sponge spicules	1	—	—

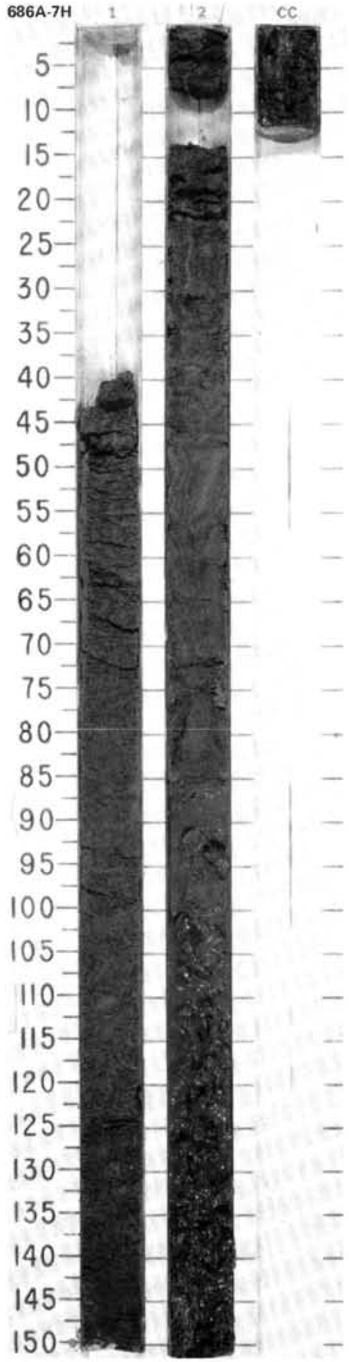

SITE 686 HOLE A CORE 8H CORED INTERVAL 508.9-511.5 mbsl; 62.1-64.7 mbsf

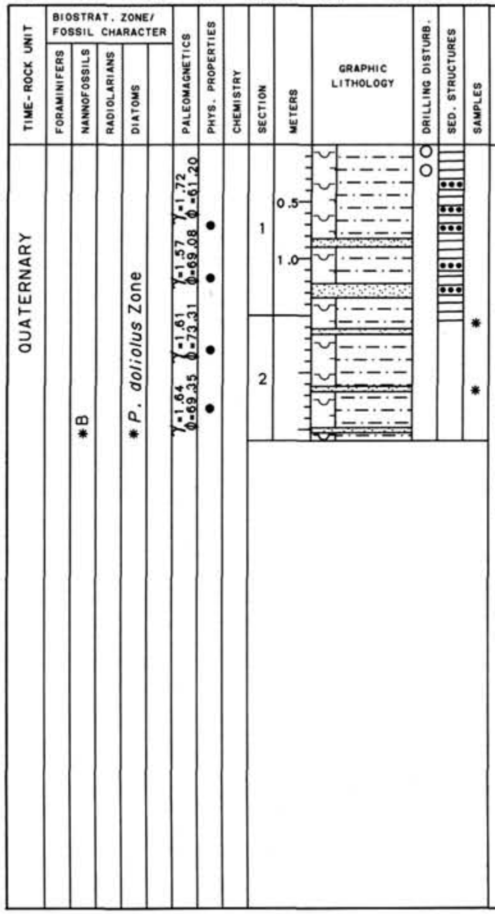

LITHOLOGIC DESCRIPTION

DIATOMACEOUS MUD and SAND

Major lithology: diatomaceous mud, olive gray (5Y 4/2 and 5/2), laminated with minor burrowing. Sand, dark gray (N 4/), quartz-rich, in graded, massive beds, 5 to 10 cm thick. With sharp, erosional basal contacts.

SMEAR SLIDE SUMMARY (%):

	2, 8 M	2, 70 D
TEXTURE:		
Sand	40	70
Silt	40	20
Clay	20	10
COMPOSITION:		
Quartz	5	47
Feldspar	5	11
Rock fragments	5	15
Mica	1	—
Clay	15	10
Calcite/dolomite	2	—
Accessory minerals		
Glauconite	1	—
Pyrite	1	12
Hornblende	Tr	5
Phosphorite	Tr	—
Foraminifers	1	—
Nannofossils	3	Tr
Diatoms	60	Tr
Radiolarians	Tr	—
Sponge spicules	1	—

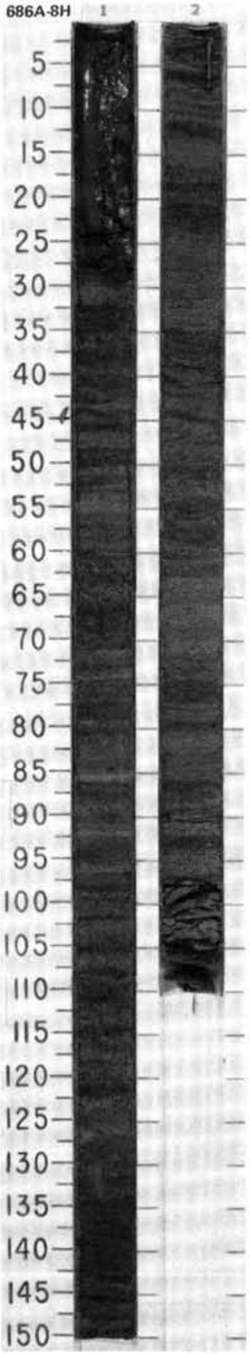

SITE 686 HOLE A CORE 9X CORED INTERVAL 511.5-519.5 mbsl; 64.7-72.7 mbsf

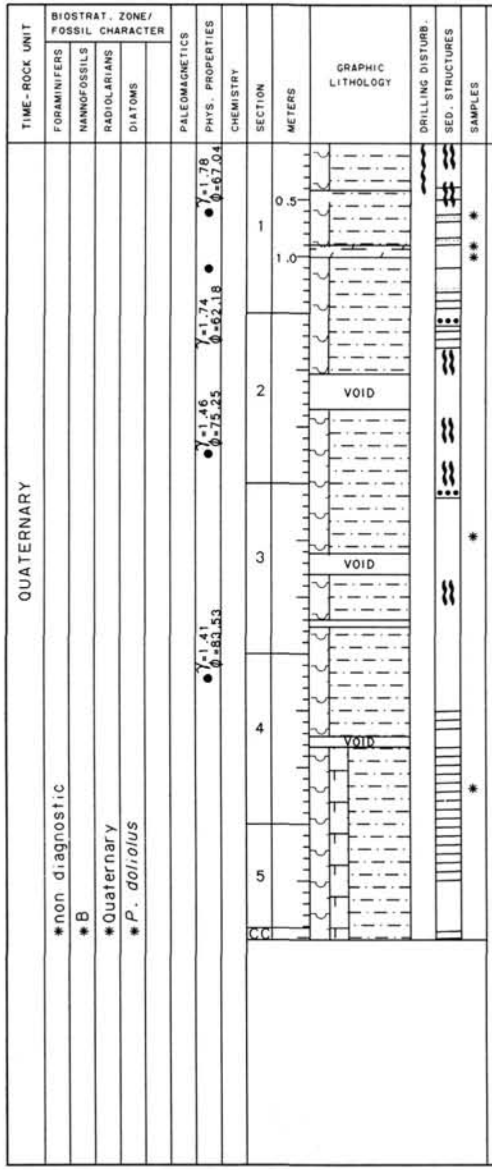

LITHOLOGIC DESCRIPTION

DIATOMACEOUS MUD, SANDY SILT, and SAND

Major lithology: diatomaceous mud, olive gray (5Y 4/2 and 5Y 5/2), olive (5Y 5/4), dark olive gray (5Y 3/2), black (5Y 2.5/1). Laminated to massive, burrowed, locally micritic or dolomitic. Sand, very dark gray (N 3/) and dark gray (N 4/). Fine-grained, massive to graded, in beds 4 to 10 cm thick with sharp, erosional basal contacts. A few thin layers of sandy silt.

SMEAR SLIDE SUMMARY (%):

	1, 60 D	1, 89 D	1, 94 M	3, 47 D	4, 130 M
TEXTURE:					
Sand	15	70	—	80	—
Silt	50	20	15	20	50
Clay	35	10	85	—	50
COMPOSITION:					
Quartz	10	62	Tr	65	2
Feldspar	2	10	Tr	20	3
Rock fragments	8	20	—	11	2
Mica	Tr	3	—	—	—
Clay	30	—	10	—	55
Volcanic glass	3	Tr	—	1	—
Calcite/dolomite	—	—	—	—	5
Accessory minerals					
Pyrite	2	1	—	—	2
Hornblende	—	4	—	2	1
Phosphate	—	—	—	—	Tr
Glauconite	—	—	—	—	1
Micrite	5	—	75	—	10
Foraminifers	—	—	—	1	4
Diatoms	40	Tr	15	—	15
Sponge spicules	—	Tr	—	—	—

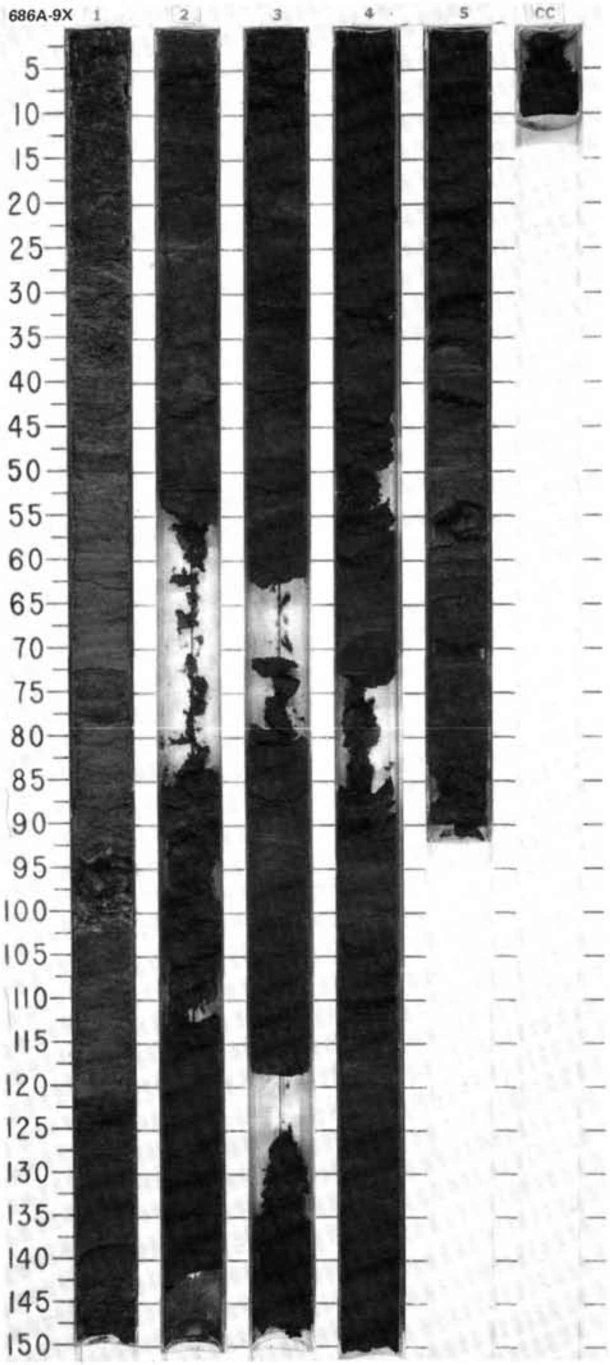

SITE 686 HOLE A CORE 10X CORED INTERVAL 519.5-529.0 mbsl; 72.7-82.2 mbsf

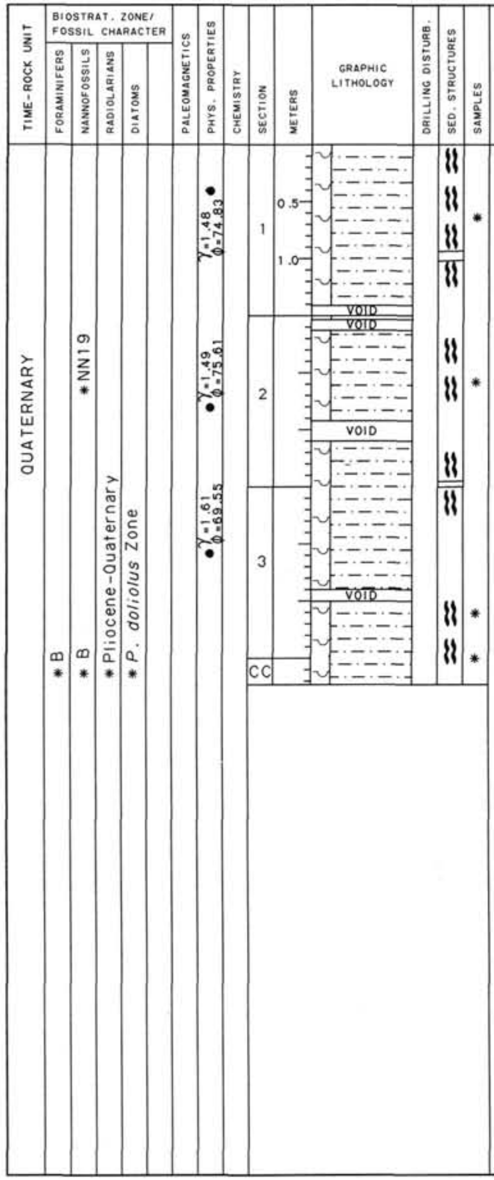

LITHOLOGIC DESCRIPTION

DIATOMACEOUS MUD and SILT

Major lithology: diatomaceous mud and silt, dark olive gray (5Y 3/2), olive (5Y 5/4), olive gray (5Y 4/2). Burrowed (massive to mottled) with some faintly laminated to thinly bedded intervals.

Minor lithologies:
1. sandy dolomite, olive (5Y 5/4).
2. diatom ooze, in olive (5Y 5/4) laminations.
3. sand, gray (N 5/) in thin (1 cm) graded beds.

SMEAR SLIDE SUMMARY (%):

	1, 63 D	2, 68 D	3, 51 M	3, 117 M
TEXTURE:				
Sand	10	10	15	20
Silt	20	45	15	20
Clay	70	45	70	60
COMPOSITION:				
Quartz	8	5	10	10
Feldspar	2	6	2	2
Rock fragments	5	4	10	6
Mica	—	—	Tr	1
Clay	68	44	63	60
Volcanic glass	—	—	Tr	Tr
Calcite/dolomite	—	5	—	—
Accessory minerals				
Pyrite	—	1	2	—
Glauconite	—	1	—	—
Hornblende	1	2	Tr	1
Micrite	1	3	3	—
Foraminifers	—	5	—	—
Nannofossils	—	3	—	—
Diatoms	15	20	10	20
Sponge spicules	—	1	—	—
Silicoflagellates	—	—	Tr	Tr

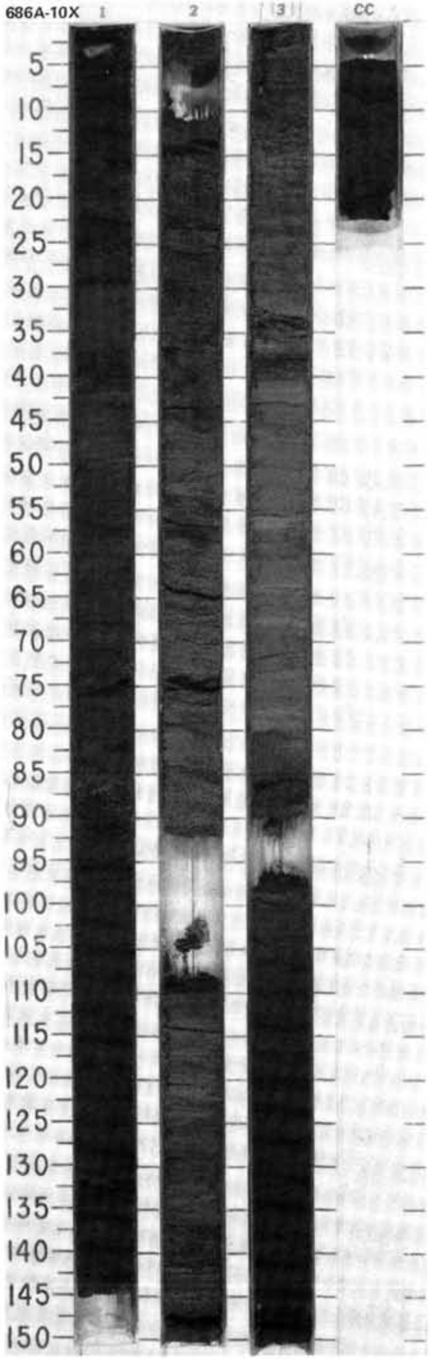

SITE 686 HOLE A CORE 11X CORED INTERVAL 529.0-538.5 mbsl; 82.2-91.7 mbsf

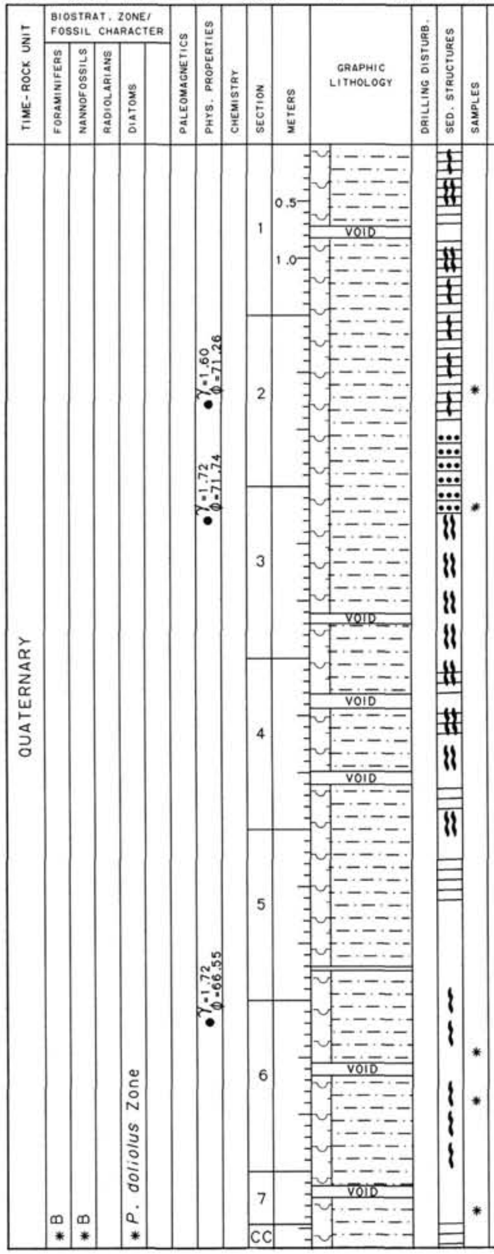

LITHOLOGIC DESCRIPTION

DIATOMACEOUS MUD

Major lithology: diatomaceous mud, olive gray (5Y 4/2), green gray (5GY 5/1), and dark olive (5Y 3/2). Laminated with minor burrowing to bioturbated, and mottled.

Minor lithologies:
1. silt and fine sand, gray (N 5/ to N 4/) in thin (1–5 cm) graded beds with sharp basal contacts.
2. diatom ooze, olive (5Y 5/4) and pale olive (5Y 6/4), in thin laminae.

SMEAR SLIDE SUMMARY (%):

	2, 65 D	3, 23 M	6, 42 M	6, 79 D	7, 34 M
TEXTURE:					
Sand	5	10	—	—	—
Silt	65	80	50	61	35
Clay	30	10	50	39	65
COMPOSITION:					
Quartz	15	40	10	1	Tr
Feldspar	15	10	10	—	—
Rock fragments	10	13	5	—	—
Mica	—	—	1	—	—
Clay	30	—	50	39	—
Volcanic glass	—	15	—	—	Tr
Calcite/dolomite	3	—	—	—	—
Accessory minerals	—	—	—	—	Tr
Pyrite	3	2	3	—	2
Glauconite	1	Tr	1	—	—
Phosphate	Tr	Tr	Tr	—	—
Hornblende	2	—	1	Tr	—
Micrite	—	5	—	Tr	—
Foraminifers	Tr	—	3	—	—
Diatoms	20	15	15	60	98
Sponge spicules	1	—	1	—	—

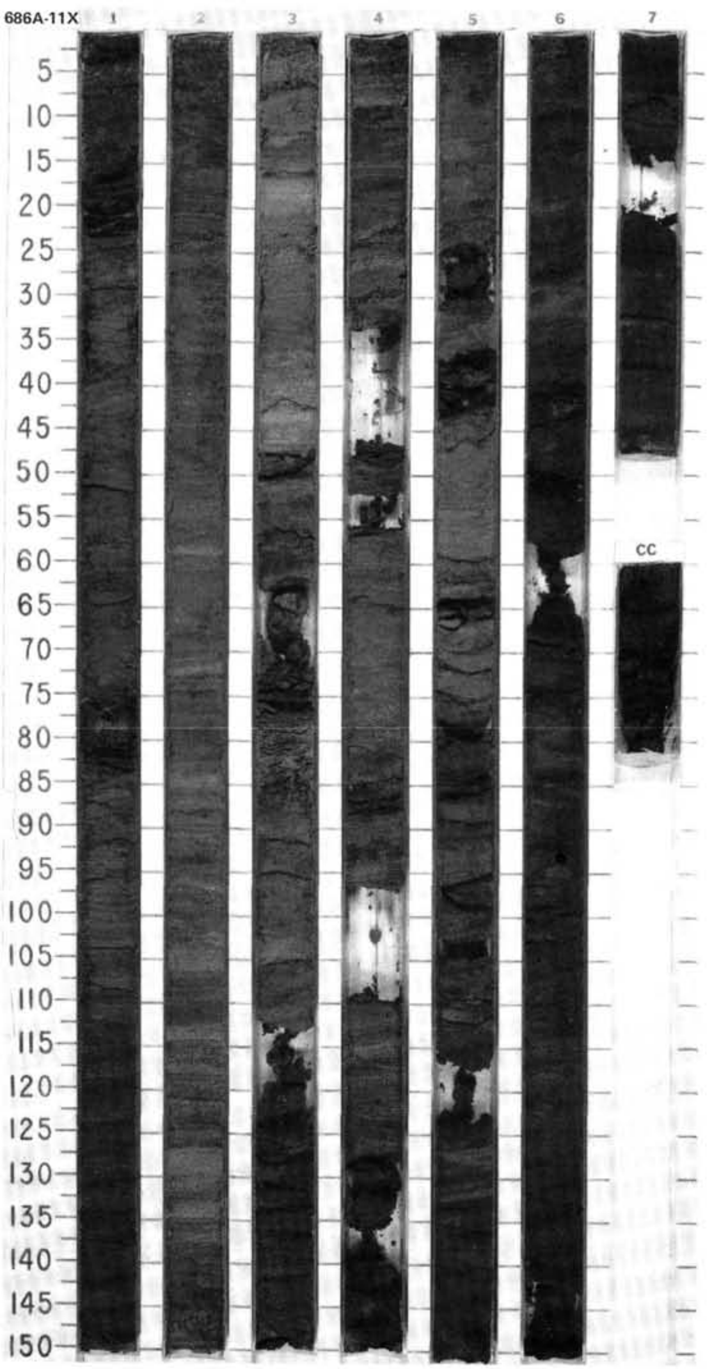

SITE 686 HOLE A CORE 12X CORED INTERVAL 538.5-548.0 mbsl; 91.7-101.2 mbsf

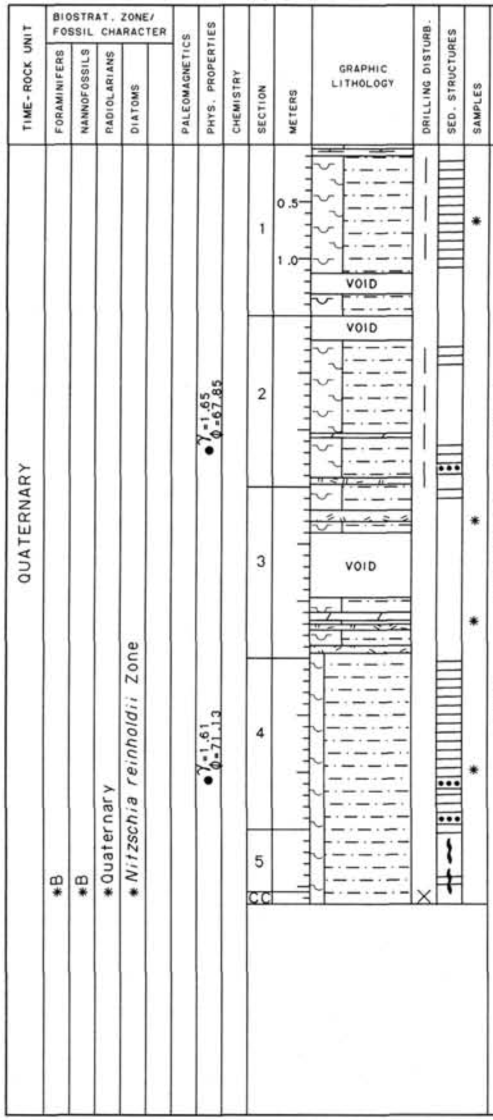

LITHOLOGIC DESCRIPTION

DIATOMACEOUS MUD

Major lithology: diatomaceous mud, olive gray and olive (5Y 4/2 and 5Y 4/3), gray (5Y 4/1) and dark olive gray (5Y 3/2). Laminated to massive, burrowed; foraminifers dispersed throughout.

Minor lithologies:
1. dolomicrite, olive (5Y 5/3).
2. silt and sand, gray (5GY 4/1), ash-bearing, in graded beds 1–5 cm thick.
3. volcanic ash, 1-cm-thick bed, gray (5Y 4/1).

SMEAR SLIDE SUMMARY (%):

	1, 72 D	3, 29 M	3, 126 M	4, 95 D
TEXTURE:				
Sand	10	10	—	30
Silt	55	40	85	50
Clay	35	50	15	20
COMPOSITION:				
Quartz	8	8	2	20
Feldspar	8	—	2	20
Rock fragments	4	2	1	5
Mica	—	—	1	1
Clay	33	48	11	23
Volcanic glass	—	15	—	—
Calcite/dolomite	7	1	5	5
Accessory minerals				
Pyrite	2	3	1	2
Glauconite	1	—	1	1
Phosphate	Tr	—	Tr	1
Hornblende	1	—	1	Tr
Micrite	—	3	65	3
Foraminifers	5	—	—	3
Nannofossils	1	Tr	—	—
Diatoms	30	20	10	15
Sponge spicules	—	—	—	1

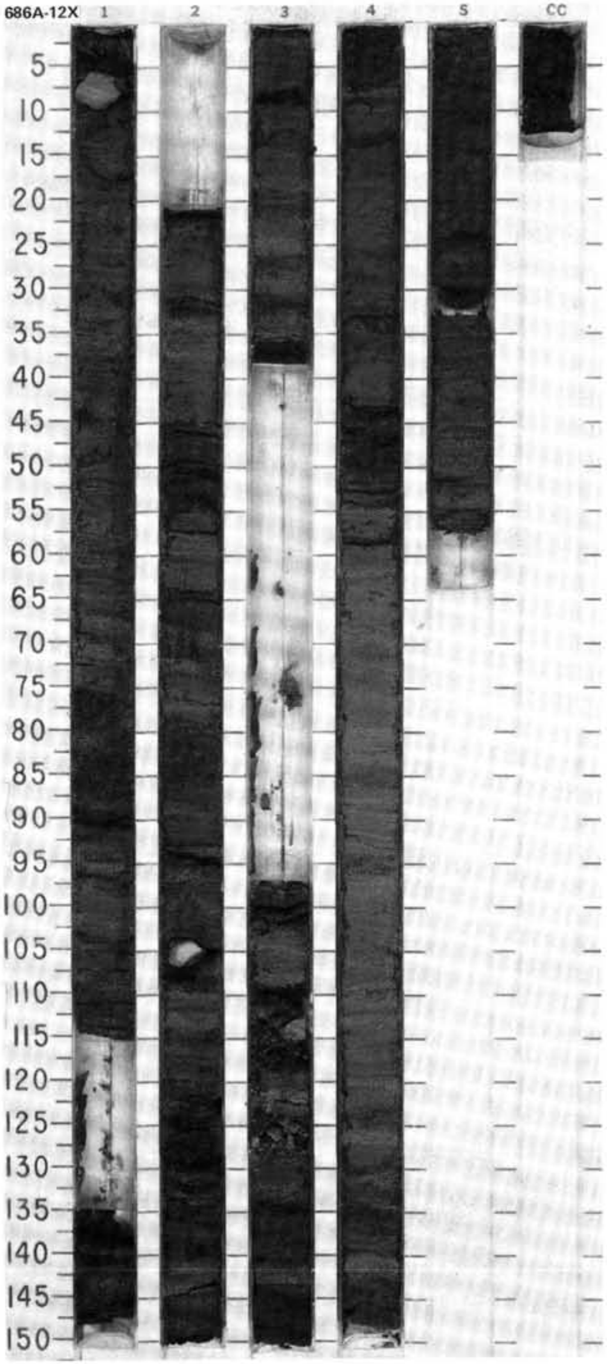

SITE 686 HOLE A CORE 13X CORED INTERVAL 548.0-557.5 mbsl; 101.2-110.7 bsf

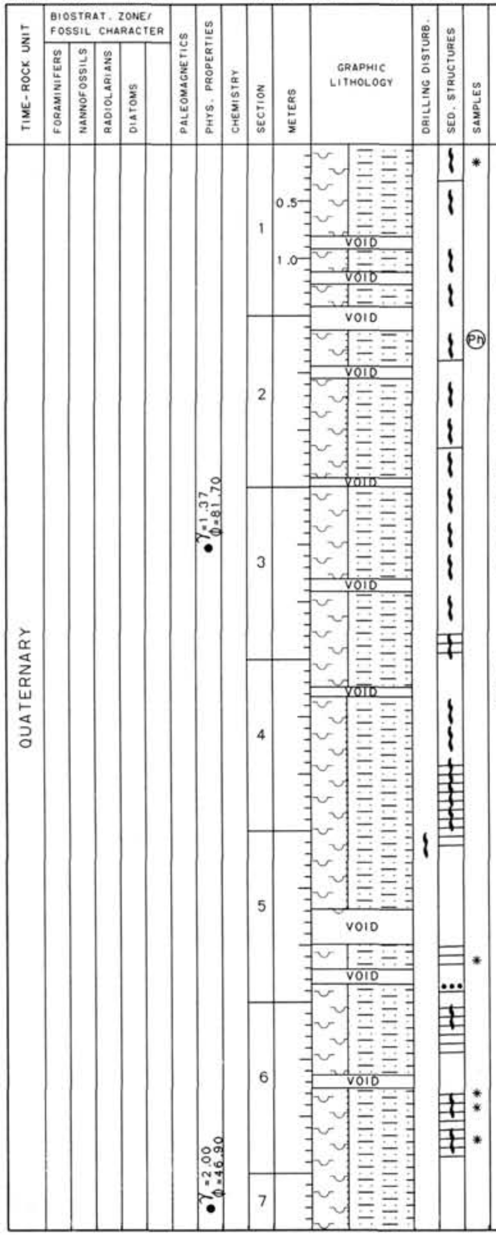

LITHOLOGIC DESCRIPTION

DIATOMACEOUS MUD

Major lithology: diatomaceous mud, dark olive gray (5Y 3/2), black (5Y 2.5/2), olive gray (5Y 4/2), laminated to massive, burrowed, minor soft sediment deformation.

Minor lithologies:
1. sand and sandy silt, olive gray (5Y 4/2) in graded beds, 1–10 cm thick.
2. diatom ooze, olive (5Y 5/4), in very thin, rare laminae.

SMEAR SLIDE SUMMARY (%):

	1, 8 D	5, 114 D	6, 82 D	6, 94 M	6, 114 M
TEXTURE:					
Sand	5	—	5	70	—
Silt	35	82	75	30	90
Clay	60	18	20	—	10
COMPOSITION:					
Quartz	4	—	20	70	—
Feldspar	5	—	20	9	—
Rock fragments	2	—	15	15	—
Mica	1	—	2	—	—
Clay	50	12	19	—	5
Volcanic glass	—	—	—	2	—
Calcite/dolomite	3	—	5	—	—
Accessory minerals					
Pyrite	2	2	1	—	—
Glauconite	1	—	1	—	—
Phosphate	1	—	1	—	—
Hornblende	Tr	—	3	4	—
Micrite	—	6	1	—	5
Collophane	—	—	Tr	—	—
Foraminifers	5	—	5	—	—
Nannofossils	Tr	—	Tr	—	—
Diatoms	25	80	5	—	90
Sponge spicules	1	—	2	—	—

(CONT.)

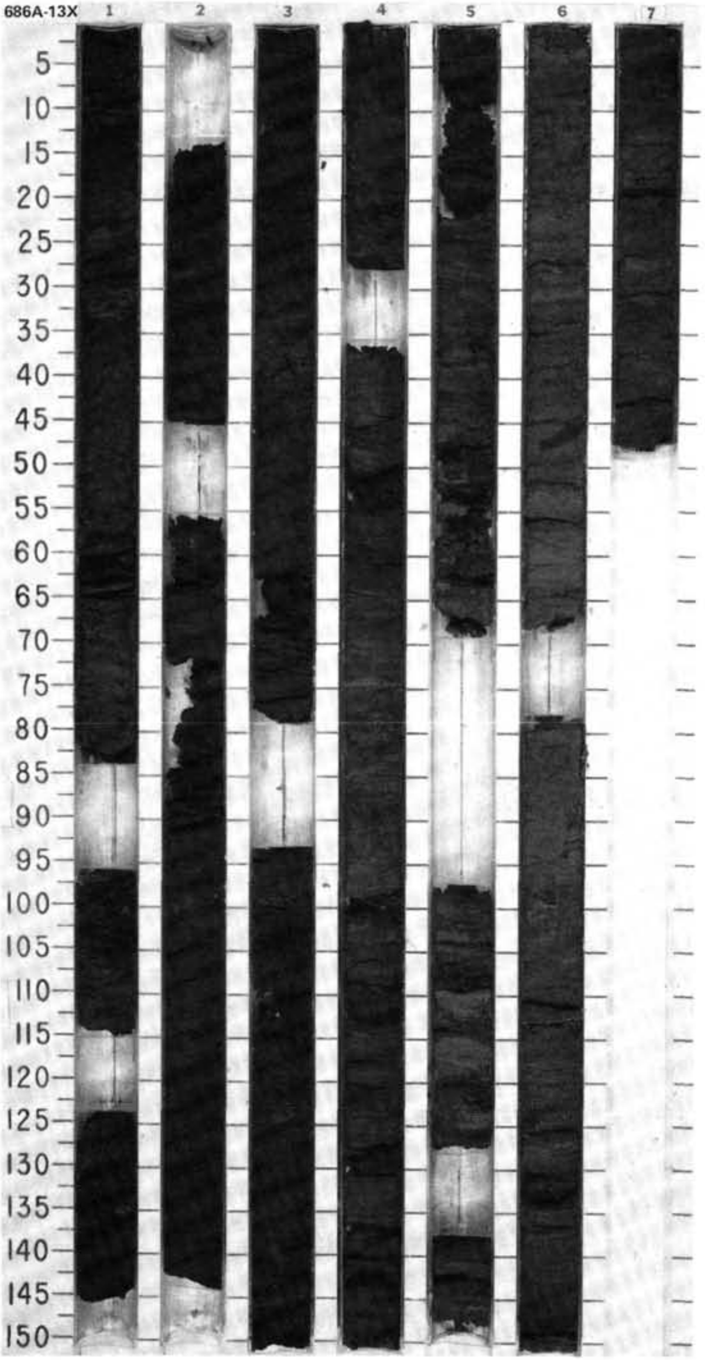

SITE 686 HOLE A CORE 13X CORED INTERVAL 548.0-557.5 mbsl; 101.2-110.7 mbsf

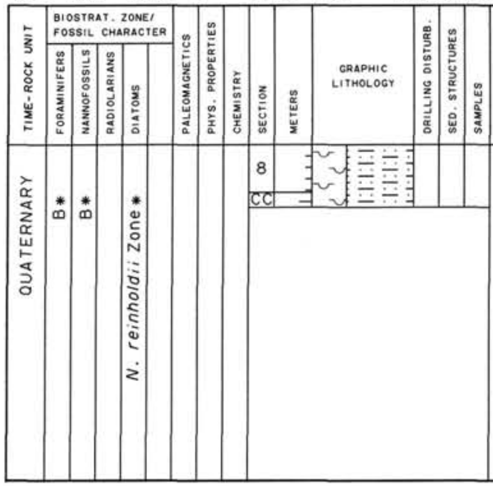

LITHOLOGIC DESCRIPTION

(CON'T.)

SITE 686 HOLE A CORE 14X CORED INTERVAL 557.5-567.0 mbsl; 110.7-120.2 mbsf

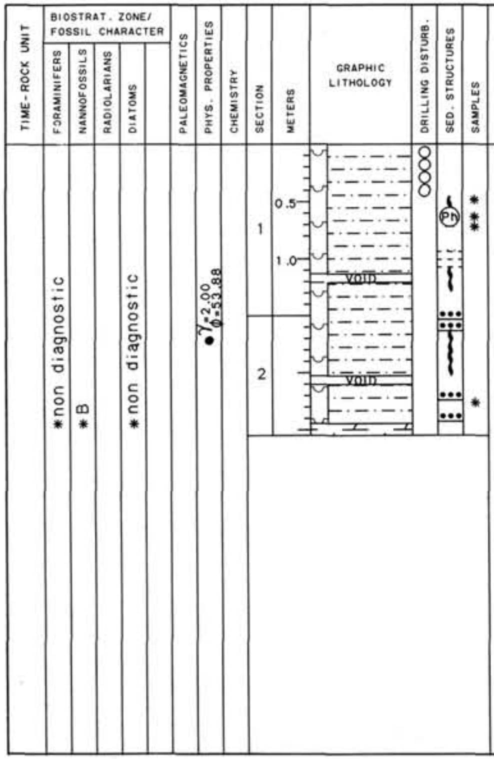

LITHOLOGIC DESCRIPTION

DIATOMACEOUS MUD, MUDDY SILT and SAND

Major lithology: diatomaceous mud and muddy silt, greenish gray (5GY 4.5/1) and dark grayish brown (2.5Y 3/2). Laminated to mottled. Sand, dark gray (2.5Y 4/1), quartz-rich, in thin graded beds.

Minor lithologies: phosphate nodule, pale olive (5Y 6/3), diatom-bearing.

SMEAR SLIDE SUMMARY (%):

	1, 46 M	1, 65 M	1, 66 M	2, 73 D
TEXTURE:				
Sand	—	80	5	10
Silt	50	20	25	50
Clay	50	—	70	40
COMPOSITION:				
Quartz	5	68	1	20
Feldspar	8	5	3	5
Rock fragments	2	20	1	15
Mica	—	Tr	—	2
Clay	48	—	10	40
Volcanic glass	—	2	—	2
Calcite/dolomite	2	—	5	—
Accessory minerals				
Pyrite	1	—	1	3
Glauconite	1	—	1	Tr
Hornblende	Tr	3	—	Tr
Micrite	3	—	5	3
Phosphorite	—	—	50	—
Foraminifers	3	Tr	5	—
Nannofossils	1	—	—	—
Diatoms	25	2	15	10
Sponge spicules	1	—	—	—
Silicoflagellates	Tr	—	3	—
Fish remains	—	—	2	—

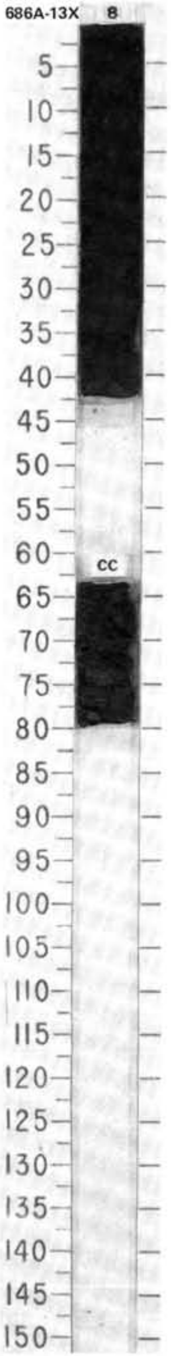

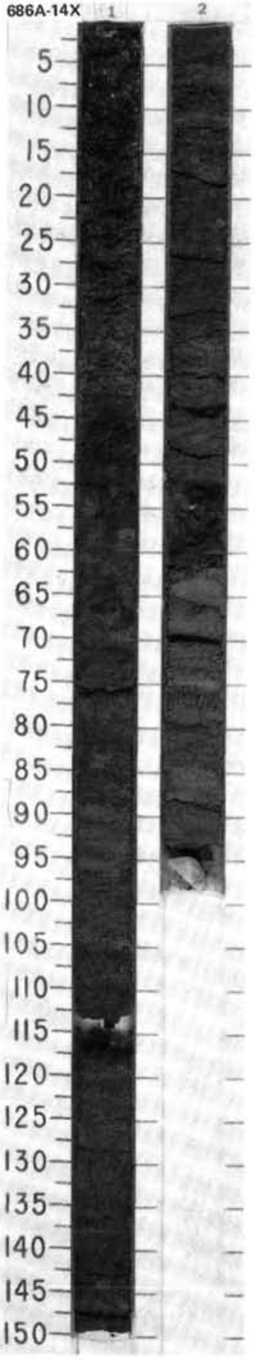

SITE 686 HOLE A CORE 15X CORED INTERVAL 567.0-576.5 mbsl; 120.2-129.7 mbsf

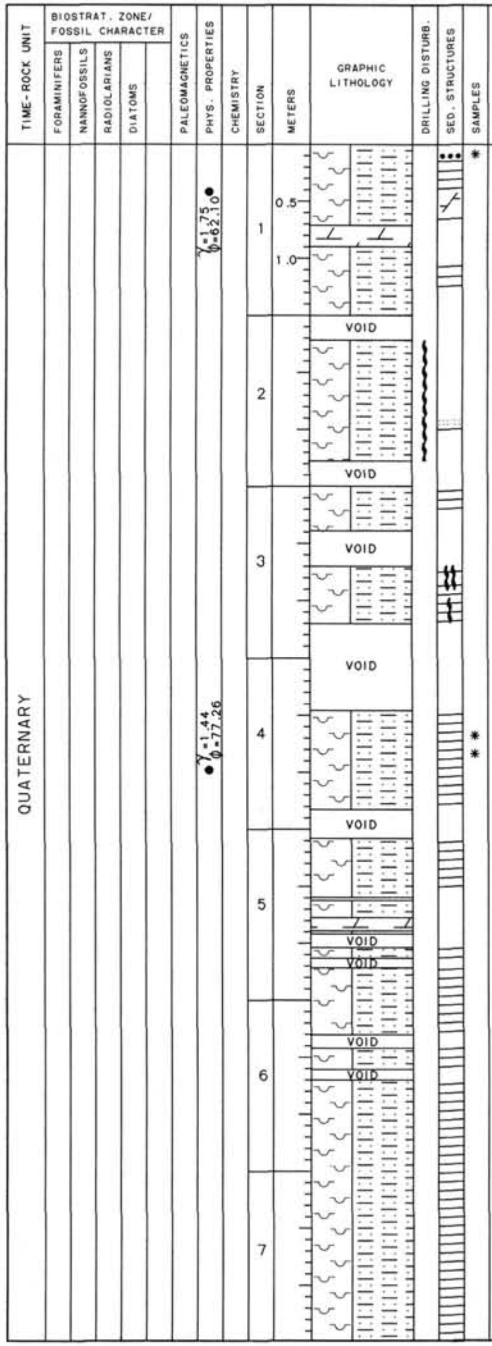

LITHOLOGIC DESCRIPTION

DIATOMACEOUS MUD

Major lithology: diatomaceous mud, olive gray (5Y 4/2 and 5/2), dark olive gray (5Y 3/2) and black (5Y 2.5/1). Laminated to faintly laminated to slightly burrowed, foraminifers dispersed throughout.

Minor lithologies:
1. dolomicrite, olive (5Y 5/3) and olive gray (5Y 5/2), with moldic porosity, in beds 2 to 10 cm thick, and as small nodules.
2. diatom ooze, olive (5Y 6/4), in thin laminae.

SMEAR SLIDE SUMMARY (%):

	1, 7 M	4, 68 D	4, 82 M	8, 102 D	8, 104 M
TEXTURE:					
Sand	80	—	—	5	5
Silt	20	60	25	30	80
Clay	—	40	75	65	15
COMPOSITION:					
Quartz	55	1	2	3	2
Feldspar	12	—	3	5	2
Rock fragments	15	—	2	2	1
Mica	6	—	1	1	—
Clay	—	37	68	40	10
Volcanic glass	5	—	—	—	—
Calcite/dolomite	—	—	5	3	Tr
Accessory minerals	5	—	—	—	—
Pyrite	2	3	2	1	Tr
Hornblende	Tr	—	—	—	—
Glaucophane	—	—	1	—	—
Micrite	—	3	—	—	—
Glauconite	—	—	—	1	—
Phosphate	—	—	—	5	2
Foraminifers	—	—	Tr	13	3
Diatoms	Tr	56	15	25	80
Sponge spicules	—	—	1	1	Tr

(CONT.)

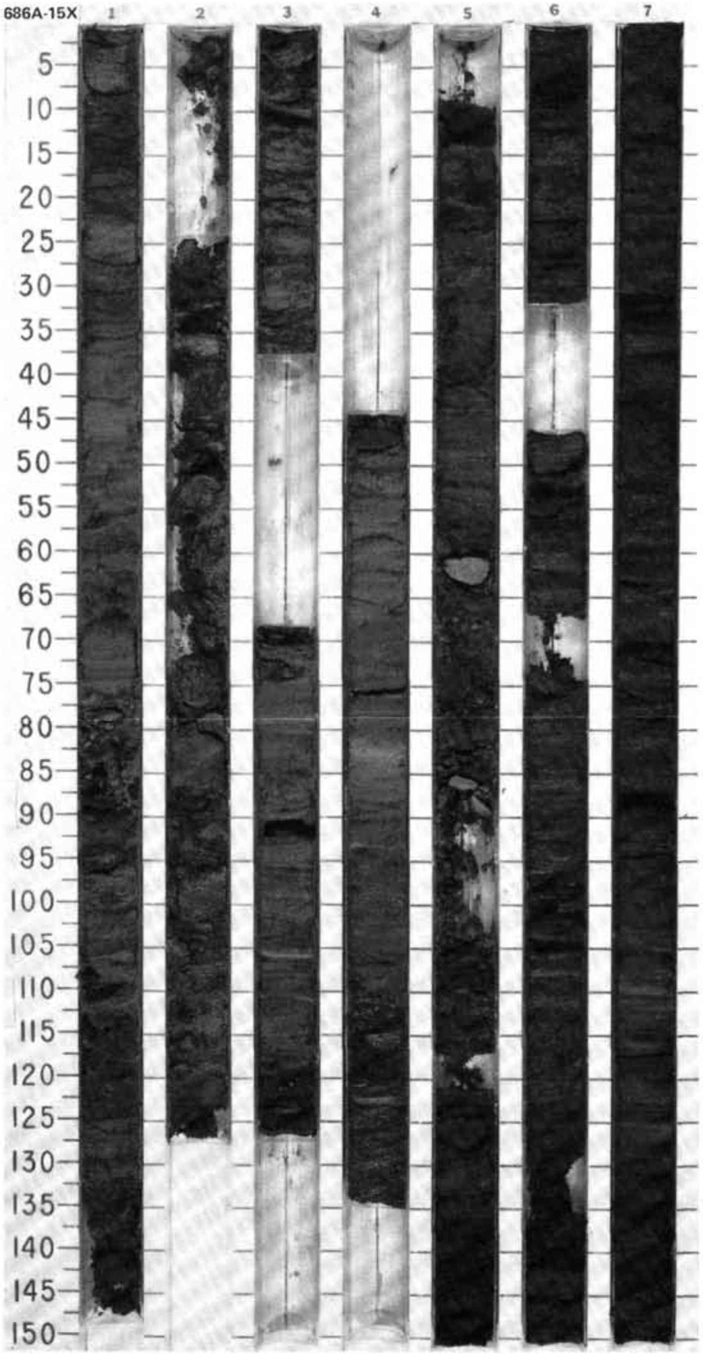

SITE 686 HOLE A CORE 15X CORED INTERVAL 567.0-576.5 mbsl; 120.2-129.7 mbsf

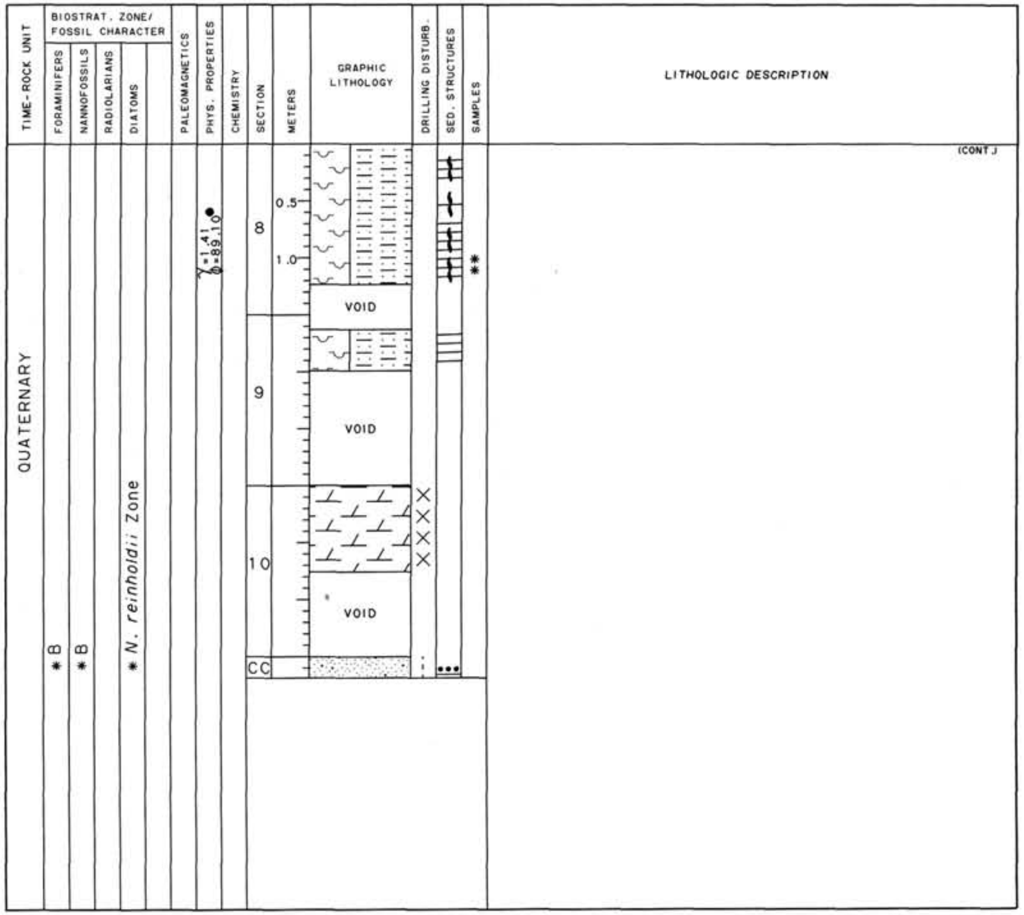

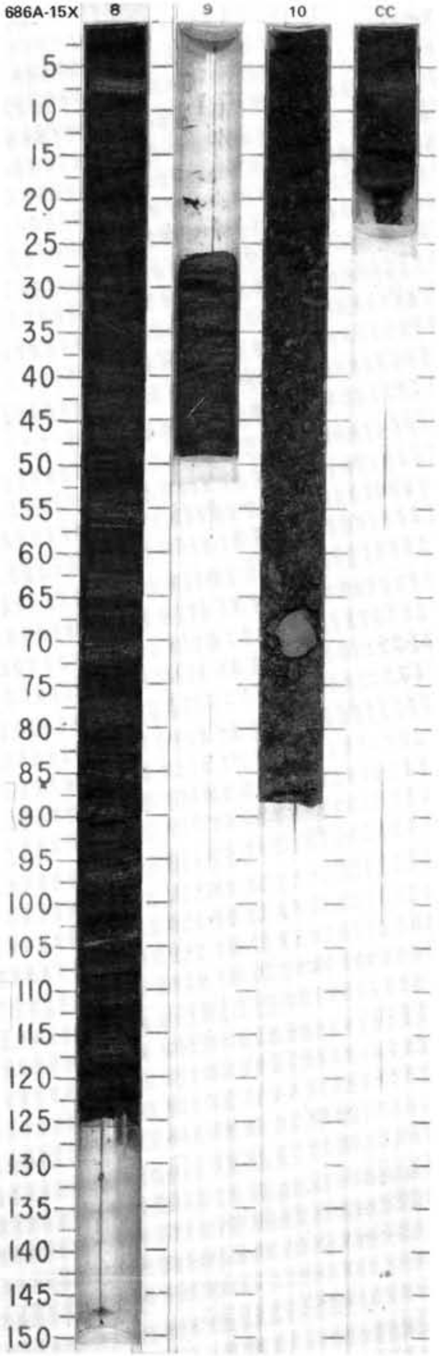

SITE 686 HOLE A CORE 16X CORED INTERVAL 576.5-586.0 mbsl; 129.7-139.2 mbsf

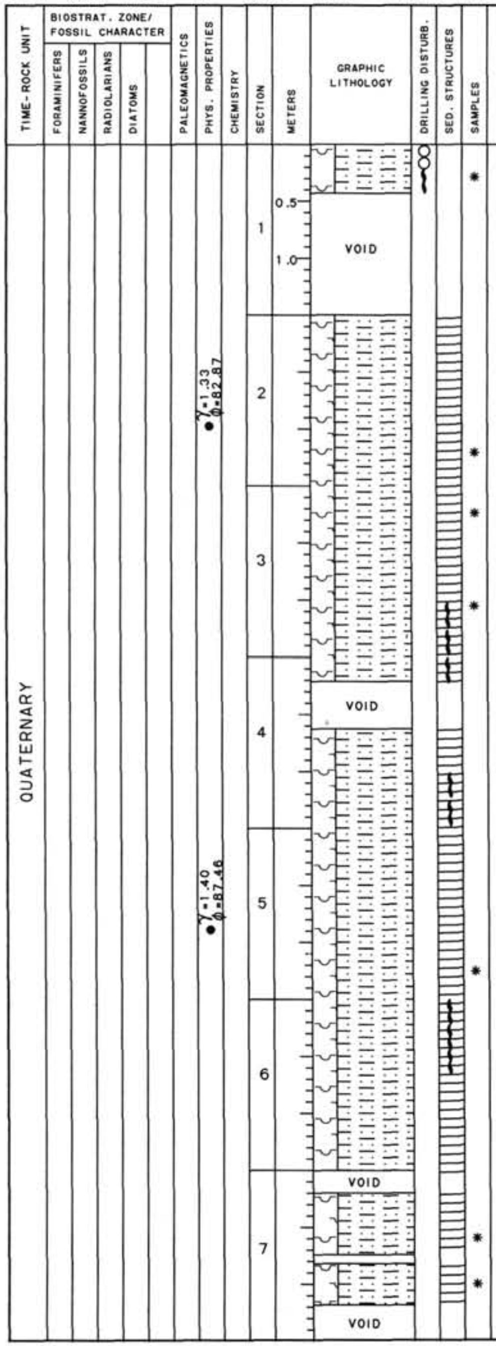

LITHOLOGIC DESCRIPTION

DIATOMACEOUS MUD

Major lithology: diatomaceous mud, olive gray to dark olive gray (5Y 4/2 to 3/2). In part well-laminated with thin laminae of olive (5Y 5/4) diatomaceous ooze, in part bioturbated; foraminifer-rich.

Minor lithologies: nodular dolomite.

SMEAR SLIDE SUMMARY (%):

	1, 20 D	2, 133 M	3, 33 M	3, 109 D	5, 125 M	7, 64 D	7, 100 D
TEXTURE:							
Sand	—	—	—	—	14	—	—
Silt	50	50	15	55	85	60	50
Clay	50	50	85	45	1	40	50
COMPOSITION:							
Quartz	3	Tr	Tr	5	—	5	10
Feldspar	5	—	—	10	—	10	10
Rock fragments	2	—	—	2	—	2	5
Mica	1	—	—	—	—	—	1
Clay	50	—	—	45	—	40	40
Calcite/dolomite	3	—	—	3	—	5	5
Accessory minerals							
Pyrite	2	1	1	2	1	2	3
Glauconite	2	—	—	1	—	—	1
Phosphate	—	—	—	3	—	3	Tr
Micrite	—	50	—	—	—	—	—
Hornblende	—	—	—	1	—	1	—
Foraminifers	2	—	—	3	—	10	3
Nannofossils	—	—	—	—	1	2	—
Diatoms	30	49	99	25	98	20	20
Radiolarians	Tr	—	—	—	—	Tr	Tr
Sponge spicules	Tr	—	—	Tr	—	—	Tr
Silicoflagellates	—	—	—	Tr	—	—	—

(CONT.)

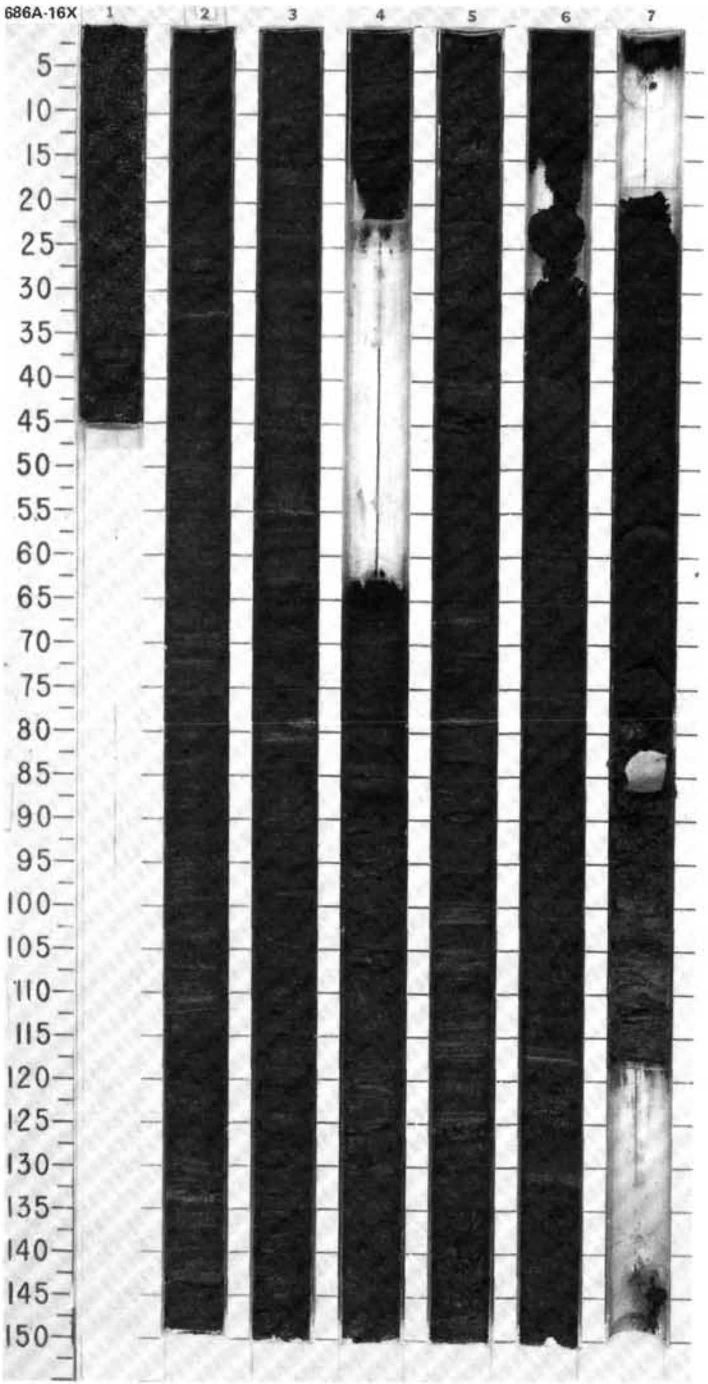

SITE 686 HOLE A CORE 16X CORED INTERVAL 576.5-586.0 mbsl; 129.7-139.2 mbsf

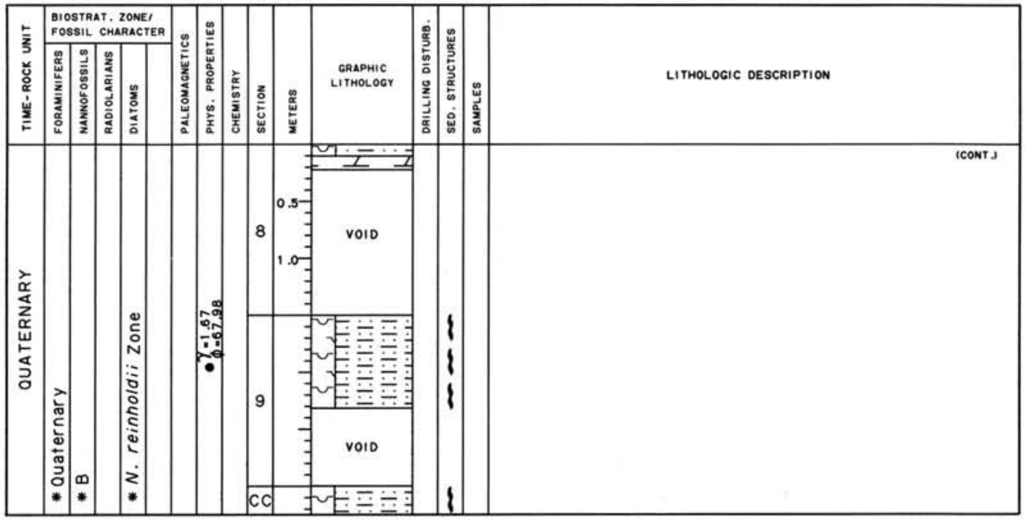

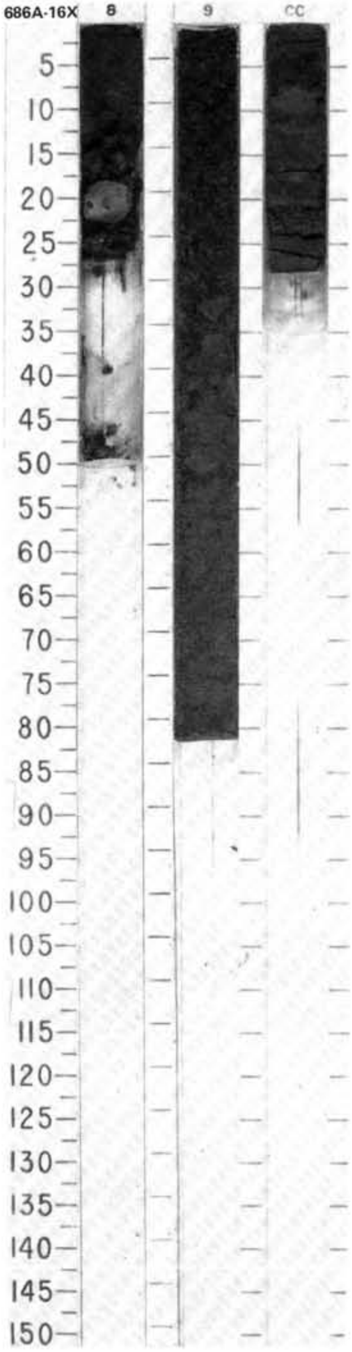

SITE 686 HOLE A CORE 17X CORED INTERVAL 586.0-595.5 mbsl; 139.2-148.7 mbsf

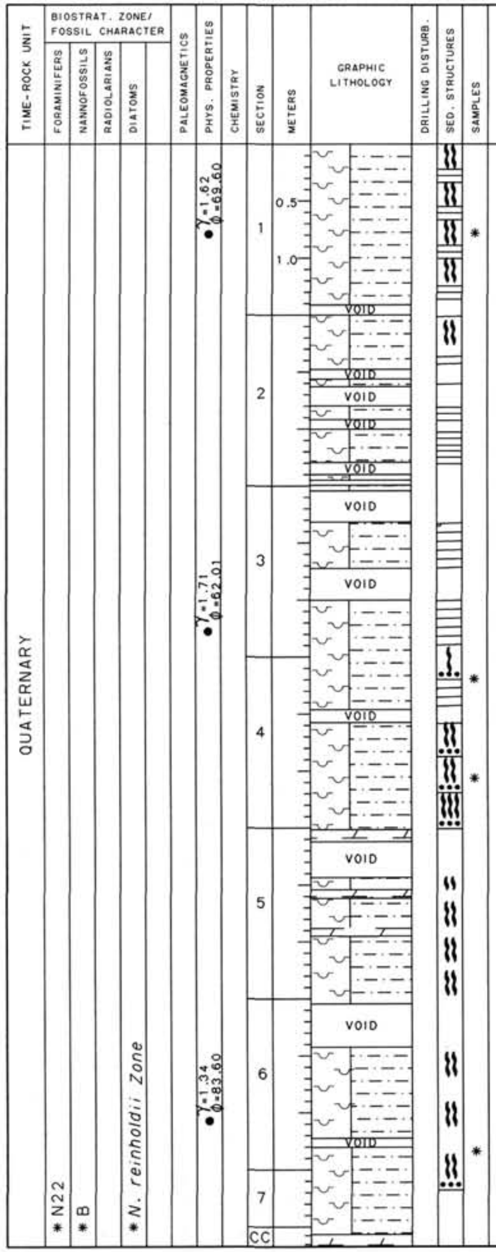

LITHOLOGIC DESCRIPTION

DIATOMACEOUS SILTY AND SANDY MUD

Major lithology: diatomaceous silty and sandy mud, olive gray to dark olive gray (5Y 4/2 to 5/2). Mostly bioturbated with a few laminated intervals; foraminifer-bearing.

Minor lithologies:
1. dolomite, olive (5Y 4/2), as lithified nodules and partly lithified layers.
2. silty sand, dark olive gray (5Y 3/2), in thin graded layers with sharp basal contacts and as diffuse, burrowed layers and patches.

SMEAR SLIDE SUMMARY (%):

	1, 75 D	4, 14 M	4, 106 D	6, 132 M
TEXTURE:				
Sand	10	45	20	—
Silt	40	35	50	2
Clay	60	20	30	98
COMPOSITION:				
Quartz	5	10	3	1
Feldspar	5	15	3	1
Rock fragments	5	25	8	—
Clay	20	20	15	—
Volcanic glass	11	5	—	—
Calcite/dolomite	2	2	2	—
Accessory minerals				
Pyrite	8	—	4	1
Phosphate	—	3	—	—
Glauconite	—	Tr	—	—
Foraminifers	1	5	—	—
Nannofossils	—	—	5	—
Diatoms	40	13	60	2
Radiolarians	—	—	—	Tr
Sponge spicules	1	—	Tr	—
Silicoflagellates	—	Tr	Tr	—
Fish remains	2	2	Tr	—
Dolomite	—	—	—	95

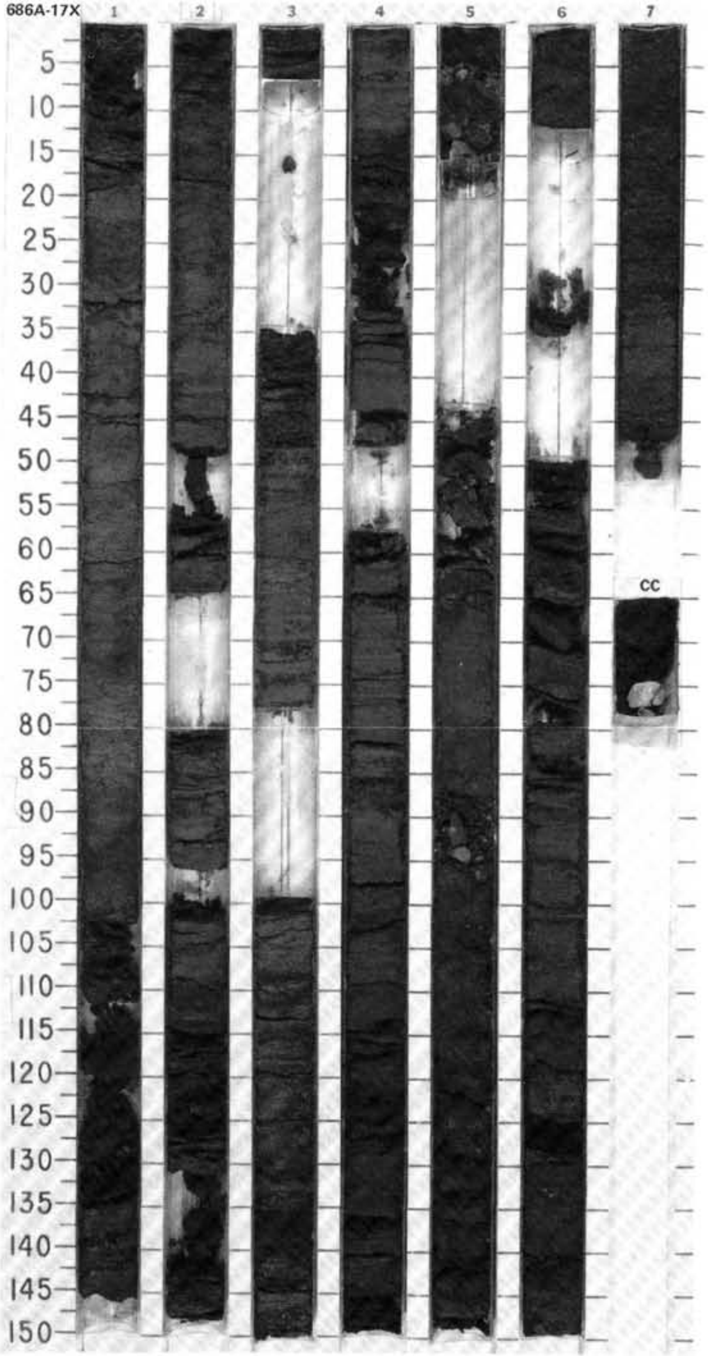

SITE 686 HOLE A CORE 18X CORED INTERVAL 595.5-605.0 mbsl; 148.7-158.2 mbsf

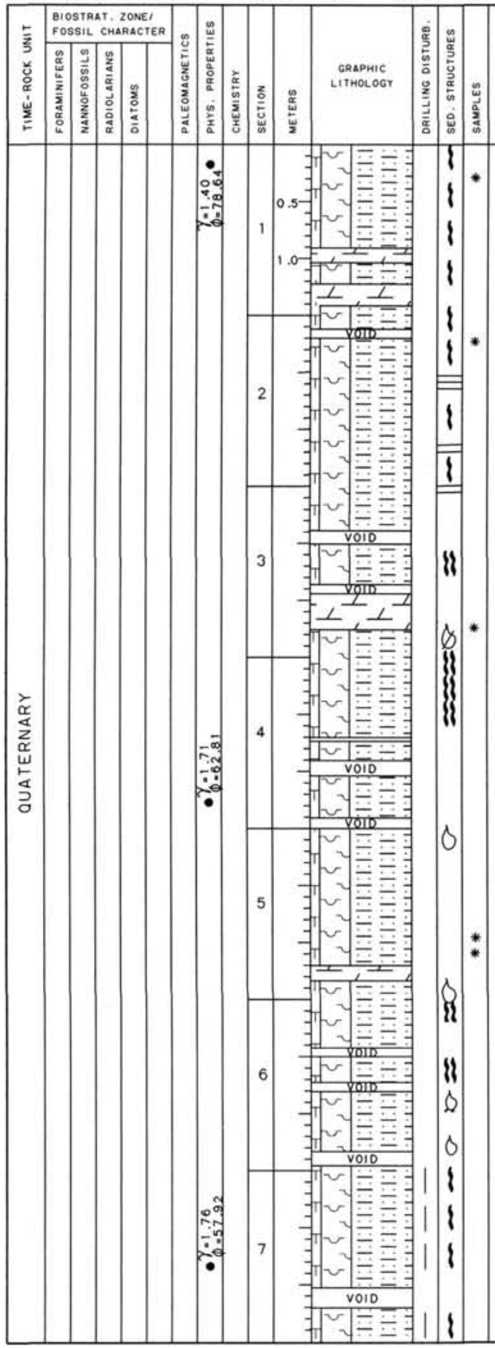

LITHOLOGIC DESCRIPTION

DIATOMACEOUS MUD

Major lithology: diatomaceous mud, olive gray (5Y 4/2). Mainly massive and burrowed, with a few small patches and thin laminae of pale olive (5Y 6/3) diatomaceous ooze, foraminifer-bearing.

Minor lithologies:
1. dolomite, olive (5Y 5/2) in layers up to 35 cm thick.
2. shelly layers in diatomaceous mud, 2–3 cm thick.
3. paired bivalve shells in Section 5, 127 and 134 cm.
4. silt, ash-rich, in layers up to 10 cm thick.

SMEAR SLIDE SUMMARY (%):

	1, 22 D	2, 25 M	3, 124 M	5, 90 M	5, 94 M
TEXTURE:					
Sand	25	20	10	15	25
Silt	35	60	75	55	55
Clay	40	20	15	30	20
COMPOSITION:					
Quartz	2	Tr	3	10	5
Feldspar	5	Tr	2	10	5
Rock fragments	3	Tr	Tr	15	15
Clay	25	10	10	15	10
Volcanic glass	Tr	Tr	—	30	40
Dolomite	—	2	30	—	—
Accessory minerals					
Pyrite	4	2	—	10	—
Micrite	15	—	40	5	15
Foraminifers	10	Tr	5	—	10
Nannofossils	—	—	—	—	Tr
Diatoms	35	86	10	5	—
Sponge spicules	—	—	Tr	—	—
Fish remains	1	—	—	—	—

(CON'T.)

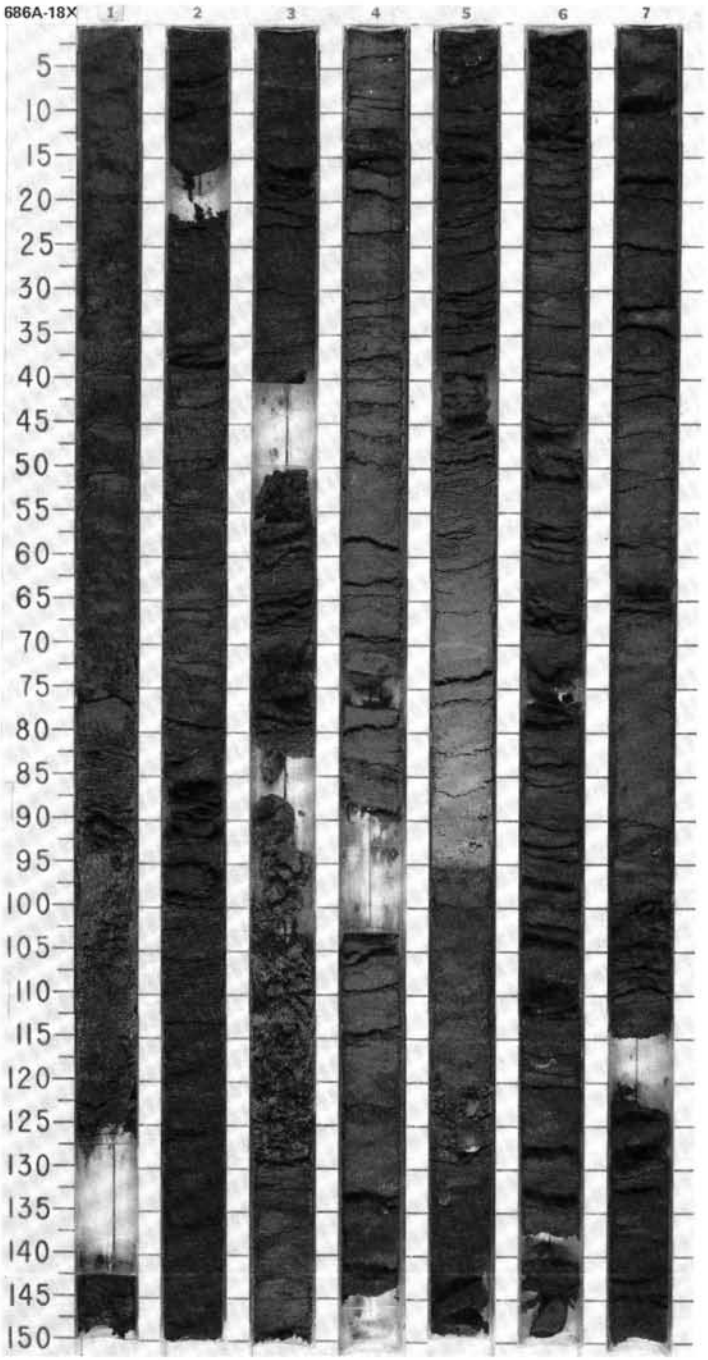

SITE 686 HOLE A CORE 18X CORED INTERVAL 595.5-605.0 mbsl; 148.7-158.2 mbsf

TIME-ROCK UNIT	BIOSTRAT. ZONE/ FOSSIL CHARACTER					PALEOMAGNETICS	PHYS. PROPERTIES	CHEMISTRY	SECTION	METERS	GRAPHIC LITHOLOGY	DRILLING DISTURB.	SED. STRUCTURES	SAMPLES	LITHOLOGIC DESCRIPTION
	FORAMINIFERS	NANNOFOSSILS	RADIOLARIANS	DIATOMS											
QUATERNARY	Pleistocene ? *	insignificant *		*N. reinholdii* Zone *					8						(CON'T.)
									CC						

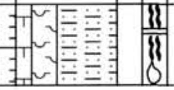

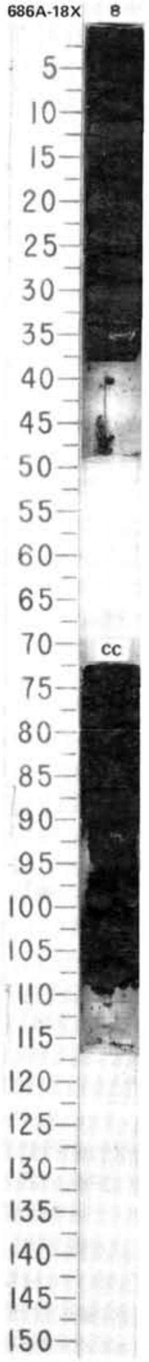

SITE 686 HOLE A CORE 19X CORED INTERVAL 605.0-614.5 mbsl; 158.2-167.7 mbsf

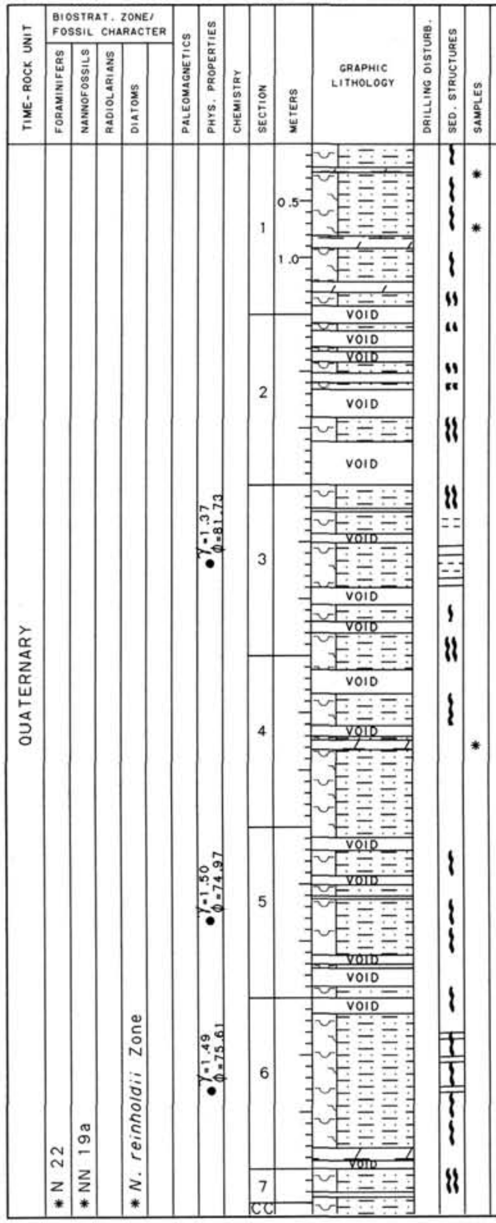

LITHOLOGIC DESCRIPTION

DIATOMACEOUS MUD

Major lithology: diatomaceous mud, dark olive gray (5Y 3/2). Foraminifer-bearing, silty to sandy, mostly bioturbated; a few laminae of olive (5Y 4/3) diatomaceous ooze.

Minor lithologies: dolomite, olive (5Y 5/2.5 and 5Y 4.5/4), as nodules and as a bed 6 cm thick.

SMEAR SLIDE SUMMARY (%):

	1, 22 M	1, 73 D	4, 82 M
TEXTURE:			
Sand	5	5	—
Silt	40	65	30
Clay	55	30	70
COMPOSITION:			
Quartz	2	10	—
Feldspar	3	15	—
Rock fragments	—	10	—
Clay	—	24	—
Volcanic glass	—	5	—
Dolomite	75	Tr	94
Accessory minerals			
Pyrite	5	5	1
Pyroxene	Tr	—	—
Diatoms	15	30	5
Radiolarians	—	1	—
Sponge spicules	Tr	Tr	—

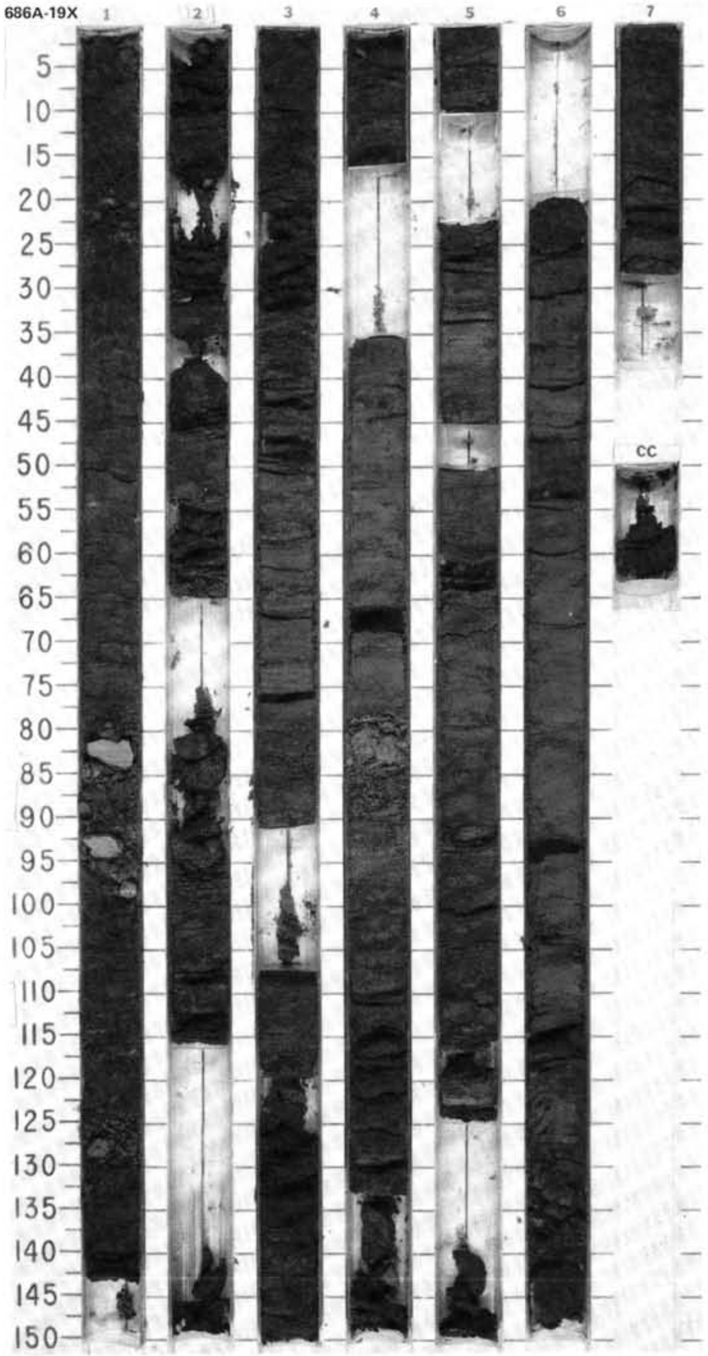

SITE 686 HOLE A CORE 20X CORED INTERVAL 614.5-624.0 mbsl; 167.7-177.2 mbsf

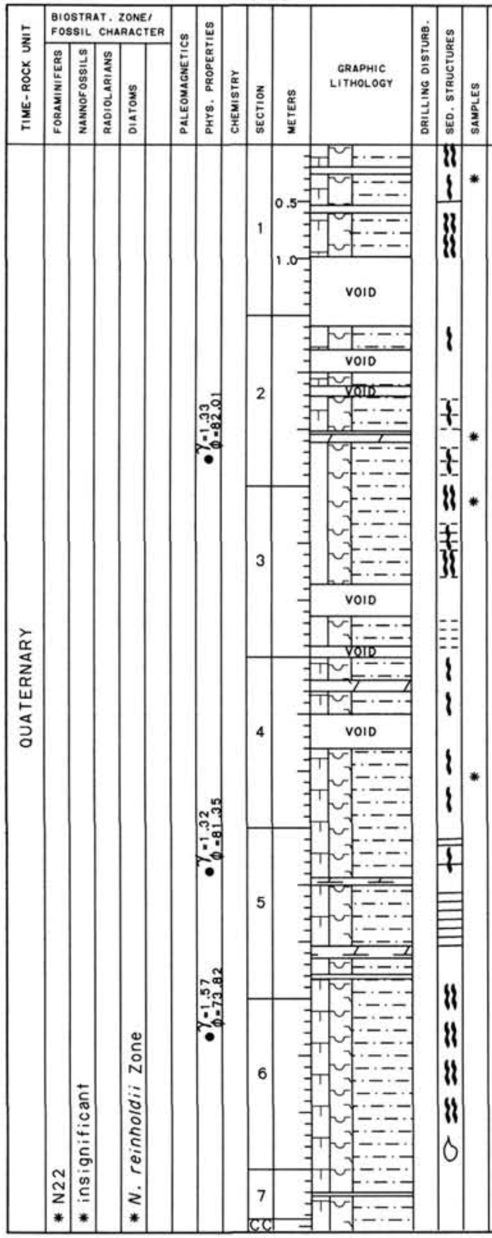

LITHOLOGIC DESCRIPTION

DIATOMACEOUS MUD

Major lithology: diatomaceous mud, dark olive gray (5Y 3/2). Foraminifer-bearing, mostly mottled and bioturbated, in part faintly bedded with thin olive (5Y 4/4) interbeds of diatomaceous ooze.

Minor lithologies:
1. dolomite, layers 2–3 cm thick, laminated to massive, pronounced moldic porosity.
2. concentrations of small bivalve shells in burrows and in thin layers.

SMEAR SLIDE SUMMARY (%):

	1, 30 D	2, 111 M	3, 23 M	4, 114 D
TEXTURE:				
Sand	5	10	10	10
Silt	55	25	50	30
Clay	40	65	40	60
COMPOSITION:				
Quartz	10	Tr	2	5
Feldspar	10	5	3	5
Rock fragments	—	—	Tr	—
Mica	—	—	Tr	—
Clay	20	10	20	50
Volcanic glass	—	—	Tr	—
Calcite	10	—	—	5
Accessory minerals				
Apatite	Tr	—	Tr	—
Pyrite	5	5	5	5
Dolomite	—	45	10	—
Foraminifers	10	—	—	10
Diatoms	35	35	60	20
Sponge spicules	—	—	Tr	—

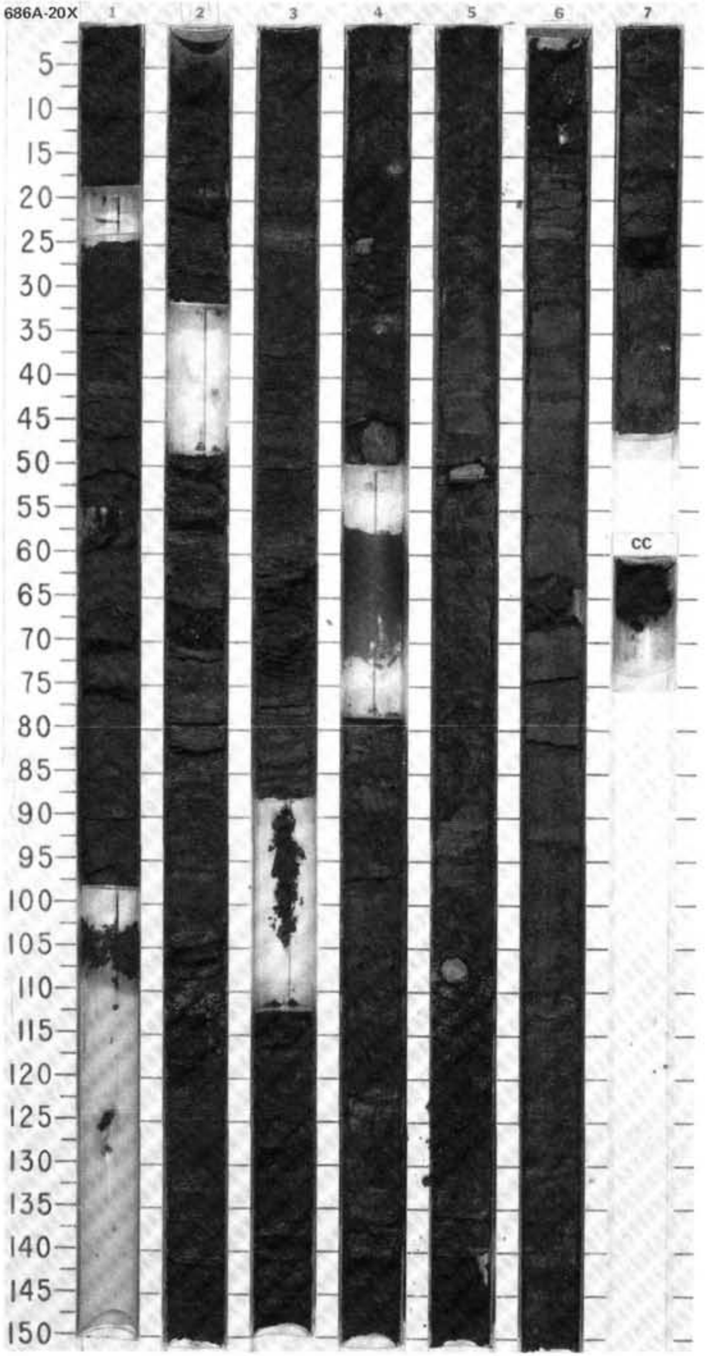

SITE 686 HOLE A CORE 21X CORED INTERVAL 624.0-633.5 mbsl; 177.2-186.7 mbsf

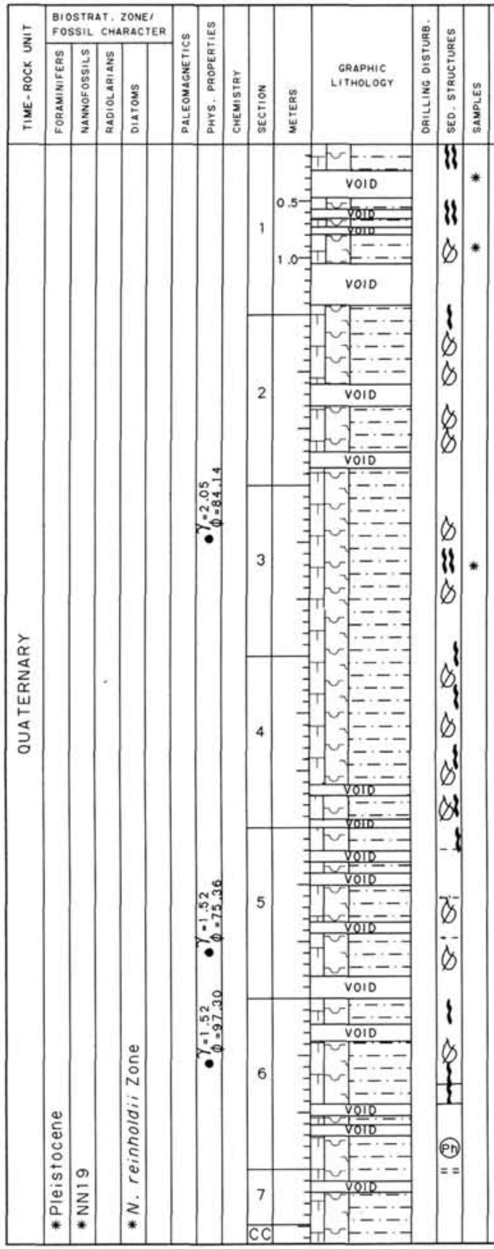

LITHOLOGIC DESCRIPTION

DIATOMACEOUS MUD

Major lithology: diatomaceous mud, dark olive gray (5Y 3/2), olive gray (5Y 4/2), dark gray (5Y 4/1) with a few thin layers of diatomaceous ooze. Faintly bedded to homogenous, burrowed.

Minor lithologies:
1. concentrations of bivalve shells in layers and burrows.
2. dolomite, olive gray (5Y 5/2).
3. phosphate nodule, olive brown (2.5Y 4/4), hard.

SMEAR SLIDE SUMMARY (%):

	1, 98 D	3, 71 D
TEXTURE:		
Sand	15	10
Silt	55	55
Clay	30	35
COMPOSITION:		
Quartz	15	19
Feldspar	10	25
Rock fragments	—	5
Clay	5	20
Volcanic glass	Tr	5
Dolomite	—	—
Accessory minerals		
Pyrite	—	5
Pyroxene	—	—
Apatite	—	Tr
Calcite	5	—
Zircon	Tr	—
Amphibole	Tr	—
Foraminifers	15	5
Diatoms	20	15
Sponge spicules	Tr	1

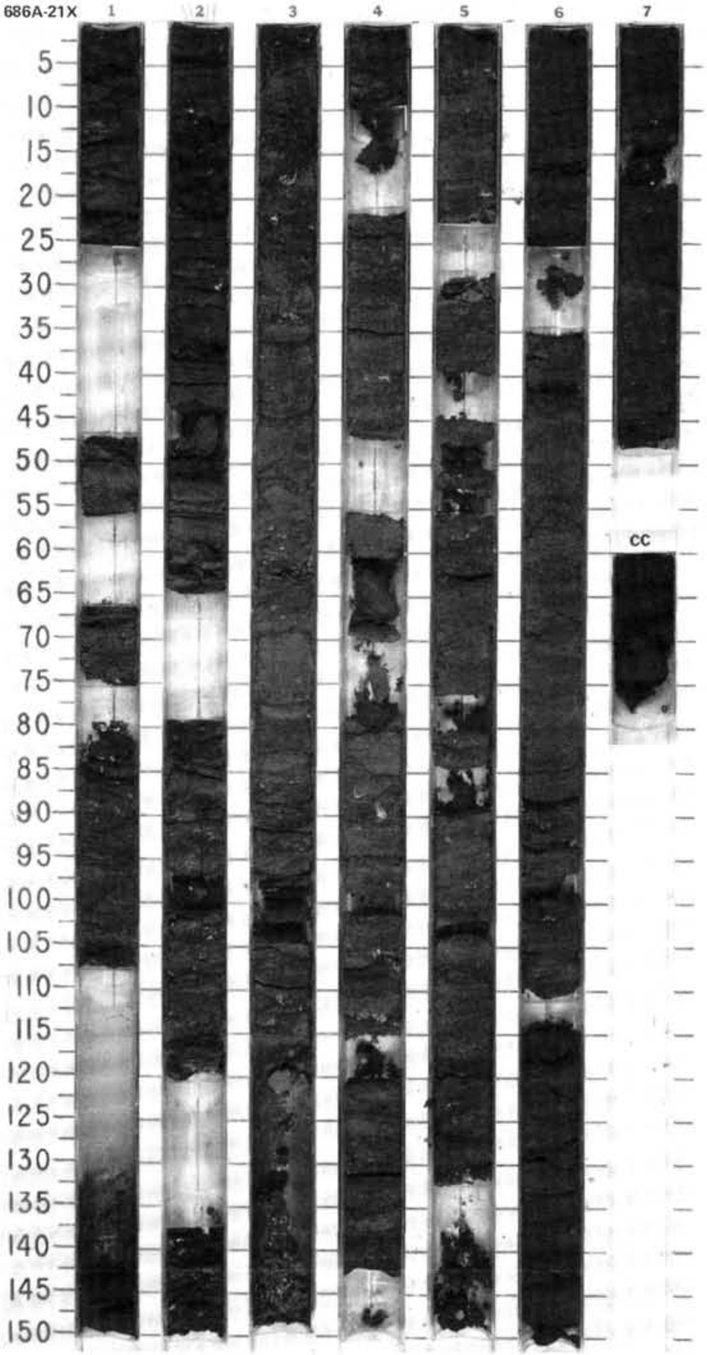

SITE 686 HOLE A CORE 22X CORED INTERVAL 633.5-643.0 mbsl; 186.7-196.2 mbsf

TIME-ROCK UNIT	BIOSTRAT. ZONE/ FOSSIL CHARACTER					PALEOMAGNETICS	PHYS. PROPERTIES	CHEMISTRY	SECTION	METERS	GRAPHIC LITHOLOGY	DRILLING DISTURB.	SED. STRUCTURES	SAMPLES
	FORAMINIFERS	NANNOFOSSILS	RADIOLARIANS	DIATOMS										
QUATERNARY	Pleistocene *	NN19a *		*N. reinholdii* Zone *					1 CC	0.5	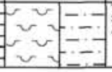	× ×	Ⓟⓗ ~	*

LITHOLOGIC DESCRIPTION

DIATOMACEOUS MUD

Major lithology: diatomaceous mud, olive gray (5Y 4/2).

Minor lithologies:
1. phosphate nodules in drilling breccia.
2. pieces of dolomite in drilling breccia.

SMEAR SLIDE SUMMARY (%):

	CC, 1 D
TEXTURE:	
Sand	10
Silt	50
Clay	40
COMPOSITION:	
Quartz	5
Feldspar	5
Clay	35
Calcite/dolomite	5
Accessory minerals	
Pyrite	5
Foraminifers	5
Nannofossils	Tr
Diatoms	40
Sponge spicules	Tr

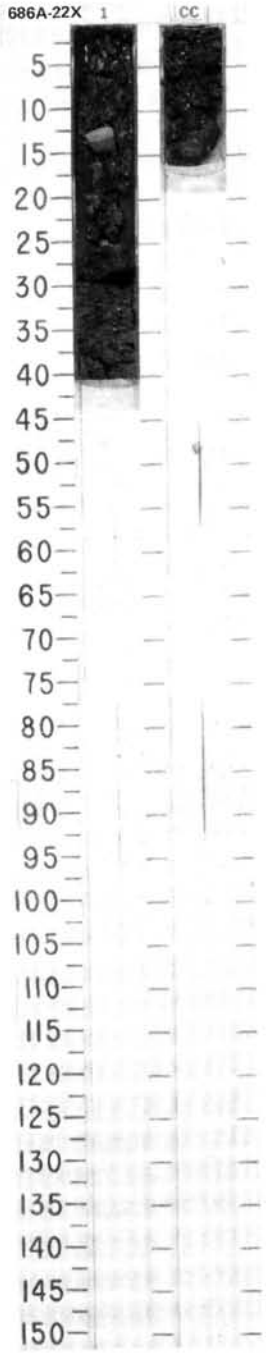

SITE 686 HOLE A CORE 23X CORED INTERVAL 643.0-652.5 mbsl; 196.2-205.7 mbsf

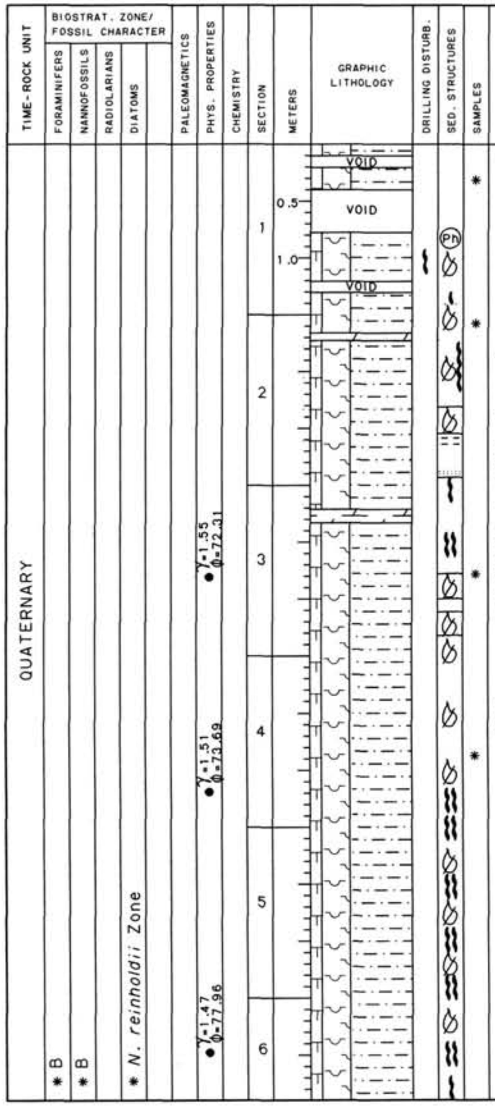

LITHOLOGIC DESCRIPTION

DIATOMACEOUS MUD

Major lithology: diatomaceous mud, olive gray (5Y 4/2) to very dark gray (5Y 3/2). Locally dolomitic; homogenous, burrowed to faintly bedded, foraminifer-bearing, with a few thin layers of diatomaceous ooze.

Minor lithologies:
1. bivalve shell fragments.
2. phosphate nodules, hard, olive brown (2.5Y 4/4).
3. phosphatically cemented sandstone.
4. sandy silt, glauconitic-phosphatic, in a 3-cm-thick layer.
5. sand, with abundant bivalve skeletal fragments, in beds 2–7 cm thick.
6. dolomite beds.

SMEAR SLIDE SUMMARY (%):

	1, 31 D	2, 6 M	3, 76 M	4, 81 D
TEXTURE:				
Sand	5	25	70	5
Silt	60	55	20	30
Clay	35	20	10	65
COMPOSITION:				
Quartz	9	5	20	8
Feldspar	20	5	20	15
Rock fragments	Tr	10	—	—
Clay	10	Tr	—	40
Volcanic glass	1	Tr	—	2
Calcite/dolomite	5	40	40	15
Accessory minerals				
Phosphate	—	5	—	—
Amphibole	—	Tr	Tr	—
Pyrite	5	—	5	5
Micrite	—	30	—	—
Zeolite(?)	—	—	5	—
Foraminifers	10	—	10	—
Nannofossils	—	—	Tr	—
Diatoms	30	5	Tr	15

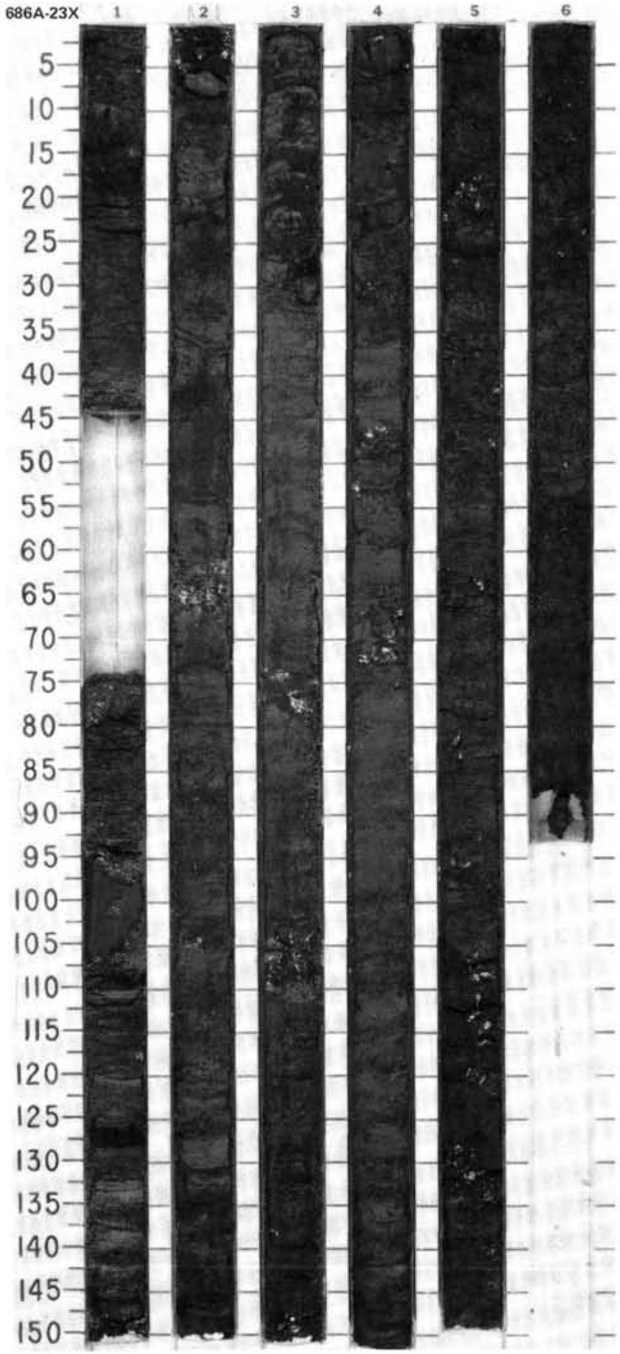

SITE 686 HOLE B CORE 1H CORED INTERVAL 446.8-455.3 mbsl; 0.0-8.5 mbsf

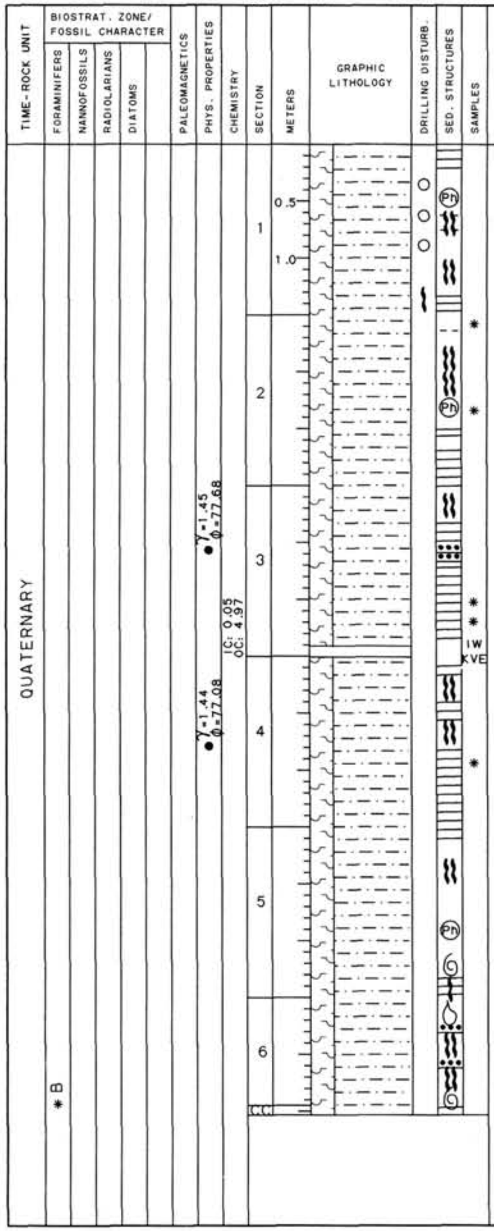

LITHOLOGIC DESCRIPTION

DIATOMACEOUS MUD

Major lithology: diatomaceous mud, black, dark olive gray, and dark gray (5Y 2.5/2, 5Y 3/2, 5Y 4/3, and 5Y 4/2). Laminated to bioturbated; foraminifer-bearing, some thin graded layers with silty basal portions, a few small slump structures.

Minor lithologies:
1. phosphate nodules, dark, hard.
2. dolomite.
3. ash-bearing quartzo-feldspathic sand.
4. diatomaceous ooze; olive (5Y 5/6), in thin laminae.
5. thin layers of bivalve shell fragments.

SMEAR SLIDE SUMMARY (%):

	2, 6 M	2, 85 M	3, 103 D	3, 116 D	4, 96 M
TEXTURE:					
Sand	5	10	—	5	—
Silt	70	5	40	40	60
Clay	25	85	60	55	40
COMPOSITION:					
Quartz	25	1	10	15	2
Feldspar	30	1	10	15	2
Rock fragments	8	—	—	Tr	—
Clay	Tr	—	55	46	30
Volcanic glass	10	4	Tr	—	Tr
Calcite/dolomite	5	2	Tr	—	—
Accessory minerals					
Pyrite	5	1	5	2	—
Hornblende	2	—	—	—	—
Apatite	Tr	90	—	—	—
Diatoms	15	1	20	20	66
Radiolarians	—	—	—	—	Tr
Sponge spicules	—	Tr	Tr	2	—

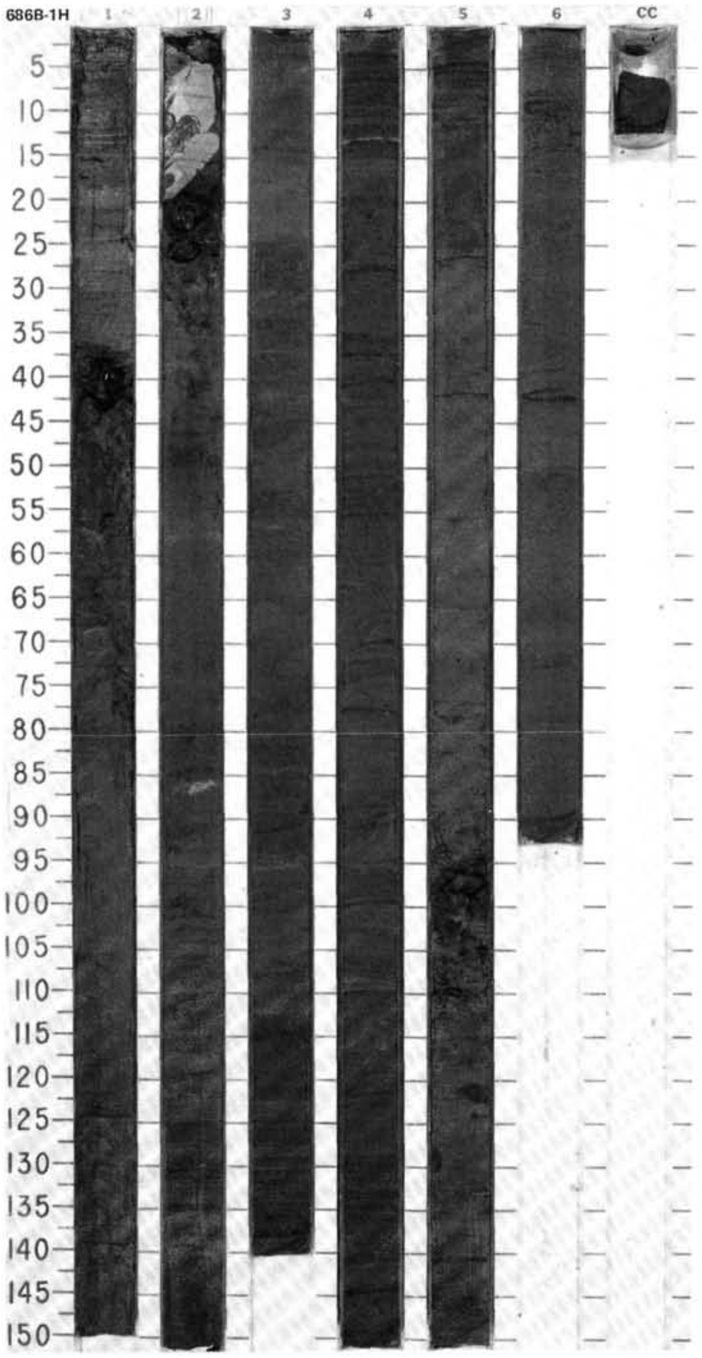

SITE 686 HOLE B CORE 2H CORED INTERVAL 455.3-464.8 mbsl; 8.5-18.0 mbsf

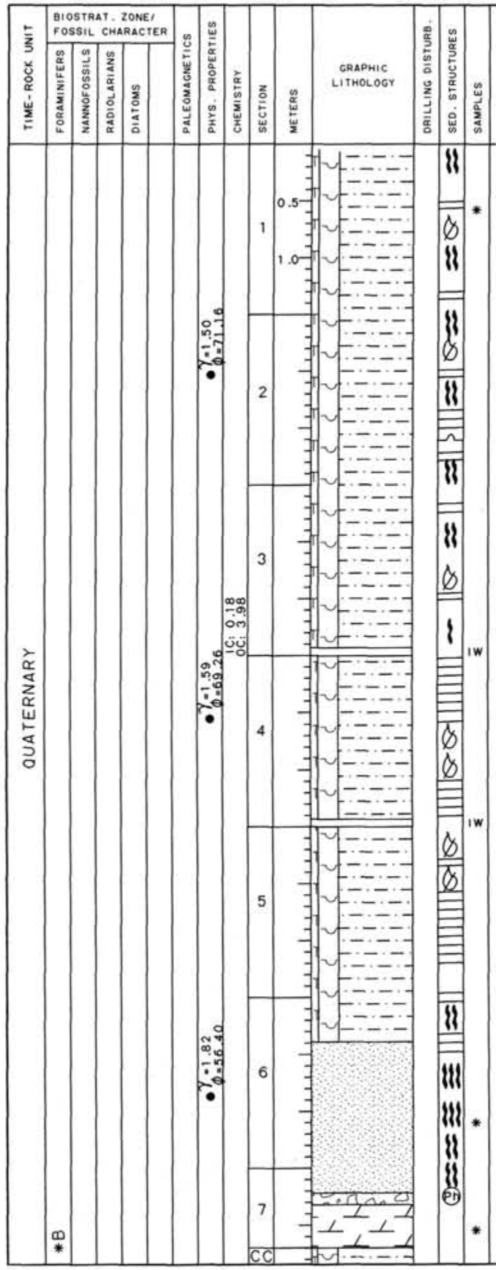

LITHOLOGIC DESCRIPTION

DIATOMACEOUS MUD

Major lithology: diatomaceous mud, dark olive gray, olive, and olive gray (5Y 3/2, 5Y 5/2, and 5Y 5/3); laminated and bioturbated.

Minor lithologies:
1. diatomaceous mud with bivalve shell fragments.
2. feldspathic-lithic sand.
3. phosphate nodules, dark, hard.
4. dolomite.

SMEAR SLIDE SUMMARY (%):

	1, 69 D	6, 114 D	7, 56 D
TEXTURE:			
Sand	20	70	—
Silt	45	20	15
Clay	35	10	85
COMPOSITION:			
Quartz	10	20	3
Feldspar	5	35	2
Rock fragments	15	25	—
Clay	25	5	—
Volcanic glass	3	—	—
Calcite/dolomite	5	3	85
Accessory minerals			
Phosphate peloids	1	—	—
Pyrite	2	2	—
Amphibole	1	1	—
Glauconite	—	1	—
Foraminifers	—	5	—
Diatoms	32	3	10
Sponge spicules	Tr	—	—
Fish remains	1	—	—

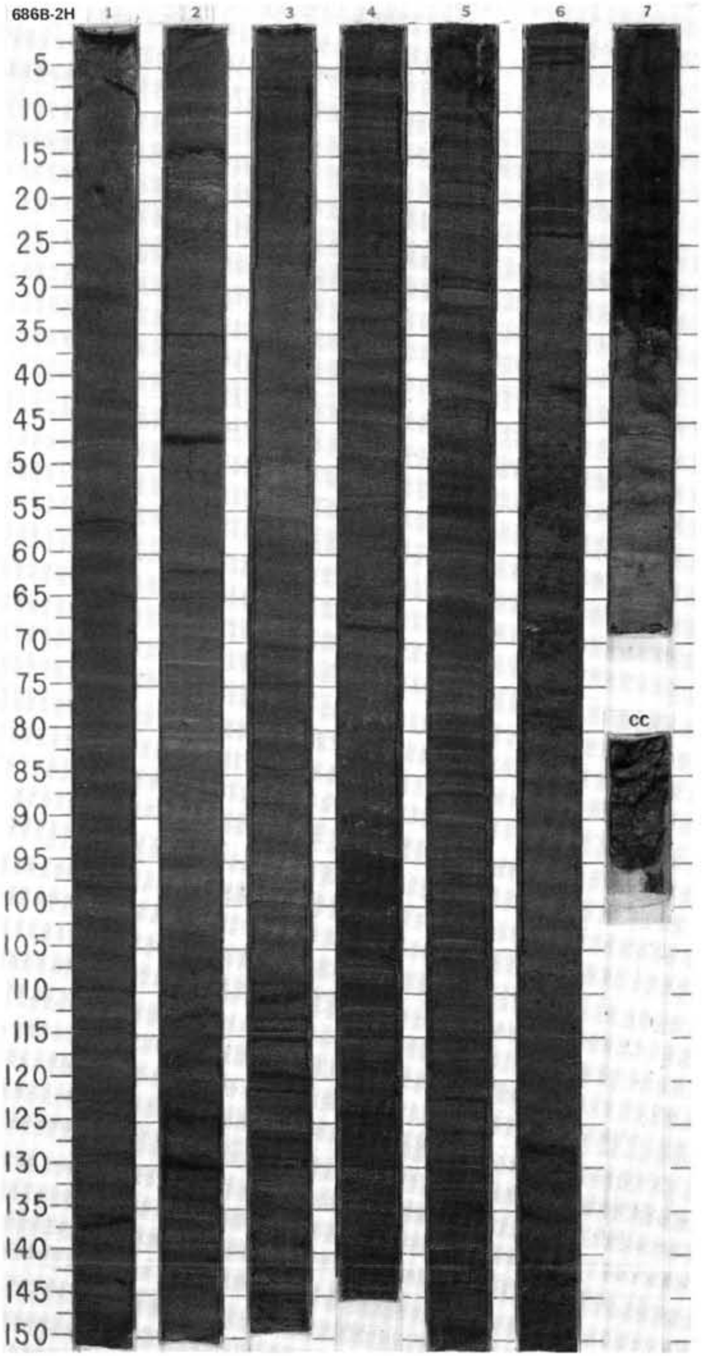

SITE 686 HOLE B CORE 3H CORED INTERVAL 464.8-474.3 mbsl; 18.0-27.5 mbsf

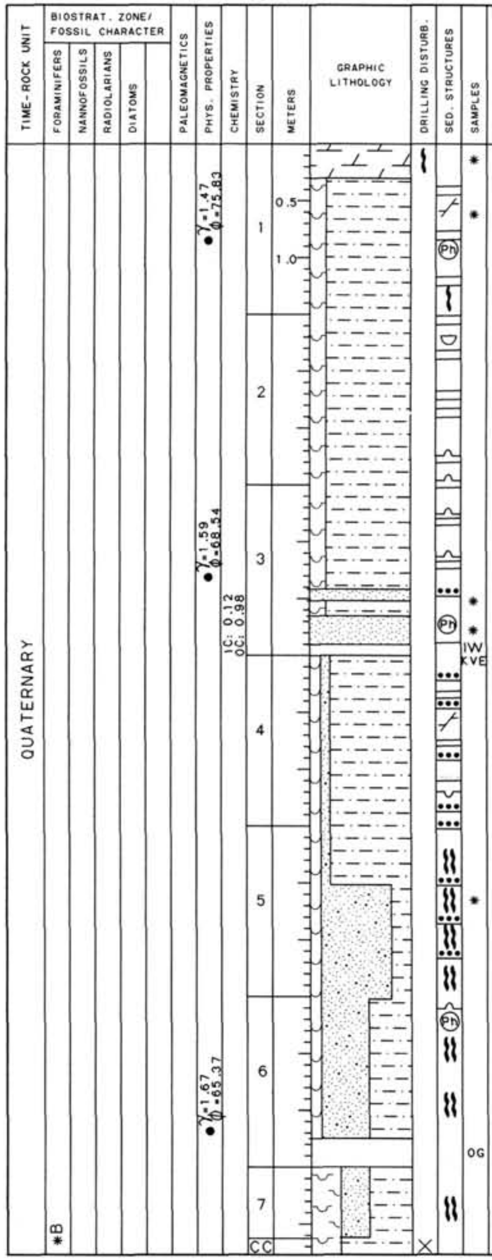

LITHOLOGIC DESCRIPTION

DIATOMACEOUS MUD

Major lithology: diatomaceous mud, olive gray and dark olive gray (5Y 5/2 and 5Y 3/2). Laminated with thin graded layers or massive and bioturbated.

Minor lithologies:
1. dolomite.
2. quartzo-feldspathic-lithic sand.
3. phosphate nodules.

SMEAR SLIDE SUMMARY (%):

	1, 9 M	1, 72 D	3, 103 M	3, 128 M	5, 65 D
TEXTURE:					
Sand	5	15	50	70	55
Silt	15	50	30	20	25
Clay	80	35	20	10	20
COMPOSITION:					
Quartz	5	10	10	35	20
Feldspar	5	10	10	15	25
Rock fragments	—	15	25	35	20
Mica	—	—	—	Tr	Tr
Clay	—	25	20	5	15
Volcanic glass	—	—	5	2	—
Dolomite	80	2	—	Tr	2
Pyrite	—	7	8	5	4
Amphibole	—	1	—	3	2
Glauconite	—	—	2	Tr	2
Calcite	—	15	15	—	—
Phosphate	—	—	—	—	5
Diatoms	10	15	5	Tr	5
Sponge spicules	—	Tr	Tr	Tr	Tr

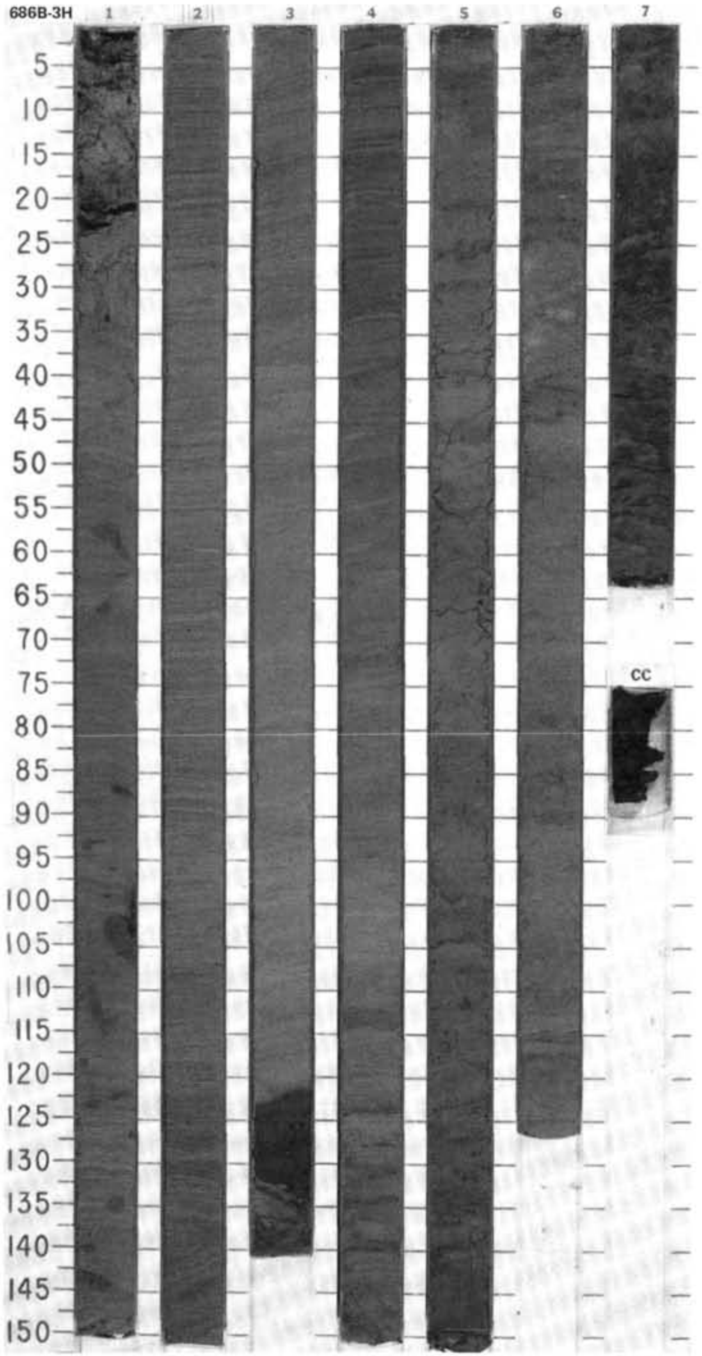

SITE 686 HOLE B CORE 4H CORED INTERVAL 474.3-483.8 mbsl; 27.5-37.0 mbsf

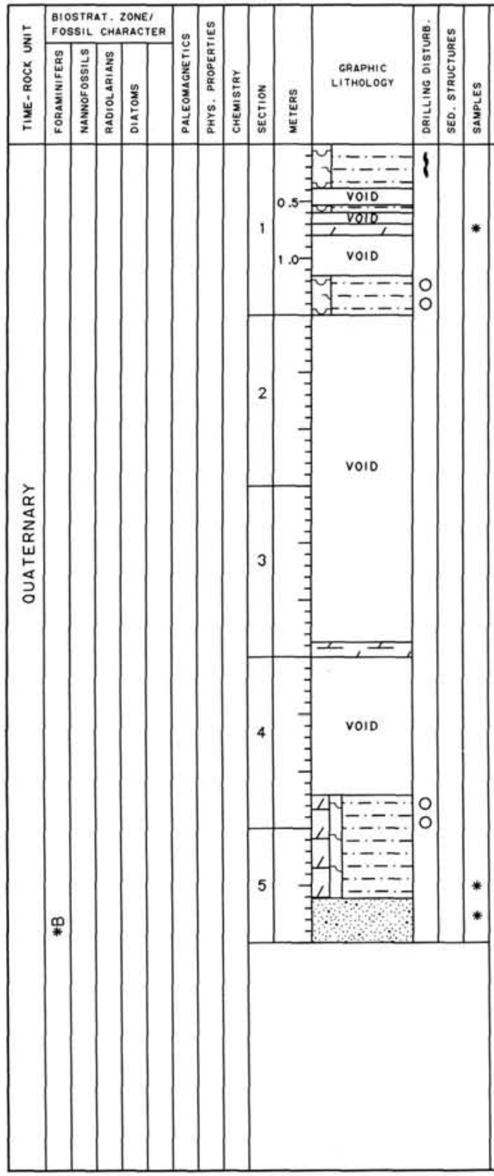

LITHOLOGIC DESCRIPTION

DIATOMACEOUS MUD

Major lithology: diatomaceous mud, olive gray, dark gray, olive, gray, light olive dark, olive gray (5Y 4/2, 5Y 4/3, 5Y 3/2, 5Y 4/4, 5Y 5/2, 5Y 4/1, and 5Y 6/2). Laminated to massive and slumped.

Minor lithologies:
1. dolomite.
2. vertebrate bone fragments and fish debris.
3. graded lithic fine sand.

SMEAR SLIDE SUMMARY (%):

	1, 74 D	5, 50 M	5, 77 D
TEXTURE:			
Sand	5	—	60
Silt	95	—	40
Clay	Tr	100	—
COMPOSITION:			
Quartz	3	—	10
Feldspar	2	—	15
Rock fragments	—	—	20
Clay	—	—	2
Dolomite	85	—	30
Accessory minerals			
Pyrite	3	—	2
Calcite	5	—	—
Apatite (bone)	—	100	—
Amphibole	—	—	1
Phosphate peloids	—	—	10
Diatoms	2	—	—
Sponge spicules	—	—	Tr
Fish remains	—	—	10

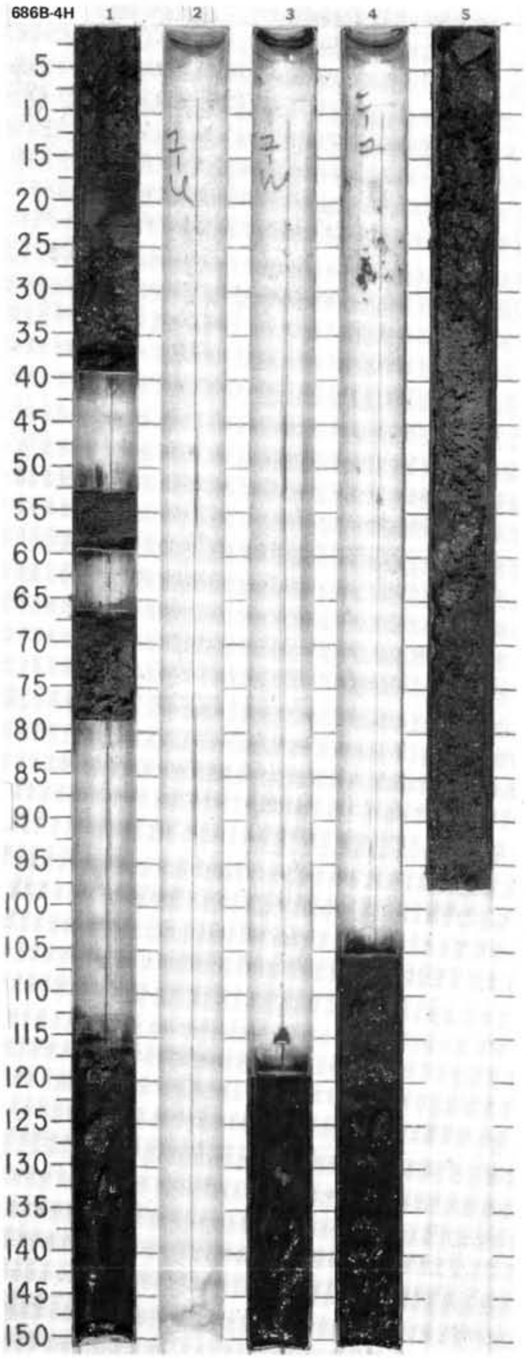

SITE 686 HOLE B CORE 5H CORED INTERVAL 483.8-493.3 mbsl; 37.0-46.5 mbsf

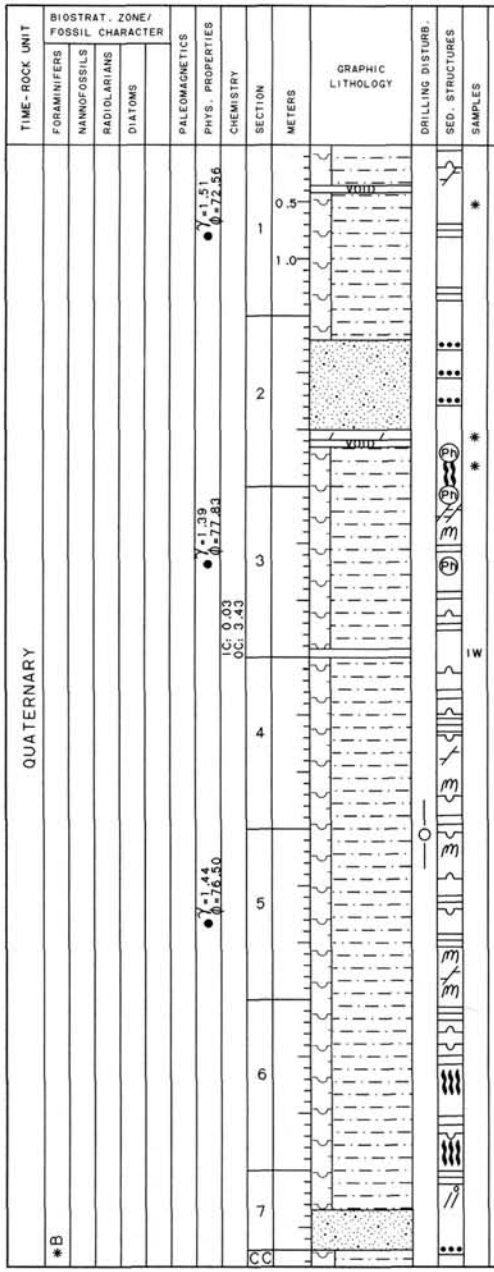

LITHOLOGIC DESCRIPTION

DIATOMACEOUS MUD

Major lithology: diatomaceous mud, dark olive gray, olive, gray, and light olive (5Y 3.5/2, 5Y 3/2, 5Y 4/4, 5Y 4/1, and 5Y 6/2). Finely laminated with thin graded base, slump folds, convolute laminations, microfaults, and dewatering veins.

Minor lithologies:
1. feldspathic-lithic sand, olive green (5Y 4/1.5), in graded beds.
2. sandy silt in graded layers.
3. dolomite.
4. phosphate nodules.

SMEAR SLIDE SUMMARY (%):

	1, 51 D	2, 104 D	2, 132 D
TEXTURE:			
Sand	10	50	25
Silt	45	20	35
Clay	45	30	40
COMPOSITION:			
Quartz	5	15	5
Feldspar	10	15	15
Rock fragments	10	25	20
Clay	35	30	20
Volcanic glass	5	—	5
Calcite/dolomite	2	3	3
Accessory minerals	—	4	3
Pyrite	3	5	5
Glauconite	2	—	—
Foraminifers	2	—	—
Diatoms	26	3	24
Sponge spicules	Tr	—	—

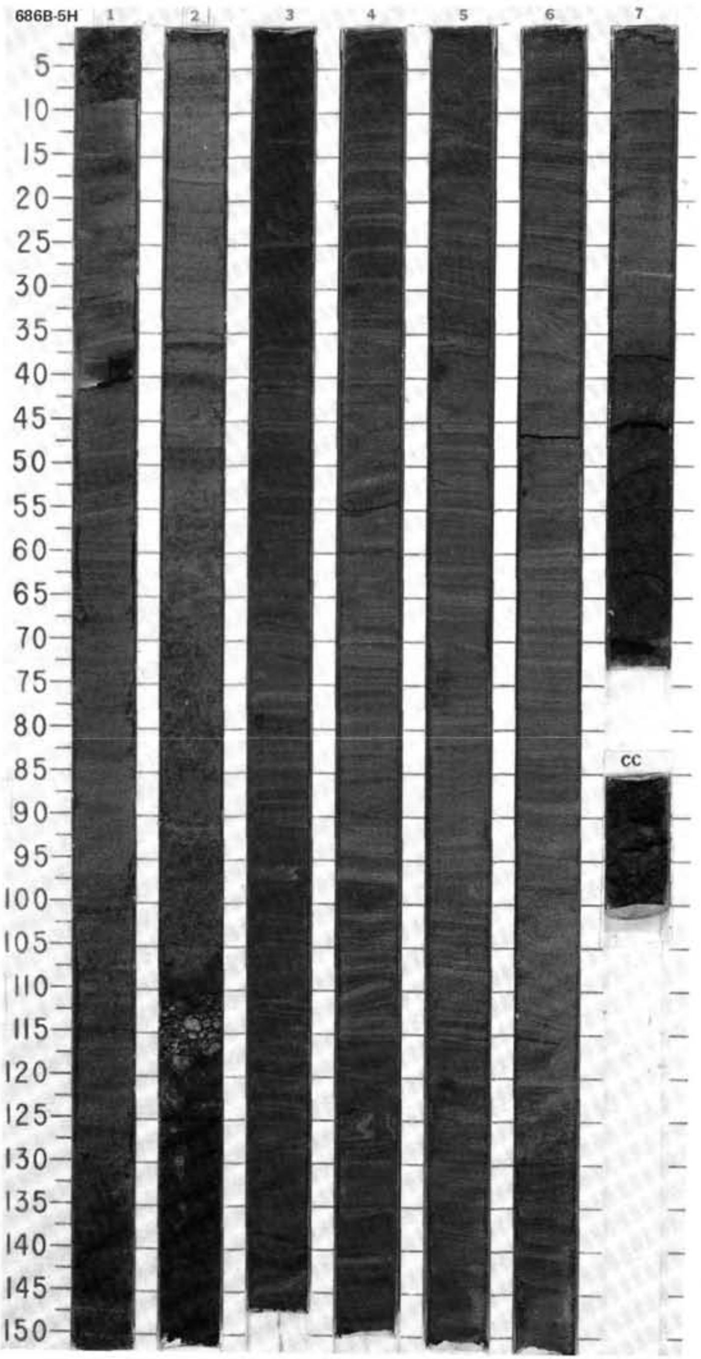

SITE 686 HOLE B CORE 6X CORED INTERVAL 493.3-502.8 mbsl; 46.5-56.0 mbsf

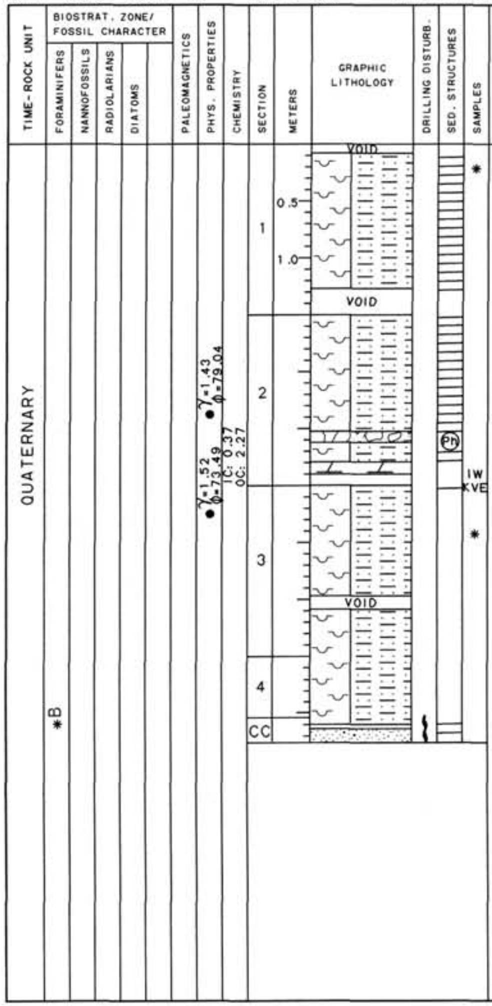

LITHOLOGIC DESCRIPTION

DIATOMACEOUS MUD

Major lithology: diatomaceous mud, olive to olive gray (5Y 3.5/2, 5Y 4/3, 5Y 4/2), laminated.

Minor lithologies:
1. phosphate nodules.
2. dolomite.

SMEAR SLIDE SUMMARY (%):

	1, 18 D	3, 43 D
TEXTURE:		
Sand	3	5
Silt	42	50
Clay	55	45
COMPOSITION:		
Quartz	6	5
Feldspar	7	5
Rock fragments	2	5
Clay	45	38
Calcite/dolomite	2	2
Accessory minerals		
Pyrite	5	5
Diatoms	30	40
Sponge spicules	—	Tr
Silicoflagellates	Tr	—
Fish remains	3	—

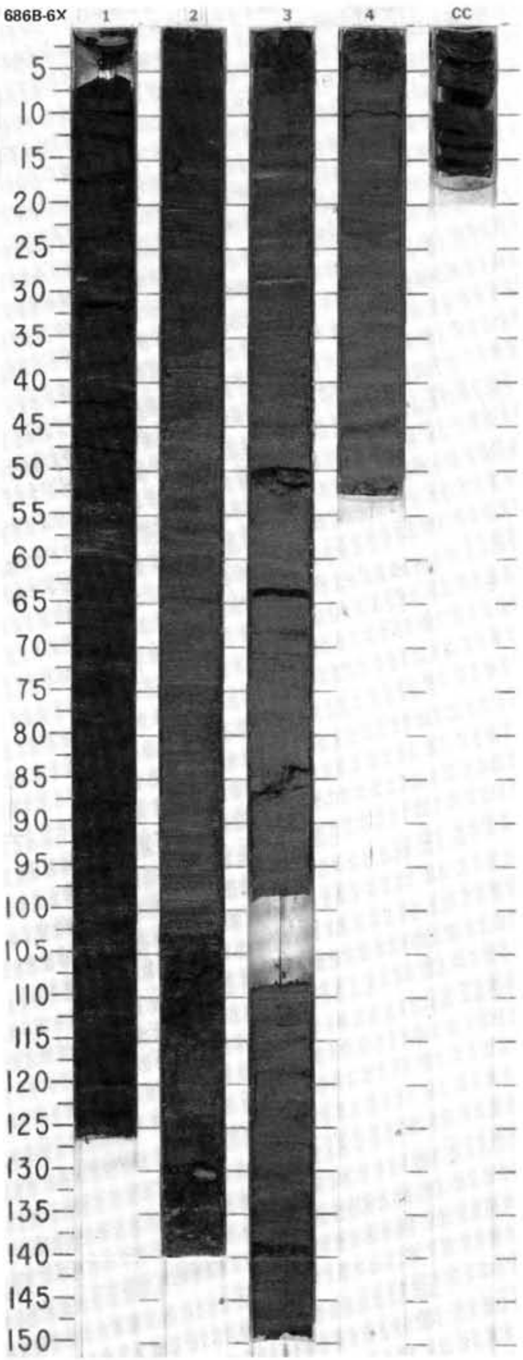

SITE 686 HOLE B CORE 7X CORED INTERVAL 502.8-512.3 mbsl; 56.0-65.5 mbsf

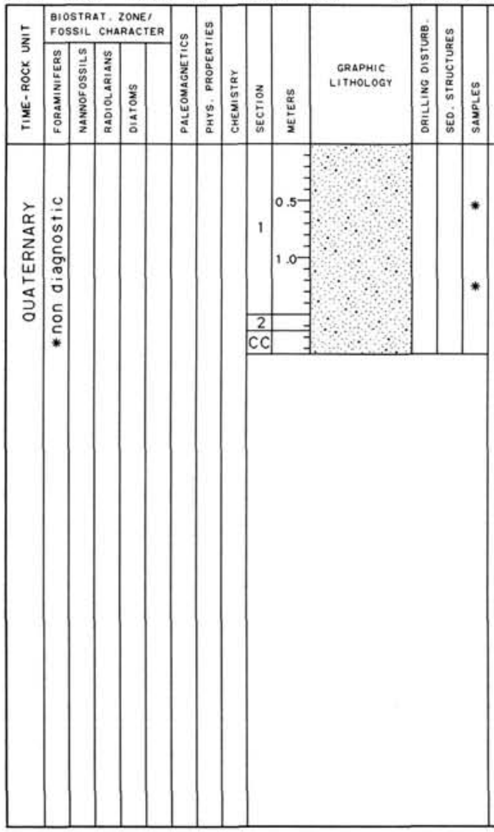

LITHOLOGIC DESCRIPTION

SAND

Major lithology: sand, olive gray, gray (5Y 4/2), and dark greenish gray (5GY 4/1), feldspathic-lithic, silty, locally phosphatic.

SMEAR SLIDE SUMMARY (%):

	1, 57 D	1, 132 D
TEXTURE:		
Sand	55	90
Silt	35	10
Clay	10	—
COMPOSITION:		
Quartz	20	25
Feldspar	30	25
Rock fragments	25	30
Mica	3	—
Dolomite	3	Tr
Calcite	—	Tr
Accessory minerals		
Pyrite	7	3
Glauconite	Tr	2
Amphibole	2	5
Phosphate peloids	—	10
Foraminifers	5	—
Diatoms	5	—

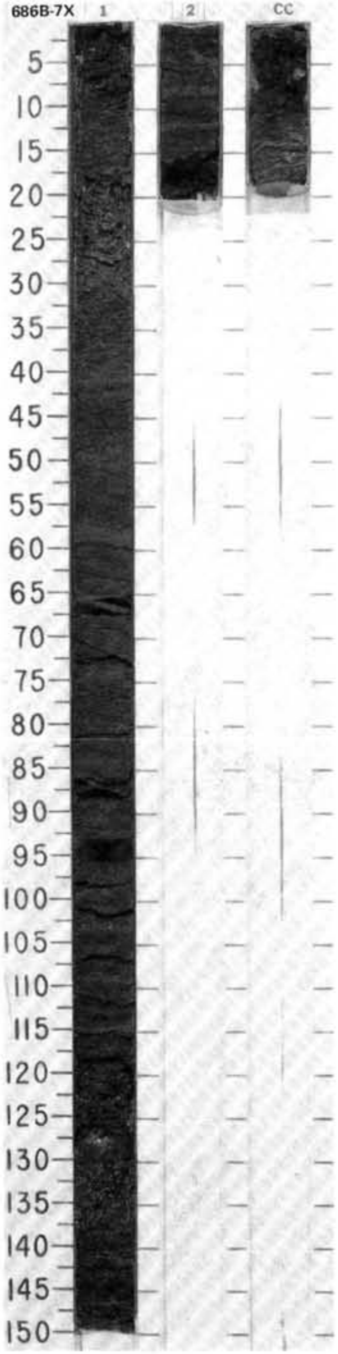

SITE 686 HOLE B CORE 8X CORED INTERVAL 512.3-521.8 mbsl; 65.5-75.0 mbsf

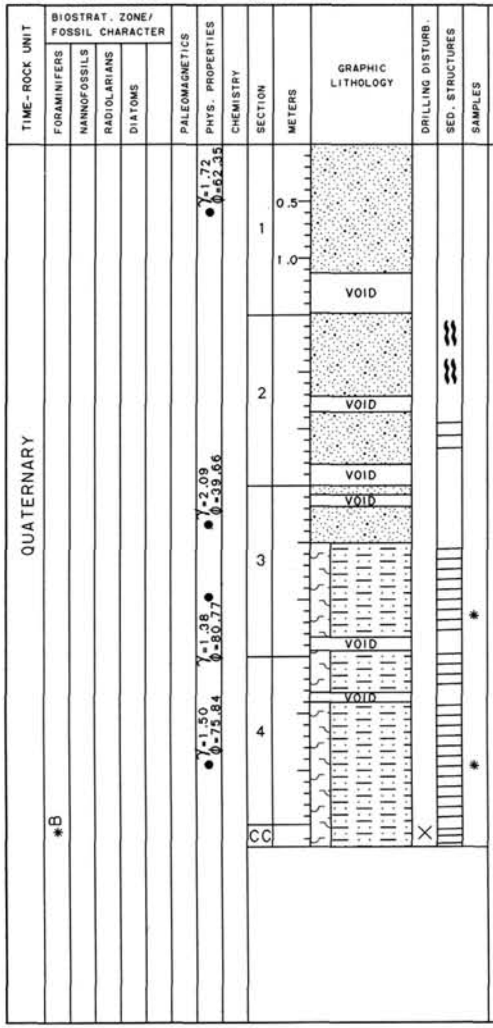

LITHOLOGIC DESCRIPTION

DIATOMACEOUS MUD and SAND

Major lithology: diatomaceous mud, dark greenish gray (5G 4/1), olive (5Y 4/3), and olive gray (5Y 4/2), laminated; sand, olive gray (5Y 4/2), burrowed.

SMEAR SLIDE SUMMARY (%):

	3, 127 M	4, 96 D
TEXTURE:		
Sand	5	10
Silt	40	40
Clay	55	50
COMPOSITION:		
Quartz	10	15
Feldspar	10	20
Rock fragments	—	5
Clay	30	35
Calcite/dolomite	Tr	Tr
Accessory minerals		
Amphibole	Tr	Tr
Pyrite	—	5
Foraminifers	5	—
Nannofossils	30	—
Diatoms	15	20
Radiolarians	—	Tr

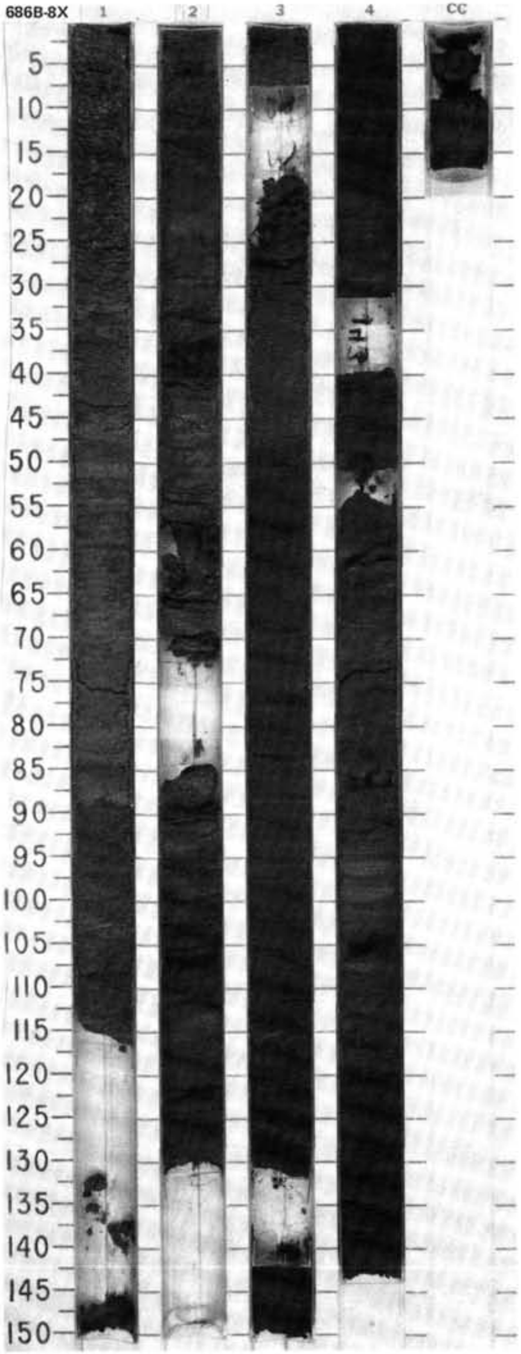

SITE 686 HOLE B CORE 9X CORED INTERVAL 521.8-531.3 mbsl; 75.0-84.5 mbsf

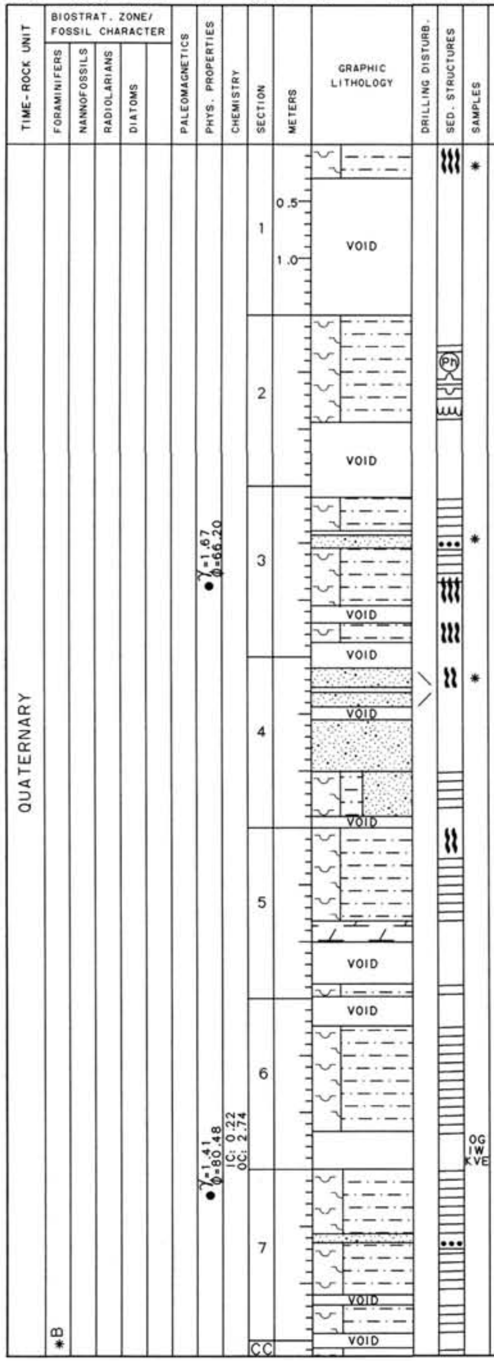

LITHOLOGIC DESCRIPTION

DIATOMACEOUS MUD, SAND and SANDY SILT

Major lithology: diatomaceous mud, black (5Y 2.5/2), dark gray (5Y 4/1 and 5Y 4/2), dark olive gray (5Y 2.5/2), laminated. Sand and sandy silt, gray (5Y 5/1) to black (5Y 2.5/2), in graded beds with sharp basal contacts.

Minor lithologies:
1. phosphate nodules.
2. dolomite.

SMEAR SLIDE SUMMARY (%):

	1, 18 D	3, 45 M	4, 17 D
TEXTURE:			
Sand	15	35	80
Silt	40	55	15
Clay	45	10	5
COMPOSITION:			
Quartz	5	10	40
Feldspar	10	20	30
Rock fragments	5	10	10
Mica	—	—	Tr
Clay	30	5	—
Dolomite	5	10	Tr
Accessory minerals			
Pyrite	10	5	—
Amphibole	—	—	15
Opaques	—	—	5
Foraminifers	5	10	Tr
Nannofossils	—	Tr	—
Diatoms	30	30	Tr

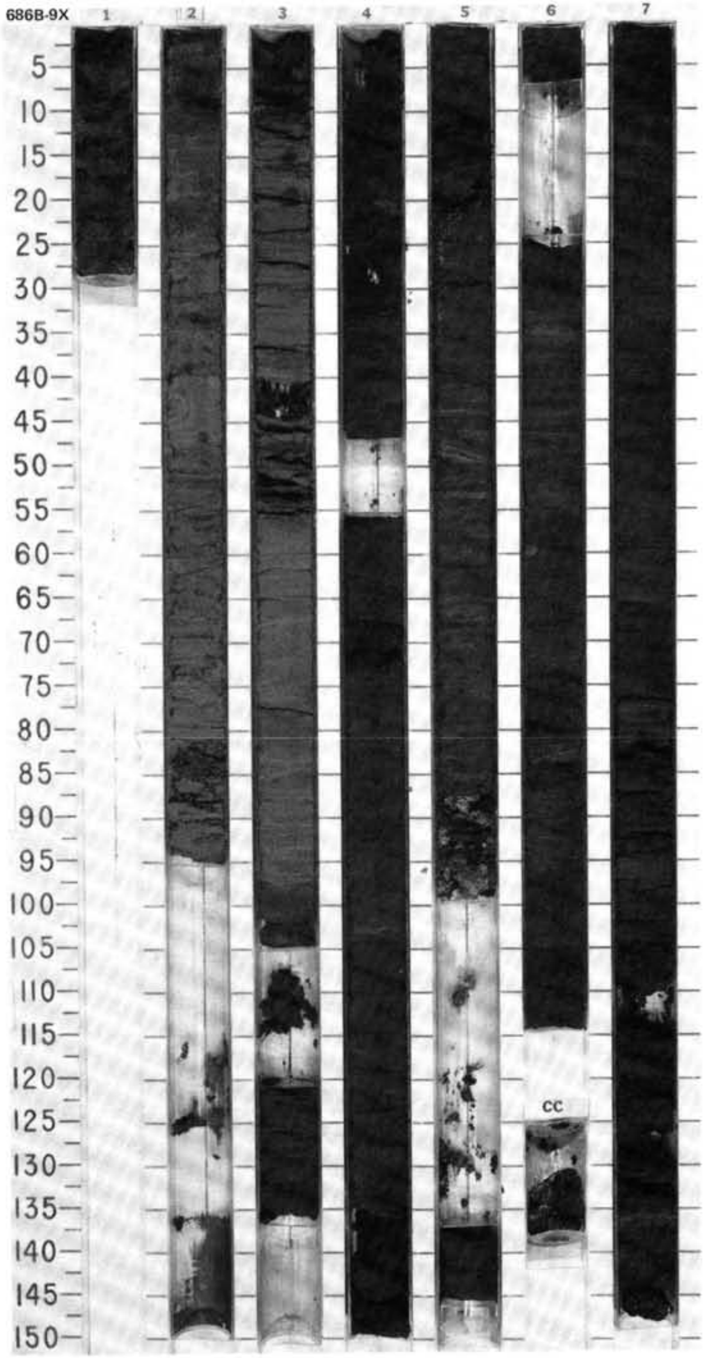

SITE 686 HOLE B CORE 10X CORED INTERVAL 531.3-540.8 mbsl; 84.5-94.0 mbsf

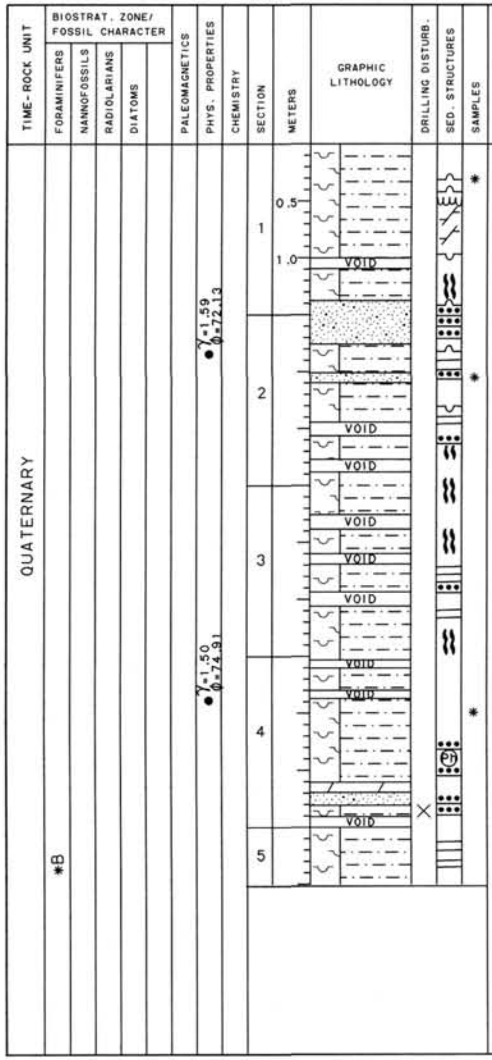

LITHOLOGIC DESCRIPTION

DIATOMACEOUS MUD and SILT AND SANDY SILT

Major lithology: diatomaceous mud, dark olive, olive, and olive gray (5Y 3.5/2, 5Y 3/2, 5Y 4/3, and 5Y 4/2). Laminated with thin graded beds, slump folds, and microfaults. Silt and sandy silt, dark gray (N 4/) to gray (5Y 5/1), feldspathic-lithic, burrowed.

Minor lithologies:
1. phosphate nodules, friable.
2. dolomite.

SMEAR SLIDE SUMMARY (%):

	1, 28 D	2, 63 M	4, 63 D
TEXTURE:			
Sand	5	80	5
Silt	50	20	40
Clay	45	—	55
COMPOSITION:			
Quartz	20	30	5
Feldspar	20	23	10
Rock fragments	Tr	35	—
Mica	—	—	Tr
Clay	30	—	35
Volcanic glass	Tr	2	—
Calcite/dolomite	2	5	2
Pyrite	6	—	8
Phosphate peloids	2	—	—
Opaques	—	5	—
Diatoms	20	—	20
Radiolarians	Tr	—	—
Sponge spicules	Tr	Tr	—
Spores/pollen	Tr	—	—

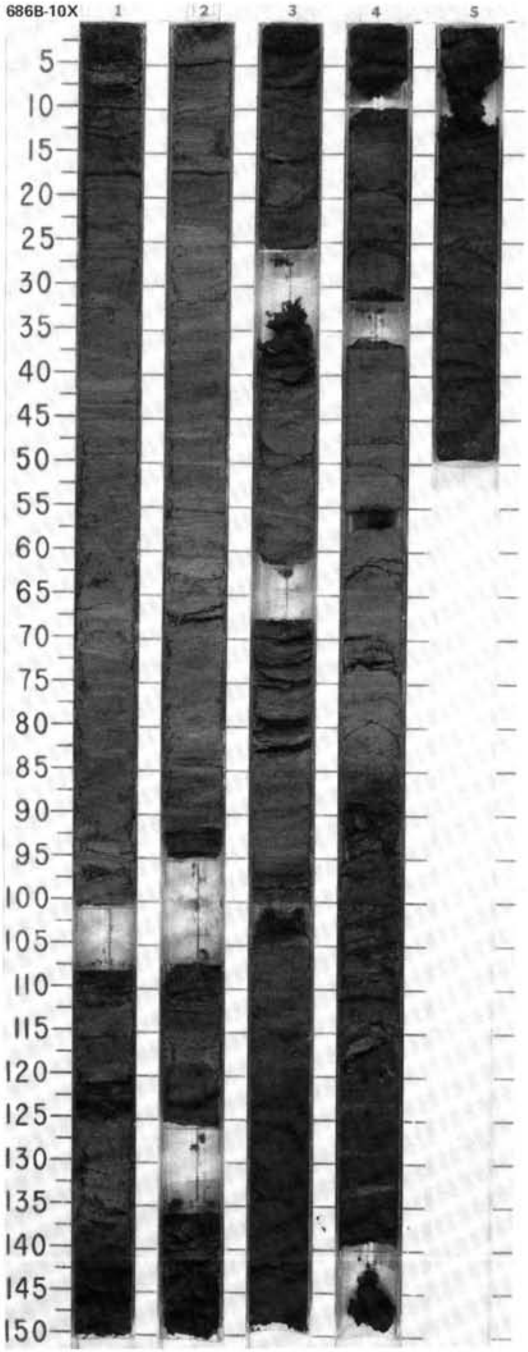

SITE 686 HOLE B CORE 11X CORED INTERVAL 540.8-550.3 mbsl; 94.0-103.5 mbsf

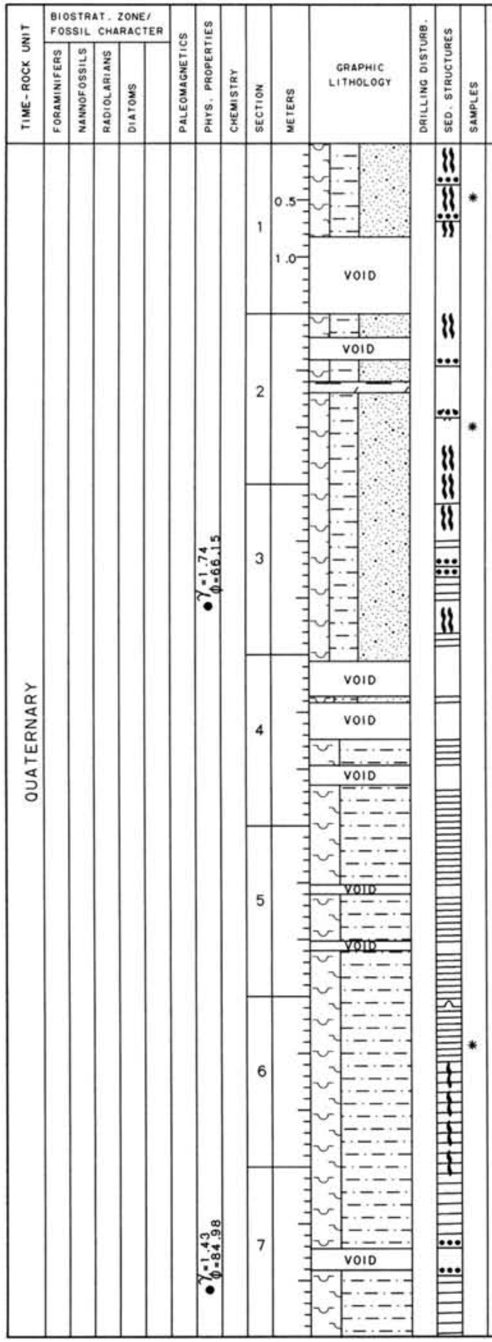

LITHOLOGIC DESCRIPTION

DIATOMACEOUS MUD and SAND

Major lithology: diatomaceous mud, olive gray (5Y 4/1, 4/2, 3.5/1 and 3/1). Laminated to burrowed, with thin graded beds. Sand, dark greenish gray (5GY 4/1), lithic-rich.

Minor lithology: dolomite.

SMEAR SLIDE SUMMARY (%):

	1, 83 D	2, 98 M	6, 72 D	8, 28 D
TEXTURE:				
Sand	20	70	40	20
Silt	55	20	40	50
Clay	25	10	20	30
COMPOSITION:				
Quartz	5	30	5	10
Feldspar	10	10	10	5
Rock fragments	25	35	20	15
Clay	15	5	15	25
Volcanic glass	Tr	Tr	2	2
Calcite/dolomite	Tr	2	8	1
Pyrite	5	2	10	12
Glauconite	1	3	Tr	—
Phosphate	—	1	2	—
Amphibole	—	Tr	—	5
Foraminifers	—	—	—	5
Nannofossils	—	—	—	Tr
Diatoms	35	10	28	20
Radiolarians	—	—	—	Tr
Sponge spicules	Tr	2	Tr	Tr
Silicoflagellates	—	—	—	Tr
Fish remains	—	—	—	Tr

(CON'T)

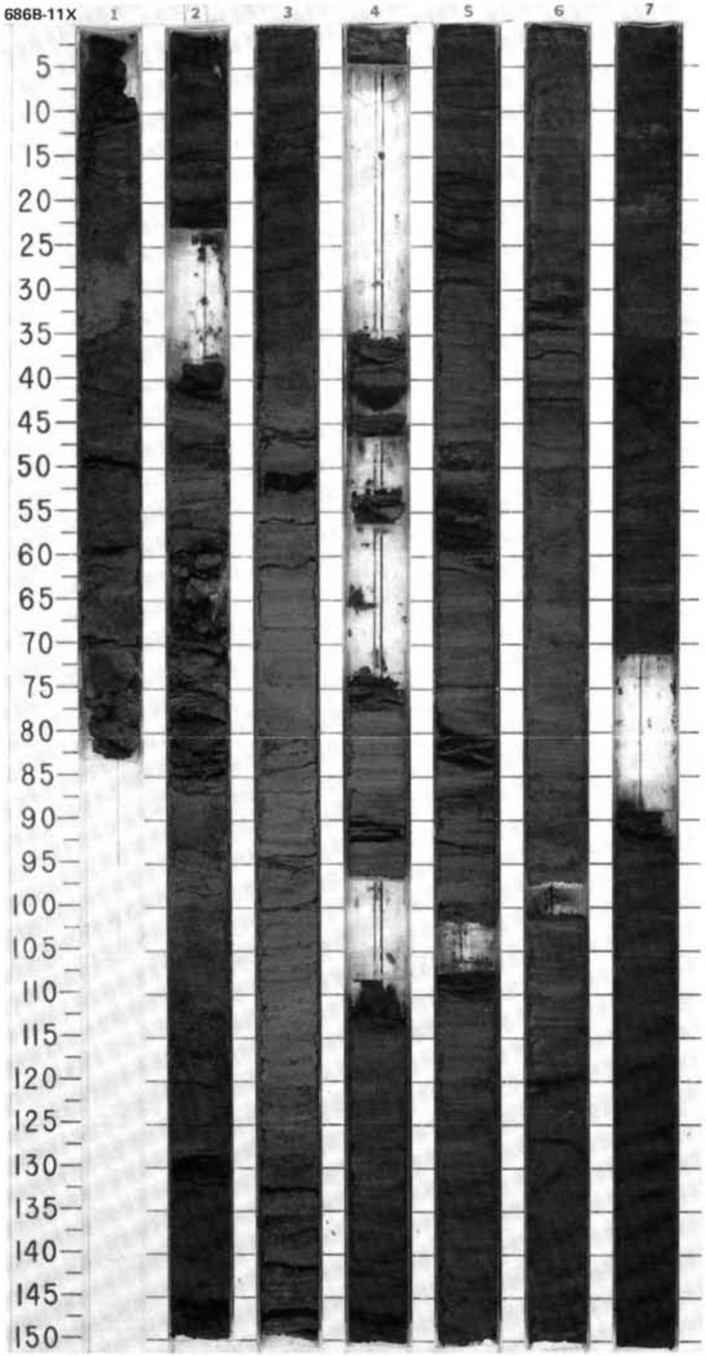

SITE 686 HOLE B CORE 11X CORED INTERVAL 540.8-550.3 mbsl; 94.0-103.5 mbsf

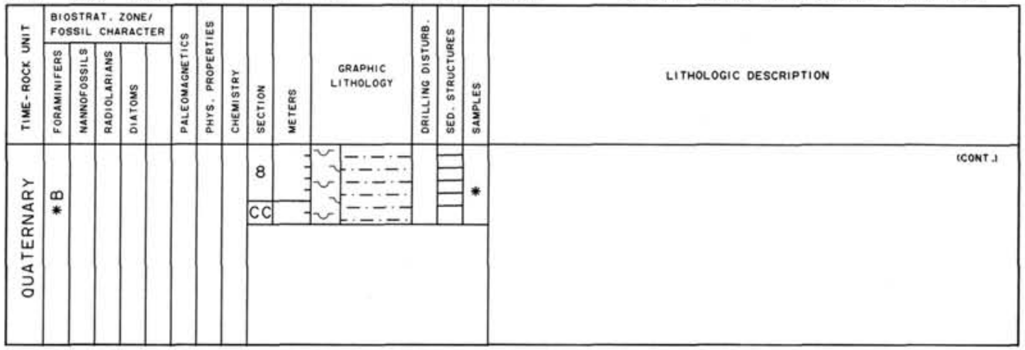

(CONT.)

SITE 686 HOLE B CORE 12X CORED INTERVAL 550.3-559.8 mbsl; 103.5-113.0 mbsf

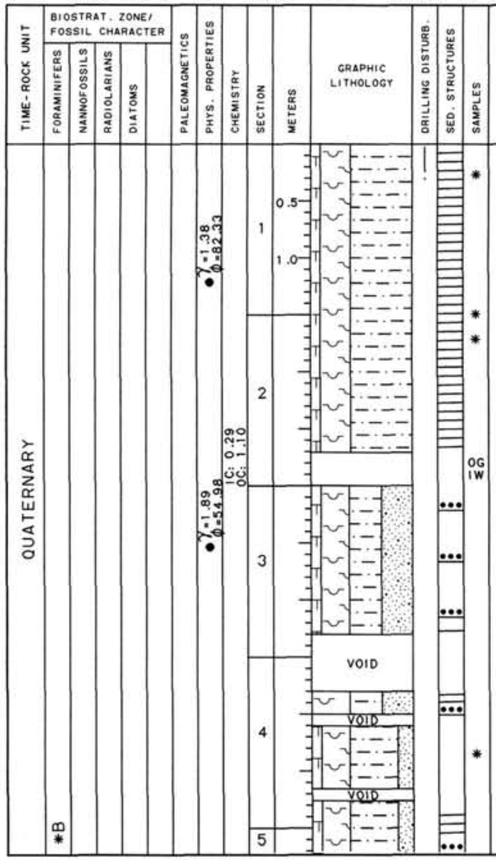

LITHOLOGIC DESCRIPTION

DIATOMACEOUS MUD and SAND

Major lithology: diatomaceous mud, dark olive to olive (5Y 2.5/3 to 5Y 3/3) and olive gray (5Y 4/2), and sand, gray (5Y 4/1.5).

SMEAR SLIDE SUMMARY (%):

	1, 29 D	2, 1 M	2, 25 M	4, 83 D
TEXTURE:				
Sand	15	—	—	40
Silt	45	70	85	30
Clay	40	30	15	30
COMPOSITION:				
Quartz	3	2	—	10
Feldspar	5	2	—	10
Rock fragments	2	1	—	10
Clay	30	20	5	18
Calcite/dolomite	—	—	1	—
Accessory minerals				
Pyrite	5	3	—	6
Phosphate	—	—	—	5
Amphibole	—	—	—	1
Foraminifers	15	5	—	10
Nannofossils	—	2	—	—
Diatoms	40	65	94	30

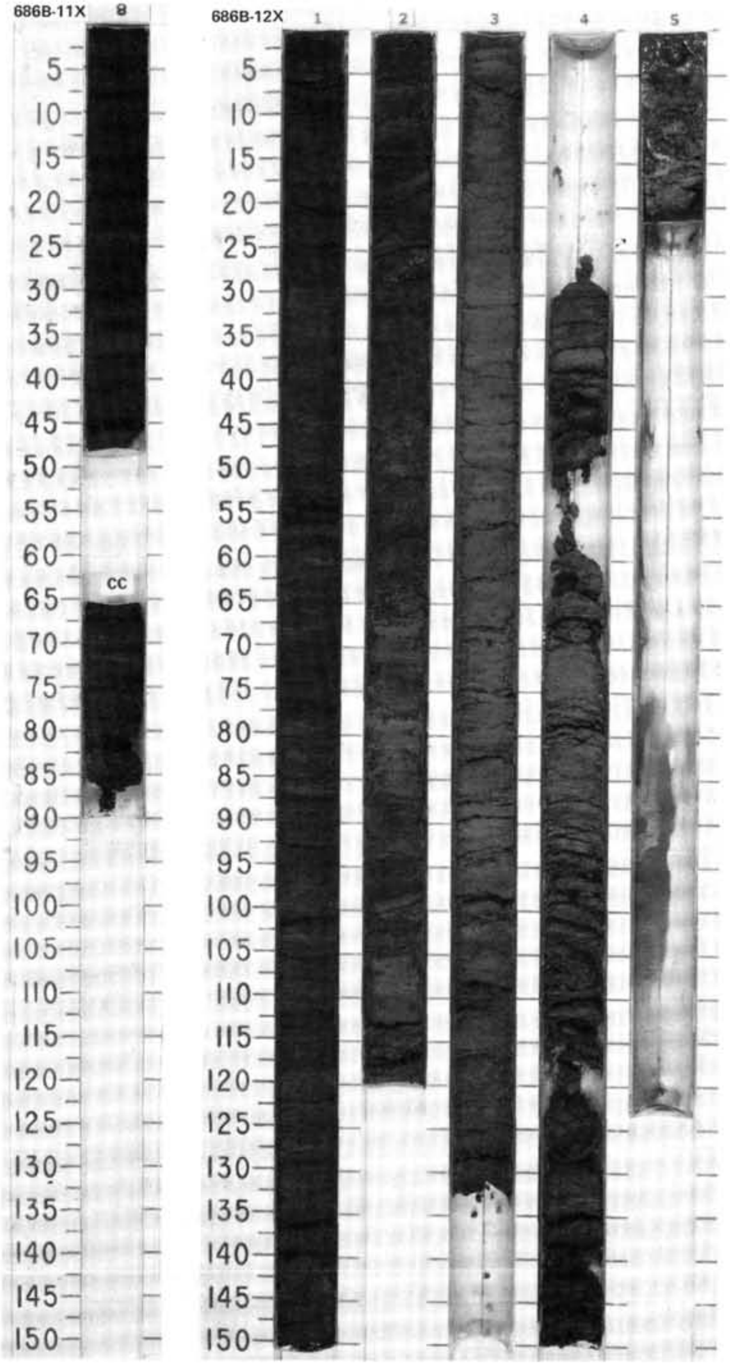

SITE 686 HOLE B CORE 13X CORED INTERVAL 559.8-569.3 mbsl; 113.0-122.5 mbsf

TIME-ROCK UNIT	BIOSTRAT. ZONE/ FOSSIL CHARACTER					PALEOMAGNETICS	PHYS. PROPERTIES	CHEMISTRY	SECTION	METERS	GRAPHIC LITHOLOGY	DRILLING DISTURB.	SED. STRUCTURES	SAMPLES
	FORAMINIFERS	NANNOFOSSILS	RADIOLARIANS	DIATOMS										
QUATERNARY									1 CC	0.5	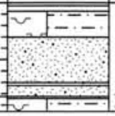	×		*

LITHOLOGIC DESCRIPTION

DIATOMACEOUS MUD and SAND

Major lithology: diatomaceous mud, greenish gray (5GY 4/1 and 5/1), and sand, gray (N 5) quartzo-feldspathic-lithic.

Minor lithologies: dolomite and dolomite-cemented sandstone.

SMEAR SLIDE SUMMARY (%):

	1, 40 D
TEXTURE:	
Sand	35
Silt	45
Clay	20
COMPOSITION:	
Quartz	30
Feldspar	15
Rock fragments	25
Clay	10
Calcite/dolomite	5
Accessory minerals	
Pyrite	5
Glauconite	Tr
Diatoms	10

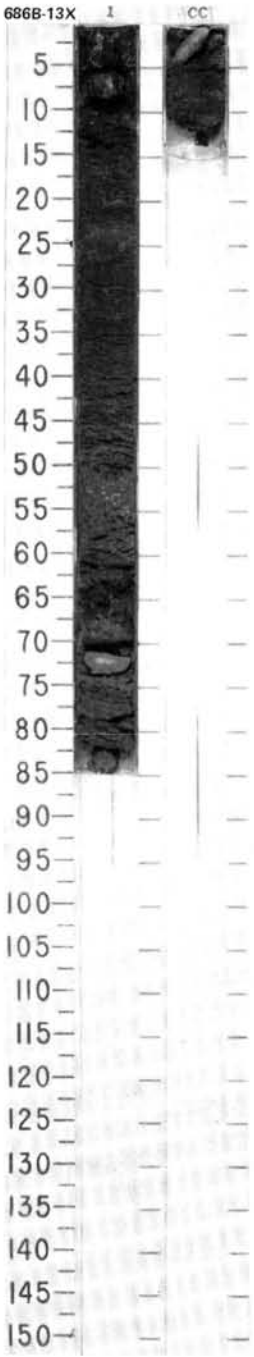

SITE 686 HOLE B CORE 14X CORED INTERVAL 569.3-578.8 mbsl; 122.5-132.0 mbsf

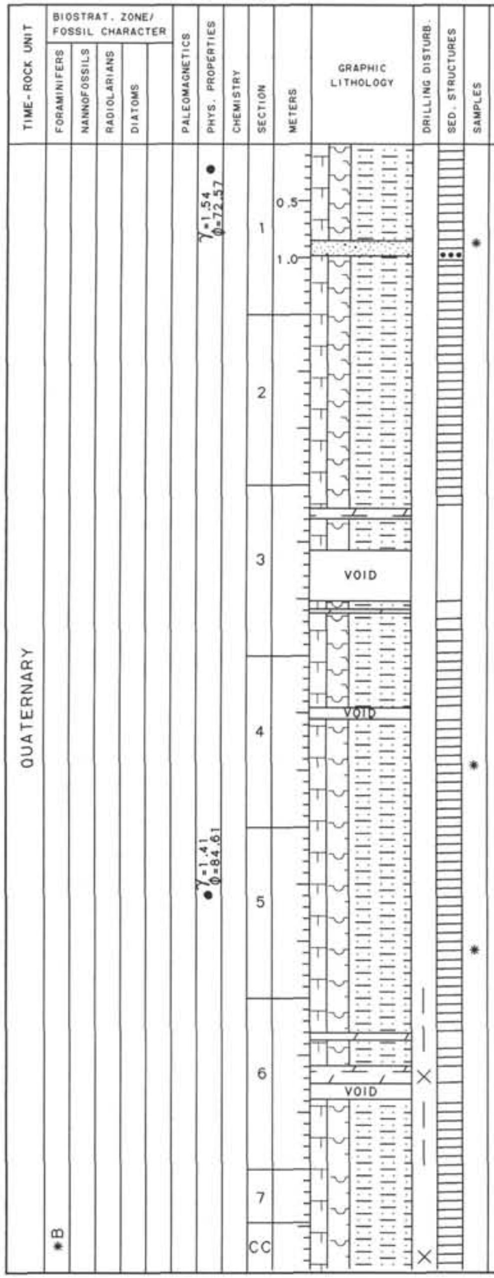

LITHOLOGIC DESCRIPTION

DIATOMACEOUS MUD and SAND

Major lithology: diatomaceous mud, dark olive gray 95Y 3/2), olive gray (5Y 4/2), and black (5Y 3/1); laminated. Sand, gray (N 5/).

Minor lithology: dolomite.

SMEAR SLIDE SUMMARY (%):

	1, 85 D	4, 82 M	5, 104 M
TEXTURE:			
Sand	—	30	—
Silt	45	60	75
Clay	55	10	25
COMPOSITION:			
Quartz	5	4	5
Feldspar	5	3	—
Rock fragments	—	—	—
Mica	Tr	3	Tr
Clay	55	10	—
Calcite	5	5	Tr
Accessory minerals	5	—	—
Foraminifers	—	15	5
Nannofossils	—	Tr	Tr
Diatoms	25	60	90
Silicoflagellates	—	—	—

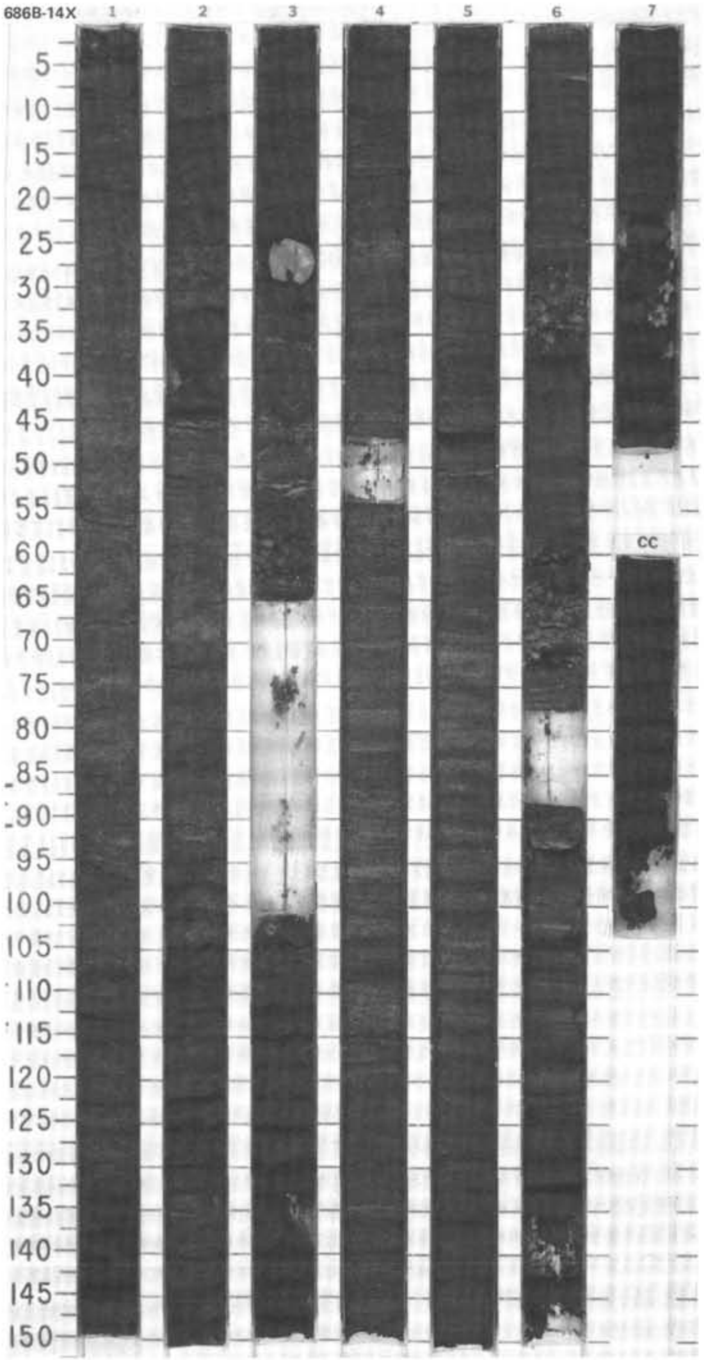

SITE 686 HOLE B CORE 15X CORED INTERVAL 578.8-588.3 mbsl; 132.0-141.5 mbsf

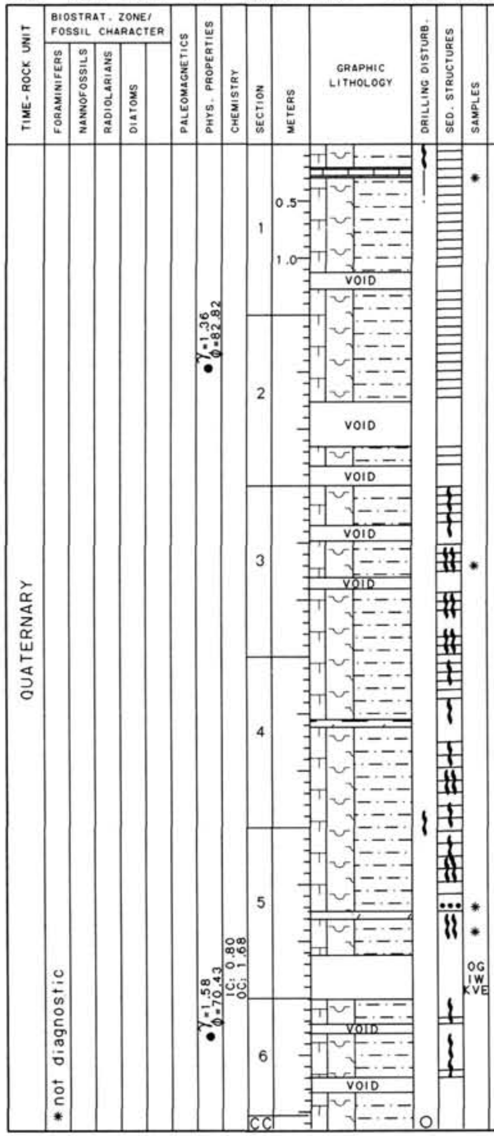

LITHOLOGIC DESCRIPTION

DIATOMACEOUS MUD

Major lithology: diatomaceous mud, olive (5Y 3/3) to dark olive (5Y 3/3) to dark olive gray (5Y 3/2) to olive gray (5Y 5/1.5). Laminated to slightly burrowed, mottled.

Minor lithologies:
1. micritic limestone.
2. dolomite.
3. sand, quartzo-feldspathic-lithic.

SMEAR SLIDE SUMMARY (%):

	1, 28 M	3, 72 D	5, 62 M	5, 92 D
TEXTURE:				
Sand	5	20	75	10
Silt	15	40	15	60
Clay	80	40	10	30
COMPOSITION:				
Quartz	Tr	5	27	5
Feldspar	—	5	15	5
Rock fragments	—	10	40	10
Clay	—	15	5	20
Volcanic glass	—	Tr	3	2
Dolomite	Tr	—	—	—
Accessory minerals				
Pyrite	1	7	5	8
Amphibole	—	—	5	—
Micrite/ authigenic calcite	84	5	—	5
Foraminifers	Tr	—	—	10
Nannofossils	—	Tr	—	—
Diatoms	15	53	—	35
Sponge spicules	—	—	Tr	—

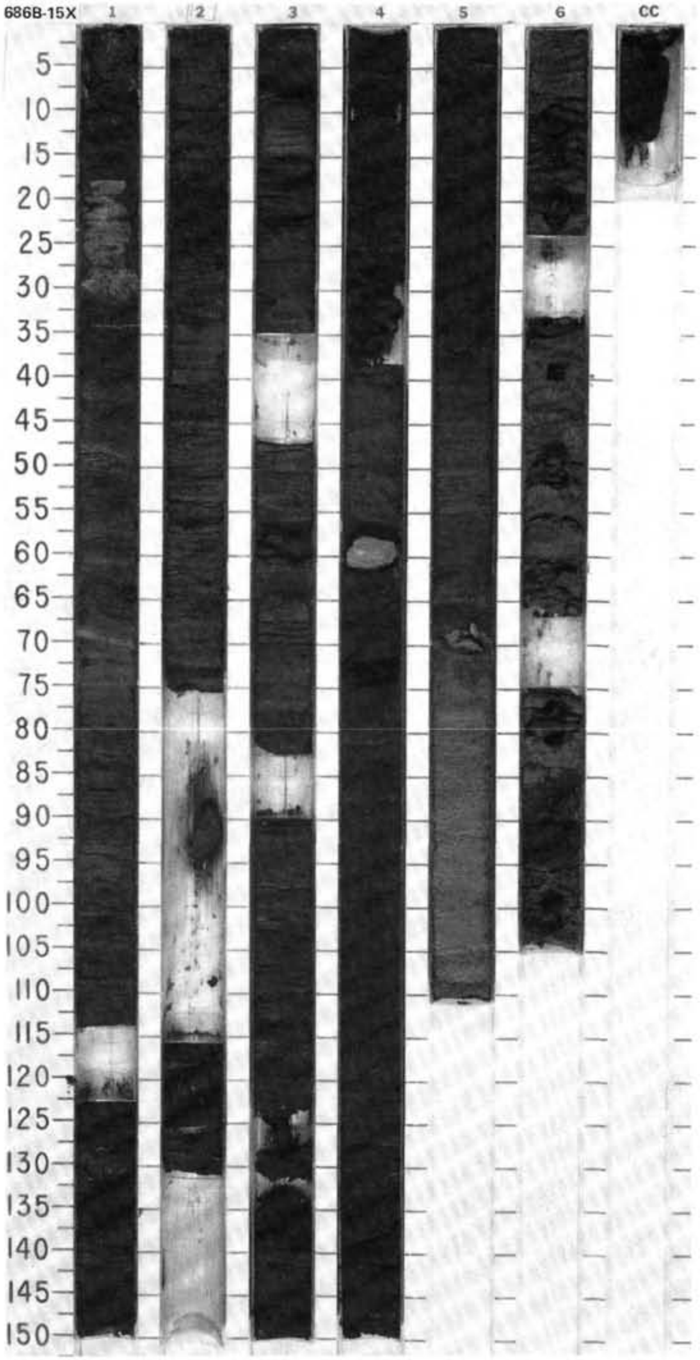

SITE 686 HOLE B CORE 16X CORED INTERVAL 588.3-597.8 mbsl; 141.5-151.0 mbsf

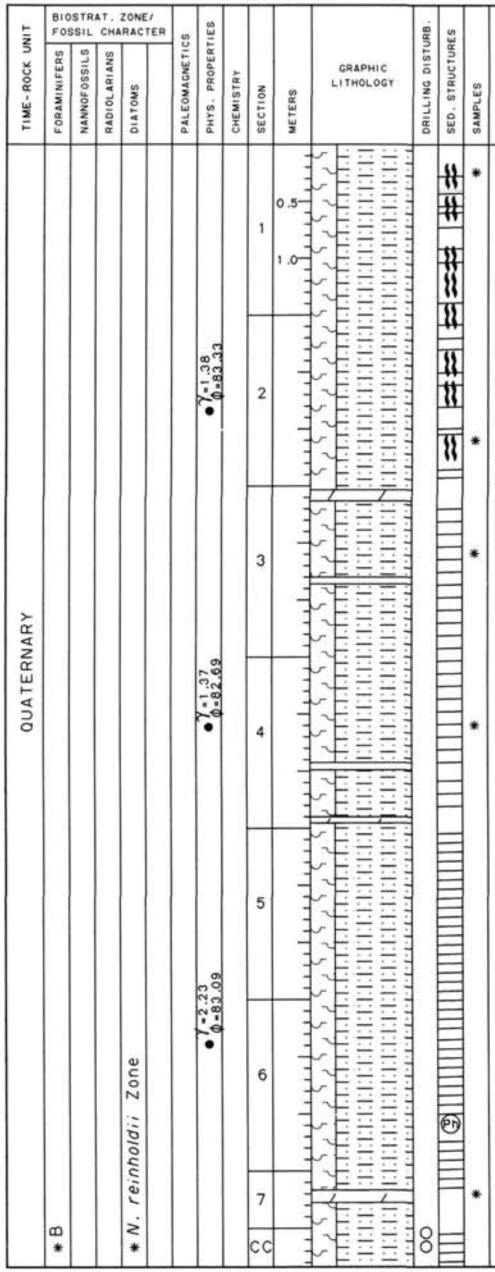

LITHOLOGIC DESCRIPTION

DIATOMACEOUS MUD

Major lithology: diatomaceous mud, olive gray (5Y 4/2), to dark gray (5Y 4/1), and olive (5Y 4/4). Burrowed to faintly laminated.

Minor lithologies:
1. dolomite and dolomite-cemented sandstone.
2. phosphatic nodule.

SMEAR SLIDE SUMMARY (%):

	1, 24 D	3, 60 M	4, 59 D	7, 22 M
TEXTURE:				
Silt	70	85	50	—
Clay	30	15	50	100
COMPOSITION:				
Quartz	10	5	5	Tr
Feldspar	15	—	5	Tr
Rock fragments	10	—	—	—
Mica	Tr	—	—	—
Clay	30	15	50	10
Volcanic glass	Tr	—	—	—
Calcite/dolomite	5	—	5	—
Accessory minerals				
Opaques	5	—	—	Tr
Glauconite	Tr	—	Tr	Tr
Dolomite	—	5	—	80
Foraminifers	—	5	5	Tr
Diatoms	25	70	30	10

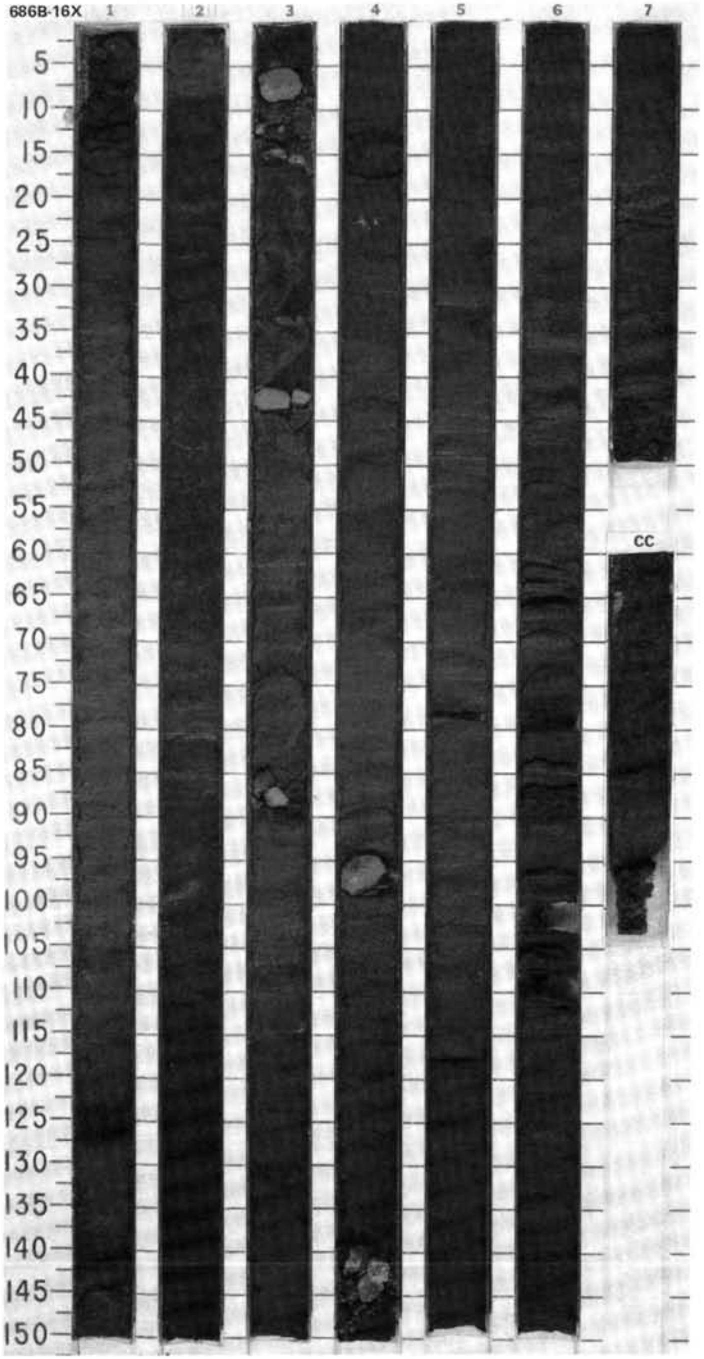

SITE 686 HOLE B CORE 17X CORED INTERVAL 597.8-607.3 mbsl; 151.0-160.5 mbsf

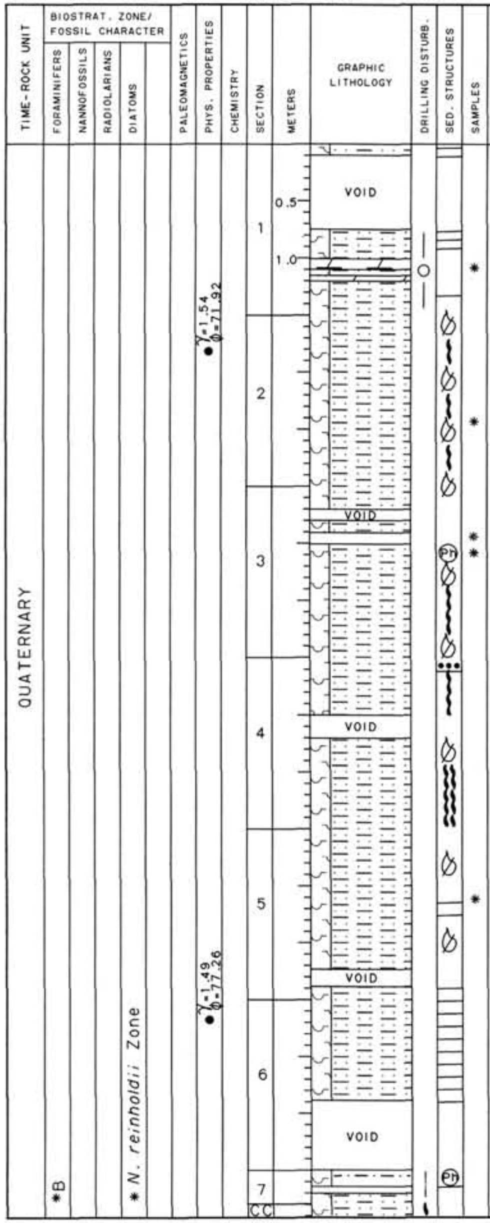

LITHOLOGIC DESCRIPTION

DIATOMACEOUS MUD

Major lithology: diatomaceous mud, dark olive, olive gray, and olive (5Y 3/3, 5Y 4/2, 5Y 4/3).

Minor lithologies:
1. limestone.
2. dolomitic mud.
3. sponge and bivalve shell fragments.

SMEAR SLIDE SUMMARY (%):

	1, 116 M	2, 91 D	3, 43 M	3, 54 M	5, 62 D
TEXTURE:					
Sand	5	—	20	5	—
Silt	80	55	70	85	55
Clay	15	45	10	10	45
COMPOSITION:					
Quartz	5	7	5	1	10
Feldspar	Tr	8	10	1	10
Rock fragments	Tr	—	—	2	5
Mica	—	Tr	Tr	—	Tr
Clay	5	45	10	5	45
Volcanic glass	Tr	—	65	90	—
Dolomite	35	—	Tr	—	—
Accessory minerals					
Pyrite	1	5	—	1	5
Micrite	44	10	5	—	5
Foraminifers	—	5	—	Tr	5
Nannofossils	—	Tr	—	—	—
Diatoms	10	20	5	—	15
Sponge spicules	—	Tr	—	—	Tr

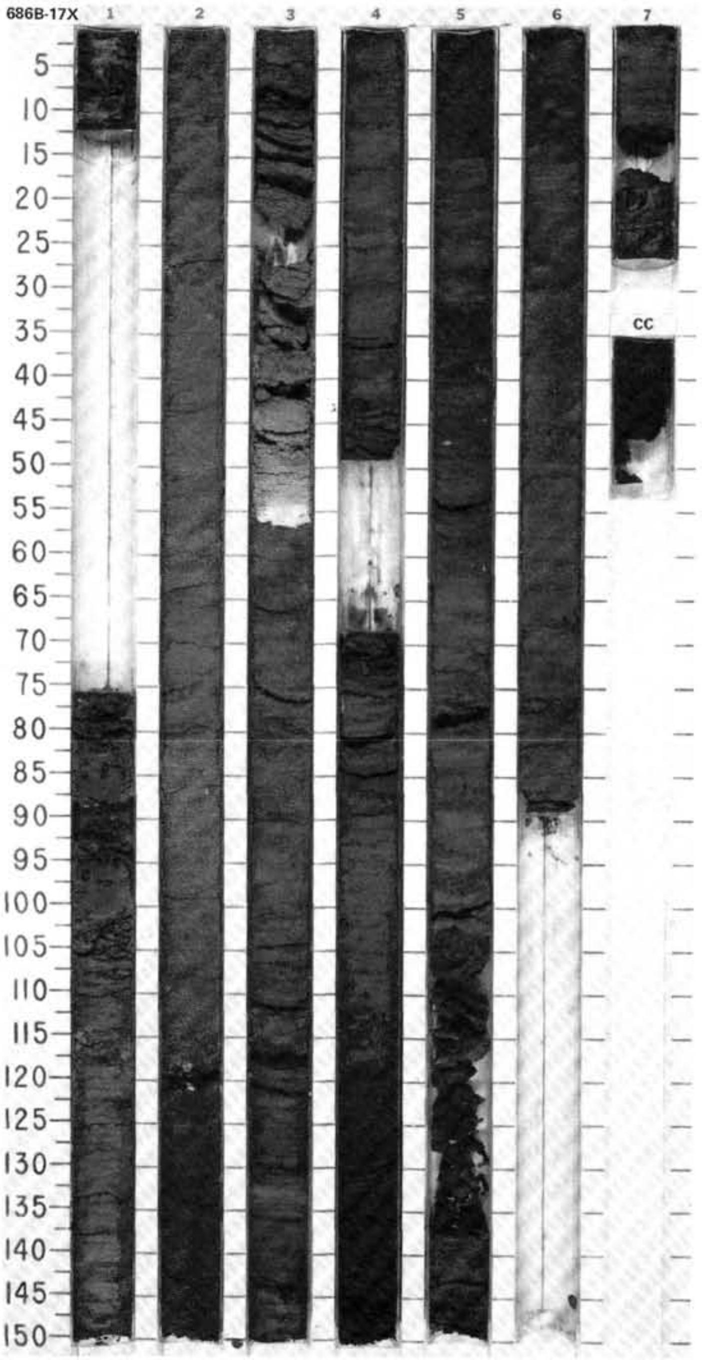

SITE 686 HOLE B CORE 18X CORED INTERVAL 607.3-616.8 mbsl; 160.5-170.0 mbsf

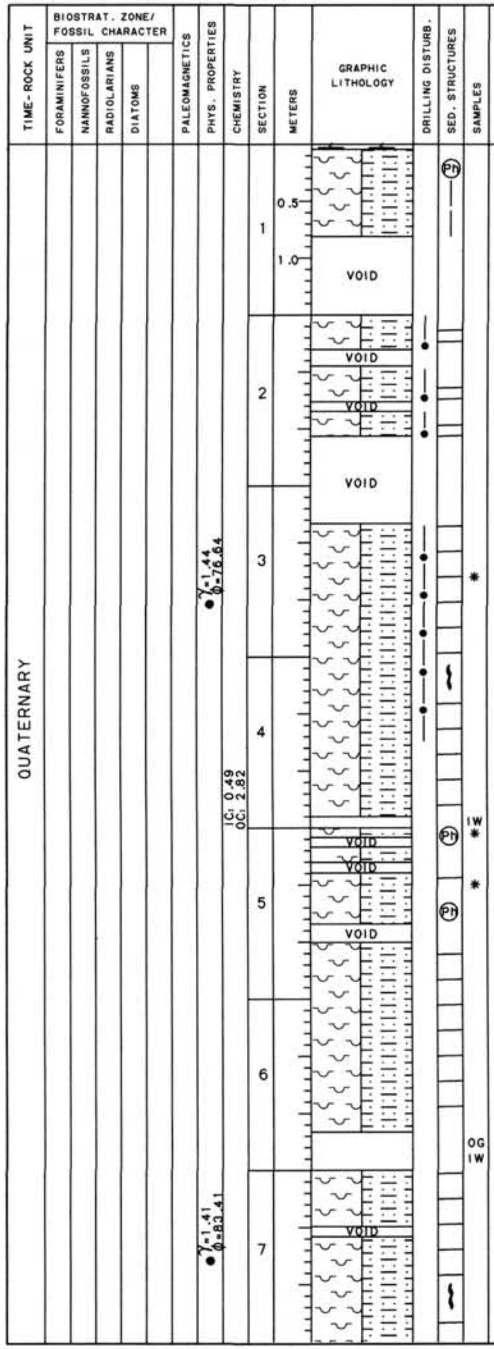

LITHOLOGIC DESCRIPTION

DIATOMACEOUS MUD

Major lithology: diatomaceous mud, olive gray to dark olive (5Y 4/2 to 5Y 3/2), faintly laminated.

Minor lithologies:
1. dolomite.
2. phosphate nodules.

SMEAR SLIDE SUMMARY (%):

	3, 86 D	5, 5 M	5, 53 D	8, 40 D
TEXTURE:				
Silt	70	50	50	55
Clay	30	50	50	45
COMPOSITION:				
Quartz	1	—	1	2
Clay	30	10	45	40
Dolomite	1	5	—	—
Accessory minerals				
Pyrite	2	2	Tr	—
Micrite	Tr	40	5	5
Nannofossils	—	—	1	Tr
Diatoms	66	43	48	53
Silicoflagellates	—	—	Tr	—

(CON'T.)

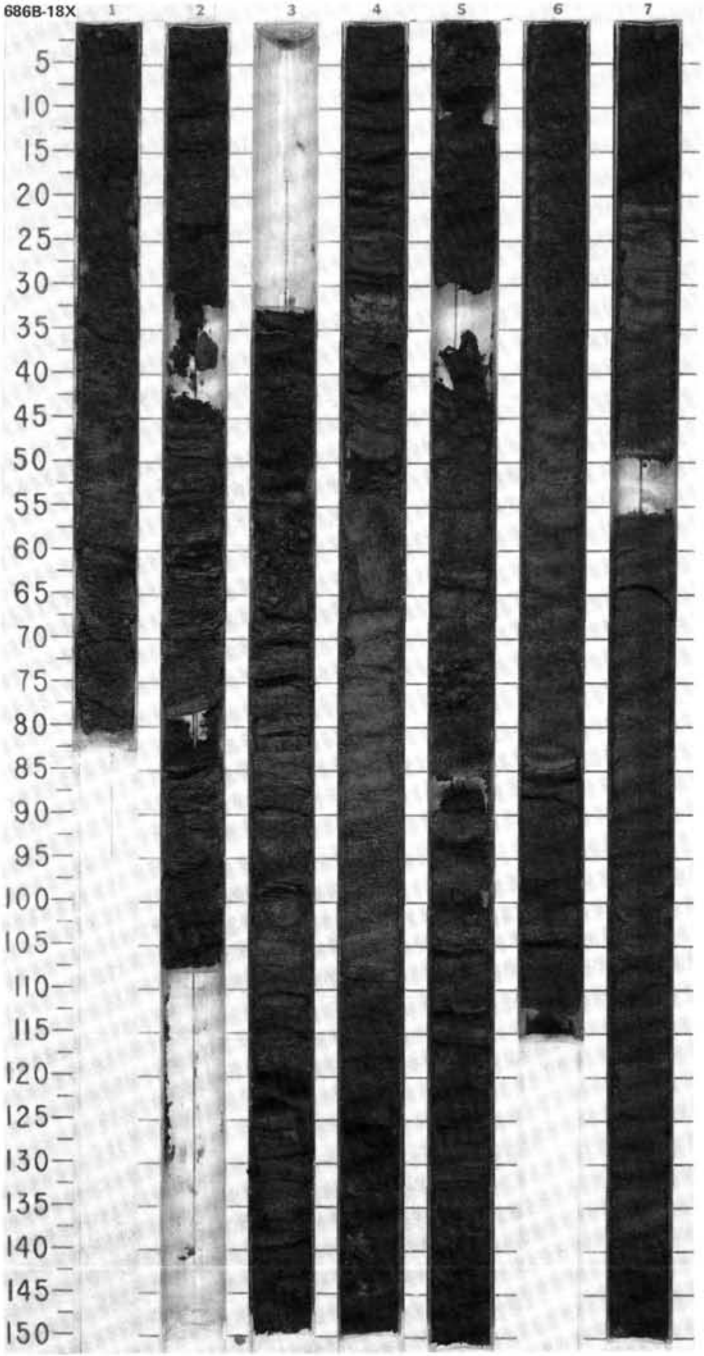

SITE 686 HOLE B CORE 18X CORED INTERVAL 607.3-616.8 mbsl; 160.5-170.0 mbsf

TIME-ROCK UNIT	BIOSTRAT. ZONE/ FOSSIL CHARACTER				PALEOMAGNETICS	PHYS. PROPERTIES	CHEMISTRY	SECTION	METERS	GRAPHIC LITHOLOGY	DRILLING DISTURB.	SED. STRUCTURES	SAMPLES	LITHOLOGIC DESCRIPTION
	FORAMINIFERS	NANNOFOSSILS	RADIOLARIANS	DIATOMS										
QUATERNARY	B*			*N. reinholdii* Zone *				8 CC	0.5	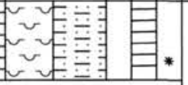			*	(CON'T.)

SITE 686 HOLE B CORE 19X CORED INTERVAL 616.8-626.3 mbsl; 170.0-179.5 mbsf

TIME-ROCK UNIT	BIOSTRAT. ZONE/ FOSSIL CHARACTER				PALEOMAGNETICS	PHYS. PROPERTIES	CHEMISTRY	SECTION	METERS	GRAPHIC LITHOLOGY	DRILLING DISTURB.	SED. STRUCTURES	SAMPLES	LITHOLOGIC DESCRIPTION
	FORAMINIFERS	NANNOFOSSILS	RADIOLARIANS	DIATOMS										
QUATERNARY	B*			*N. reinholdii* Zone *				1 CC	0.5 1.0	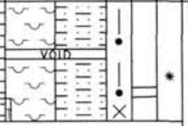 VOID			*	DIATOMACEOUS MUD

DIATOMACEOUS MUD

Major lithology: diatomaceous mud, dark olive gray (5Y 3/2), massive.

SMEAR SLIDE SUMMARY (%):

	1, 63 D
TEXTURE:	
Silt	55
Clay	45
COMPOSITION:	
Clay	40
Accessory minerals	
Pyrite	2
Micrite	5
Diatoms	53

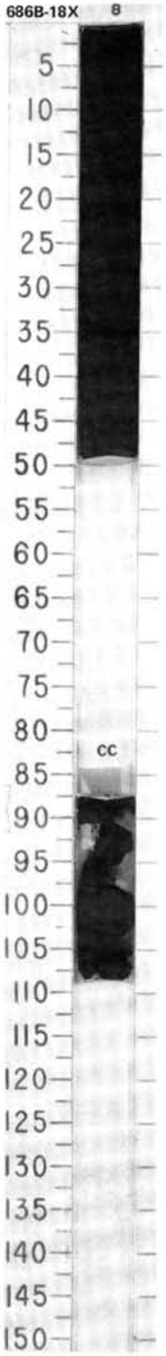

SITE 686 HOLE B CORE 20X CORED INTERVAL 626.3-635.8 mbsl; 179.5-189.0 mbsf

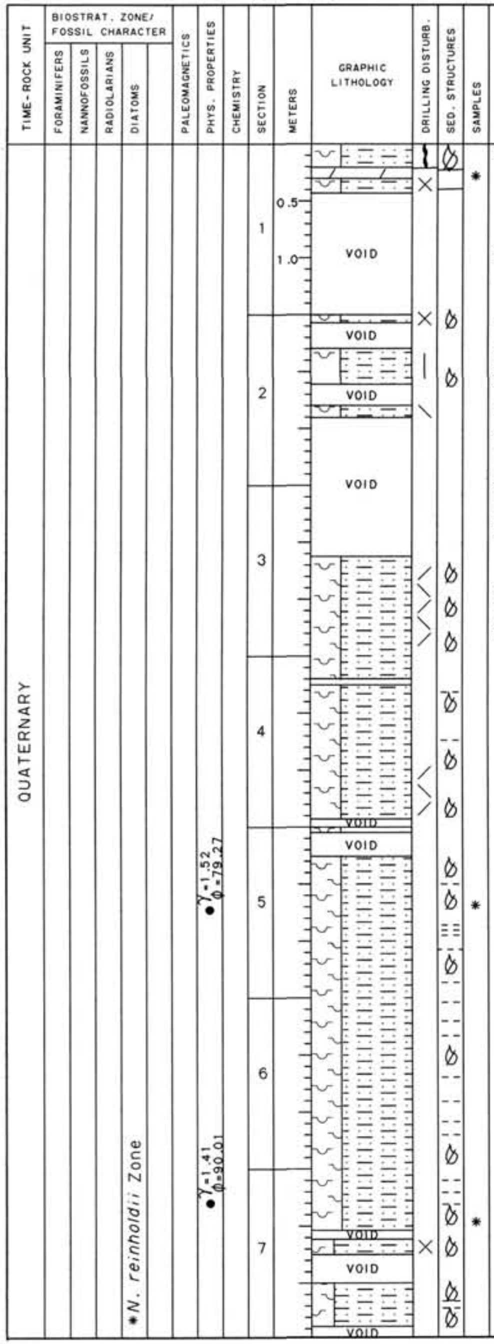

LITHOLOGIC DESCRIPTION

DIATOMACEOUS MUD

Major lithology: diatomaceous mud, dark olive to dark olive gray (5Y 3/3 to 5Y 3/2). Massive to faintly laminated, scattered bivalve shells.

Minor lithologies: dolomite.

SMEAR SLIDE SUMMARY (%):

	1, 25 D	5, 73 D	7, 44 M
TEXTURE:			
Sand	—	—	15
Silt	40	40	25
Clay	60	60	60
COMPOSITION:			
Quartz	7	Tr	5
Feldspar	3	—	5
Rock fragments	1	—	—
Mica	1	—	Tr
Clay	26	57	60
Volcanic glass	2	2	Tr
Calcite	—	—	5
Accessory minerals			
Pyrite	—	2	—
Glauconite	—	—	Tr
Micrite	35	4	—
Foraminifers	—	—	10
Nannofossils	—	Tr	Tr
Diatoms	25	35	15
Sponge spicules	—	Tr	—

(CONT.)

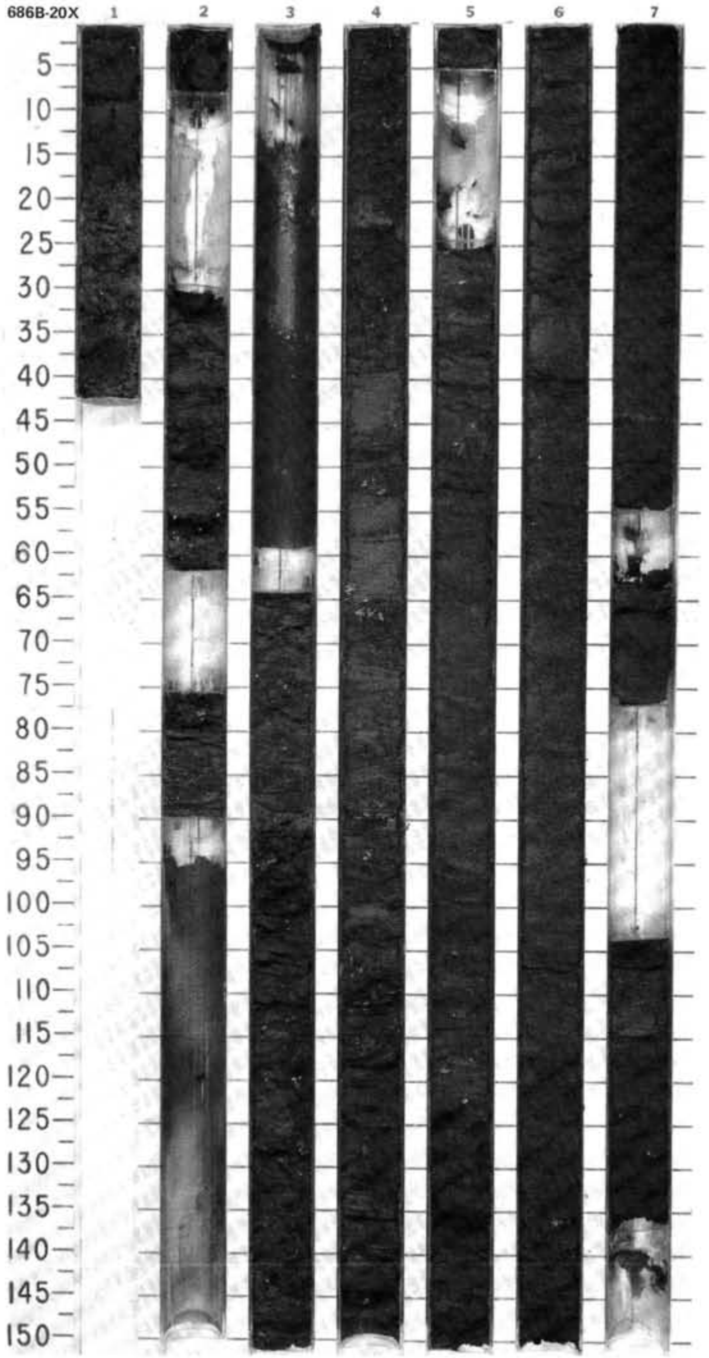

SITE 686 HOLE B CORE 20X CORED INTERVAL 626.3-635.8 mbsl; 179.5-189.0 mbsf

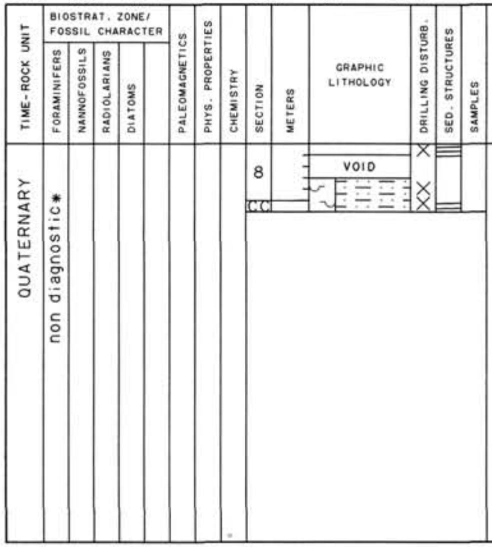

LITHOLOGIC DESCRIPTION

(CONT.)

SITE 686 HOLE B CORE 21X CORED INTERVAL 635.8-645.3 mbsl; 189.0-198.5 mbsf

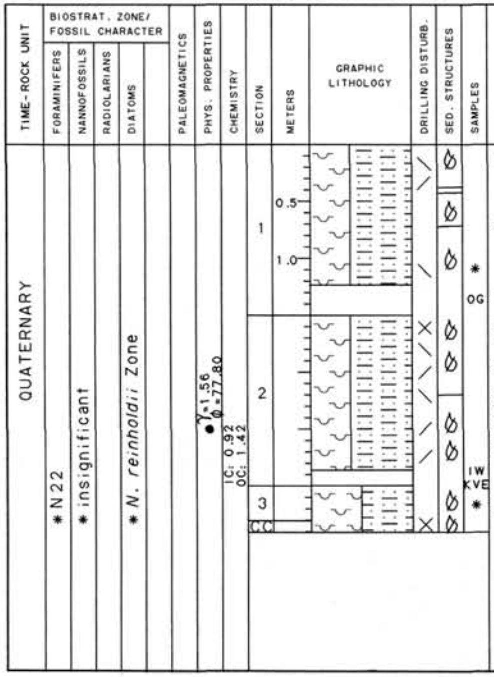

LITHOLOGIC DESCRIPTION

DIATOMACEOUS MUD

Major lithology: diatomaceous mud, olive gray to dark olive (5Y 4/1.5, 5Y 4/2, 5Y 3/3). Massive, with scattered bivalve shells.

SMEAR SLIDE SUMMARY (%):

	1, 114 M	3, 16 D
TEXTURE:		
Silt	47	46
Clay	53	54
COMPOSITION:		
Quartz	—	1
Clay	52	48
Volcanic glass	1	1
Calcite/dolomite	—	2
Accessory minerals		
Pyrite	1	2
Micrite	1	6
Nannofossils	Tr	—
Diatoms	45	40

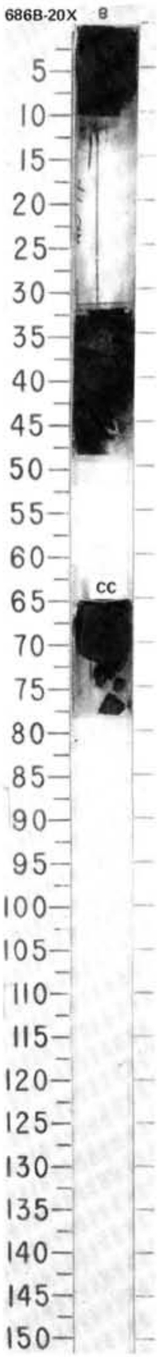

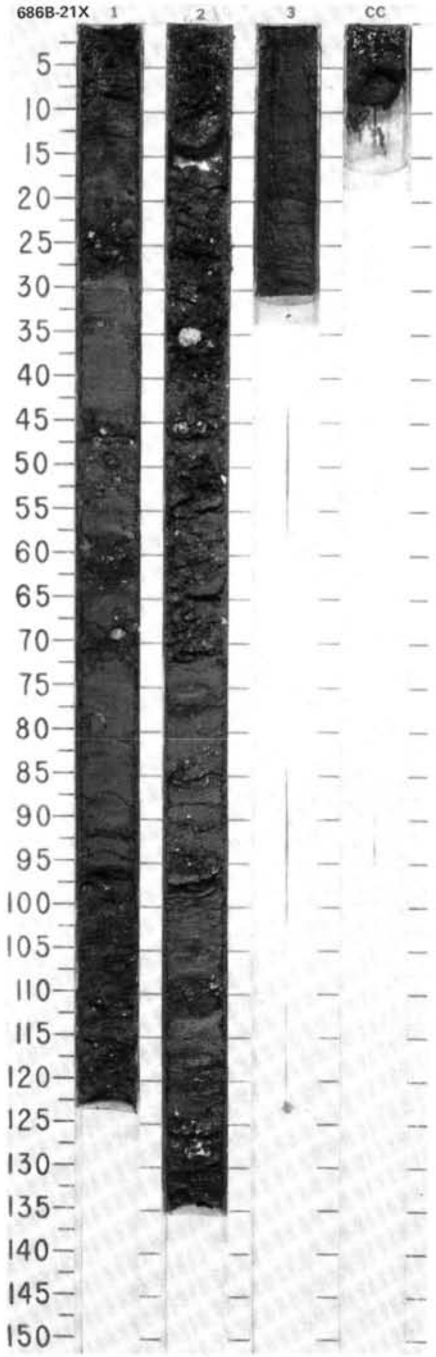

SITE 686 HOLE B CORE 22X CORED INTERVAL 645.3-654.8 mbsl; 198.5-208.0 mbsf

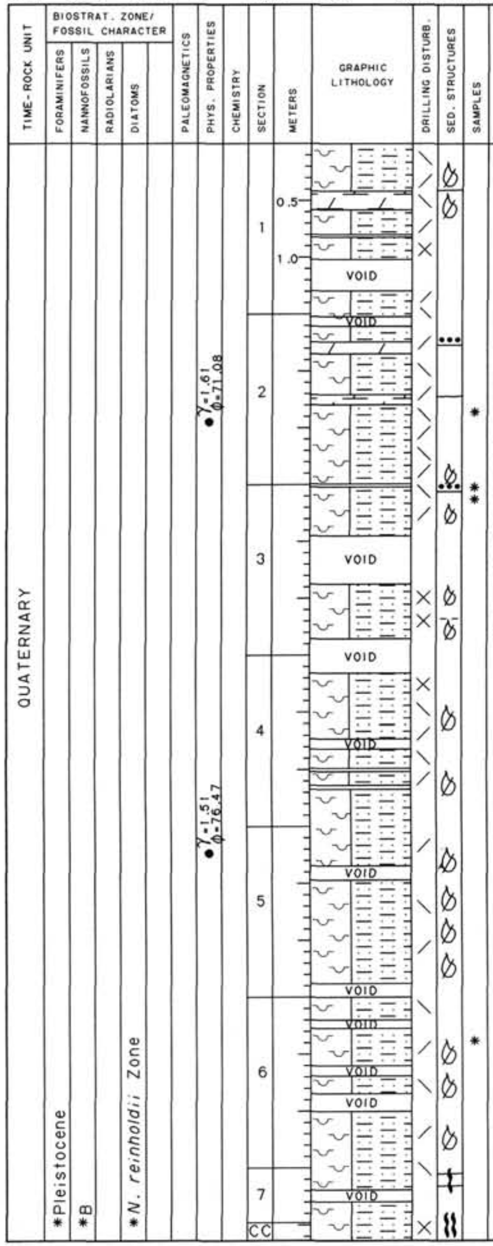

LITHOLOGIC DESCRIPTION

DIATOMACEOUS MUD and SILT

Major lithology: diatomaceous mud and silt, dark olive, olive gray, dark olive gray, olive (5Y 3/3, 5Y 4/1.5, 5Y 3/2, 5Y 4/4); massive.

Minor lithologies:
1. dolomite.
2. sand with bivalve shell fragments.

SMEAR SLIDE SUMMARY (%):

	2, 90 D	3, 6 M	3, 9 D	6, 34 D
TEXTURE:				
Sand	—	50	—	—
Silt	45	30	25	58
Clay	55	20	75	42
COMPOSITION:				
Quartz	1	10	1	Tr
Feldspar	—	15	—	Tr
Rock fragments	—	10	—	—
Mica	—	—	—	Tr
Clay	30	15	45	40
Volcanic glass	—	—	—	6
Dolomite	30	15	25	2
Accessory minerals	—	5	—	—
Pyrite	3	—	2	2
Glauconite	—	Tr	—	—
Foraminifers	—	15	—	—
Diatoms	36	15	27	50
Sponge spicules	—	—	Tr	Tr

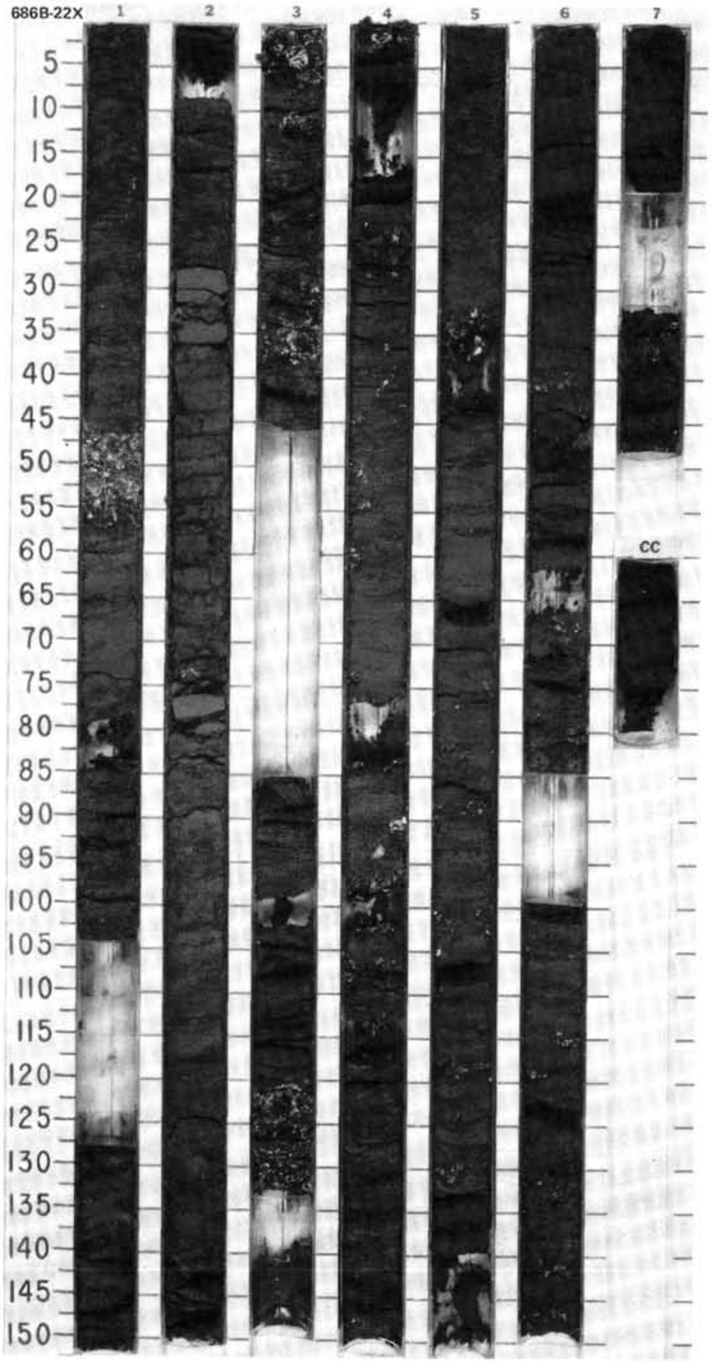

SITE 686 HOLE B CORE 23X CORED INTERVAL 654.8-664.3 mbsl; 208.0-217.5 mbsf

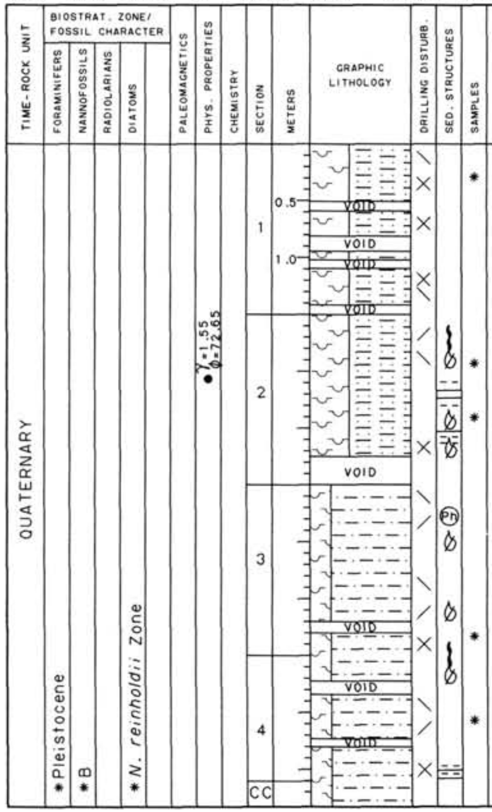

LITHOLOGIC DESCRIPTION

DIATOMACEOUS MUD

Major lithology: diatomaceous mud, very dark gray and dark gray (5Y 3/1, 5Y 4/1), massive.

Minor lithologies:
1. phosphate nodule, small, friable.
2. bivalve shells and shell fragments.
3. muddy sand, foraminifer-rich.

SMEAR SLIDE SUMMARY (%):

	1, 26 D	2, 43 M	2, 99 D	3, 139 D	4, 56 D
TEXTURE:					
Sand	—	—	5	40	35
Silt	49	80	45	40	35
Clay	51	20	50	20	30
COMPOSITION:					
Quartz	2	5	4	15	10
Feldspar	—	—	—	15	10
Rock fragments	1	—	1	15	5
Mica	Tr	Tr	—	Tr	—
Clay	51	10	48	20	30
Volcanic glass	4	—	5	10	10
Calcite	—	75	—	5	—
Accessory minerals					
Pyrite	2	—	2	—	—
Phosphate	—	—	—	—	Tr
Glauconite	—	—	—	—	Tr
Micrite	Tr	—	5	—	—
Foraminifers	—	—	—	20	20
Diatoms	40	10	35	—	15
Sponge spicules	Tr	—	—	—	—

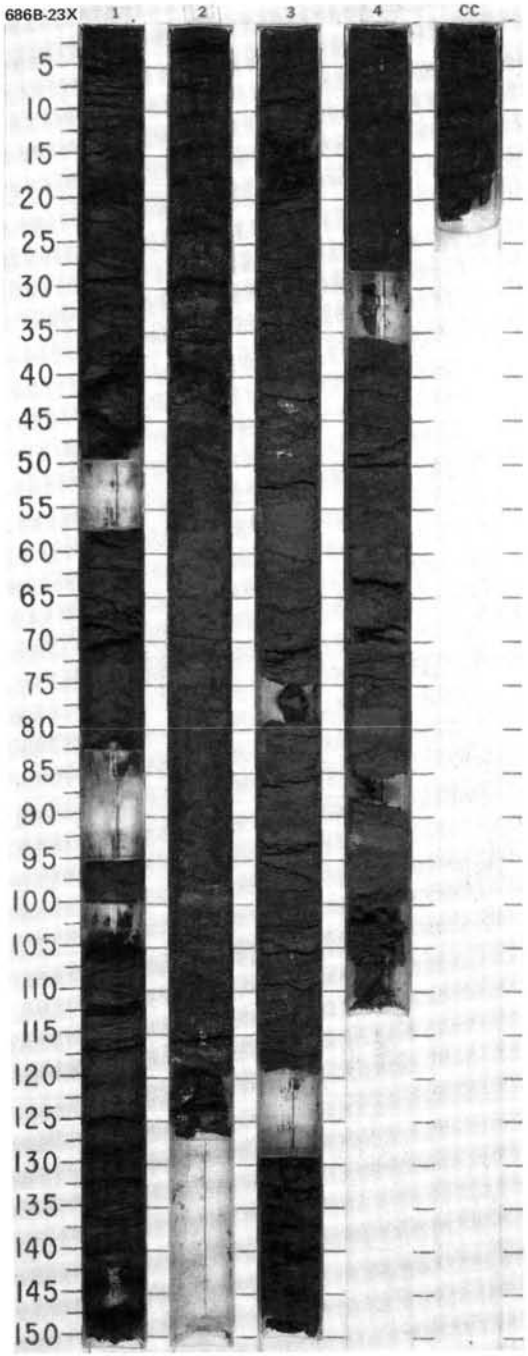

SITE 686 HOLE B CORE 24X CORED INTERVAL 664.3-673.8 mbsl; 217.5-227.0 mbsf

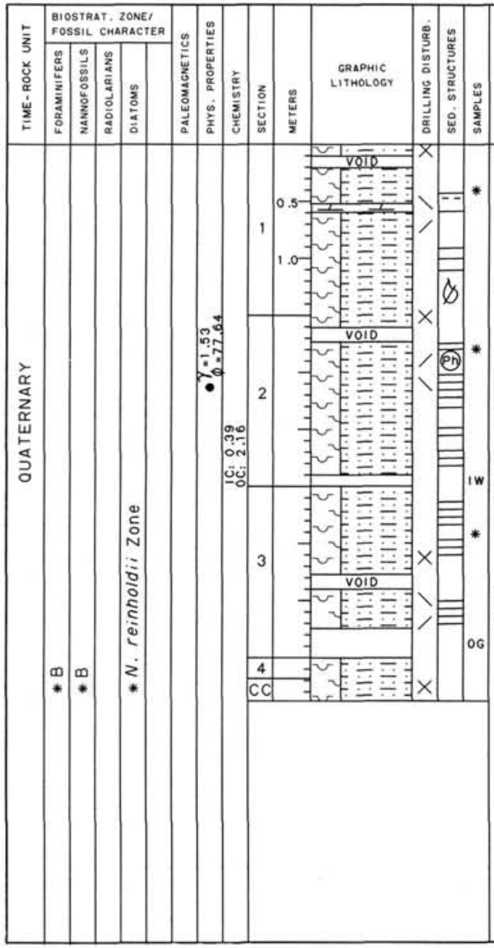

LITHOLOGIC DESCRIPTION

DIATOMACEOUS MUD

Major lithology: diatomaceous mud, dark olive and dark olive gray (5Y 3/3, 5Y 3/2), Foraminifer-bearing, massive to mottled to faintly laminated.

Minor lithologies:
1. dolomite.
2. phosphate nodules, small, friable.

SMEAR SLIDE SUMMARY (%):

	1, 33 D	2, 33 M	3, 47 D
TEXTURE:			
Silt	45	70	42
Clay	55	30	58
COMPOSITION:			
Quartz	5	5	1
Feldspar	1	—	—
Rock fragments	3	Tr	1
Clay	45	30	56
Volcanic glass	2	—	2
Calcite/dolomite	—	Tr	—
Accessory minerals			
Pyrite	3	—	3
Glauconite	Tr	—	—
Micrite	15	—	2
Foraminifers	Tr	Tr	—
Nannofossils	—	Tr	—
Diatoms	26	65	35

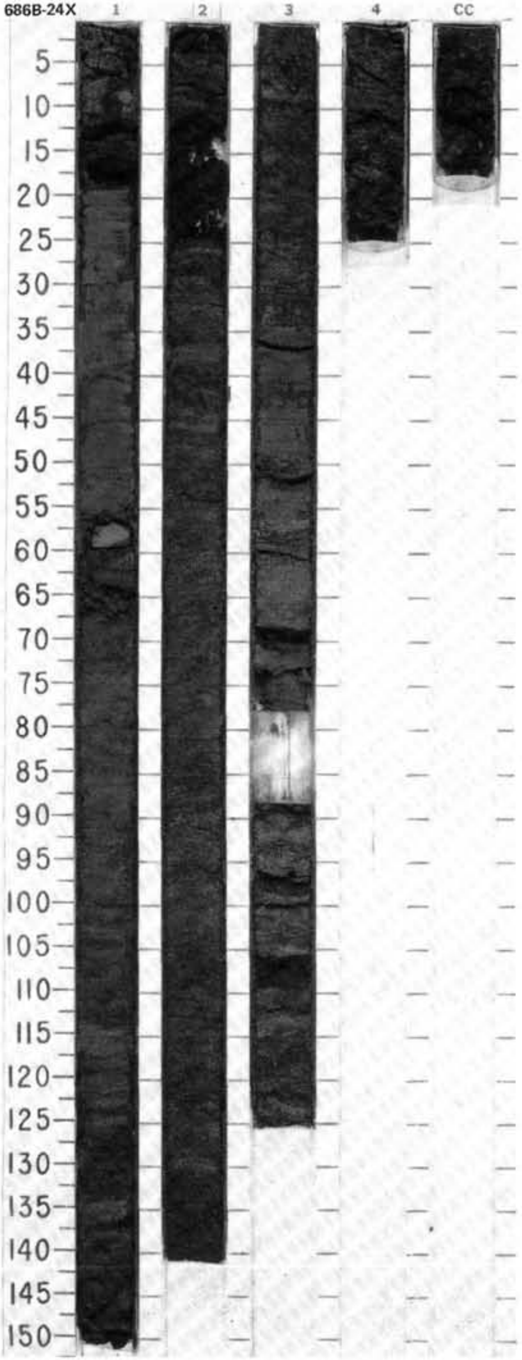

SITE 686 HOLE B CORE 25X CORED INTERVAL 673.8-683.3 mbsl; 227.0-236.5 mbsf

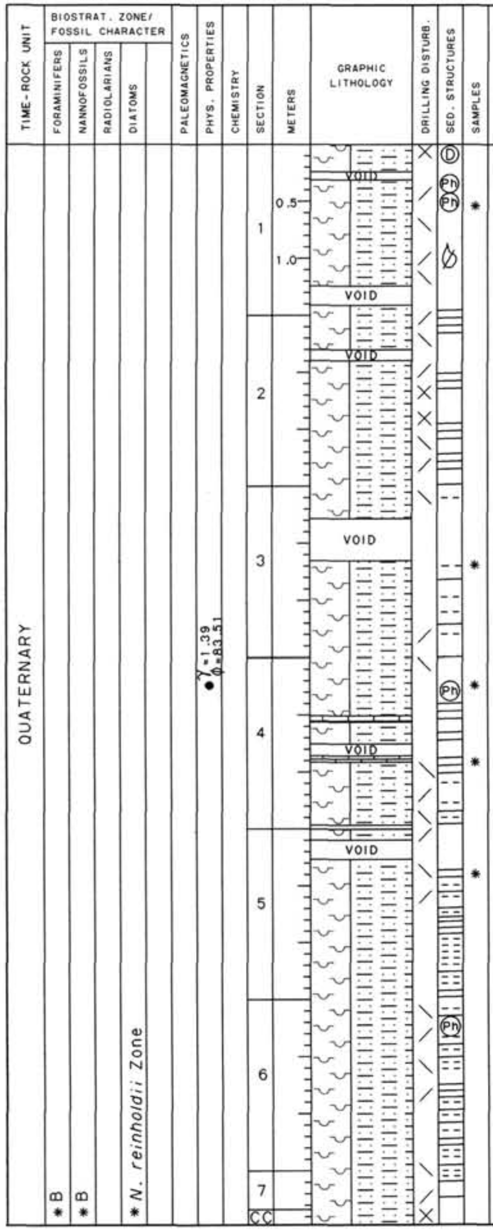

LITHOLOGIC DESCRIPTION

DIATOMACEOUS MUD

Major lithology: diatomaceous mud, olive gray to black, (5Y 3/2, 5Y 4/2, 5Y 2.5/1, 5Y 3.5/2). Massive to laminated or faintly laminated.

Minor lithologies:
1. dolomite.
2. phosphate nodules, small, friable.
3. micritic mud.

SMEAR SLIDE SUMMARY (%):

	1, 53 M	3, 64 D	4, 36 M	4, 92 M	5, 37 M
TEXTURE:					
Sand	40	—	30	—	—
Silt	15	56	40	—	30
Clay	45	44	30	100	70
COMPOSITION:					
Quartz	5	4	5	—	5
Feldspar	—	1	—	—	—
Rock fragments	—	2	—	—	—
Mica	—	1	—	—	—
Clay	40	41	—	10	10
Volcanic glass	—	3	—	—	—
Accessory minerals					
Phosphate	40	—	85	—	Tr
Micrite	5	3	3	80	60
Foraminifers	Tr	—	2	—	5
Diatoms	10	45	5	10	20
Fish remains	—	—	Tr	—	—

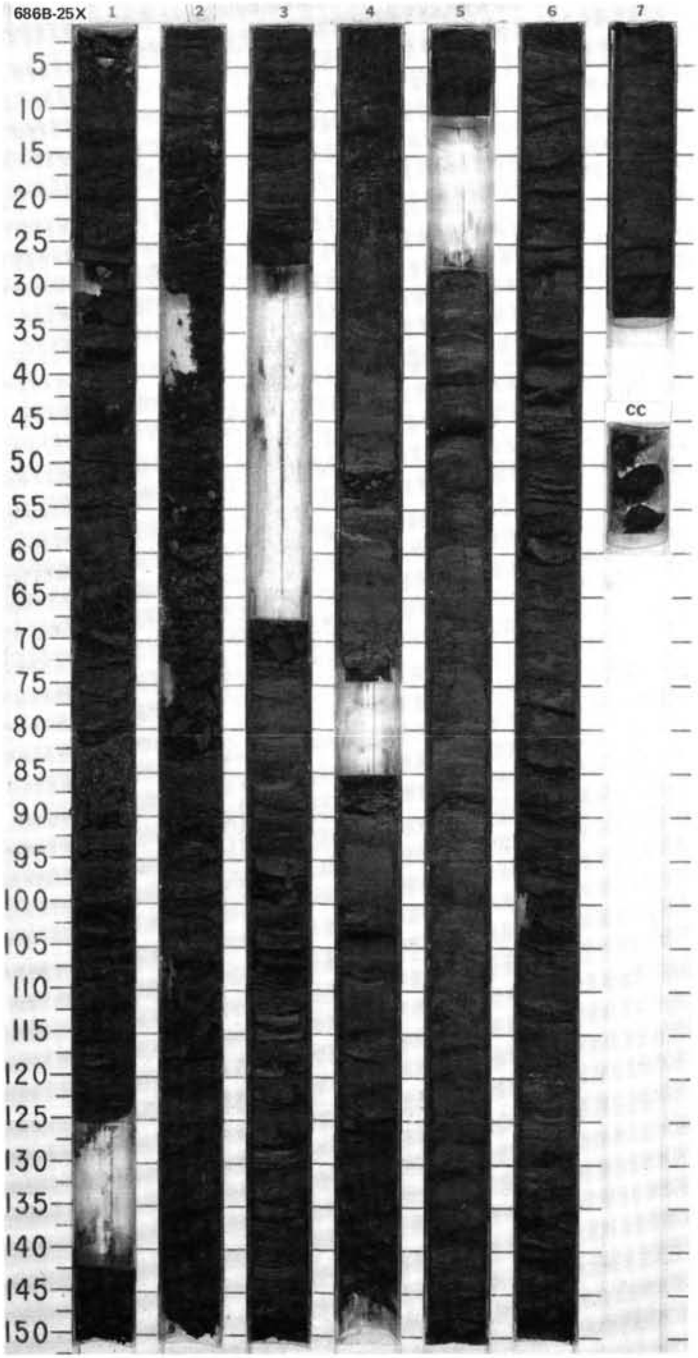

SITE 686 HOLE B CORE 26X CORED INTERVAL 683.3-692.8 mbsl; 236.5-246.0 mbsf

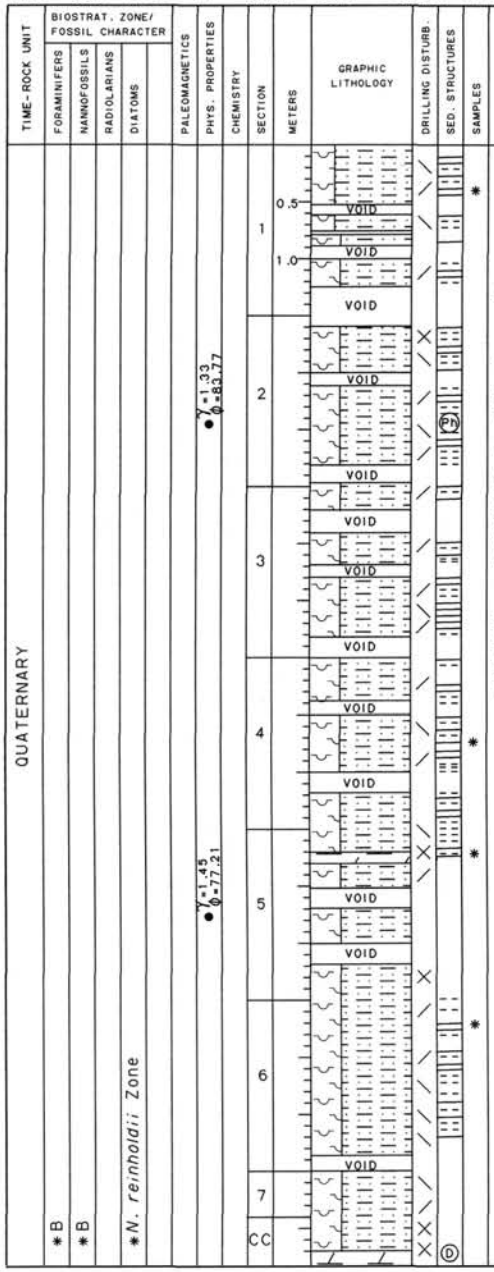

LITHOLOGIC DESCRIPTION

DIATOMACEOUS MUD and SILT

Major lithology: diatomaceous mud and silt, dark olive and olive, (5Y 3/3, 5Y 4/3). Laminated to slightly burrowed, mottled to massive.

Minor lithologies:
1. phosphate nodules, small.
2. dolomite and dolomitic mud.
3. micritic mud.

SMEAR SLIDE SUMMARY (%):

	1, 48 D	4, 76 M	5, 23 D	6, 21 D
TEXTURE:				
Sand	5	—	5	—
Silt	45	56	35	49
Clay	50	44	60	51
COMPOSITION:				
Quartz	5	2	Tr	2
Feldspar	5	1	—	1
Rock fragments	—	1	Tr	1
Clay	50	40	8	50
Volcanic glass	—	2	2	2
Calcite	5	—	—	—
Accessory minerals				
Opaques	5	—	—	—
Hornblende	—	—	—	Tr
Pyrite	—	—	—	2
Micrite	—	4	60	1
Foraminifers	10	—	—	—
Nannofossils	Tr	—	—	—
Diatoms	20	50	20	41
Silicoflagellates	Tr	—	—	—
Pellets	—	—	10	—

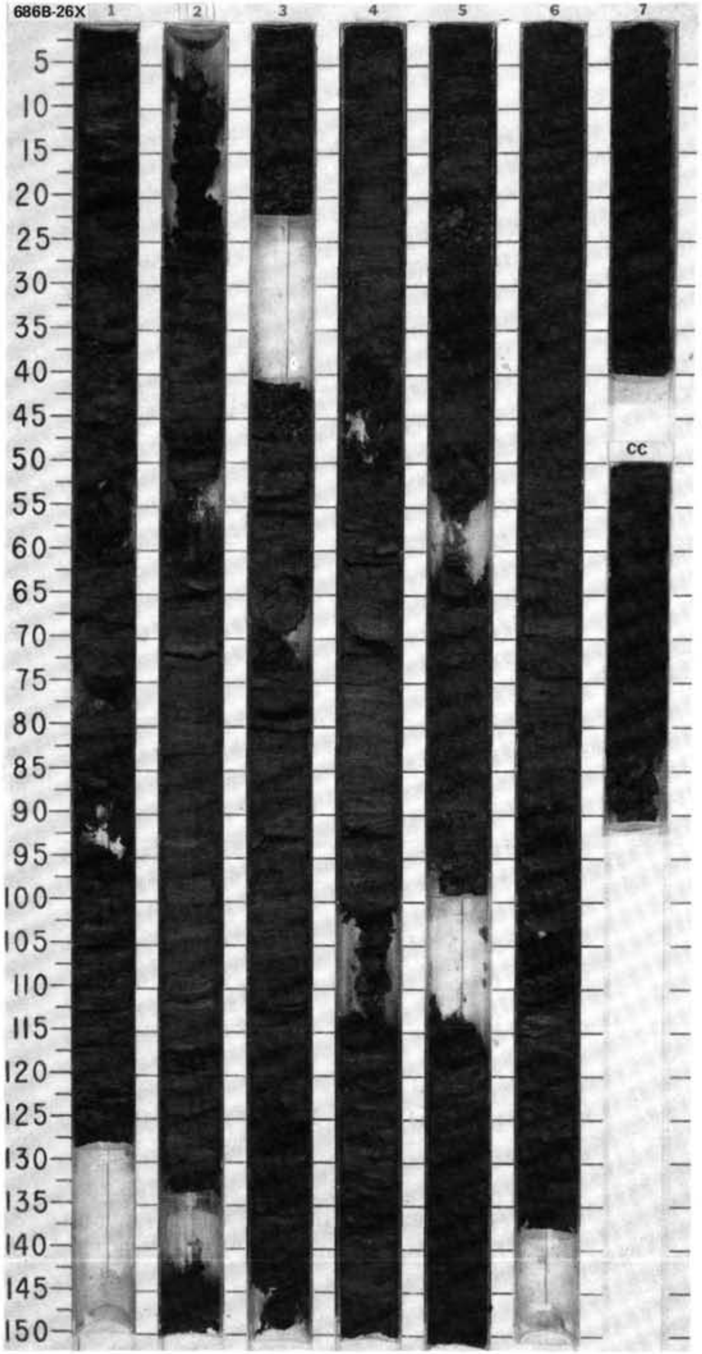

SITE 686 HOLE B CORE 27X CORED INTERVAL 692.8-702.3 mbsl; 246.0-255.5 mbsf

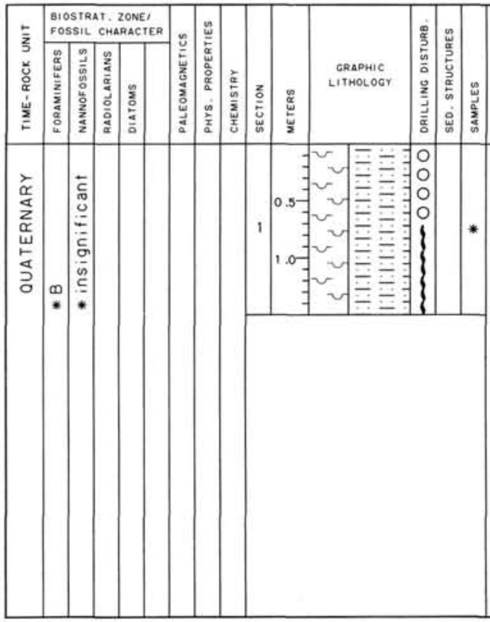

LITHOLOGIC DESCRIPTION

DIATOMACEOUS MUD

Major lithology: diatomaceous mud, dark olive gray (5Y 3/2), disturbed by drilling.

SMEAR SLIDE SUMMARY (%):

	1, 75 D
TEXTURE:	
Silt	58
Clay	42
COMPOSITION:	
Quartz	2
Feldspar	1
Rock fragments	1
Mica	Tr
Clay	48
Volcanic glass	1
Accessory minerals	
Pyrite	3
Micrite	3
Diatoms	40
Sponge spicules	1

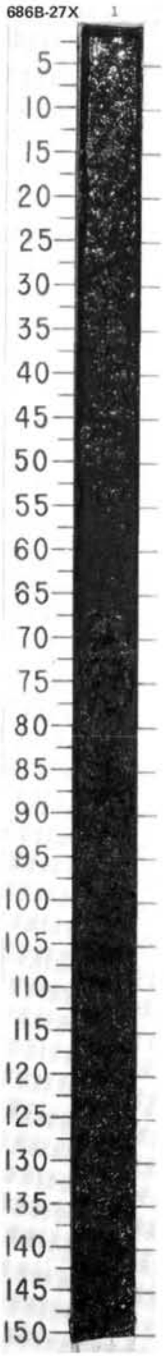

SITE 686 HOLE B CORE 28X CORED INTERVAL 702.3-711.8 mbsl; 255.5-265.0 mbsf

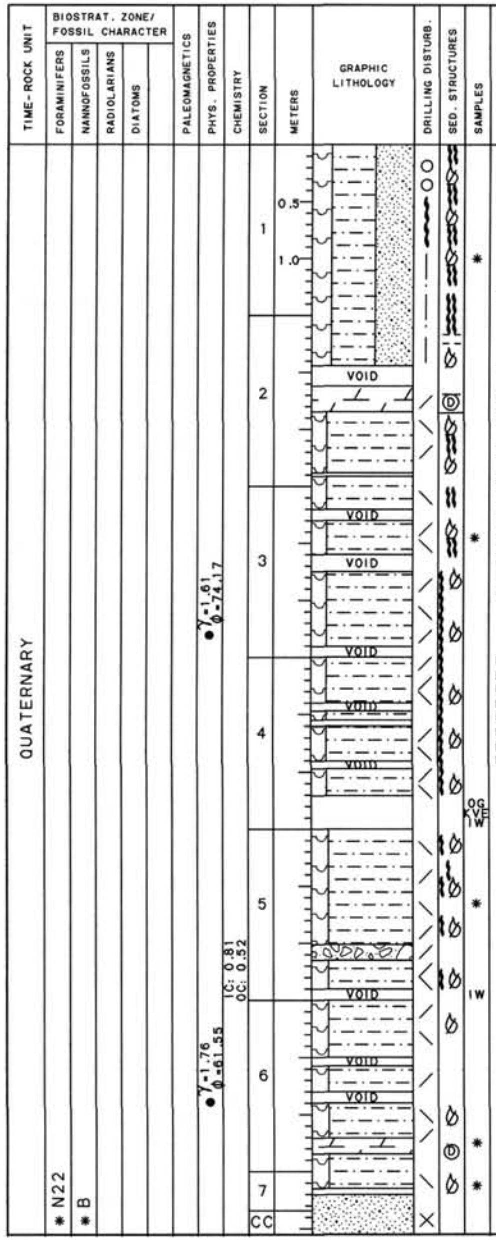

LITHOLOGIC DESCRIPTION

DIATOMACEOUS MUD and SILT

Major lithology: diatomaceous mud and silt, dark olive gray, olive, and greenish gray (5Y 3/2, 5Y 4/3, 5GY 4.5/1). Sandy with scattered bivalve shells, massive, burrowed.

Minor lithologies:
1. dolomite.
2. sand, olive gray (5Y 4/2), muddy and silty.
3. shell beds, concentration of abraded bivalve shells.

SMEAR SLIDE SUMMARY (%):

	1, 100 D	3, 46 D	5, 66 D	6, 133 M	7, 12 D
TEXTURE:					
Sand	10	—	10	5	60
Silt		50	63	85	20
Clay		50	27	10	20
COMPOSITION:					
Quartz	10	8	35	3	20
Feldspar	15	10	5	1	25
Rock fragments	3	5	10	1	5
Mica	—	1	Tr	—	1
Clay	20	37	26	5	16
Volcanic glass	3	3	2	1	5
Calcite	7	—	—	—	—
Dolomite	—	8	—	25	5
Accessory minerals					
Pyrite	5	5	5	1	5
Glauconite	2	2	—	—	2
Hornblende	Tr	—	—	—	2
Micrite	—	7	5	60	3
Foraminifers	5	3	—	—	5
Nannofossils	—	—	—	—	Tr
Diatoms	25	10	12	3	5
Radiolarians	Tr	—	—	—	—
Sponge spicules	2	1	Tr	Tr	1
Silicoflagellates	—	Tr	—	—	—
Fish remains	Tr	—	—	—	—
Spar cement	3	—	—	—	—

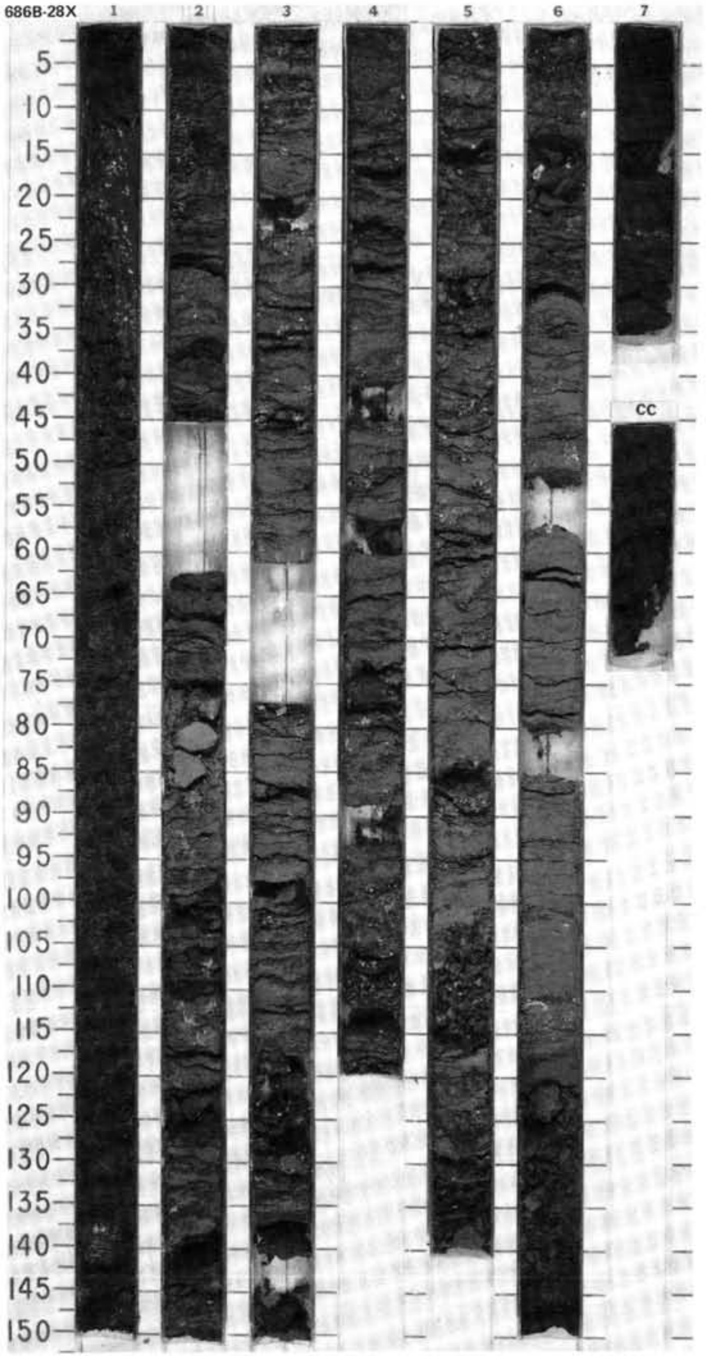

SITE 686 HOLE B CORE 29X CORED INTERVAL 711.8-721.3 mbsl; 265.0-274.5 mbsf

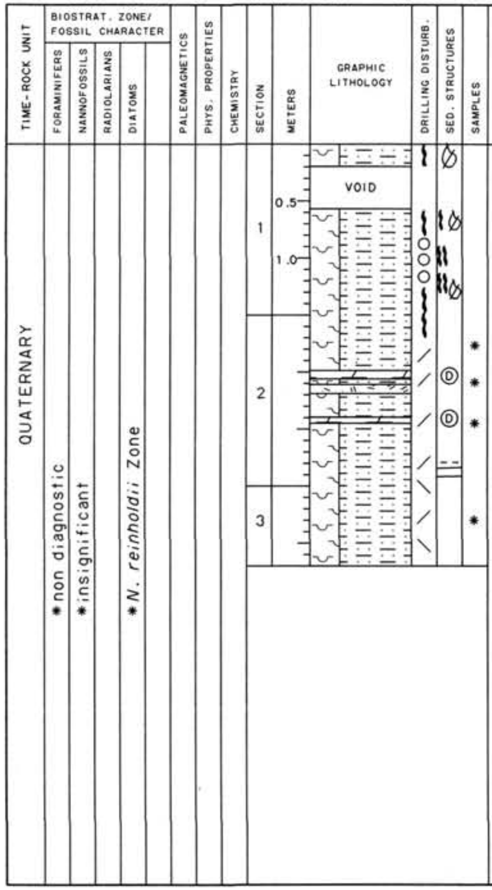

LITHOLOGIC DESCRIPTION

DIATOMACEOUS MUD

Major lithology: diatomaceous mud, greenish gray, gray, olive gray, dark olive gray (5GY 4/1, 5Y 4/1, 5Y 4/2, 5Y 3/2); massive.

Minor lithologies:
1. volcanic ash.
2. dolomite.
3. micritic mud.

SMEAR SLIDE SUMMARY (%):

	2, 37 D	2, 66 M	2, 92 M	3, 35 D
TEXTURE:				
Sand	—	5	—	—
Silt	50	90	65	60
Clay	50	5	35	40
COMPOSITION:				
Quartz	7	2	Tr	—
Feldspar	8	2	—	—
Rock fragments	2	1	—	—
Mica	2	3	—	—
Clay	47	3	89	40
Volcanic glass	2	87	Tr	2
Calcite	5	—	—	—
Dolomite	—	—	10	—
Accessory minerals				
Pyrite	3	1	1	2
Glauconite	2	—	—	—
Hornblende	Tr	—	—	—
Micrite	5	—	—	1
Foraminifers	2	—	—	—
Nannofossils	Tr	—	—	Tr
Diatoms	15	1	—	55
Sponge spicules	Tr	—	—	—

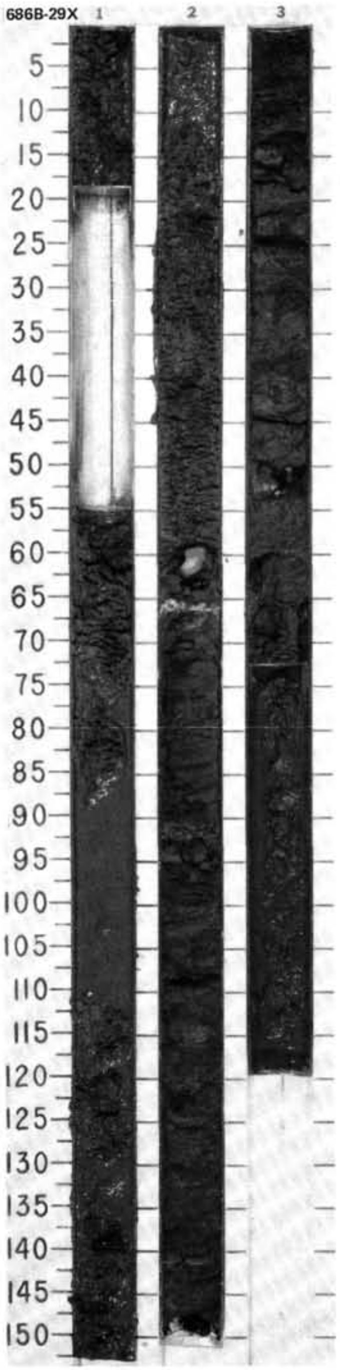

SITE 686 HOLE B CORE 30X CORED INTERVAL 721.3-730.8 mbsl; 274.5-284.0 mbsf

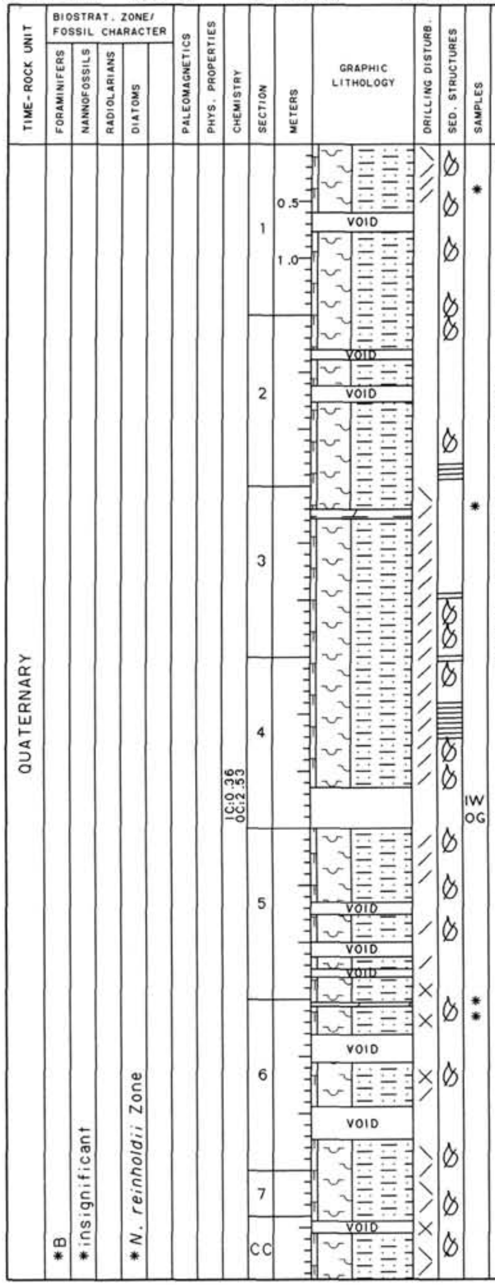

LITHOLOGIC DESCRIPTION

DIATOMACEOUS MUD

Major lithology: diatomaceous mud, dark greenish gray, dark olive gray, olive, and olive gray (5GY 4/1, 5GY 3/2, 5Y 4/3, 5Y 4/2). Massive to faintly laminated, scattered bivalve shells.

Minor lithologies:
1. *dolomite and dolomitic mud.*
2. shelly beds.

SMEAR SLIDE SUMMARY (%):

	1, 49 *D*	3, 20 *M*	6, 3 *M*	6, 9 *M*
TEXTURE:				
Sand	15	—	—	—
Silt	70	60	60	67
Clay	15	40	40	33
COMPOSITION:				
Quartz	10	1	1	1
Feldspar	3	1	—	—
Rock fragments	5	1	1	—
Mica	1	Tr	—	—
Clay	10	—	40	33
Volcanic glass	5	—	—	Tr
Dolomite	5	86	2	40
Accessory minerals				
Pyrite	1	1	3	1
Micrite	—	—	3	—
Foraminifers	15	—	—	25
Diatoms	45	10	50	—
Sponge spicules	—	—	—	Tr
Silicoflagellates	—	Tr	—	—

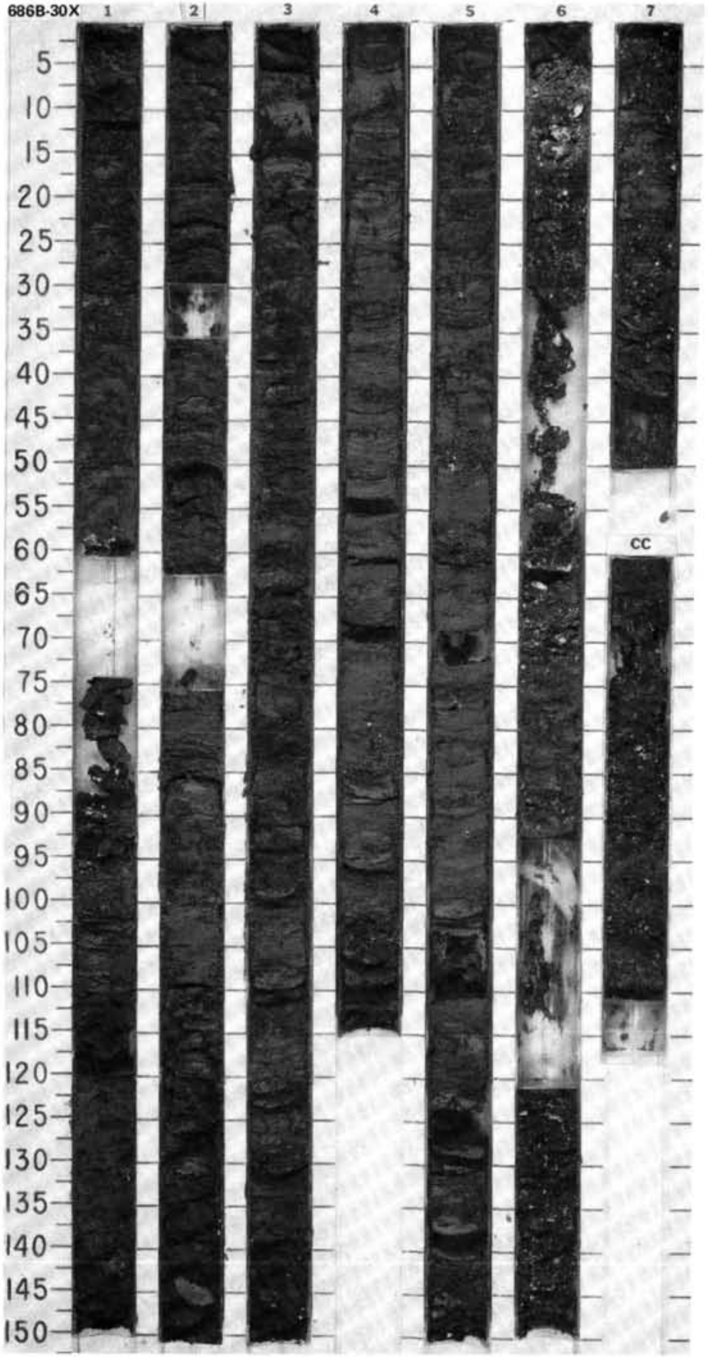

SITE 686 HOLE B CORE 31X CORED INTERVAL 730.8-740.3 mbsl; 284.0-293.5 mbsf

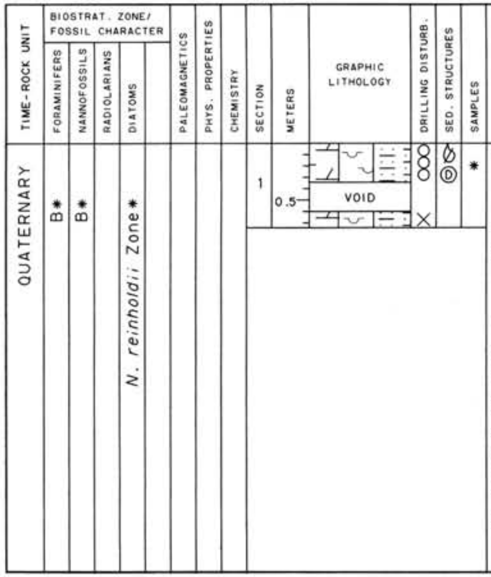

LITHOLOGIC DESCRIPTION

DIATOMACEOUS MUD

Major lithology: diatomaceous mud, olive gray (5Y 4/2). Massive with scattered bivalve shells.

Minor lithology: dolomite.

SMEAR SLIDE SUMMARY (%):

	1, 19 D
TEXTURE:	
Sand	5
Silt	75
Clay	20
COMPOSITION:	
Quartz	8
Feldspar	2
Rock fragments	2
Dolomite	60
Accessory minerals	1
Pyrite	2
Diatoms	25

SITE 686 HOLE B CORE 32X CORED INTERVAL 740.3-749.8 mbsl; 293.5-303.0 mbsf

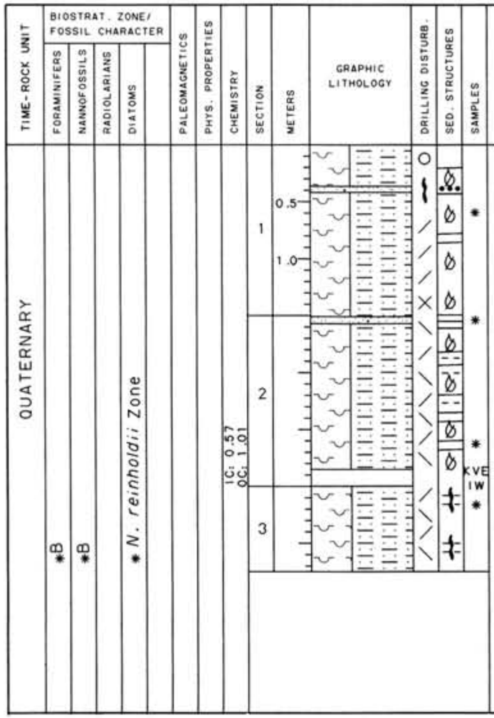

LITHOLOGIC DESCRIPTION

DIATOMACEOUS MUD and SILT

Major lithology: diatomaceous mud and silt, dark olive, dark gray, olive gray, olive (5Y 3/3, 5Y 3/1.5, 5Y 4/2, 5Y 5/4). Massive to laminated with slight mottling, with scattered bivalve shells.

Minor lithologies: sand, dark olive gray (5Y 3/2) and quartzo-feldspathic occurs in thin beds.

SMEAR SLIDE SUMMARY (%):

	1, 61 D	2, 4 M	2, 123 D	3, 9 D
TEXTURE:				
Sand	—	60	—	—
Silt	58	35	60	65
Clay	42	5	40	35
COMPOSITION:				
Quartz	5	38	20	1
Feldspar	3	27	5	—
Rock fragments	2	10	7	1
Mica	—	1	Tr	—
Clay	42	4	40	20
Volcanic glass	5	3	—	—
Calcite/dolomite	—	2	—	1
Accessory minerals	—	4	—	—
Pyrite	3	5	Tr	2
Glauconite	—	Tr	—	—
Micrite	Tr	—	3	15
Diatoms	40	5	25	60
Sponge spicules	—	1	—	—